MULTI-DIMENSIONAL ESTIMATION OF THERMAL PROPERTIES AND SURFACE HEAT FLUX USING EXPERIMENTAL DATA AND A SEQUENTIAL GRADIENT METHOD

By

Kevin J Dowding

A DISSERTATION

Submitted to

Michigan State University

in partial fulfillment of the requirements

for the degree of

DOCTOR OF PHILOSOPHY

Department of Mechanical Engineering

1997

ABSTRACT

MULTI-DIMENSIONAL ESTIMATION OF THERMAL PROPERTIES AND SURFACE HEAT FLUX USING EXPERIMENTAL DATA AND A SEQUENTIAL GRADIENT METHOD

By

Kevin J Dowding

Inverse theory is an emerging field of study with application to a diverse range of problems. Inverse thermal problems are the focus of this dissertation; specifically, the parameter estimation problem and inverse heat conduction problem (IHCP) are investigated. Although one-dimensional inverse thermal problems have been widely investigated, multi-dimensional problems are beginning to receive an increasing amount of attention. One- and two-dimensional cases are addressed for both the noted inverse problems, including an experimental application.

Parameter estimation techniques are applied to estimate the thermal properties of a carbon-carbon composite from transient experiments. Properties are determined as a function of temperature and direction relative to the fiber orientation. The thermal conductivity is assumed to be orthotropic, varying in the direction normal and parallel to the fibers; the volumetric heat capacity is assumed isotropic. Thermal properties from room temperature up to 500C are obtained. The thermal conductivity normal to the fiber is found to be less than one-tenth of the thermal conductivity parallel to the fiber. Agreement within 7% is demonstrate between independent one- and two-dimensional results.

A sequential-in-time implementation is proposed for a conjugate gradient method, utilizing an adjoint equation approach, to solve the IHCP. Because the IHCP is generally ill-posed, Tikhonov regularization is included to stabilize the solution. The proposed sequential method benefits from the efficiency and on-line capabilities of a sequential implementation, without requiring *a priori* information about the (unknown) surface heat flux. Aspects of the sequential gradient method are discussed and examined. Several promising features of the sequential gradient method are noted. Simulated one- and two-dimensional test cases are presented to study the sequential implementation. Numerical solutions are obtained using a finite difference procedure. Results indicate the sequential implementation has accuracy comparable to a standard whole domain solution, but in certain cases requires significantly more computational time. Methods to improve the computational requirements, which make the method competitive, are presented.

to my wife

ACKNOWLEDGMENTS

The input and help of the my Ph.D. guidance committee, James Beck, Patti Lamm, Alex Diaz, and Craig Somerton, is acknowledged. Special thanks are due Patti Lamm for her patience working with an engineer, help with understanding the gradient methods, and availability to discuss the research. To my advisor James Beck, I thank for his encouragement and introduction to the field of inverse problems. His enthusiasm and dedication were inspiring, not only in helping realize this work, but as a teacher and researcher.

I have benefited from interaction with several fellow students and researchers. Input and help from Arafa Osman, Bob McMasters, Heidi Relyea, and Matt White is appreciated.

Completing this work would not have been possible if it were not for the endless support my parents. To my wife I'm indebted for her understanding, support, and patience.

TABLE OF CONTENTS

LIST OF TABLES

LIST OF FIGURES

NOMENCLATURE

a	dimension of two-dimensional simulated case $[m]$
A	area $[m^2]$
$A_{1,i}$	sub-diagonal of tri-diagonal matrix
b	dimension of two-dimensional simulated case $[m]$
$\boldsymbol{b}$	parameter vector
$\hat{\boldsymbol{b}}$	estimated parameter vector
$B_{1,i}$	sup-diagonal of tri-diagonal matrix
C	specific heat $[J/kgC]$
$C_{1,i}$	main diagonal of tri-diagonal matrix
$\boldsymbol{d}_j$	location for temperature sensor j $[m]$
e_j	temperature residual sensor j $[°C]$
E	function space
f_i	nonhomogeneous term for boundary surface $[\Gamma_i]$
h	convection coefficient $[W/(m^2°C)]$
h_i	boundary coefficient
I	number of components retained in sequential implementation
I_p	current $[Amps]$
J	objective function $[°C^2\text{sec}]$
J_S	sum-of-squares term in objective function $[°C^2\text{sec}]$
J_R	regularization (Tikhonov) term if objective function $[°C^2\text{sec}]$

k thermal conductivity $[W/m°C]$

k_i boundary coefficient

L length $[m]$

L_2 function space of all "square integrable" functions

M number of temporal components for estimated heat flux on $[\Gamma_4]$

$\hat{\boldsymbol{n}}$ outward pointing unit normal vector

N_t number of measurement times

N_p number of estimated parameters

p number of parameters

p^n search direction $\left[\frac{°C^2}{(W/m^2)m}\right]$

P number of spatial components for heat flux on $[\Gamma_4]$

q heat flux $[W/m^2]$

$\hat{q}$ estimated heat flux $[W/m^2]$

$\hat{q}_e$ estimated heat flux with measurement errors $[W/m^2]$

q_{prior} prior information for heat flux, equation (4-2.4) $[W/m^2]$

q_{est} stored flux for sequential solution $[W/m^2]$

$\boldsymbol{r}$ two-dimensional coordinate vector $[m]$

r number of future time steps

S sum-of-squares function $[°C^2]$

S_Y temperature error, equation (5-4.2) $[°C]$

$S_{i,k,j,l}$ basis for finite-dimensional heat flux, equation (4-7.6)

t time [sec]

t_h heating time [sec]

T temperature $[°C]$

$\hat{T}$ calculated temperature $[°C]$

$\boldsymbol{u}$ prior information vector

$\boldsymbol{U}$ weighting matrix for prior information

$\boldsymbol{v}$ velocity vector $[m/s]$

V voltage $[V]$

$\boldsymbol{W}$ weighting matrix for sensors $\left[\frac{1}{°C^2}\right]$

$X, \boldsymbol{X}$ sensitivity coefficient, matrix

$\overline{X}, \overline{\boldsymbol{X}}$ normalized sensitivity coefficient, matrix $[°C]$

$Y, \boldsymbol{Y}$ measured temperature, vector $[°C]$

Greek

α thermal diffusivity $[m^2/s]$

α_T Tikhonov regularization parameter $\left[\left(\frac{°C}{(W/m^2)}\right)^2 \frac{1}{m}\right]$

β conjugate gradient search direction parameter, equation (4-6.10)

β_i coefficient in tri-diagonal solution, equation (5-2.3b)

γ_i coefficient in tri-diagonal solution, equation (5-2.3d)

$\gamma_{i,k}$ weighting for finite-dimensional heat flux, equation (4-7.5)

Γ_i boundary surface i for domain Ω

Δ optimality criteria

Δt time step [sec]

Δq update to heat flux $[W/m^2]$

ε convergence tolerance

ε_n temperature error $[°C]$

η_i Lagrange multiplier, equation (4-4.3)

θ sensitivity function $[°C]$

$\bar{\theta}$ adapted sensitivity function $\left[\left(\frac{°C}{W/m^2}\right)^2 \frac{°C}{m}\right]$

λ Lagrange multiplier, equation (4-4.3)

Λ Lagrangian function, equation (4-4.3)

ρ density $[kg/m^3]$

$\hat{\rho}^n$ step size, equation (4-6.13) $\left[\left(\frac{W/m^2}{°C}\right)^2 m\right]$

σ standard deviation of temperature noise $[°C]$

$\hat{\sigma}_D$ estimated error in heat flux, no measurement errors, equation (5-4.3) $[°C]$

$\hat{\sigma}_{S_\epsilon}$ estimated error in heat flux, random measurement errors, equation (5-4.7) $[°C]$

$\hat{\sigma}_q$ estimated error in heat flux, experimental data $[°C]$

$\hat{\sigma}_{\bar{Y}_k}$ estimated error in measured temperature $[°C]$

τ relaxation parameter for Residual Principle

ϕ_1, ϕ_2, ϕ_3 one-dimensional solutions for basic heat flux functions $[°C]$

ϕ_i basis parameter on time, equation (4-7.1)

φ_k basis function on space, equation (4-7.1)

ψ adjoint function (Lagrange multiplier) $\left[\frac{°C}{(W/m^2)} \frac{1}{m}\right]$

Ω two-dimensional domain

Subscripts

0 initial

cc carbon-carbon composite material

f final

ins insulating material

kapton kapton heater assembly

mica	mica heat assembly
x	direction parallel to the fiber direction
y	direction normal to the fiber direction

Superscripts

e	effective
n, *k*	iteration index
+	dimensionless variable

Chapter 1

INTRODUCTION

Study of direct (well-posed) problems has progressed for nearly two centuries. In heat conduction, a direct problem represents a situation when the coefficients of the describing differential equation, such as thermal conductivity, density, and specific heat, in addition to the magnitude and location of internal energy generation (if it exist), are specified. The geometry of the body, boundary conditions, and initial conditions are also specified. Then given this specified information, the temperature at any point in the body is calculated. Direct problems have been examined for nonlinear and multi-dimensional cases as well as irregular geometries. Study of direct problems is widely described in the literature, including issues of uniqueness and stability. Although analytical solution methods, Beck, et al. (1992) and Ozisik (1993), are restricted to mainly linear problems with a regular geometry, many numerical methods are available for solving more complex direct problems, Minkowycz et al. (1988).

Direct problems are typically in a class called well-posed problems because their solutions exist, are unique, and depend continuously on the data (coefficients of describing equation, internal energy generation, and boundary and initial conditions), Lamm (1993). We can think of the direct problem as a cause-effect relationship. Given the *cause* (coefficients of describing equation, energy generation, and boundary and initial conditions), the

effect (temperature) can be determined. In contrast to the direct problem, an inverse problem attempts to determine the *cause* for a given *effect*; the inverse of the direct problem. That is, given the *effect* (temperature), the *cause* (coefficients of describing equation, energy generation, or boundary and initial conditions) is determined. Inverse problems are typically ill-posed because they do not satisfy the criteria for a well-posed problem. Problems that do not satisfy the criteria for being well-posed were initially thought to be of little practical and physical significance. As it turns out, inverse problems are not only important, but are applicable to a wide range of practical problems.

Inverse thermal methods have numerous applications. Specific examples include: the determination of the outer surface heat flux during re-entry of a space vehicle, estimating surface conditions at the exhaust of a rocket or jet engine, determining conditions in the cylinder of an internal combustion engine, analysis of quenching in material processing, industrial process control, optimal design of experiments, estimating thermophysical properties of materials, analysis of casting processes, etc. Two popular applications of inverse methods are concerned with the estimation of surface conditions from temperature measurements, typically called the inverse heat conduction problem (IHCP) and the estimation of thermophysical properties or parameter estimation (PE). Both of these problems are addressed in this dissertation.

The study of inverse problems is relatively recent, particularly in comparison to the study of the direct problem. The earliest (engineering) papers on the subject were published near the beginning of the nineteen-sixties. Mathematicians were thinking about such problems much earlier; in 1923 Hadamard formalized the concept of well-posed, and hence ill-posed, Lamm (1993). Due to the recent nature of the field, there are few

comprehensive books on the subject. Books by Kurpisz and Nowak (1995), Hensel (1991), Beck et al. (1985), and Beck and Arnold (1977) summarize and present various methods and discuss practical applications of inverse methods. These aforementioned books tend to be the broadest in coverage of inverse methods. Less comprehensive, but more theoretical approaches are given in Alifanov et al. (1996), Alifanov (1994), Ingham and Yuan (1994), Murio (1993a), Baumeister (1987), Tikhonov and Arsenin (1977), and Lawson (1974). These book present a more limited discussion, typically focusing on a particular approach for inverse methods. They also tend to be more mathematically rigorous. Additional references (most in Russian) are found in Kurpisz and Nowak (1995); a relatively large Russian contingent is studying inverse problems.

As the importance and wide-spread application of inverse methods are realized, so too have the demands on the complexity of the problems that can be solved. For twenty years one-dimensional problems were the main subject of attention. Over the past decade multi-dimensional problems have come under scrutiny, as well as inverse radiation problems and most recently inverse convection problem. (Specific references are given in subsequent chapters.) The demands on the complexity of the inverse problems that can be solved are certainly increasing.

Multi-dimensional inverse problems are the main focus of this dissertation. In particular, the estimation of coefficients in a describing partial differential equation and the estimation of surface conditions from internal measurements for the two-dimensional case are studied. These two problems were previously referred to as PE and IHCP, respectively. The problems are closely related. In the former problem coefficients in the

describing partial differential equation are estimated. While the latter problem estimates boundary conditions, or functions, in the describing partial differential equation.

An additional complexity addressed in this dissertation is the experimental application of the multi-dimensional inverse methods. Although the contingency studying inverse problems continues to grow, a relatively small faction applies the methods to experimental studies, and even a smaller number have addressed multi-dimensional experimental applications. This dissertation studies inverse methods to experimentally estimate thermal properties and surface conditions.

Experiments with carbon-carbon composite are used to study one and two-dimensional inverse applications. Carbon-carbon composite, which is known to have thermophysical properties that depend on direction within the material (Loh and Beck, 1991), is studied for the PE problem. For the IHCP a sequential method is proposed. This method is hybrid in nature, although not completely, in that a sequential implementation on time of the conjugate gradient method using an adjoint equation approach is proposed to solve the IHCP. The sequential method was previously proposed for use with the function specification method (Beck et al., 1985). Although a sequential implementation of the gradient method has been proposed by Reinhardt and Hao (1996a), a very limited study of its implementation was addressed for the one-dimensional problem. This is the first known application of the method to a multi-dimensional problem. Issues of implementation and benefits of such a sequential method are also investigated and discussed in detail.

Specifically there two major objectives, both related to multi-dimensional inverse problems, of this dissertation:

1. Measurement of thermal properties of a carbon-carbon composite from experiments with one- and two-dimensional heat flow. Two components of

thermal conductivity and the volumetric heat capacity are simultaneously measured from transient temperature and heat flux measurements from room temperature to $500°C$.

2. Develop a conjugate gradient method using an adjoint equation approach for solving the IHCP with a sequential-in-time concept. The sequential concept is contrasted with the standard whole domain approach and variations of the sequential approach are proposed. Applications of these methods are studied with experimental data.

An outline of the dissertation is given. Carbon-carbon composite material and the experimental aspects to estimate its thermophysical thermal properties are discussed in Chapter 2 with the estimated one-dimensional properties presented. Chapter 3 gives the two-dimensional thermal properties for the carbon-carbon and a comparison between the one- and two-dimensional properties. A derivation of the conjugate gradient method with adjoint equation for the IHCP is given in Chapter 4, including a sequential implementation of the method. Chapters 5 and 6 investigate one- and two-dimensional applications of the sequential method, respectively. A summary and conclusions are given in Chapter 7, and recommended future work is suggested in Chapter 8.

Chapter 2

CARBON-CARBON THERMAL PROPERTIES: ONE-DIMENSIONAL EXPERIMENTS

2-1.0 Introduction

Composite materials are defined as materials in which two or more constituent materials are combined to produce a resultant material that has different properties from the individual constituents. Often the resulting properties (mechanical and/or thermal) of a composite material are far better than that of the constituents, hence the advantage of the composite materials. Carbon matrix carbon fiber composites are an important widely-used family of such composite materials.

Carbon-carbon composites (CC) display the mechanical benefits of fiber-reinforced materials, such as high strength-to-weight ratios, stiffness, and in-plane toughness, while maintaining these mechanical properties at elevated temperatures. Carbon-carbon's retention of mechanical properties at elevated temperatures (up to 2000 $^{\circ}C$) is unprecedented (Savage, 1993). As a consequence, carbon-carbon is used in structural materials for space vehicles, rocket nozzles, and aircraft brakes. Additionally, carbon-carbon is used for biomedical applications in hip replacement joints and for automotive applications in brakes, clutches, engine blocks, and piston rings. Most automotive applications are associated with motor sports, such as Formula I, or advanced applications. Presently, costs are too prohibitive for commercial automotive applications.

The mechanical and thermal properties of the carbon-carbon composite are quite varied. Depending on the weave and precursor used for the fiber and the method used to form the matrix, the resulting properties (thermal and mechanical) will vary, possibly orders of magnitude. In general, however, the properties tend to be anisotropic, varying with direction in the material. The complexity of the anisotropy depends on the weave and form of the fiber used. For some carbon-carbon materials (such as the one studied herein) it is sufficient to describe the properties based on two principal components, one describing the properties in the direction parallel to the fibers and a second component for the direction normal to the fibers. This type of material is referred to as orthotropic. Fortunately in the material studied, the fibers are oriented to align the fiber direction to coincide with the planes of the outer surfaces.

Although carbon-carbon can maintain structural integrity at extreme temperatures, it does so only in an inert atmosphere. At moderate temperatures (500 $^{\circ}C$) in an air atmosphere oxidation will occur (Bines, 1993). To prevent oxidation and extend the temperature range the carbon-carbon requires protection. Typically, oxidation protection is obtained by coating the surface with a form of silicon (silicon-carbide, SiC) through one of many application processes (chemical vapor deposition (CVD), infiltration (CVI), or reaction (CVR), or "pack coated"). After coating the surface, a film (tetraethylorthosilicate, TEOS) is applied to the oxidation protective coating to seal the coating. The TEOS film significantly decreases relative weight loss (oxidation) through the porous SiC coating. Since the SiC has a relatively high thermal conductivity (Incropera and Dewitt, 1990) and appreciable thickness, the properties of the carbon-carbon are even more complex

with the oxidation protective coating. (For this investigation, the effects of the CC and SiC are lumped and effective thermal properties are estimated.)

The carbon-carbon composite is known to be a thermally complex material. The simplest description for the thermal properties of the material, beyond isotropic, are orthotropic. Hence, multi-dimensional experiments are required to fully characterize the properties. (A series of one-dimensional experiments would not verify the adequacy of the orthotropic assumption.) Furthermore, with the number of different fiber/matrix variations and manufacturing methods a wide range of thermal properties are possible (Savage, 1993). Consequently, methods, experimental and analysis, are required to measure the multi-dimensional thermal properties for accurate modeling of the material. Parameter estimations techniques permit the measurement of thermal properties from appropriate experimental measurements. These methods are applied and studied to estimate the orthotropic thermal conductivity and isotropic volumetric heat capacity of the carbon-carbon.

The remainder of this section gives a problem description and literature review. Experimental aspects are discussed in Section 2-2.0. Parameter estimation methods for analyzing the experiments are covered in Section 2-3.0. Section 2-4.0 presents and discusses the thermal properties estimated for the one-dimensional experiments. Experimental uncertainty is analyzed in Section 2-5.0.

2-1.1 Problem Description

The development of composites materials is proceeding at an ever increasing rate. Advanced materials are used in automotive, airplane, and aerospace applications. The strength-to-weight ratio and survivability in harsh conditions are two main advantages of these materials. However, the emergence of these materials requires experimental

techniques and solution methods to determine their thermal properties. This chapter is about the estimation of thermal properties from temperature and heat flux measurements for a carbon-carbon composite material.

The investigated material is an advanced carbon matrix-carbon fiber material made by Carbon-Carbon Advanced Technologies, Inc. of Fort Worth, Texas. There are six specimens, 7.62cm square and 0.953cm thick. (Testing, presented herein, was performed on two of these specimens.) The specimens are described (by the manufacturer) as CC1 2-D composite made from fiberite K-641 fully densified, SiC pack coated with sealant. Because the specimens were not flat as received, the specimens were ground to produce flat surfaces.

2-1.2 Literature review

Several methods have been used to measure the thermal properties of composite materials. These methods include: the guarded hot plate (Lee and Taylor, 1975), flash method (Lee and Taylor, 1975, Taylor et al., 1985, and, Harris et al., 1982, and parameter estimation (Beck and Osman, 1991 and Garnier et al., 1992). In addition, modeling of the composite has been investigated to derive properties from constituent or laminate properties; see Kulkarni and Brady (1997), Balageas and Luc (1986), Han and Cosner (1981), and Chamis (1973). In comparison to the other methods, parameter estimation provides interaction between the model (analysis) and the experiment. For example, in the flash method a small sample is heated on one side for a very short duration, typically with a laser, and the temperature is measured on the opposite side. Early methods to calculate the thermal diffusivity (α) used the relationship

$$\alpha = \frac{k}{\rho C} = \frac{0.1388\, l^2}{t_{1/2}} \tag{2-1}$$

where $t_{1/2}$ is the time required for the temperature to reach one-half the maximum temperature rise and l is the sample thickness. An advantage of this method is that it is relatively simple. However, the method has certain disadvantages:

1. The (heat conduction) model equation is not necessarily satisfied nor checked
2. Typically few measurements are used
3. The properties k and ρC cannot be obtained independently
4. Generalizing these methods, i.e. multi-dimensional, more complex model, or temperature dependent thermal properties, is difficult, if not impossible
5. Use of statistics to quantify estimates or improve the experiment is not easily done

Parameter estimation does not posses the limitations of this other method. Beck (1996) discusses applying parameter estimation techniques to the flash diffusivity experiment. Beck shows by observing parameter estimation results that the model can be refined to improve the accuracy of the estimated thermal diffusivity. Not only by improving the analysis, but by using the analysis to better understand the experiment. Using equation (2-1) to calculate the thermal diffusivity does not permit such an analysis or provide insight. Hence, the more general method applying parameter estimation techniques is used in this dissertation.

The theory of the techniques in this research using electric heaters for estimating the thermal properties is detailed in the book Beck and Arnold (1977, see Chapter 7 in particular). A consequence of using electric heaters is that typically both thermal properties can be estimated simultaneously. This research uses the electric heaters.

Other methods with the known heat flux and transient measurements are described in Beck, et al. (1991), Scott and Beck (1992a,b), and Beck and Osman (1991). The first of these papers uses an internal heat flux transducer. The papers by Scott and Beck (1992a, 1992b) relate to composite materials during and after cure. A method to sequentially estimate thermal properties by mathematically connecting a series of discrete experiments with various temperature ranges is presented by Beck and Osman (1991). Loh (1991) has given results for experimentally determining two components of the thermal conductivity for a carbon-carbon composite. The papers by Garnier et al. (1992,1993) describe a method for estimating thermal properties without requiring the temperature sensor inside the specimen(s). This was also attempted in the present work, but the method (at least for one-dimensional cases) is only appropriate for materials with relatively low thermal conductivities because of the contact conductance. The carbon-carbon composite material does not have low values, however. Also relevant is the study of optimal experiments, which are discussed in Chapter 8 of Beck and Arnold (1977) and in Taktak et al. (1993).

2-2.0 Experimental Aspects

2-2.1 Experimental Description

A sketch of the experimental set-up used to estimate the thermal properties of the carbon-carbon material is shown in Figure 2-1. It consist of two nominally identical carbon-carbon specimens (7.62cm x 7.62cm x 0.914cm) and ceramic insulations (7.62cm x 7.62cm x 2.54cm, Zircar Products Inc., Florida, NY) with a mica heater assembly (Thermal Circuits, Inc., Salem, MA., $\Omega(T_{room})$ = 33 Ohms) located between the identical halves. Five thermocouples (Type E, 0.254mm nominal wire diameter) are embedded on

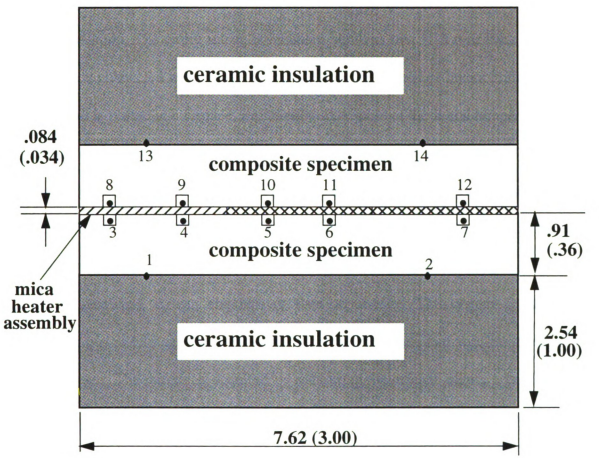

Figure 2-1 Schematic of experimental set-up used for estimating thermal properties of carbon-carbon composite. For one-dimensional experiments all heaters are activated.

the surface of each carbon-carbon specimen at the heater/specimen interface. The thermocouples (insulation removed) are attached with electrically insulating high temperature cement into grooves (0.38 mm by 0.46 mm) that extend the length of the specimen. Two thermocouples are located at each interface of the carbon-carbon specimen and the ceramic insulation. The entire set-up is mounted between two 3.18 mm thick aluminum plates that are connected with threaded rods and hold the numerous layers firmly in place; the apparatus is placed in a furnace, which allows variation of the initial temperature. Further details of the experimental procedures are discussed in Ulbrich et al. (1993).

The experiments are conducted and processed using a 12-bit data acquisition system (National Instruments) with a 486 PC. The system provides accurate data acquisition with minimum sampling intervals in the μsec range. Two eight-channel data acquisition boards are linked providing sixteen channels of data acquisition. The system controls and acquires the power (voltage and current) delivered to the heaters and acquires the thermocouple voltages. The current is acquired by measuring the voltage across a known resistance. The heat flux is calculated from the power measurements assuming the heating is uniform over the heating area (7.62 cm x 7.62 cm) and divides equally to the symmetric experimental halves.

The measured temperatures are averaged on opposite sides of the heater assembly to determine the temperature at each location. The location of the thermocouples are shown in Figure 2-1 and given in Table 2-1. The sensors that are embedded in the specimen are assumed to measure the temperature at the surface of the specimen. Since thermal conductivity normal to the fiber is much greater than the conductivity of the insulation $(k^e_{y,\,cc} \gg k^e_{ins})$, small temperature gradients near the specimen / insulation interface. The

Table 2-1 Sensor locations in experimental apparatus

Sensor Location	Sensor Number	Location cm (in)	
		x	y
A	3,8	0.89 (.35)	0
B	4,9	1.91 (.75)	0
C	5,10	3.18 (1.25)	0
D	6,11	4.45 (1.75)	0
E	7,12	6.73 (2.65)	0
F	1,13	1.27 (0.5)	0.91 (0.36) (L_y)
G	2,14	6.35 (2.5)	0.91 (0.36) (L_y)

non-embedded sensors are assumed to measure the temperature at the backside of the carbon-carbon specimen.

The thermal experimental model for the one-dimensional case is shown in Figure 2-2. All outer surfaces are assumed to be insulated, except for the surface where the energy is introduced by the heater. The energy to the heater is assumed to divide equally between the two halves and emanate from the middle of the heater assembly ($y = -0.042\,\text{cm}$). The adequacy of the assumed insulated outer surfaces for the model can be verified by a comparison of heat losses from natural convection with the anticipated applied heat flux from the heater assembly. Since a temperature rise of 20 to $25°C$ above the ambient is expected for a typical experiment, the heat loss is mainly due to natural convection ($h \approx 4W/m^2C$). These losses are negligible ($q_{conv} \approx 100W/m^2$) in comparison to the applied heat flux, which was a minimum of $7800W/m^2$ for the one-dimensional testing. Hence, insulated boundary conditions on the outer surfaces are applicable.

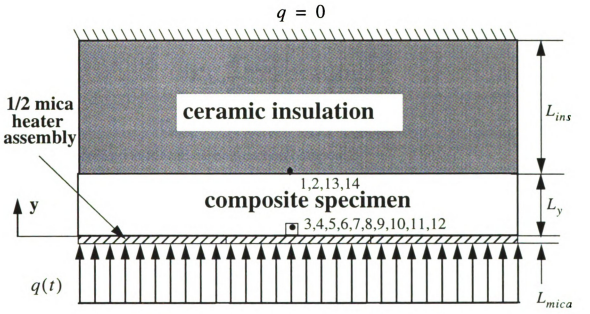

Figure 2-2 Heat transfer model for one-dimensional experiment

The thermal model is mathematically represented as three coupled problems. In the analysis of a particular experiment the thermal properties are assumed constant in the model. Temperature dependence of the thermal properties is developed by combining experiments over the temperature range. The first problem is for the mica heater/contact conductance

$$k^e_{mica}\frac{\partial^2 T_{mica}}{\partial y^2} = (\rho C)^e_{mica}\frac{\partial T_{mica}}{\partial t},\ -L_{mica} < y < 0,\ t > 0 \tag{2-2}$$

$$-k^e_{mica}\frac{\partial T_{mica}}{\partial y}\bigg|_{y=0} = q(t) \tag{2-3a}$$

$$T_{mica}(y, 0) = T_o,\ -L_{mica} \le y \le 0 \tag{2-3b}$$

The second problem is for the carbon-carbon composite

$$k^e_{y,cc}\frac{\partial^2 T_{cc}}{\partial y^2} = (\rho C)^e_{cc}\frac{\partial T_{cc}}{\partial t},\ 0 < y < L_y,\ t > 0 \tag{2-4}$$

$$T_{cc}(y, 0) = T_o,\ 0 \le y \le L_y \tag{2-5}$$

The third problem represents the insulation material

$$k^e_{ins}\frac{\partial^2 T_{ins}}{\partial y^2} = (\rho C)^e_{ins}\frac{\partial T_{ins}}{\partial t},\ L_y < y < L_y + L_{ins},\ t > 0 \tag{2-6}$$

$$\frac{\partial T_{ins}}{\partial y}\bigg|_{y = L_{ins} + L_y} = 0 \tag{2-7a}$$

$$T_{ins}(y, 0) = T_o,\ L_y \le y \le L_y + L_{ins} \tag{2-7b}$$

The problems are coupled through interface conditions that assume perfect contact

$$k^e_{mica}\frac{\partial T_{mica}(0, t)}{\partial y} = k^e_{y,cc}\frac{\partial T_{cc}(0, t)}{\partial y}, \tag{2-8a}$$

$$T_{mica}(0, t) = T_{cc}(0, t) \tag{2-8b}$$

$$k^e_{ins} \frac{\partial T_{ins}(L_y, t)}{\partial y} = k^e_{y, cc} \frac{\partial T_{cc}(L_y, t)}{\partial y} \tag{2-8c}$$

$$T_{ins}(L_y, t) = T_{cc}(L_y, t) \tag{2-8d}$$

Although perfect contact is not reasonable between the mica heater and carbon-carbon, effective properties are used to represent the mica heater and contact conductance due to imperfect contact. Effective thermal conductivity is defined

$$k^e = \bar{q} / \overline{\frac{\partial T}{\partial y}} \tag{2-9}$$

where $\bar{q}$ is the average heat flux and $\overline{\frac{\partial T}{\partial y}}$ is the average temperature gradient. Both averages are in the direction normal to the heat flow. The effective volumetric heat capacity is defined

$$(\rho C)^e = \frac{1}{V} \int_V \rho C dv \tag{2-10}$$

where V is the volume. By experimentally measuring effective properties for the mica heater assembly and insulation the contact conductance due to imperfect contact is accounted for in the model. In addition, the effective properties of the mica heater account for the effects of other materials in the heater and the cement used to install the thermocouples in grooves in the carbon-carbon composite. Modeling the effects of several materials with an effective property is much easier (and in most cases more accurate) then accounting for all effects individually. Effective properties of the carbon-carbon represent the non-homogenous construction of the material. To protect from oxidation a thin layer (approximately 10% of the overall thickness) of silicon-carbide protects the outer surfaces

of carbon-carbon. Consequently, effective properties that represent the carbon-carbon and silicon-carbide are estimated.

Including the mica heater and ceramic insulation in the model (Figure 2-2) requires the thermal properties of the materials to be known, or also estimated, to determine the properties of the carbon-carbon specimen. Neglecting the mica heater in the model is not appropriate because the contact conductance results in a large temperature drop across the heater. If the heater is neglected, the carbon-carbon properties will incorrectly reflect this effect. Also, including the heat loss to the insulation, instead of assuming a perfect insulated condition (at the specimen/insulation interface), increases the accuracy of the properties estimated for the carbon-carbon. If known (tabulated or published) properties are used for these materials (mica and insulation), several problems arise. First, thermal properties are typically not known very accurately. Second, contact conductance between adjacent layers is typically not negligible and must be considered. Third, the ceramic insulation was treated by spraying with a ridigizing material, possibly changing its thermal properties. By experimentally estimating effective properties of these materials, these problems are less influential in the estimated properties of the carbon-carbon.

This approach requires additional experimental work, however. The experimental conditions (length of experiment and heating duration) to determine the properties of the mica and insulation are quite different from the conditions necessary to estimate the properties of the carbon-carbon. A separate series of tests are performed, one set with the carbon-carbon specimen removed, to determine the properties of the insulation and mica heater assembly. These are effective properties, which will account for any contact conductance due to imperfect contact between the different material layers.

With the separate series of experiments the effective thermal properties of the ceramic insulation and mica heater assembly were determined. However, when the set-up is reconfigured to test the carbon-carbon composite, the contact conductance may vary. Therefore, for each experiment to determine the properties of the carbon-carbon composite, a short duration experiment is conducted to characterize the effective thermal properties of the mica heater and contact conductance. The short duration experiment is conducted such that the thermal properties of the mica heater, including the contact resistance, are important in the thermal model, but the properties of the carbon-carbon are not important. Importance of the materials in the model is quantified by the sensitivity coefficients (discussed in Section 2-3.0). A duration is selected that is sensitive to the properties of the mica, but relatively insensitive to the properties of the properties of the carbon-carbon.

For a typical set of experiments to determine the properties of the carbon-carbon composite, the furnace is set at a given temperature and the experimental apparatus is allowed to reach a uniform temperature (usually this required several hours). A short duration experiment (heating for approximately 2 seconds) is run first, which is used to estimate the effective properties of the mica heater. After allowing the set-up to stabilize at a uniform temperature, a second experiment is run. The second experiment (heating for approximately 20 seconds) is longer in duration and is used to estimate the properties of the carbon-carbon composite specimen.

2-2.2 Experimental Design

During the initial stages of this research a different heater design was used. The heater was constructed of a Kapton material with resistance temperature sensors (RTD) integral in the heater assembly. This approach had the advantage of being non-intrusive and

required no machining to install thermocouples. A major difficultly with this design was that the magnitude of the contact conductance resulted in the one-dimensional thermal resistance of the heater/contact conductance being on the same order of magnitude as the composite specimen in the thermal model

$$\frac{L_y}{k^e_{y,cc}} \approx \frac{L_{kapton}}{k^e_{kapton}} \tag{2-11}$$

where k^e_{kapton} is the effective thermal conductivity of the kapton heater/contact conductance and L_{kapton} is its thickness. Hence, the measured RTD temperature depends as much on the thermal properties specified for the heater/contact conductance as it does on the thermal properties specified for the composite specimen. (Sensitivity coefficients, discussed in Section 2-3.0, for the two materials would be comparable in magnitude.) In general, when other materials are present in the model, their effect on the temperature should be small in comparison to the material for which the properties are sought. For this case, the sensitivity coefficients (discussed below) for $k^e_{y,cc}$ should be larger, compared to the sensitivity coefficients for k^e_{kapton}. To improve the accuracy and reduce the dependence on the thermal properties of the heater/contact conductance, the sensors were embedded in the surface of the specimen.

The choice of the boundary condition on the backside of the specimen is dependent on the thermal conductivity of the test specimen. For a test specimen with a relatively high thermal conductivity (which this carbon-carbon does have) it is more practical to simulate an insulation condition. An insulating boundary condition is less sensitive to the contact conductance at this surface. However, for a relatively low thermal conductivity material it is more practical to simulate a temperature boundary condition. For a test specimen with a

relatively low thermal conductivity, the boundary temperature is again less sensitive to the contact conductance. Based on optimality criteria for the one-dimensional case with an applied surface heat flux, a specified temperature boundary condition on the back surface is an optimal experiment for estimating thermal conductivity. An insulating condition is optimal for estimating the volumetric heat capacity, Beck and Arnold (1977).

An approximate insulation boundary condition on the back of the specimen is chosen, instead of a temperature boundary condition (which was initially used), to minimize the sensitivity to the contact conductance at this location. With the insulation boundary condition, the heat flux (and temperature gradients) at the specimen/insulation interface is small and the temperature is not sensitive to the contact conductance or location for the non-embedded sensors. A temperature boundary condition, however, has a larger heat flux at the boundary and the temperature (at the sensor) is very sensitive to the magnitude of the contact conductance and the specified location for the sensors at the interface.

2-3.0 Analysis Procedures

The techniques to estimate thermal properties are detailed in a book by Beck and Arnold (1977). The basic process involves minimizing a sum-of-squares function

$$S = (\boldsymbol{Y} - \hat{\boldsymbol{T}})^T \boldsymbol{W} (\boldsymbol{Y} - \hat{\boldsymbol{T}}) + (\boldsymbol{u} - \boldsymbol{b})^T \boldsymbol{U} (\boldsymbol{u} - \boldsymbol{b}) \qquad (2\text{-}12)$$

where $\boldsymbol{Y}$ and $\hat{\boldsymbol{T}}$ are vectors of the measured and calculated temperatures and $\boldsymbol{W}$ is a weighting matrix (typically the identity matrix). The last term in equation (2-12) serves as regularization or allows for the inclusion of prior information about the thermal properties. It contains the difference between the prior information $\boldsymbol{u}$ and present estimates $\boldsymbol{b}$ with a symmetric weighting matrix $\boldsymbol{U}$. To determine the thermal properties the function S is

minimized with respect to the thermal properties, i.e., $b_1 = (\rho C)^e_{cc}$, $b_2 = k^e_{y,cc}$, and $b_3 = k^e_{x,cc}$. This is accomplished by setting the first derivative of S with respect to each parameter equal to zero, and solving for the estimated parameters ($\hat{\boldsymbol{b}}$). The resulting expression for the estimated thermal properties (Beck and Arnold, equation 7.4.6, 1977) is

$$\hat{\boldsymbol{b}}^{(k+1)} = \hat{\boldsymbol{b}}^{(k)} + \boldsymbol{P}^{(k)}[\boldsymbol{X}^T\boldsymbol{W}(\boldsymbol{Y} - \hat{\boldsymbol{T}}) + \boldsymbol{U}(\boldsymbol{u} - \hat{\boldsymbol{b}}^{(k)})] \tag{2-13}$$

$$\boldsymbol{P}^{(k)} = [\boldsymbol{X}^T\boldsymbol{W}\boldsymbol{X} + \boldsymbol{U}]^{-1} \tag{2-14}$$

The superscript (k) defines the iteration number, iteration is required even for the linear conduction problem, due to the non-linear nature of the estimation problem; the sensitivity coefficients $\boldsymbol{X}$ depend on the parameters (thermal properties). The columns of the sensitivity matrix are the first derivative of temperature (for each time and sensor location) with respect to the parameters

$$\boldsymbol{X} = [\boldsymbol{X}_{b_1}, \boldsymbol{X}_{b_2}, \ldots, \boldsymbol{X}_{b_p}] \tag{2-15}$$

$$\boldsymbol{X}_{b_i} = \frac{\partial \boldsymbol{T}}{\partial b_i} \tag{2-16}$$

The sensitivity coefficients can provide considerable insight to the estimation problem and aid in the design of the experiment for optimum accuracy in the estimates (Beck and Arnold, Chapter 8, 1977). One criteria for an "optimal" experiment, valid for additive, zero mean normal errors in $\boldsymbol{Y}$, and errorless independent variables, is to maximize

$$\Delta = |\boldsymbol{X}^T\boldsymbol{X}| \tag{2-17}$$

This criteria is appropriate because it corresponds to minimizing the volume of the confidence region for the estimated parameters. By studying the experimental design prior to conducting experiments, such that equation (2-17) is maximized, the maximum information is available from an experiment. In addition to the criteria proposed in

equation (2-17), a constraint requiring a fixed number of observations and/or the same temperature rise, may be required to provide consistency in comparing experimental designs with multiple sensors. Taktak et al., (1993) discuss the design of an experiment to estimate thermal properties of composites with relatively low thermal conductivity. Additional investigations on experimental design concerning the optimal placement of sensors (Fadale et al., 1995a) and the design of experiments using uncertainty information (Fadale et al., 1995b and Emery and Fadale, 1996) use the Fisher information matrix.

The sensitivity matrix and the temperatures are linearized about the thermal properties from the previous iteration in equation (2-13) and (2-14). Iteration continues until convergence of the estimated parameters is reached, as defined by, $\left|\hat{\boldsymbol{b}}^{(k+1)} - \hat{\boldsymbol{b}}^{(k)}\right| \leq \varepsilon \hat{\boldsymbol{b}}^{(k)}$, where ε is a small number to quantify convergence, such as $\varepsilon = 0.0001$.

These solution procedures are implemented with the computer program PROP1D to estimate the thermal properties. PROP1D provides a means to estimate thermal properties of multi-layer bodies from appropriate measurements. Thermal conductivity and volumetric heat capacity may be determined simultaneously and for more than one material, if desired. Layers of different materials may also be lumped and effective thermal properties determined. Garnier et al. (1992) performed experiments on materials with well-known published thermal properties to support the accuracy of PROP1D.

2-4.0 Results and Discussion

Three types of experiments were conducted. The first type removed the carbon-carbon from apparatus and replaced it with a 1.25 cm thick insulation. These type-one experiments estimated effective thermal properties of the mica heater and insulation.

Experiments of type-two and type-three replaced the carbon-carbon specimen in the experiment. Type-two experiments heated for a short duration, providing information about the effective properties of the mica heater. Type-three experiments estimate the properties of the carbon-carbon. Results from experiments of type-one and type-two are discussed in Section 2-4.1 and type-three is discussed in Section 2-4.2.

The reason that three types of experiments were used, is to quantify three separate, quite different, effects. Type-one experiments, with the carbon-carbon composite removed, provide effective thermal properties of the insulation. Experiment type-two was relatively short in duration, so that temperature is mainly influenced by the properties of mica heater, contact conductance, and associate materials used to install thermocouples. Type-three experiments were longer in duration and characterized the properties of the carbon-carbon composite. Each of the three experiments focuses on an individual aspect of the thermal model and has minimal effects from other material's thermal properties.

2-4.1 Effective Properties for Mica Heater and Insulation

An independent set of experiments was conducted to determine the effective thermal properties of the insulation material (Ulbrich, 1993). These tests used a set-up similar to Figure 2-1, except that the carbon-carbon specimen was replaced by a 1.25 cm-thick piece of insulation. The goal of these experiments was to estimate the thermal properties of the insulation. The results are given in Table 2-2. The values estimated for the insulation are considerably higher than the values reported by the manufacturer. This is not a surprising outcome. Manufacturers do not typically measure thermal properties. Also, this material was treated with a solution to make it more structurally strong. The effective properties for the mica heater were also measured. Because these values are sensitivity to the contact

Table 2-2 Thermal properties of the ceramic insulation

	Present Investigation		Manufacturer
Temperature	k^e_{ins}	$(\rho C)^e_{ins} x 10^{-6}$	k_{ins}
$°C$	$W/(m°C)$	$J/(m^3°C)$	$W/(m°C)$
40	.088	.419	
175	.093	.570	
200			.055
600			.110

Table 2-3 Effective thermal properties for the mica heater assembly

Experimental Case	**Initial Temp**	$\hat{\sigma}$	k^e_{mica}	$(\rho C)^e_{mica} x 10^{-6}$
	$(°C)$	$(°C)$	$W/(m°C)$	$J/(m^3°C)$
1010@30.1	30	0.066	0.142 +/- 0.002	2.030
1010@41.1	41	0.070	0.131 +/- 0.002	2.030
1007@134.1	134	0.067	0.102 +/- 0.001	2.030
1007@143.1	143	0.072	0.110 +/- 0.002	2.030
1008@180.1	180	0.057	0.125 +/- 0.001	2.030
1012@195.1	195	0.053	0.123 +/- 0.001	2.030
1008@245.1	245	0.070	0.114 +/- 0.001	2.030
1013@254.1	254	0.057	0.123 +/- 0.002	2.030
1008@295.1	295	0.058	0.123 +/- 0.002	2.030

conductance they were measured again after the apparatus was re-assembled with the carbon-carbon specimen. These experiments were referred to as type-one experiments.

Having established the properties of the insulation, type-two experiments were conducted to determine the effective properties of the mica heater. It was found that estimating the thermal conductivity and volumetric heat capacity simultaneously is not possible due to correlated sensitivity coefficients (see Beck and Arnold, 1977). Therefore, the volumetric heat capacity of the mica heater is set at the value estimated during the experiments to determine the properties of the ceramic insulation (type-one). The effective thermal conductivity of the mica heater is estimated. The thermal conductivity is estimated because it is most influenced by the contact conductance, which may have changed from the previous estimates.

The effective thermal conductivity estimated for the mica heater assembly, assuming $(\rho C)^e_{mica} = 2.0\times10^6\ J/m^3C$, demonstrated no specific trend with temperature over the range $(30-295)°C$. See Table 2-3. The largest value is $k^e_{mica}(30°C) = 0.14\ W/mC$ and the smallest is $k^e_{mica}(134°) = 0.10\ W/mC$. For temperatures up to $295°C$ the thermal conductivity of the mica heater is estimated at each temperature. After which, the magnitudes of these thermal properties were shown to minimally affect the outcome of the estimation for the carbon-carbon properties. A variation of 50% in the thermal properties specified for the mica heater results in variations in the estimated properties of the carbon-carbon that are within the magnitude of the confidence intervals (discussed below). For temperatures greater than $295°C$, the thermal conductivity estimate of the mica heater at $295°C$ is used in the analysis. The fact that it is difficutlt to estimate the thermal properties of the mica heater suggests that these properties are not significant in the estimation of

Table 2-4 Thermal properties estimated for the carbon-carbon composite from one-dimensional experiments and analysis

Experimental Case	Initial Temp	$\hat{\sigma}$	$k^e_{y,cc}$	$(\rho C)^e_{cc}\times 10^{-6}$
	$(°C)$	$(°C)$	$W/(m°C)$	$J/(m^3°C)$
1010#30.1	31	0.128	3.40 +/- 0.05	1.42 +/- 0.01
1010#41.1	42	0.114	3.48 +/- 0.04	1.47 +/- 0.01
1012#94.1	95	0.161	3.85 +/- 0.07	1.74 +/- 0.02
1012#108.1	109	0.161	3.93 +/- 0.07	1.81 +/- 0.02
1011#143.1	143	0.121	4.12 +/- 0.07	1.90 +/- 0.02
1011#159.1	159	0.089	4.22 +/- 0.06	2.08 +/- 0.01
1012#195.1	195	0.091	4.35 +/- 0.06	2.20 +/- 0.02
1013#259.1	259	0.075	4.60 +/- 0.04	2.47 +/- 0.02
1008#295.1	295	0.090	4.76 +/- 0.05	2.52 +/- 0.02
1013#304.1	304	0.103	4.74 +/- 0.05	2.58 +/- 0.02
1023#403.2	403	0.100	4.86 +/- 0.05	2.76 +/- 0.02
1023#455.2	455	0.082	4.93 +/- 0.03	2.88 +/- 0.02
1023#508.2	508	0.096	4.99 +/- 0.05	2.97 +/- 0.02
1023#571.2	571	0.278	3.93 +/- 0.23	3.06 +/- 0.10
1023#623.2	623	0.205	3.73 +/- 0.15	3.23 +/- 0.07

the carbon-carbon properties (or thermal model). This is a desirable characteristic for additional materials (i.e. mica heater and ceramic insulation) in the experimental model. A similar insensitivity is demonstrated for the thermal properties of the insulation.

2-4.2 Effective Properties of Carbon-Carbon

The properties estimated for the carbon-carbon composite are given in Table 2-4. The first column identifies the experimental case and the second column the initial

temperature. The third column is the estimated standard deviation of the analysis, which is defined as

$$\hat{\sigma} = \left[\frac{1}{(N_t - N_p)} \sum_{i=1}^{I} \sum_{j=1}^{J} (Y_{ij} - \hat{T}_{ij})^2 \right]^{0.5} \tag{2-18}$$

where N_t is the total number measurements (from both sensor locations, $N_t = I + J$) and N_p is the number of estimated parameters. Variables I and J are the number of measurement times and number of sensors, respectively. The last two columns present the estimated properties with the associated confidence interval (calculated by PROP1D and discussed below).

Insight about the estimated properties is gained by plotting the properties as a function of temperature; Figure 2-3 gives a plot of the one-dimensional properties of the carbon-carbon composite as a function of the temperature, with the estimated confidence intervals. Note that the analysis assumes that the thermal properties were constant during an experiment, but varied between experiments; the initial temperature of the experiment is used to plot the properties. Using an F-test (Beck and Arnold, chapter 6, 1977) it is concluded that a second order (in temperature) model adequately represents the results. The equations determined for the properties with a least squares fit are

$$k^e_{y,cc} = 3.42 + 3.38\left(\frac{T - T_0}{T_3 - T_0}\right) - 1.86\left(\frac{T - T_0}{T_3 - T_0}\right)^2 \tag{2-19}$$

$$(\rho C)^e_{cc} = \left[1.41 + 2.65\left(\frac{T - T_0}{T_3 - T_0}\right) - 1.11\left(\frac{T - T_0}{T_3 - T_0}\right)^2\right] x10^6 \tag{2-20}$$

where $T_0 = 31°C$ and $T_3 = 508°C$ are the minimum and maximum temperatures. By normalizing the temperature in equation (2-19) and (2-20) the coefficients in the describing equations have units equivalent to the respective thermal properties. A physical

appreciation of the magnitudes is more easily realized in this form. The relationships are also shown in Figure 2-3. The thermal conductivities determined from the last two experiments are not used in the least squares analysis. The validity of the thermal properties estimated at temperatures of $571°C$ and $623°C$ is uncertain. The residuals and confidence intervals for these two cases are relatively large. When the set-up was disassembled after these experiments, the outer coating of the specimen (which protects from oxidation) had separated from the inner composite material. Because the estimated thermal conductivities are lower it is quite possible that the failure of the specimen occurred just before or during these experiments.

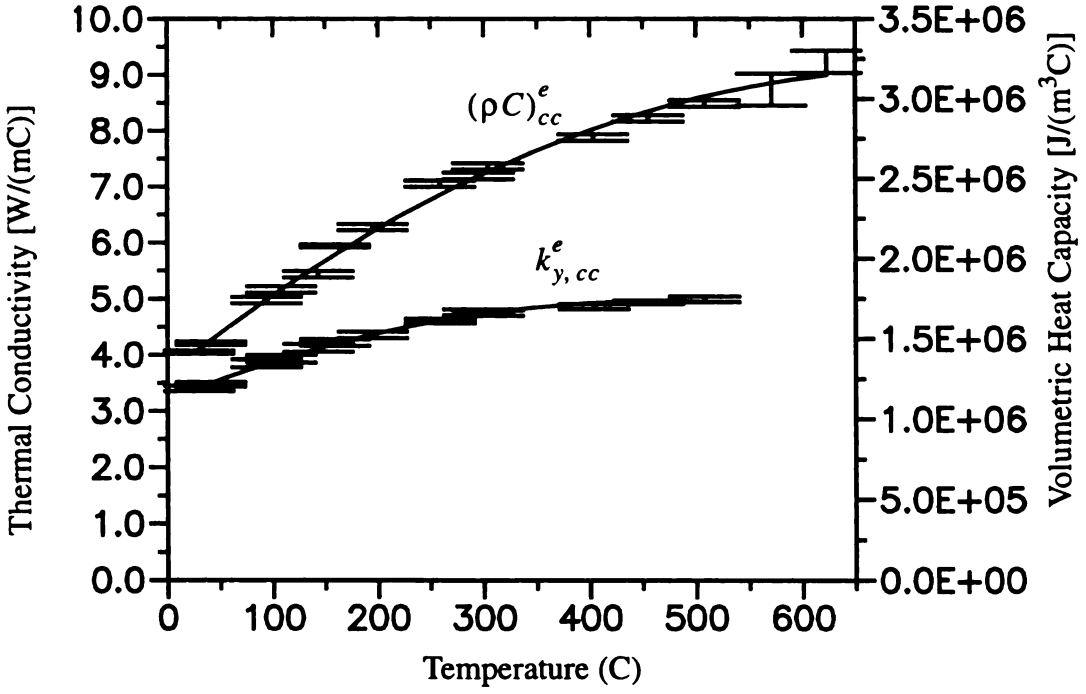

Figure 2-3 Temperature dependence of thermal properties estimated from one-dimensional experiments

The details of the parameter estimation are quite similar at different initial temperatures. For this reason, and for brevity, only one case (1023#508.2), at an initial temperature of $508°C$, is discussed. The experimental data for this case are presented in Figure 2-4. The temperatures shown represent the average of all thermocouples at the referenced locations. The results closely approximate the case of a finite slab heated with a constant heat flux at the surface and insulated at the backside. Initially, the temperature at the heated surface increases rapidly, while the backside temperature remains constant. Later both the temperatures at the heated surface and backside increase linearly with time until the power to the heater is turned off. Then the temperatures at both surfaces tend to approach the same temperature, demonstrating that there is little heat loss to the insulation (even though it is considered in the analysis).

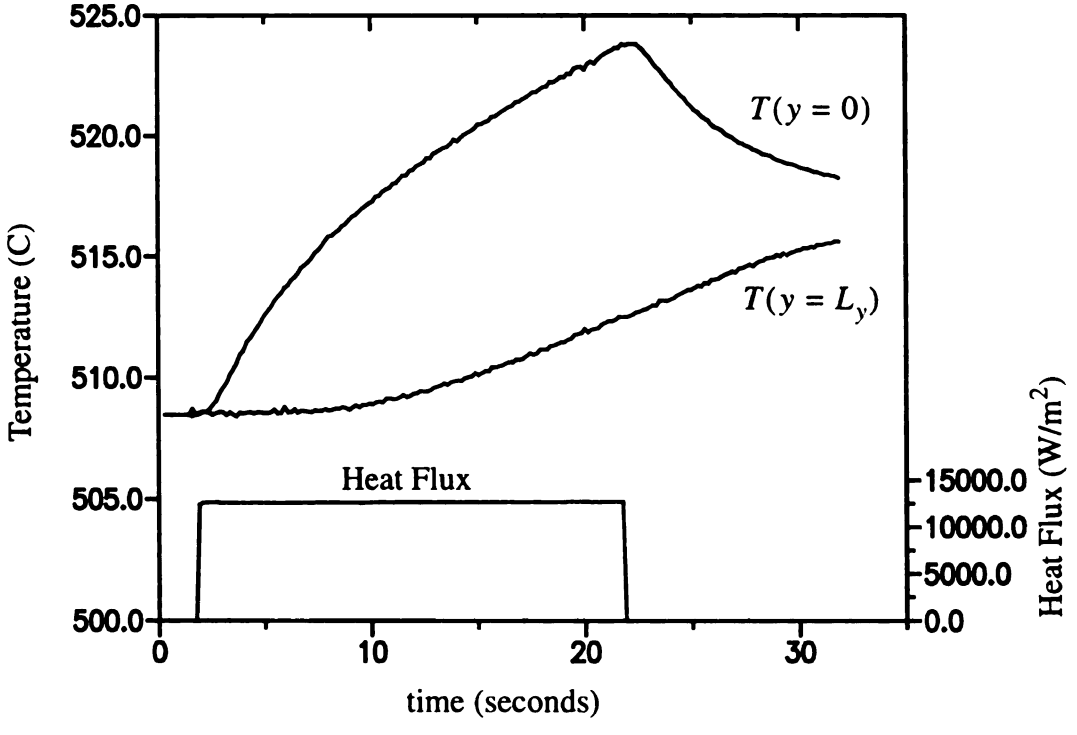

Figure 2-4 Experimental data for one-dimensional case 1023#508.2

In addition to estimating the thermal properties, PROP1D provides some means to quantify the accuracy of the estimates. The previously discussed estimated standard deviation, equation (2-15), provides an indication of how well the calculated match the measured temperatures. The magnitude of $\hat{\sigma}$ can be compared to the temperature rise of the experiment, which is approximately $15°C$. Except for the last two experiments, $\hat{\sigma}$ is within 1% of the temperature rise. Also given with the estimates of the parameters is a confidence interval (Beck and Arnold, Chapter 6, 1977). The calculation of the confidence intervals has associated assumptions. First, the model for the experiment is correct. Second, the dominant errors in the analysis are in the temperature measurements, modeled with a first order auto-regressive model, and the errors are not biased (Beck and Arnold, 1977).

Other quantities can be observed to demonstrate the accuracy of the estimated properties. These include the sequential estimates of the properties, the residuals, and the sensitivity coefficients. The quantities are important to provide insight to the estimation, as well as insight to the experiment. Observing them can help improve the experiment and support the accuracy of the estimated properties. Each is discussed below.

The sequential estimates demonstrate how the estimated properties vary as additional measurements are considered. The analysis assumes that the estimates are linearized about the converged parameter values using <u>all</u> experimental data. Figure 2-5 shows the sequential estimates for this case. The sequentially estimated property, at time t_i, represents the outcome if only data up to that time is used in the analysis (and linearized about the converged property values). In other words, if the data is analyzed by adding one data pair, $Y(y = 0)$ and $Y(y = L_y)$, at each time, it shows how the estimated properties change as

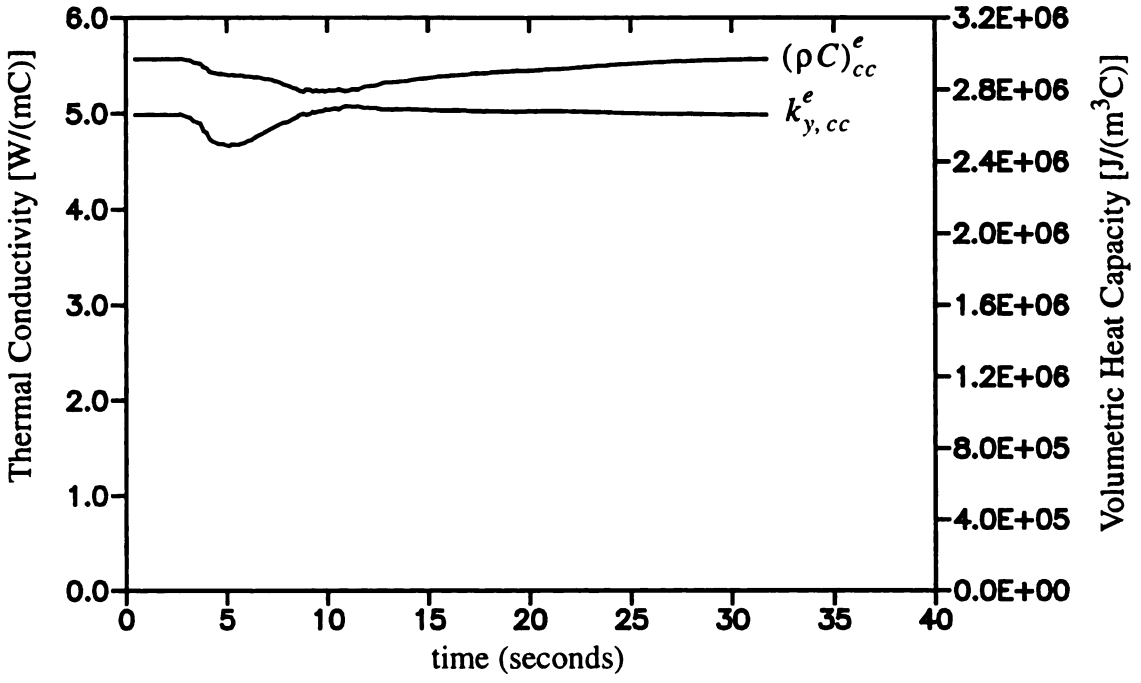

Figure 2-5 Sequential parameter estimates for one-dimensional case 1023#508.2

an additional data pair is added to the analysis. Initially the sequential estimates vary because there is not enough information to determine the parameters. However, as more data is considered, the property estimates approach constants and the linearization approximation is accurate. Meaning, if the experiment (or analysis) is ended at 15 seconds, the estimated properties would not differ significantly from the properties at 30 seconds. In general, for a good estimation, the sequential estimates converge to a constant and are fairly steady with time. For times greater than fifteen seconds, the sequential estimates of $k^e_{y,cc}$ and $(\rho C)^e_{cc}$ vary 0.9 and 3.5%, respectively. These values can be compared with the confidence regions predicted in Table 2-4 for this case of 1% and 0.67%, respectively. These sequential results for $(\rho C)^e_{cc}$ at $508°C$ are not as accurate as the confidence interval in Table 2.4. Uncertainty in the other experimental measurements account for the difference; the confidence intervals include error in the temperature measurements only.

The residuals are related to the estimated standard deviation and are calculated using

$$e_{ij} = Y_{ij} - \hat{T}_{ij} \tag{2-21}$$

and represent the difference between the measured and calculated temperature for a particular time (t_i) and sensor location (j). The estimated standard deviation gives an indication of the magnitude of the residuals; the signs and magnitudes of the residuals can provide considerable insight. Figure 2-6 presents the residuals for this case. The magnitude of the residuals is approximately $0.1°C$. The residuals are correlated; most of the residuals are positive during the heating. This outcome may signify that some inconsistency exists in the model or that a small effect was omitted. However, the magnitudes of these residuals are small, within 1% of the temperature rise during the experiment, indicating that errors in the model are minimal.

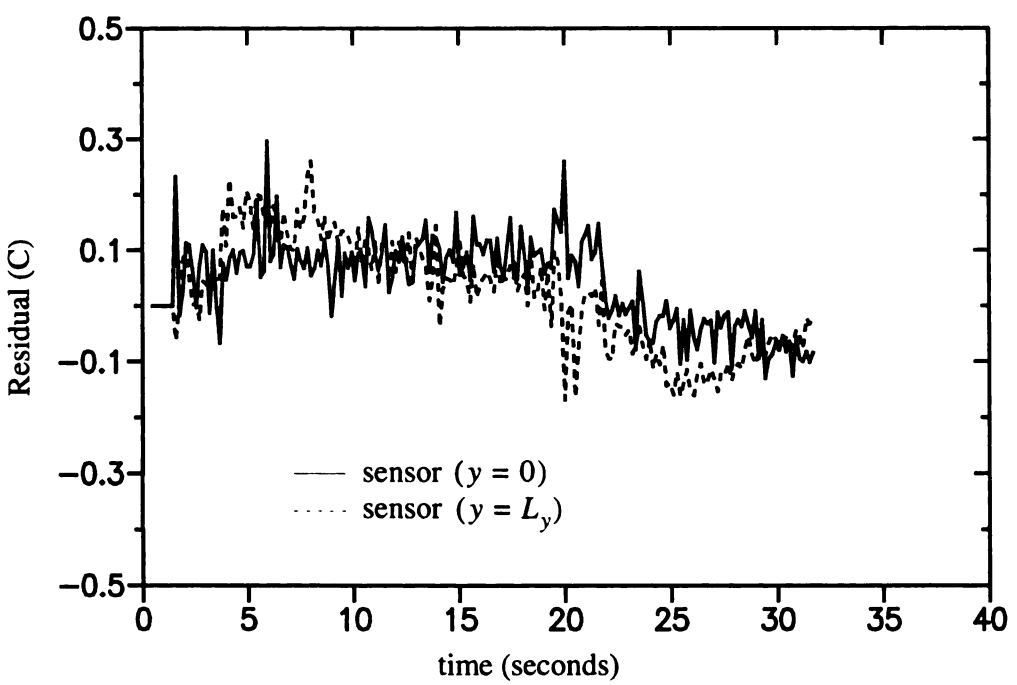

Figure 2-6 Temperature residuals for one-dimensional case 1023#508.2

Sensitivity coefficients are the first derivative of the temperature with respect to the parameters, thermal conductivity and volumetric heat capacity. They are indicators of how well designed the experiment is. In general, the sensitivity coefficients are desired to be large and uncorrelated (linearly independent). A sense of the magnitude of the sensitivity coefficients is gained through normalizing the sensitivity coefficients by multiplying by parameters, resulting in units of temperature for the normalized sensitivity coefficients. A comparison is then possible with the temperature rise of the experiment. For a well designed experiment, with boundary conditions similar to the case investigated in this study, the sum of the normalized sensitivity coefficients for the thermal conductivity and volumetric heat capacity is nearly equal to the negative of the temperature rise (equal only if perfectly insulated at $y = L_y$). Sensitivity coefficients are useful in the design of experiments, i.e., determining the heating and experiment duration, location of sensors, heating area (for two-dimensional case), etc. A study of the sensitivity coefficients, prior to performing experiments, can lead to better experiment designs.

Figure 2-7 shows the sensitivity coefficients for the representative experimental case (1023#508.2). The sensitivity to the thermal conductivity and volumetric heat capacity are shown for both sensor locations. The magnitudes are about equal to the temperature rises, which is a good feature. Notice that the sensitivity coefficients are correlated (linearly dependent) for times up to 10 seconds for the sensor at the surface of the specimen ($y = 0$). This is similar to the situation that resulted in only being able to estimate one parameter for the effective properties of the mica heater in the analysis of the short duration experiment. In this case, however, information is available from another sensor ($y = L_y$) where the normalized sensitivity coefficients for $k^e_{y,cc}$ and $(\rho C)^e_{cc}$ have quite

different shapes (i.e., not correlated). Even though the $(\rho C)^{\sim}_{cc}$ normalized sensitivity coefficient at $(y = 0)$ and L_y are both negative and decrease with time, the $k^e_{y,cc}$ normalized sensitivity coefficients are different shapes with one decreasing $(y = 0)$ and the $(y = L_y)$ values being positive. The difference in the $k^e_{y,cc}$ and $(\rho C)^e_{cc}$ normalized sensitivity coefficients at $(y = 0)$ and L_y is more pronounced as time increases and also after 22 seconds when the power to the heater is turned off. These sensitivity coefficients for $k^e_{y,cc}$ and $(\rho C)^e_{cc}$ show that the experiment is well-designed because 1) the sensitivity coefficients for $k^e_{y,cc}$ are quite different from those for $(\rho C)^e_{cc}$ and 2) the normalized magnitudes are large (relative to the temperature rise of the experiment).

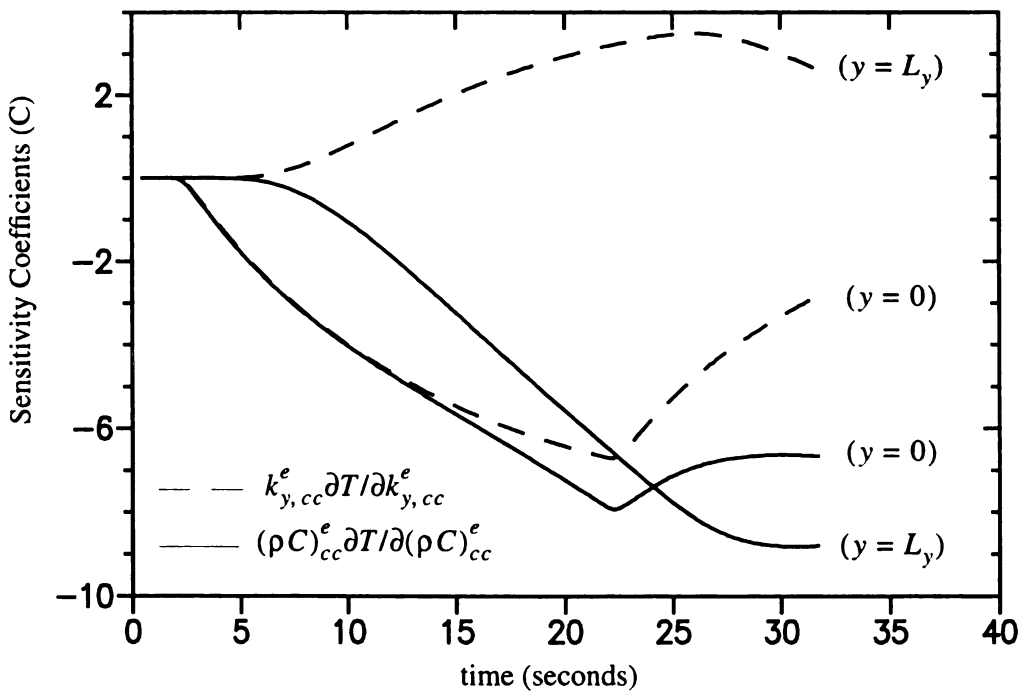

Figure 2-7 Sensitivity coefficients for one-dimensional case 1023#508.2

2-5.0 Experimental Uncertainty

The estimated thermal properties are presented with confidence intervals indicating the error in the estimates due to errors in temperature measurements. Only errors in the temperature measurements are considered in such an analysis. Errors in other experimental measurements are not included in the confidence interval. Several other experimental aspects influence the estimated thermal properties. These other experimental issues are not the same nature as the errors in temperature. They are systematic errors and not random in nature. The uncertainty in the estimate parameters ($\hat{\boldsymbol{b}}$), based on the uncertainty in the experimental parameters, is calculated as

$$d\hat{\boldsymbol{b}} = \left\{ \left(\frac{\partial \hat{\boldsymbol{b}}}{\partial z_1} dz_1 \right)^2 + \left(\frac{\partial \hat{\boldsymbol{b}}}{\partial z_2} dz_2 \right)^2 + \ldots + \left(\frac{\partial \hat{\boldsymbol{b}}}{\partial z_{n_z}} dz_{n_z} \right)^2 \right\}^{1/2} \tag{3-22}$$

where $\boldsymbol{z} = [z_1, z_1, \ldots, z_{n_z}]$ are experimentally measured parameters. In the experiment to estimate the thermal properties of the carbon-carbon, uncertainties in the measured heat flux, location (depth) of the thermocouple, thickness of the carbon-carbon specimen, effective thermal properties of the mica heater, and effective thermal properties of the insulating material are considered. An experimental uncertainty in the thicknesses of the mica heat and insulation are not included. This is because effective thermal properties were experimentally estimated for these materials, implicit in the effective thermal properties is the prescribed thickness of the material. Consequently, uncertainty in the material properties includes an uncertainty in the thickness. Experimental uncertainty for each experimental parameter and its contribution to the total uncertainty in the estimated parameters are given in Table 2-5.Uncertainty in the measured heat flux was computed as

Table 2-5 Experimental uncertainty for the two-dimensional experiments

Exp. Parameter	**Uncertainty**	**Contribution** $\left(\frac{\partial \hat{b}}{\partial z}dz\right)$	
z	dz	$(\rho C)^e_{cc} x 10^{-6}$	$k^e_{y,cc}$
		$J/(m^3 °C)$	$W/(m°C)$
q	125 W/m^2	0.033	0.049
L_y	0.05 mm	0.016	0.027
y_1	0.025 mm	0.014	0.015
k^e_{mica}	20%	0.04	0.0
$(\rho C)^e_{mica}$	20%	0.06	0.06
k^e_{ins}	20%	0.0	0.0
$(\rho C)^e_{ins}$	20%	0.0	0.0
TOTAL		**0.082**	**0.083**

$$dq = \left\{\left(\frac{\partial q}{\partial A}dA\right)^2 + \left(\frac{\partial q}{\partial V}dV\right)^2 + \left(\frac{\partial q}{\partial I}dI_p\right)^2\right\}^{\frac{1}{2}} \tag{3-23}$$

where uncertainties in measurements of area (A), voltage (V), and current (I_p) are included.

There is not a dominant term in the uncertainty analysis. All experimental conditions considered are of the same order. Overall, the uncertainty due to other experimental measurements are excellent. The uncertainty represents a maximum of 2.4% in $k^e_{y,cc}$ and 5.8% in $(\rho C)^e_{cc}$ for the experiment at the lowest temperature and 1.6% and 2.8%, respectively at the highest temperature. These values assume the uncertainties do not vary with temperature, which is reasonable for these experiments.

Chapter 3

CARBON-CARBON THERMAL PROPERTIES: TWO-DIMENSIONAL EXPERIMENTS

3-1.0 Introduction

In this chapter two-dimensional experiments are presented to estimate two components of the thermal conductivity and the volumetric heat capacity for the carbon-carbon composite. As in the previous chapter, effective thermal properties are estimated that represent the carbon matrix carbon fiber composite with a silicon-carbide protective coating. The properties, $k^e_{y,cc}$, $(\rho C)^e_{cc}$, determined from the one-dimensional experiments are not imposed on the two-dimensional solution. All the thermal properties are estimated simultaneously for the two-dimensional case. This permits a comparison between the results from one-dimensional and two-dimensional experiments to demonstrate the consistency of the methods.

3-1.1 Motivation

Interest in the solution of multi-dimensional inverse problems has gained momentum, particularly in recent years. As the importance and wide-spread application of inverse methods are realized, so too have the demands on the complexity of the problems that can be solved. Such is the case for the application of inverse methods to the field of heat transfer. Two examples are the estimation of the thermal properties of a material and the

determination of the heat flux at a boundary, both from experimental measurements. The latter problem is the inverse heat conduction problem (IHCP), which has been the main focus of research on multi-dimensional inverse problems in heat transfer. The application of inverse methods to evaluate the IHCP or estimate thermal properties are closely related, however.

A variety of methods which are used to solve the one-dimensional IHCP, have been extended to the multi-dimensional case. Osman and Beck (1990), Hsu et al. (1992) and Bass (1980) use methods based on the function specification method (Beck, et al., 1985). Murio (1993b) has presented a mollified space-marching algorithm. The adjoint method is employed by Jarny et al. (1991) and Truffart et al. (1993). Alifanov and Egorov (1985), Alifanov and Kerov (1981), and Alifanov (1994) have presented formulations for iterative regularization methods to solve the two-dimensional problem. The Monte-Carlo method was investigated by Haji-Sheikh and Buckingham (1993). Solving the multi-dimensional IHCP is further discussed in Chapter 4.

Although much energy has been focussed on the multi-dimensional IHCP, less work has been afforded to the estimation of thermal properties using inverse methods for the multi-dimensional case. Loh (1991) performed an experimental investigation for the estimation of thermal properties, orthotropic thermal conductivity and isotropic volumetric heat capacity, in a carbon-carbon composite. Jarny et al. (1991) formulated the analysis to estimate the thermal conductivity using a conjugate gradient method with an adjoint equation.

The lack of research on the multi-dimensional estimation of thermal properties may be due to the small number of materials that display an appreciable anisotropy. Due to the

construction and advancement of composite materials, however, anisotropic thermal properties are inherent in the composite; the magnitude of the anisotropy depends on the type of materials. For the carbon-carbon material investigated by Loh the thermal conductivity varied nearly an order of magnitude for directions normal and parallel to the fiber direction. This anisotropic nature of the composite material requires multi-dimensional inverse solution methods to accurately determine the thermal properties.

Although this chapter focuses on a laboratory method, the extension of a method to the field, i.e. while the aircraft is on the runway or in the hanger, is of particular interest for the carbon-carbon material because of the variability that the thermal properties demonstrate. An *in situ* method also allows changes in the material properties to be tracked during development and operation of the vehicle. The methods presented herein are not easily extended experimentally to a field application, due to the practicality of instrumenting the material. What is demonstrated, however, is the applicability of the analysis and algorithms to determine the thermal properties given experimental data. More work on the design and optimization of the experiments is required to move the methods to the field.

3-2.0 Experimental Aspects

The same experimental apparatus, shown in Figure 2-1, is used, except that only one of three heaters is energized. The two-dimensional thermal model is shown in Figure 3-1. The locations for the thermocouples are given in Table 2-1. The thermal model is mathematically represented as three coupled problems. Although the techniques used herein can be extended to temperature variable properties in a given experiment, the models given below are for thermal properties that are temperature independent.

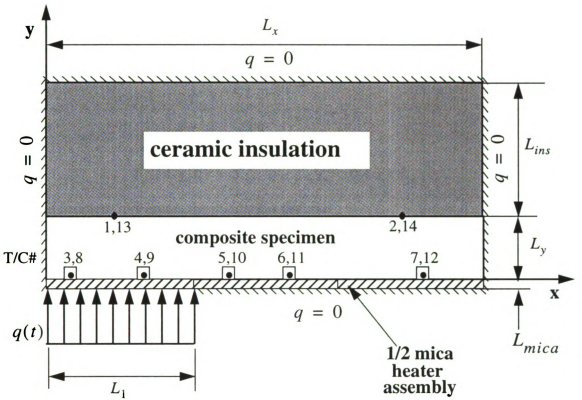

Figure 3-1 Heat transfer model for two-dimensional experiments

The first problem models the mica heater/contact resistance

$$k^e_{mica}\left(\frac{\partial^2 T_{mica}}{\partial y^2}+\frac{\partial^2 T_{mica}}{\partial x^2}\right)=(\rho C)^e_{mica}\frac{\partial T_{mica}}{\partial t},\quad \begin{matrix}-L_{mica}<y<0\\ 0<x<L_x\end{matrix},\ t>0 \tag{3-1}$$

$$-k^e_{mica}\left.\frac{\partial T_{mica}}{\partial y}\right|_{y=0}=\begin{cases} q(t) & 0\le x\le L_1\\ 0 & L_1\le x<L_x\end{cases} \tag{3-2a}$$

$$\left.\frac{\partial T_{mica}}{\partial x}\right|_{x=0,\,L_x}=0,\quad -L_{mica}\le y\le 0 \tag{3-2a}$$

$$T_{mica}(x,y,0)=T_o,\quad -L_{mica}\le y\le 0\ ,\ 0\le x\le L_x \tag{3-2b}$$

The second problem is for the carbon-carbon composite

$$k^e_{y,cc}\frac{\partial^2 T_{cc}}{\partial y^2} + k^e_{x,cc}\frac{\partial^2 T_{cc}}{\partial x^2} = (\rho C)^e_{cc}\frac{\partial T_{cc}}{\partial t}, \quad \begin{matrix} 0 < y < L_y \\ 0 < x < L_x \end{matrix}, \; t > 0 \tag{3-3}$$

$$\left.\frac{\partial T_{cc}}{\partial x}\right|_{x = 0, L_x} = 0, \; 0 \le y \le L_y \tag{3-4}$$

$$T_{cc}(x, y, 0) = T_o, \quad 0 < y < L_y \;, \; 0 < x < L_x \tag{3-5}$$

The third problem represents the insulation material

$$k^e_{ins}\left(\frac{\partial^2 T_{ins}}{\partial y^2} + \frac{\partial^2 T_{ins}}{\partial x^2}\right) = (\rho C)^e_{ins}\frac{\partial T_{ins}}{\partial t}, \quad \begin{matrix} L_y < y < L_y + L_{ins} \\ 0 < x < L_x \end{matrix}, \; t > 0 \tag{3-6}$$

$$\left.\frac{\partial T_{ins}}{\partial x}\right|_{x = 0, L_x} = 0, \; L_y < y < L_y + L_{ins} \tag{3-7a}$$

$$\left.\frac{\partial T_{ins}}{\partial y}\right|_{y = L_{ins} + L_y} = 0, \; 0 \le x \le L_x \tag{3-8b}$$

$$T_{ins}(x, y, 0) = T_o, \quad L_y < y < L_y + L_{ins} \;, \; 0 < x < L_x \tag{3-8c}$$

The problems are coupled through interface conditions that assume perfect contact

$$k^e_{mica}\frac{\partial T_{mica}(x, 0, t)}{\partial y} = k^e_{y,cc}\frac{\partial T_{cc}(x, 0.t)}{\partial y} \tag{3-9}$$

$$T_{mica}(x, 0, t) = T_{cc}(x, 0, t) \tag{3-10}$$

$$k^e_{ins}\frac{\partial T_{ins}(x, L_y, t)}{\partial y} = k^e_{y,cc}\frac{\partial T_{cc}(x, L_y, t)}{\partial y} \tag{3-11}$$

$$T_{ins}(x, L_y, t) = T_{cc}(x, L_y, t) \tag{3-12}$$

Taktak (1992) investigated optimal experimental conditions to estimate the orthotropic thermal conductivity for this geometry. However, his model specified a temperature boundary condition at the backside of the composite, instead of (an approximate) insulation condition which is used here. Taktak showed that for two sensors, the extremes (x = 0, 7.62 cm) on the heated surface ($y = 0$) , was optimal for the condition that heating occurred over one-half of the surface. For this case, which is approximately insulated at the backside of the specimen, includes the thermal effects of the heater assembly, and heats over one-third of the surface, a similar outcome would be expected. Measurement of the temperature on the surface where the heater is active and locations where it is not active provides contrasting effects (sensitivity coefficients), which improves the accuracy of the estimates. See the optimality criteria in Section 2-3.0.

3-3.0 Analysis Procedures

The same analysis procedures presented in Section 2-3.0 are used for the two-dimensional case. However, now a two-dimensional heat conduction thermal model is solved.

Computer program **PROP2D** implements this inverse method to determine two components of thermal conductivity and the volumetric heat capacity. The program was developed at Michigan State University by taking the finite element code **TOPAZ2D** (Shapiro, 1986) and combining this direct problem solver with these parameter estimation methods, to create a powerful algorithm. **PROP2D** allows for the estimation of the thermal properties for multiple materials, with possibly irregular geometries, from transient measurements. The thermal conductivity can be orthotropic and temperature dependent thermal properties are allowed.

3-4.0 Results and Discussion

A separate, independent set of one-dimensional experiments (Chapter 2) were performed to determine the thermal properties of the mica heater and ceramic insulation in the model (Figure 3-1). Effective properties were determined to account for imperfect contact between the layers. Therefore, only the thermal properties of the carbon-carbon composite are unknown in the model (Figure 3-1). Furthermore, one-dimensional experiments were performed to determined the thermal conductivity normal to the fibers ($k^e_{y,\,cc}$) and the volumetric heat capacity (ρC^e_{cc}) in the previous chapter. The one-dimensional results provide initial estimates for the two-dimensional analysis and permit for a comparison to demonstrate the accuracy and consistency of the methods; one-dimensional results are not used as prior information in the analysis.

For the two-dimensional experiments, the analysis is more sensitive to the experimental conditions. For example, the magnitude and duration of the heat flux must produce adequate response (sensitivity coefficients) for the sensors nearer the active heater, as well as for the sensors farther from the active heater. This requires a longer heating duration than that used for the one-dimensional experiments. The locations of the thermocouples must also be known accurately, especially on the active heater where temperature gradients are large. Although it is not too difficult to locate the position of the thermocouples in the carbon-carbon specimen, it is difficult to align the mica heater assembly relative to the specimens since the heating elements are not visible in the heater assembly.

The two-dimensional thermal properties of the carbon-carbon composite determined for temperatures up to $400°C$ are given next. Experiments were conducted at regular intervals over this temperature range and analyzed assuming the thermal properties were

constant for the duration of an experiment, but varied between experiments. The measured experimental data and details of the parameter estimation are presented and discussed for a typical experiment.

3-4.1 Experimental Data

Experimental data for a test started at a temperature of $297°C$ (experiment case 1022$297) are shown in Figure 3-2. A sampling interval of 0.64 seconds is used to acquired data for this experiment. The heating begins at approximately 16 seconds and ends at 56 seconds. For experiments at lower initial temperatures the heating duration is 80 seconds. However, based on observation of the sensitivity coefficients and the criteria for optimal experiments, "D-optimality", (Beck and Arnold, Chapter 8, 1977) a shorter

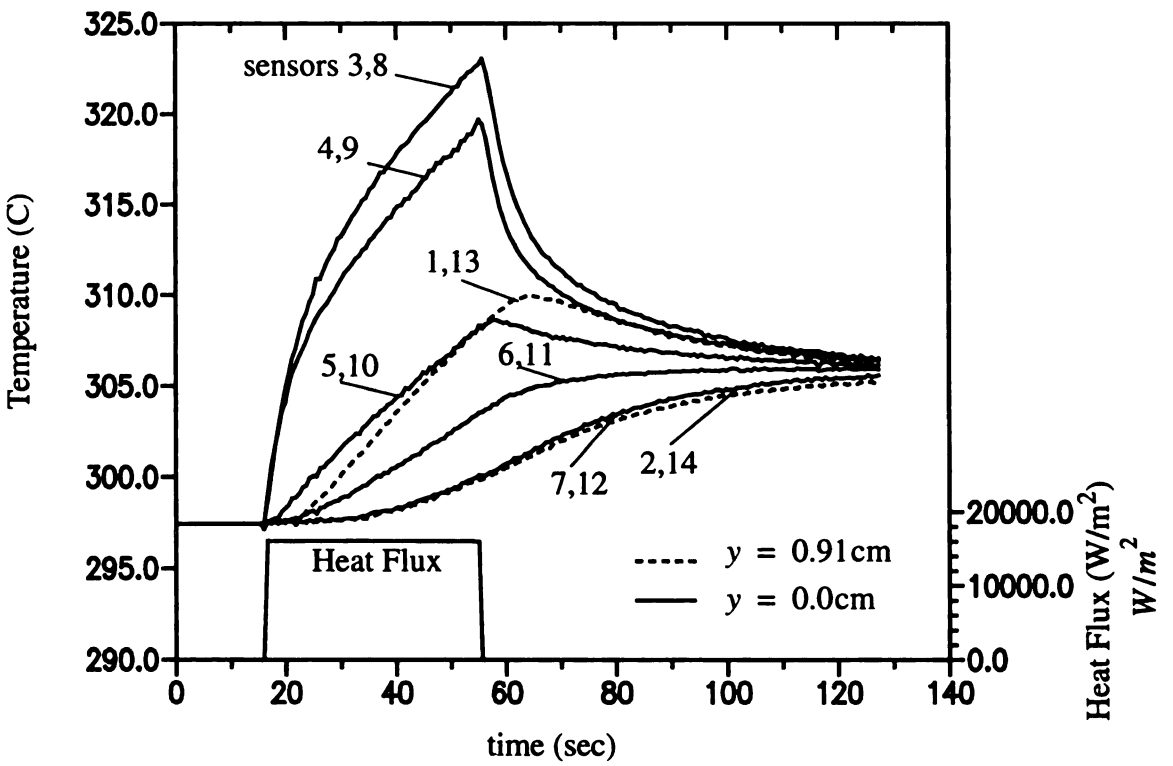

Figure 3-2 Experimental data for two-dimensional case 1022$297, see Table 2-1 for sensor locations

duration, higher magnitude heat flux is selected to be closer to optimal experimental conditions for determining the two components of the thermal conductivity and the volumetric heat capacity. The complexity of this experiment is that two components of thermal conductivity and volumetric heat capacity are simultaneously estimated. The experimental conditions must be selected to provide information about all three effects. An alternative is to conduct an series of experiments, each experiment providing information on one (or more) particular effect. Then analyze the different experiments in a sequential manner. Osman and Beck (1991) used such a procedure to estimate temperature dependent thermal properties. For this model, a single experiment provides adequate information on all thermal properties (effects) and a sequential procedure is not required.

The effect of the orthotropic thermal conductivity is seen by comparing in Figure 3-2 the temperature rise for the sensors at $x = 3.81\,\text{cm}$ (Figure 3-1) on the heated surface (sensors 5,10) and $x = 1.27\,\text{cm}$ on the insulated surface (sensors 1,13). The larger thermal conductivity in the x-direction results in a nearly instantaneous response at $x = 3.81\,\text{cm}$ on the heated surface, while the sensor at $x = 1.27\,\text{cm}$ on the insulated surface has approximately a four second time delay before responding. This delay exists even though the sensors are approximately the same distance from the active heater (~10% difference, 0.835 and 0.914 cm from the sensor on the heated surface and insulated surface, respectively).

Notice that temperature data are acquired after the heating ends. Continuing to acquire data after stopping the heat flux results in better estimates. This is because it causes the sensitivity coefficients to be of different shape from one another after heating. These effects result in a more accurate estimation of multiple thermal properties based on

the criteria "D-optimality with constraints" (Beck and Arnold, pp. 459, 1977). Possible heat losses in the experimental set-up can also be monitored with this data, although it does not appear that there are significant losses in this experiment, since all temperature sensors converge to a constant.

3-4.2 Estimated Thermal Properties

Numerical issues are more important for the two-dimensional analysis than they are for the one-dimensional. The mesh size and time step selected for the finite element method can greatly influence the amount of time required to obtain a solution and the accuracy of this solution. The mesh used for this analysis contains 525 (quadrilateral) elements. Twenty-five elements are along the 7.62 cm surface (x-direction) for all materials. There is one element across the mica heater assembly and ten elements across each the carbon-carbon specimen and ceramic insulation (y-direction). The computational time step chosen was 0.64 seconds, the same as the experimental time step. A typical two-dimensional analysis required 2-4 hours on a VAXstation 4000 Model 60 running VMS V5.5-2, depending on the number of iterations and accuracy of the initial parameter estimates; typically 4-5 iterations (16-20 direct solutions) were required. Although a detailed investigation was not performed, the time step and mesh size were varied and shown to have little influence on the resulting estimated thermal properties.

Two-dimensional thermal properties determined for the carbon-carbon composite are summarized in Table 3-1. The experiment case number and initial temperature are given in columns one and two. The next four columns present the estimated standard deviation ($\hat{\sigma}$) and the two-dimensional thermal properties determined from the analysis with confidence intervals. The final two columns give the duration and magnitude of the applied heat flux.

Table 3-1 Thermal properties estimated for the carbon-carbon composite from two-dimensional experiments and analysis

Exp Case	Init Temp	$\hat{\sigma}$	$k^e_{x,cc}$	$k^e_{y,cc}$	$(\rho C)^e_{cc} x10^{-6}$	Heat Flux	
	$(°C)$	$(°C)$	W/mC	W/mC	J/m^3C	sec	W/m^2
1020&65	65	0.168	58.4 +/- 0.34	3.89 +/- 0.04	1.52 +/- 0.003	80	5276
1020&111	111	0.183	61.0 +/- 0.39	4.17 +/- 0.04	1.74 +/- 0.004	80	6095
1021&157	158	0.163	60.7 +/- 0.34	4.24 +/- 0.04	1.93 +/- 0.003	80	6910
1021&205	205	0.210	61.8 +/- 0.33	4.55 +/- 0.04	2.13 +/- 0.004	80	8905
1021&256	256	0.202	61.6 +/- 0.30	4.73 +/- 0.05	2.34 +/- 0.004	80	8792
1022$297	297	0.295	58.8 +/- 0.38	4.97 +/- 0.06	2.36 +/- 0.007	40	17304
1022$352	353	0.277	58.7 +/- 0.37	5.07 +/- 0.06	2.56 +/- 0.007	40	17259
1022$403	403	0.256	57.4 +/- 0.34	5.09 +/- 0.05	2.66 +/- 0.007	40	17096

A plot of the thermal properties ($k^e_{x,cc}$, $k^e_{y,cc}$, and $(\rho C)^e_{cc}$) with estimated confidence interval as a function of the initial temperature is shown in Figure 3-3. A F-test (Beck and Arnold, Chapter 7, 1977) indicated a second order model (in temperature) for these properties. Because limited results are available, the relationship for $k^e_{x,cc}$ remains linear. The relationships determined with a least squares fit, are shown in Figure 3-3 and given by the following relationships:

$$k^e_{y,cc} = 3.87 + 1.93\left(\frac{T-T_1}{T_2-T_1}\right) - 0.656\left(\frac{T-T_1}{T_2-T_1}\right)^2 \tag{3-13}$$

$$k^e_{x,cc} = 60.8 - 2.07\left(\frac{T-T_1}{T_2-T_1}\right) \tag{3-14}$$

$$\rho C^e_{cc} = \left[1.52 + 1.68\left(\frac{T-T_1}{T_2-T_1}\right) - 0.543\left(\frac{T-T_1}{T_2-T_1}\right)^2\right]\times 10^6 \tag{3-15}$$

where $T_1 = 65°C$ and $T_2 = 403°C$. The thermal conductivity parallel to the fibers

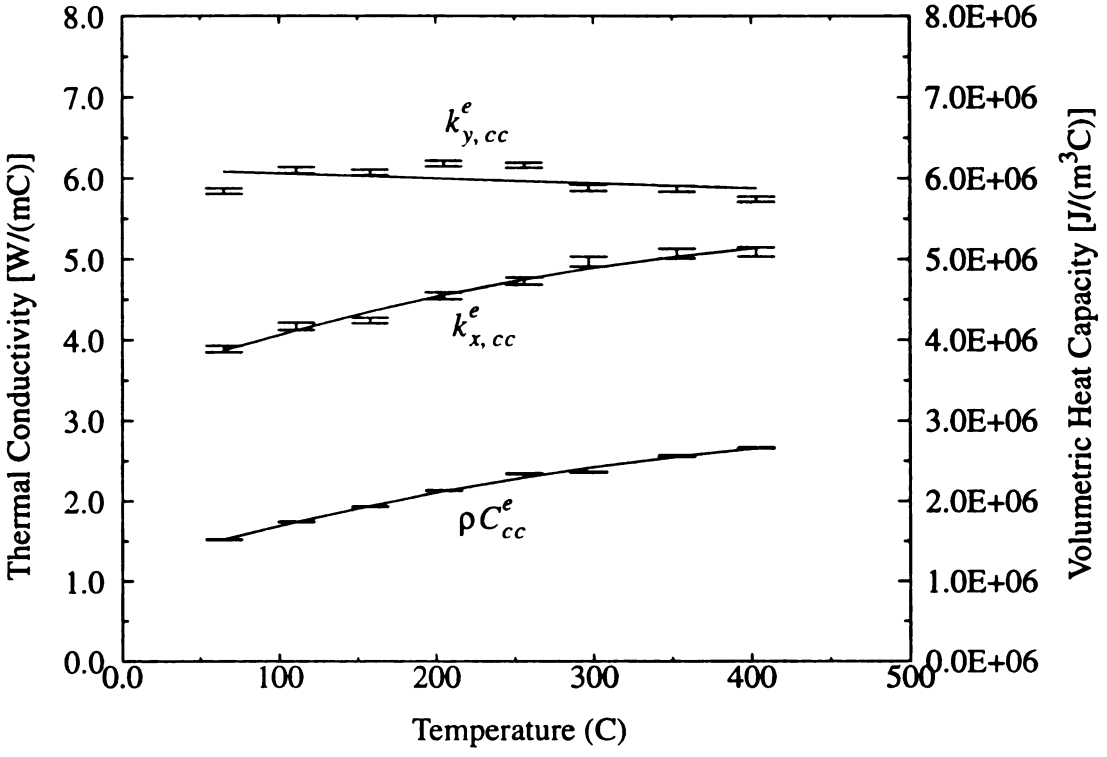

Figure 3-3 Temperature dependence of estimated thermal properties from two-dimensional experiments

($k^e_{x,cc}$) is 12 to 15 times as large as that normal to the fibers ($k^e_{y,cc}$). Testing was halted at $400°C$ due to the failure of the carbon-carbon specimen during subsequent one-dimensional testing at higher temperatures.

In addition to estimating the thermal properties, PROP2D provides some means to quantify the accuracy of the estimates. The estimated standard deviation, $\hat{\sigma}$ computed in equation (2-18), which is given in Table 3-1, provides an indication of how well the calculated temperatures match the experimentally measured temperatures. The magnitude of the estimated standard deviation can be compared to the temperature rise of the experiment, which is approximately 20 to $25°C$. The magnitude of the estimated standard deviation is within 1.2% of the maximum temperature rise for all the experiments and many

are less than 1%. The estimated standard deviation is largest for the last three experiments, which applied a larger heat flux for a shortened duration.

There are other quantities that can be observed to demonstrate the accuracy of the estimated properties. These quantities are the sequential estimates of the thermal properties, the temperature residuals, and sensitivity coefficients. These quantities are sensitive indicators to provide insight to the estimation and experiment. Each is discussed below for experiment 1022$297.

The sequential estimates demonstrate how the estimated properties vary as additional experimental measurements are considered. Figure 3-4 shows the sequential estimates for this experiment. A sequentially estimated property, at time t_i, represents the outcome if

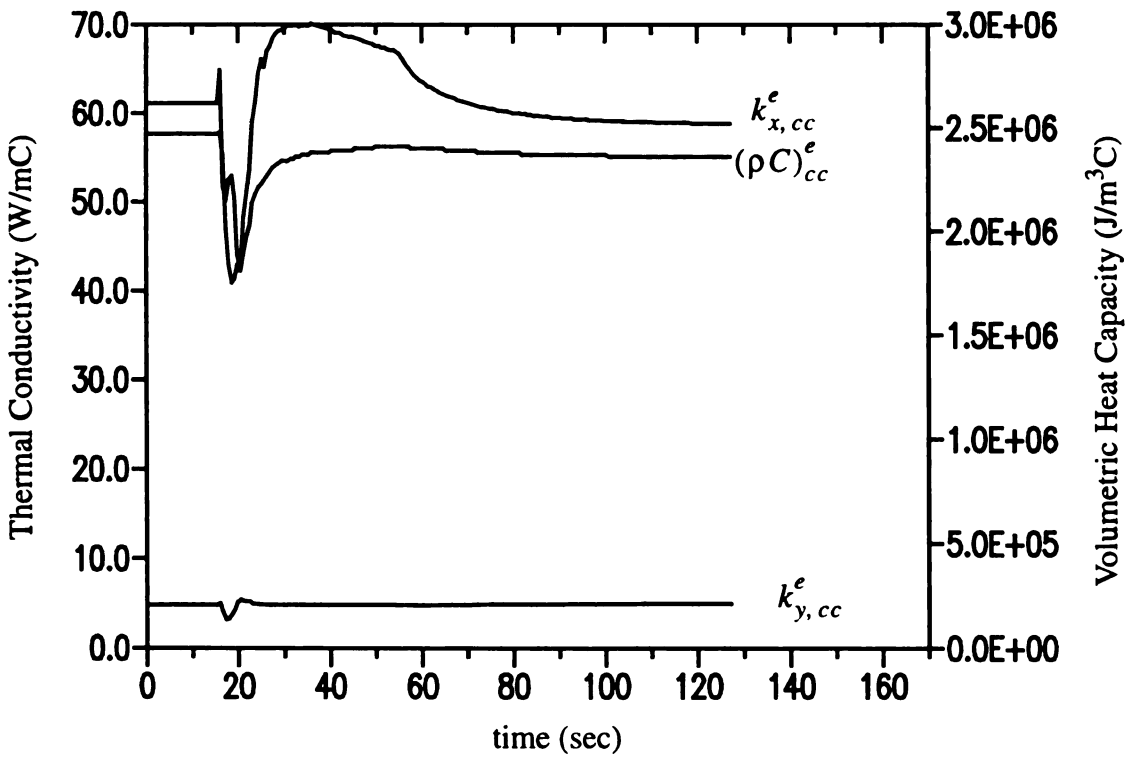

Figure 3-4 Sequential parameter estimates for two-dimensional case 1022$297

only data up to that time is used in the analysis and the results are linearized about the converged parameter values. In other words, if the data is analyzed by adding one data set at each time, it shows how the estimated properties change as one more data set is added to the analysis. Initially the sequential estimates vary because there is not enough information (data) to accurately determine the properties. However, as more data is considered, the property estimates approach constants. If the experiment (or analysis) is ended at 80 seconds, the estimated properties would not differ significantly from the properties at 100 seconds. In general, for a good estimation the sequential estimates converge to a constant and are steady with time. For this experiment the sequential estimates for $k^e_{x,\,cc}$, $k^e_{y,\,cc}$, and $(\rho C)^e_{cc}$ vary only 7.7, 3.0, and 1.6% over the final one-half of the experiment. The values are quite large compared to the confidence intervals, which were 0.6%, 1.2% and 0.3%, respectively. The confidence interval models error in temperature only. Uncertainty in other experimental measurements account for the discrepancy.

The temperature residuals are related to $\hat{\sigma}$ and are calculated as shown in equation (2-18). They represent the difference between the measured and calculated temperature for a particular time (t_i) and sensor location (x_j, y_j). The estimated standard deviation gives an indication of the magnitude of the residuals; the sign and magnitude of the individual residual can provide considerable insight. The residuals for this experiment (1022$297) are shown in Figure 3-5a, b and c. Figure 3-5a presents the residuals for the sensors on the active heater, Figure 3-5b the residuals for the sensors on the heated surface but not on the active heater, and Figure 3-5c the residuals for the sensors at the insulated surface. The residuals for the sensors on the heated surface, but not on the active heater (Figure 3-5b), are slightly correlated. The other residuals, Figure 3-5a and 3-5c, are highly correlated and

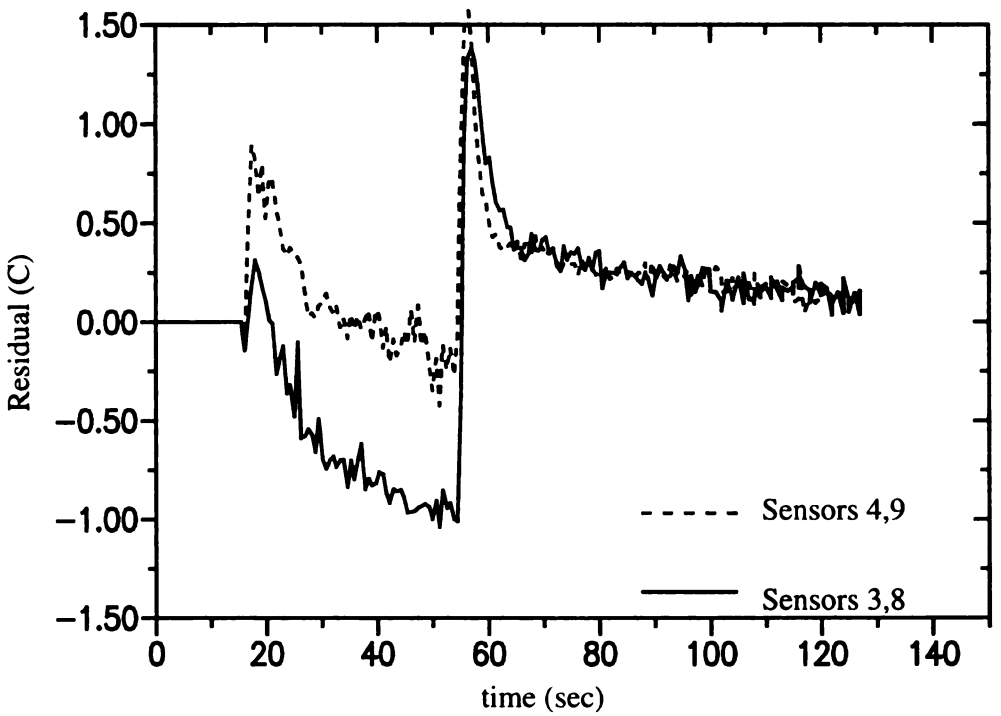

Figure 3-5a Temperature residuals for two-dimensional case 1022$297 on surface below active heater

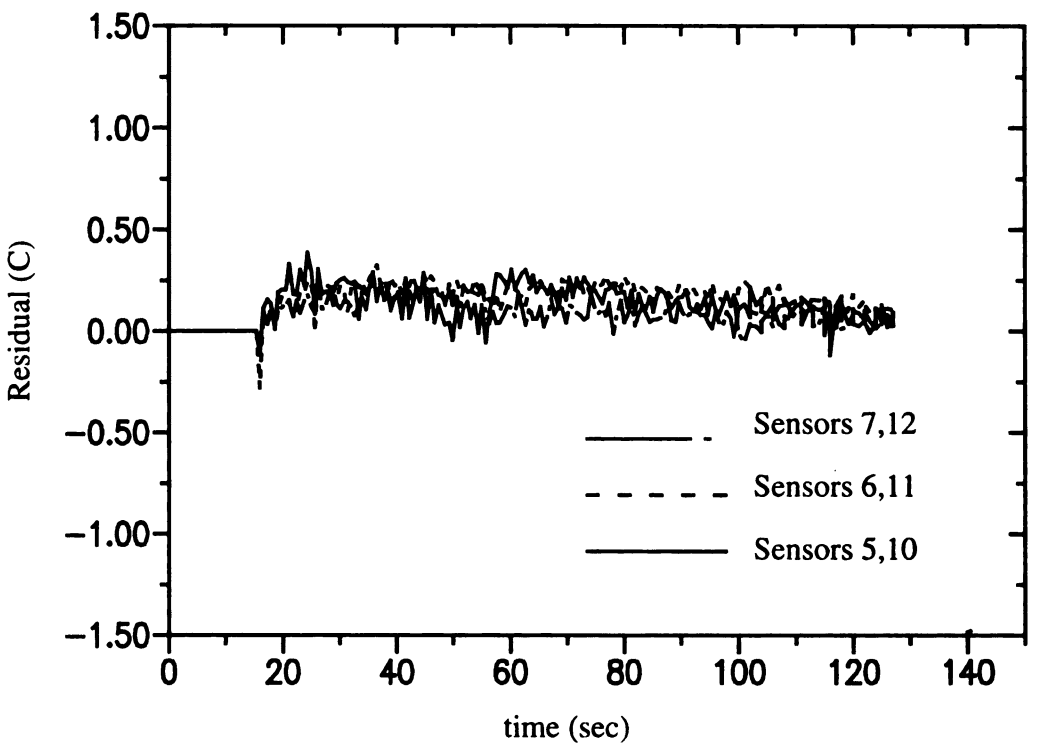

Figure 3-5b Temperature residuals for two-dimensional case 1022$297 on the heated surface, but not on the are of the active heater

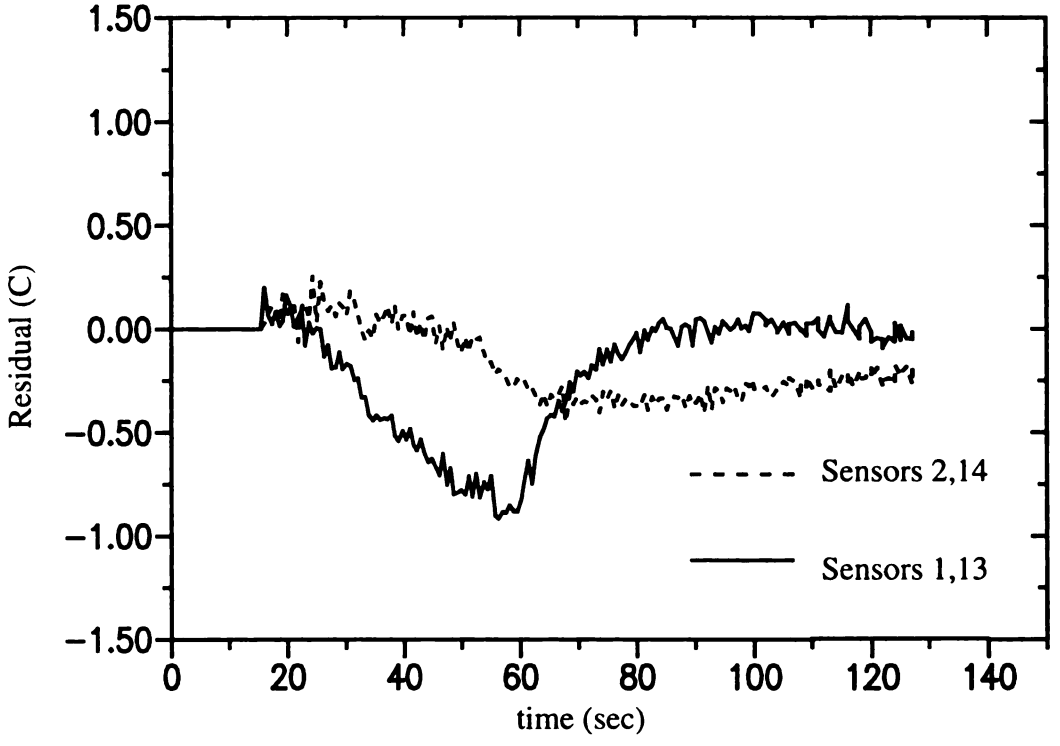

Figure 3-5c Temperature residuals for two-dimensional case 1022$297 at the specimen/insulation interface

larger, 4-5% of the temperature rise on the heated surface and 8-10% of the temperature rise at the insulated surface. It is not clear exactly why the residuals are so highly correlated. Two possible reasons are the uncertainty in the location of the sensors with respect to the heater and a non-uniform heat flux produced by the heater. First, there is some uncertainty in the alignment of the heater assembly and the specimen. The heating elements are contained within an opaque fiberglass with a mica layer on the outside. Since the fiberglass and mica extend beyond the heating elements, the alignment of the edge of the heater (element) with the specimen is difficult. Second, the design of the heating element has a gap between successive coils allowing for areas of localized heating. If the sensors align with a gap, the actual heat flux will be larger than that calculated flux, which assumes a uniform profile. Similarly, the sensors aligned with the heating element will have a larger heat flux than the calculated uniform flux. The residuals for sensors away from the active heater are less sensitive to the location and uniformity of the heat flux and therefore are less affected.

To investigate the correlated residuals, two numerical experiments were conducted. The first numerical experiment investigated an error in the location of the heater and the second investigated a non-uniform heat flux; no other measurement errors were present. These experiments were analyzed assuming no error in the location of the heater and a uniform heat flux to investigate the effect on the residuals. Unfortunately, the results of these numerical experiments were not conclusive. In particular, the two errors had opposite effects on the residuals. An error in the location of the heater resulted in a residual that had an opposite sign to the residuals for a non-uniform heat flux. The shapes of the residual curves for the numerical experiments were quite different from the

experimental case (Figure 3-5), especially for sensors not at the location of the applied heat flux.

As previously noted, observation of the sensitivity coefficients can provide insight to the estimation problem. An advantage of parameter estimation, compared to other inverse methods, such as gradient methods (Jarny et al., 1991), is that the sensitivity coefficients are computed in the analysis. Hence, no additional computation are required to observe the coefficients. Observation of the sensitivity coefficients at this stage may be too late, since the experiment is essentially designed and moving sensors or changing the heated area is not easily done. However, some minor modifications may improve the accuracy, such as changing the heating duration or magnitude. When possible, an analysis of the sensitivity coefficients should be conducted prior to running the experiments.

Sensitivity coefficients provide insight to design experiments. In general, the normalized sensitivity coefficients are desired to be large for each parameter and uncorrelated (linearly independent) for different parameters. A sense of the magnitude of the sensitivity coefficients is gained through normalizing the sensitivity coefficients. Normalization is performed by multiplying by the parameters, resulting in units of temperature for the normalized sensitivity coefficients. The normalized sensitivity coefficient for parameter η is

$$\bar{X}_\eta = \eta \frac{\partial T}{\partial \eta} \tag{3-16}$$

A comparison is then permitted with the temperature rise of the experiment. For the current experimental design, the normalized sensitivity coefficients are shown in Figure 3-6a-c. Figure 3-6a shows the sensitivity to ρC^e_{cc}, $\bar{X}_{\rho C}$, and Figure 3-6b and c shows the sensitivity to the thermal conductivities $k^e_{y,cc}$ and $k^e_{x,cc}$, $\bar{X}_{k_y}$ and $\bar{X}_{k_x}$. Because the sensitivity

coefficients are normalized, a direct comparison of their magnitudes is possible. Some observations are drawn from the sensitivity coefficient plots.

The most information is available on the active heater (sensor locations x = 0.89 cm and 1.91 cm for y = 0). At these locations the sensitivity coefficients have the largest magnitudes and therefore are most influential on the values of the estimated properties. Notice that $\overline{X}_{k_y}$ undergoes a sign change across the specimen (in the y-direction) and $\overline{X}_{k_x}$

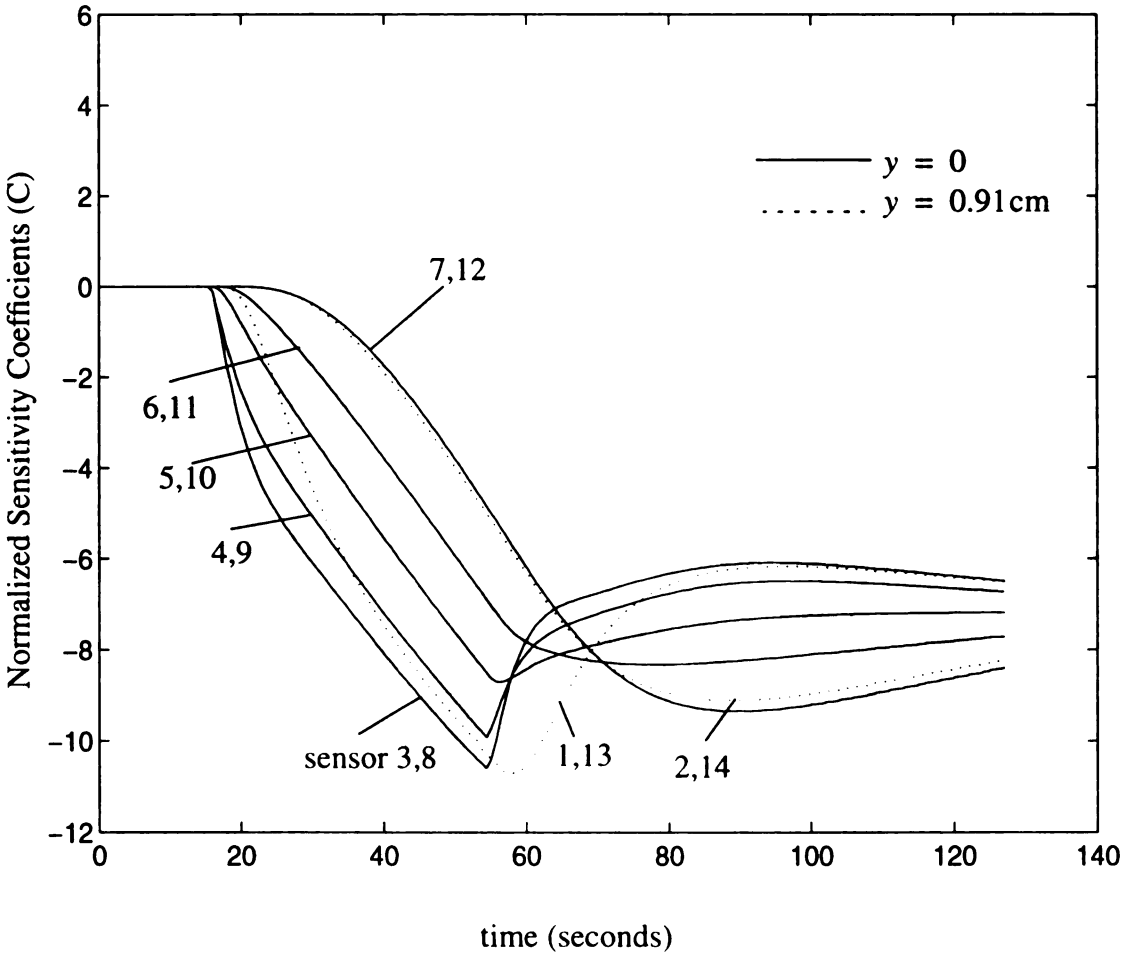

Figure 3-6a Normalized sensitivity coefficient for volumetric heat capacity, $\overline{X}_{\rho C}$, for two-dimensional case 1022$297

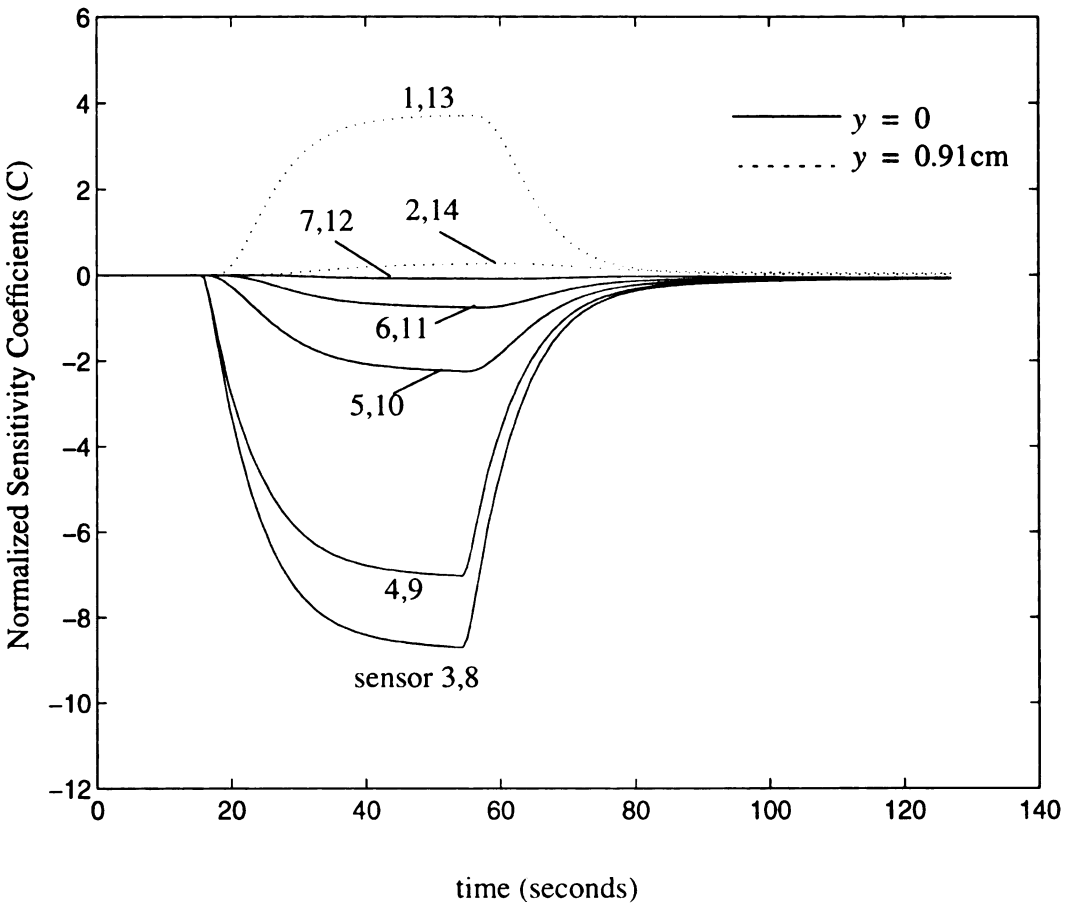

Figure 3-6b Normalized sensitivity coefficient for thermal conductivity in y-direction, $\bar{X}_{k_y}$, for two-dimensional case 1022$297

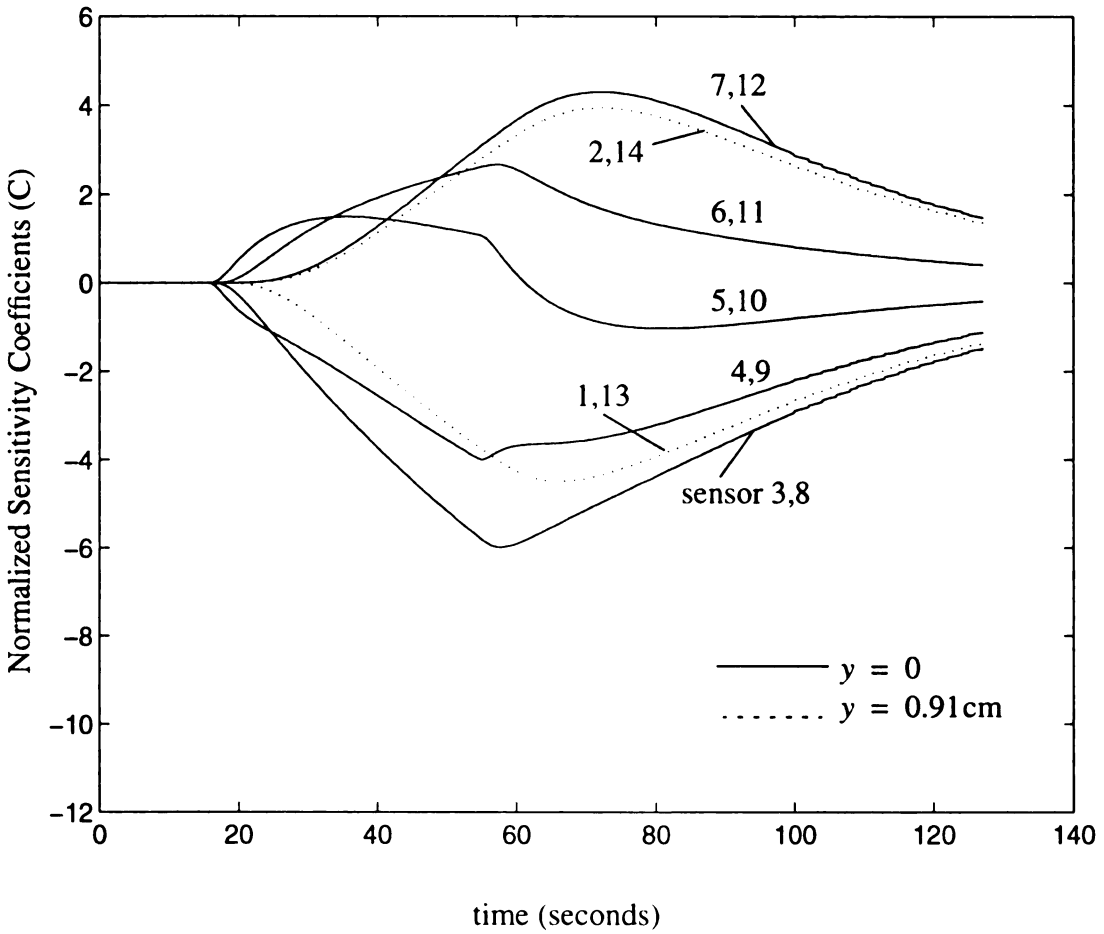

Figure 3-6c Normalized sensitivity coefficient for thermal conductivity in x-direction $\bar{X}_{k_x}$ for two-dimensional case 1022$297

undergoes a sign change along the specimen (in the x-direction). The implications of the these sign changes are that there exist 1) a y-location within the body where the temperature is insensitivity to $k_{y,cc}$ and more importantly 2) a x-location where the temperature is insensitivity to $k_{x,cc}$. The latter result is more important for this case where surfaces temperatures are measured, because seemingly logical locations along the measurement surfaces $y = 0, L_y$ may be insensitive to $k_{x,cc}$. Although it is desirable to avoid locations where the sensitivity coefficients changes sign because the sensitivity is quite small, sensor locations that have sensitivity coefficients with opposite signs are a beneficial result. This situation produces contrasting effects which improves the accuracy of the estimates. Hence, the choice of the locations near the edges of the specimen ($x = 0, 7.62$ cm), which have oppositely signed sensitivity coefficients, for the measurement locations. Fortunately, the surfaces of the specimen ($y = 0, L_y$) are the most sensitive in that direction. Finally, the experiment was halted after heating for approximately 40 seconds to make comparable the magnitudes of the sensitivity coefficients for all thermal properties. In Figure 3-6b $\overline{X}_{k_y}$ is approaching a steady-state value, while the sensitivity to $\overline{X}_{k_x}$ and $\overline{X}_{\rho C}$ have not. The sensitivity coefficient $\overline{X}_{\rho C}$ does not have a steady-state solution and will continue to increase linearly with time. If the experiment heated for a longer duration $\overline{X}_{k_y}$ and $\overline{X}_{\rho C}$ would be much larger than $\overline{X}_{k_x}$. Consequently, the estimates for the two former properties would be considerably more accurate than the latter property.

3-4.3 Comparison of One- and Two-Dimensional Results

The two-dimensional results can be compared to the one-dimensional results in chapter two for the thermal conductivity normal to the fiber and the volumetric heat capacity. The results obtained for the one-dimensional analysis were used as initial estimates for the

two-dimensional analysis; however, the thermal properties were not constrained in the two-dimensional analysis using the one-dimensional results.

The properties determined from the one- and two-dimensional experiments are compared in Figure 3-7a and 3-7b. Overall, the results are quite close. The two-dimensional results are slightly higher for $k^e_{y,cc}$ and slightly lower for $(\rho C)^e_{cc}$. Recall that the properties were estimated assuming they were constant over the duration of an experiment and therefore are applicable for a 20-25°C temperature range. Noting this, the one and two-dimensional estimates for $k^e_{y,cc}$ are within 6%, with the largest errors at the higher temperatures where limited two-dimensional data is available. There is also a dip downward for the estimates near the maximum temperature, an unexpected result that may indicate the thermal conductivity is approaching a constant, but more testing (at higher temperatures) is needed for verification. The results for $(\rho C)^e_{cc}$ have a maximum of 7% deviation between the one and two-dimensional estimates.

The temperature dependence determined using both one- and two-dimensional results, which were also indicated to be second order in temperature using a F-test, are

$$k^e_{y,cc} = 3.46 + 3.59\left(\frac{T-T_0}{T_3-T_0}\right) - 2.08\left(\frac{T-T_0}{T_3-T_0}\right)^2 \tag{3-17}$$

$$(\rho C)^e_{cc} = \left[1.41 + 2.42\left(\frac{T-T_0}{T_3-T_0}\right) - 0.894\left(\frac{T-T_0}{T_3-T_0}\right)^2\right]\times 10^6 \tag{3-18}$$

The relationship for $k^e_{x,cc}$ has only two-dimensional results and is given by equation (3-12). The estimated thermal properties, from both one- and two-dimensional experiments, are within 4% and 6% of the relationships given in equation (3-17) and (3-18) for $k^e_{y,cc}$ and $(\rho C)^e_{cc}$.

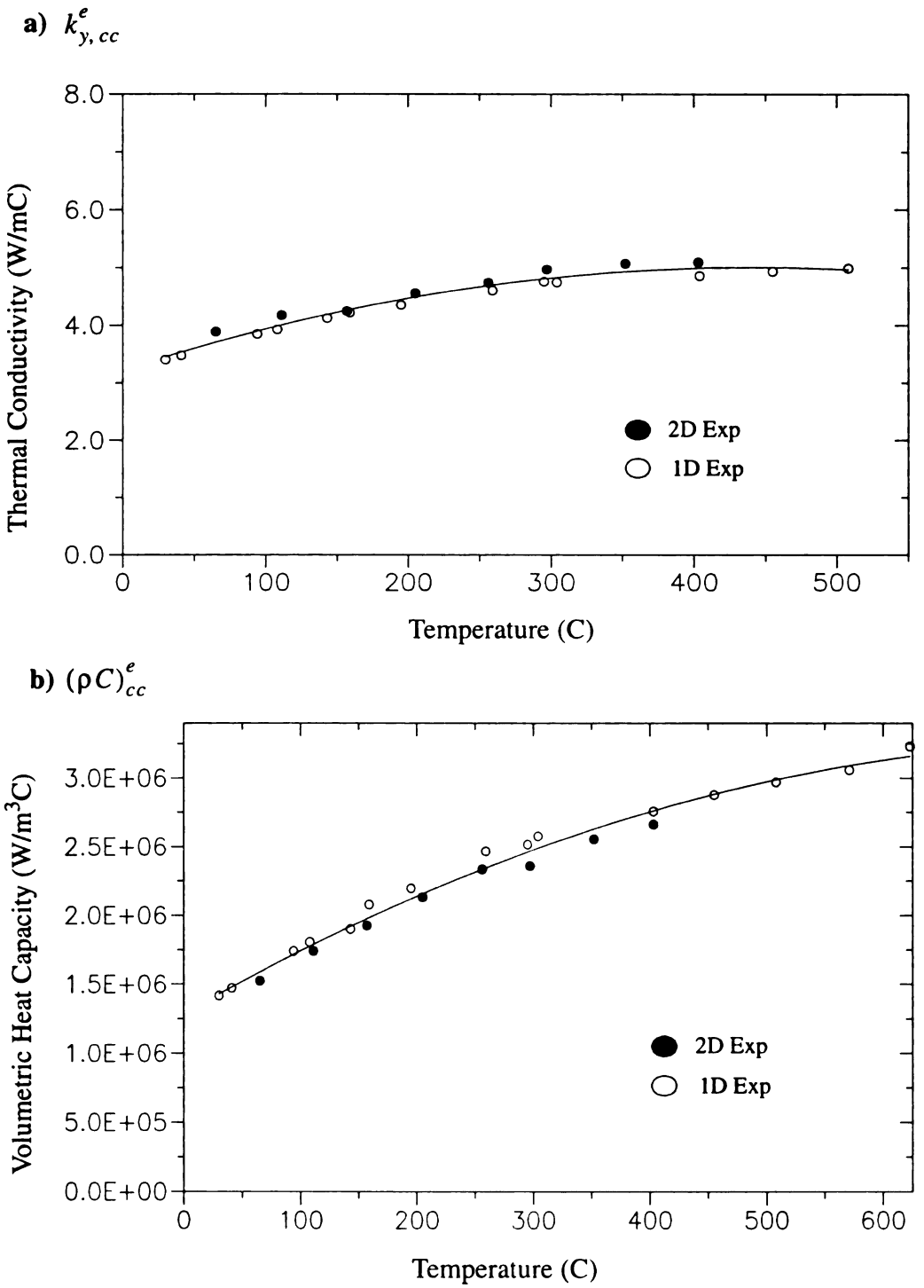

Figure 3-7 Comparison of thermal properties estimated from one- and two-dimensional experiments **a)** thermal conductivity $k^e_{y,cc}$ and **b)** volumetric specific heat $(\rho C)^e_{cc}$

Table 3-2 Experimental uncertainty for the two-dimensional experiments

Exp. Parameter	Uncertainty	Contribution $\left(\frac{\partial \hat{b}}{\partial z} dz\right)$		
z	dz	$(\rho C)^e_{cc} x 10^{-6}$	$k^e_{x,\,cc}$	$k^e_{y,\,cc}$
		$J/(m^3 C)$	$W/(mC)$	$W/(mC)$
q	3%*q W/m^2	0.086	1.9	0.15
L_y	0.05 mm	0.014	0.43	0.066
y_1	0.025 mm	5.5 E-04	0.14	0.016
x_j (j=1,2, J)	1.0 mm	8.0 E-04	0.72	0.20
k^e_{mica}	20%	0.018	0.55	0.073
$(\rho C)^e_{mica}$	20%	0.020	1.2	0.14
k^e_{ins}	20%	0.0	0.0	0.0
$(\rho C)^e_{ins}$	20%	0.0	0.0	0.0
TOTAL		**0.091**	**2.5**	**0.30**

3-5.0 Experimental Uncertainty

Using the techniques described in Section 4-5.0 for the one-dimensional properties, the experimental uncertainty for the two-dimensional thermal properties is assessed. For the two-dimensional experiment uncertainties in the measured surface heat flux, thickness of the carbon-carbon specimen, y-location and x-locations of sensors on the surface nearest the heater (experiment is insensitive to locations specified for sensors on back surface of specimen), thermal properties of mica heater, and thermal properties of insulation are considered. As in the one-dimensional analysis, the uncertainty in the thicknesses of mica heater and ceramic insulation are not considered because they are implicit in the effective properties estimated for these materials. Table 3-2 gives the uncertainties in the estimated

thermal properties due to the uncertainties in the measured quantities. For the two-dimensional case there are three important uncertainties. The uncertainty in the measured heat flux, x-location of the sensors, and the thermal properties of the mica heater are dominant terms. All terms contribute significantly to the overall uncertainty, but vary depending on the thermal property. The heat flux is important because there is a large uncertainty in the area associated with locating the heater relative to the sensors. The x-location of the sensors are important due to alignment issues. The two-dimensional uncertainties are larger than one-dimensional results. However, uncertainties are still a maximum of 6.0, 4.2, and 7.7% of $(\rho C)^e_{cc}$, $k^e_{x,\,cc}$, and $k^e_{y,\,cc}$, respectively.

Chapter 4

SOLUTION OF IHCP USING A GRADIENT METHOD WITH ADJOINT EQUATION APPROACH

4-1.0 Introduction

Estimating the conditions at the surface of a conducting body from internal measurements is typically called the inverse heat conduction problem (IHCP). Inverse describes this type of conduction problem because conditions at the boundary or surface of a body are estimated using internal measurements. Whereas a direct conduction problem, sometimes called just the direct problem, uses conditions specified on the boundary to compute the internal temperature. While the direct problem is generally a well-posed problem, the inverse problem tends to be ill-posed and very sensitive to measurement errors. A sequential method to solve the IHCP is discussed in this chapter.

Applications of the IHCP are abundant. A classic problem is determining the heat flux at the surface of space vehicles during re-entry. A related problem is the estimation of the heat flux at the leading edges of hypersonic vehicles. Other examples are estimating the heat flux, or convection coefficients during quenching, which enables control in the resulting material properties. During casting processes, estimates of the heat flux can be used to the control the cooling rate and movement of the cooling front to minimize residual stresses and void formation. Measurements on the outside of the cylinder wall of a internal

combustion engine can estimate the heat flux in the combustion chamber. Additional examples are cited in Kurpisz and Nowak (1995).

Several methods are applied to solve the IHCP. Function specification (Beck et al., 1985), Tikhonov regularization (Tikhonov and Arsenin, 1977), gradient methods (Alifanov, 1994 and Ozisik, 1993), and mollification (Murio, 1993) are more frequently cited methods. However, other approaches also applied are, dynamic programming (Busby and Truijillo, 1985), Kalman filter (Tuan et al., 1996), Monte Carlo method (Haji-Sheikh and Buckingham, 1993). In addition, combining methods is useful. Beck and Murio (1986) formulated a combined function specification and Tikhonov regularization method, similar concepts were used in Osman et al. (1997). Jarny et al. (1991) combined an iterative search method with Tikhonov regularization. Since this dissertation focuses on multi-dimensional problems, the literature review will narrow its attention to the two-dimensional problem. Refer to books by Alifanov (1994), Beck et al. (1985), Hensel (1991), and Kurpisz and Nowak (1995), for a comprehensive survey of the literature.

Many methods applied to the one-dimensional problem have been extended for the two-dimensional problem. Function specification and gradient methods have received the most attention. Function specification specifies a functional form for the heat flux over a future interval (Beck et al., 1985). Specifying a functional form over the future interval provides regularization to stabilize the ill-conditioned problem (Lamm, 1995). In conjunction with specifying a function form, function specification solves the problem in a sequential manner.

Several researchers have investigated the two-dimensional application of the function specification method. It was applied to estimate spatially and time varying convective heat

transfer coefficients, Osman and Beck (1989, 1990), and surface heat flux, Osman et al. (1997). A boundary element method was coupled with function specification to investigate multi-dimensional problems by Zabaras and Liu (1988). Hsu et al. (1992) applied a finite element method to solve the general two-dimensional problem with inverse methods similar to function specification.

Gradient methods, which typically apply a conjugate gradient iterative scheme, couple iterative or Tikhonov regularization to stabilize the solution and solve the multi-dimensional problem. Iterative regularization depends on the slowness or "viscosity" of the solution and uses the iteration index as the regularization parameter. Several papers use iterative regularization; see Alifanov and Kerov (1981), Kerov (1983), and Alifanov and Egorov (1985). Additional investigations using gradient methods, but not iterative regularization, are given in Zabaras and Yang (1996), Reinhardt (1996a.b) and Jarny et al. (1991).

Others have studied the multi-dimensional inverse problem with a variety of approaches. Tuan et al. (1996) uses Kalman filter to develop an on-line algorithm. A new method, called "direct sensitivity coefficient," is claimed by Tseng and Zhao (1996) and Tseng et al. (1996). Pasquetti and Le Niliot (1991) employ Tikhonov regularization with the boundary element method. An adjoint equation approach to compute sensitivities and relate measured temperature to unknown surface conditions is used by Hensel and Hills (1989). A Monte-Carlo method is given by Haji-Sheikh and Buckingham (1993). Mollification with a space marching technique is used by Murio (1993) and Guo and Murio (1991). Busby and Trujillo (1985) use dynamic programming. An analytical solution is developed by Mosaad (1995) and transform methods are used by Imber (1974, 1975).

Function specification and gradient methods are popular approaches. An advantage of the function specification method is that the problem retains the causal nature, represented with a Volterra operator (Lamm, 1995), and can be solved sequentially with possible savings in computational time and memory. The method, however, requires assuming *a priori* information about the (unknown) function. Gradient methods require no *a priori* information but typically solve for a function on the whole time domain, not taking advantage of the causal nature of the problem.

The demonstrated success of gradient methods and the efficiency of a sequential implementation suggest a sequential implementation of a gradient method would be a powerful combination. A method that sequentially implements a gradient scheme, using an adjoint equation approach, is proposed and to be developed; additional stability is introduced by including Tikhonov regularization. The method is anticipated to benefit from not requiring a prescribed functional form, which is particularly useful on space, and the computational aspects of a sequential implementation. Other researchers who have proposed a sequential implementation are Reinhardt and Hao (1996a,b) and Artyukhin and Gedzhadze (1994); however, past implementations have addressed the one-dimensional problem with a very limited investigation of the method. This dissertation addresses the one- and two-dimensional problems for the sequential implementation. Although applying the sequential gradient method to linear one-dimensional problems is probably not needed or recommended, addressing the one-dimensional problem provides valuable insight to the method. This is the first known two-dimensional implementation of a sequential gradient method and the most comprehensive, to the best of the author's knowledge, study of the gradient methods.

Derivation of the equations to solve the IHCP using a conjugate gradient search method with an adjoint equation approach are presented in this chapter. Gradient methods that apply an adjoint equation approach have been widely discussed in the literature. In particular, the Russian community has championed these methods (Alifanov, 1994). However, the mathematical basis of the method seems to have limited application of the methods (at least for engineers), more so in the USA than elsewhere. Reasons for the limited use of the method in the USA can be partially attributed to the strong advocacy of the FSM there (Beck et al., 1985). However, more recently the power of the methods, particularly for multi-dimensional problems and problems with many estimated components in the author's opinion, has been realized. In particular, Ozisik (1993), is an advocate of gradient methods. In addition, the methods have been presented in a less mathematically rigorous form (Jarny et al., 1991, Lamm, 1990, and Jarny and Beck, 1995).

Section 4-2.0 to 4-6.0 develop the describing equations to solve the general multi-dimensional IHCP. Equations are developed in differential form and presented in the form of an algorithm in Section 4-7.1 for a whole domain solution. A sequential implementation is discussed and an algorithm is presented in Section 4-7.2. Derivations up to this point in the chapter assume that the unknown function resides in a prescribed function space E, which is an infinite-dimensional space. Restricting the solution to a finite-dimensional space, R^n, is addressed in Section 4-8.0. The chapter is concluded with a section to summarize the chapter and provide some insight to the method.

4-2.0 Problem Statement of the Multi-Dimensional IHCP

A schematic of the general multi-dimensional IHCP is shown in Figure 4-1. In the analysis that follows, the conduction problem is assumed linear, i.e., thermal properties do not depend on temperature. Extending the gradient methods for non-linear problems is discussed in Artyukhin (1996) and Loulou et al. (1996). For the sequential implementation to be developed, it is possible to temporarily linearize the problem and not consider it non-linear. Assuming the thermal properties are independent of temperature, the problem is mathematically formulated as follows:

$$\nabla \cdot (k(\boldsymbol{r})\nabla T(\boldsymbol{r}, t)) = \rho C(\boldsymbol{r})\left[\frac{\partial}{\partial t}T(\boldsymbol{r}, t) + \boldsymbol{v} \cdot \nabla T(\boldsymbol{r}, t)\right], \quad \begin{matrix}(\boldsymbol{r}) \text{ in } \Omega \\ (t_0 < t \le t_f)\end{matrix} \tag{4-2.1}$$

$$-k_i \frac{\partial}{\partial \hat{\boldsymbol{n}}}T(\boldsymbol{r}, t) + h_i\, T(\boldsymbol{r}, t) = f_i(\boldsymbol{r}, t), \quad \begin{matrix}(\boldsymbol{r}) \text{ on } \Gamma_i, (i = 1, 2, 3) \\ (t_0 < t \le t_f)\end{matrix} \tag{4-2.2a}$$

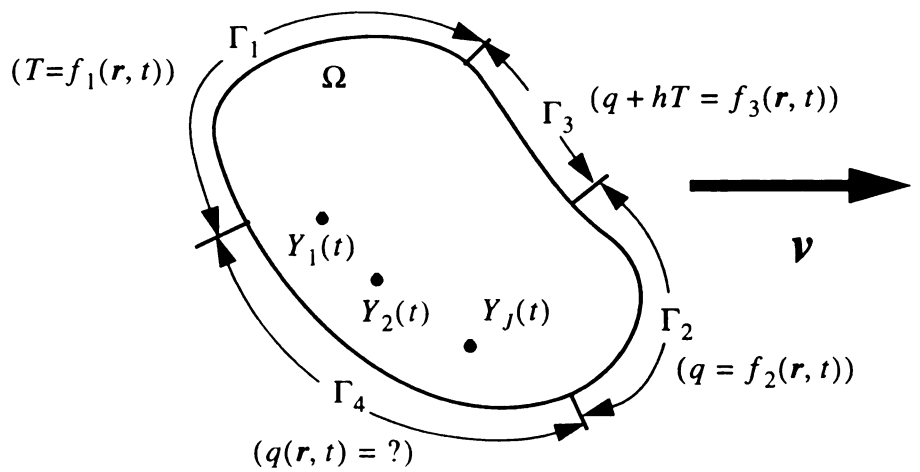

Figure 4-1 Schematic of multi-dimensional general IHCP

$$-k(\boldsymbol{r})\frac{\partial}{\partial \hat{\boldsymbol{n}}}T(\boldsymbol{r}, t) = q(\boldsymbol{r}, t), \quad \begin{matrix}(\boldsymbol{r}) \text{ on } \Gamma_4 \\ (t_0 < t \le t_f)\end{matrix} \tag{4-2.2b}$$

$$T(\boldsymbol{r}, t_0) = T_o(\underline{r}) \tag{4-2.2c}$$

where $k(\boldsymbol{r})$ and $\rho C(\boldsymbol{r})$ are the thermal conductivity and volumetric heat capacity. The spatial domain Ω is moving at a constant velocity of $\boldsymbol{v}$ and the symbols Γ_i $(i = 1, 2, 3, 4)$ representing the domain boundaries. The outward pointing normal vector is denoted $\hat{\boldsymbol{n}}$. Functions $f_1(\boldsymbol{r}, t)$, $f_2(\boldsymbol{r}, t)$, $f_3(\boldsymbol{r}, t)$, and $T_o(\boldsymbol{r})$ are assumed known. Boundary coefficients k_i and h_i are specified to form different boundary conditions, i.e. $k_1 = 0$ and $h_1 = 1$ specifies a temperature boundary condition (first kind), $k_2 = k(\boldsymbol{r})$ and $h_2 = 0$ a flux condition (second) kind, and $k_3 = k(\boldsymbol{r})$ and $h_3 = h(\boldsymbol{r})$ a convective condition (third kind). Surface Γ_4 has the unknown heat flux, $q(\boldsymbol{r}, t)$, to estimate. Excess information of transient temperature measurements exists within the body (or at the surface of the body) at locations $(\boldsymbol{r} = \boldsymbol{d}_j)$ $j = 1, \ldots\ldots J$. These measured temperatures are denoted

$$Y(\boldsymbol{d}_j, t_k) = Y_j(t_k) \tag{4-2.3}$$

and are available at discrete times t_k, $0 < t_k \le t_f$, $k = 1, 2 \ldots, N$. The analysis is first developed for measurements being at discrete locations but continuous on time.

The objective is to estimate $q(\boldsymbol{r}, t)$ using the measured temperatures. Hence, the heat flux $q(\boldsymbol{r}, t)$ is estimated such that the calculated temperatures match the measured temperatures, $T(\boldsymbol{d}_j, t_k; q) = Y_j(t_k)$, where $T(\boldsymbol{d}_j, t_k; q)$ is the solution of equation (4-2.1) and

(4-2.2). Due to the ill-conditioned nature of this problem, the matching is accomplished in a least squares sense by minimizing the function

$$J(q) = \underbrace{\frac{1}{2}\sum_{j=1}^{J}\int_{t_0}^{t_f}[T(\boldsymbol{d}_j, t, ;q) - Y_j(t)]^2 dt}_{J_S} + \underbrace{\frac{1}{2}\alpha_T\int_{t_0}^{t_f}\int_{\Gamma_4}[q(\boldsymbol{r}, t) - q_{pri}(\boldsymbol{r}, t)]^2 d\boldsymbol{r}\, dt}_{J_R} \tag{4-2.4}$$

The last term in equation (4-2.4), J_R, serves as regularization to stabilize the ill-conditioned problem; the function $q_{pri}(s, t)$ is known and could be zero. Regularization of this form is similar to zeroth order Tikhonov regularization (Tikhonov and Arsenin, 1977).

Schemes to minimize $J(q)$ in equation (4-2.4), which use iterative methods such as steepest descent and conjugate gradient, require the gradient of $J(q)$. Methods to compute this gradient depend on the function space where $q(\boldsymbol{r}, t)$ is assumed to reside. Two possibilities are a *finite dimensional* space and an *infinite dimensional* space. For the infinite dimensional problem *a priori* information is not required concerning the (unknown) function $q(\boldsymbol{r}, t)$. However, computation of the gradient requires solving two additional problems, which are the adjoint and sensitivity problems. For the special case when *a priori* information is available (or assumed) concerning the function, the problem is considered finite dimensional and standard differential calculus is used to compute the gradient.

The approach considered here is the more general infinite dimensional problem. The heat flux is assumed to be in the function space E on $\Gamma_4 \times (t_0, t_f)$ with the scalar product defined by

$$\langle Z_1, Z_2\rangle_E = \int_{t_0}^{t_f}\int_{\Gamma_4} Z_1(\boldsymbol{r}, t) Z_2(\boldsymbol{r}, t) d\boldsymbol{r}\, dt \tag{4-2.5}$$

for functions $Z_1(\boldsymbol{r}, t)$ and $Z_2(\boldsymbol{r}, t)$. The associated norm or function $Z(\boldsymbol{r}, t)$ is

$$\|Z\|_E^2 = \int_{t_0}^{t_f} \int_{\Gamma_4} |Z(\boldsymbol{r}, t)|^2 d\boldsymbol{r}\, dt \tag{4-2.6}$$

One possible choice for the function space is $E = L_2$, all square integrable functions on $\Gamma_4 \times (0, t_f)$. The finite dimensional problem, i.e. $E = R^n$, is discussed in section 4-8.0.

4-3.0 Gradient Calculation

The gradient of the function $J(q)$ in equation (4-2.4) is required for gradient search methods. In all derivations that follow it is assumed that the function $J(q)$ is given by equation (4-2.4). This is an important point because $J(q)$ is quadratic, since temperature is a linear function of the heat flux q. Application of the methods for non-linear problems is discussed in Artyukhin (1996) and Loulou et al. (1996). Because a functional heat flux is assumed, $(q \in E)$, the mathematics are more complex. The gradient of $J(q)$ at q, denoted $\nabla J(q)$, is related to the variation of J at this point by the general relationship

$$J(q + \Delta q) - J(q) = \langle \nabla J(q), \Delta q \rangle_E + (\text{terms nonlinear in } \|\Delta q\|_E) \tag{4-3.1}$$

Although more mathematics are required to correctly interpret this gradient, it is analogous to the generalization of a Taylor series expansion in standard differential calculus.

For the function $J(q)$, the Gateaux differential with increment Δq, henceforth referred to as the directional derivative at q in the direction Δq, denoted $D_{\Delta q} J(q)$, is defined as (Luenberger, 1973)

$$D_{\Delta q} J(q) = \lim_{\mu \to 0} \frac{J(q + \mu \Delta q) - J(q)}{\mu} \tag{4-3.2}$$

The directional derivative $D_{\Delta q} J(q)$ is therefore related to the gradient

$$D_{\Delta q}J(q) = \langle \nabla J(q), \Delta q \rangle_E \tag{4-3.3}$$

The directional derivative is computed using equation (4-3.2); however, identifying the gradient requires the derivation of two additional problems, typically called the sensitivity and adjoint problems.

To compute the directional derivative of $J(q)$ the limit in equation (4-3.2) is evaluated

$$J(q+\mu\Delta q) - J(q) =$$

$$\frac{1}{2}\sum_{j=1}^{J}\int_{t_0}^{t_f}[T(\boldsymbol{d}_j, t;q+\mu\Delta q) - Y_j(t)]^2 dt + \frac{1}{2}\alpha_T\int_{t_0}^{t_f}\int_{\Gamma_4}[q(\boldsymbol{r}, t) + \mu\Delta q(\boldsymbol{r}, t) - q_{pri}(\boldsymbol{r}, t)]^2 d\boldsymbol{r}\, dt$$

$$-\frac{1}{2}\sum_{j=1}^{J}\int_{t_0}^{t_f}[T(\boldsymbol{d}_j, t, ;q) - Y_j(t)]^2 dt - \frac{1}{2}\alpha_T\int_{t_0}^{t_f}\int_{\Gamma_4}[q(\boldsymbol{r}, t) - q_{pri}(\boldsymbol{r}, t)]^2 d\boldsymbol{r}\, dt \tag{4-3.4}$$

After expanding the terms, dividing by μ, and some manipulation, equation (4-3.4) is rearranged as

$$\frac{J(q+\mu\Delta q) - J(q)}{\mu} =$$

$$\frac{1}{2}\sum_{j=1}^{J}\int_{t_0}^{t_f}\left\{[T(\boldsymbol{d}_j, t;q+\mu\Delta q) + T(\boldsymbol{d}_j, t;q) - 2Y_j(t)]\frac{[T(\boldsymbol{d}_j, t;q+\mu\Delta q) - T(\boldsymbol{d}_j, q)]}{\mu}\right\}dt$$

$$+\frac{1}{2}\alpha_T\int_{t_0}^{t_f}\int_{\Gamma_4}\frac{\{2[q(\boldsymbol{r}, t) - q_{pri}(\boldsymbol{r}, t)]\mu\Delta q(\boldsymbol{r}, t) + [\mu\Delta q(\boldsymbol{r}, t)]^2\}}{\mu}d\boldsymbol{r}\, dt \tag{4-3.5}$$

The resulting change in the temperature caused by a variation of magnitude $\mu\Delta q$ in the heat flux is related to the directional derivative of the temperature. The directional derivative of T at q in the direction Δq, evaluated at $(\boldsymbol{r}, t)$ is

$$D_{\Delta q}T(\boldsymbol{r}, t;q) = \lim_{\mu \to 0}\frac{T(\boldsymbol{r}, t;q+\mu\Delta q) - T(\boldsymbol{r}, t;q)}{\mu} \tag{4-3.6}$$

Taking the limit of equation (4-3.5) as $\mu \to 0$ while using the definition of the directional derivative of temperature in equation (4-3.6) gives

$$D_{\Delta q}J(q) = \sum_{j=1}^{J}\int_{t_0}^{t_f}[T(\boldsymbol{d}_j, t;q) - Y_j(t)]D_{\Delta q}T(\boldsymbol{d}_j, t;q)dt$$

$$+ \alpha_T\int_{t_0}^{t_f}\int_{\Gamma_4}[q(\boldsymbol{r}, t) - q_{pri}(\boldsymbol{r}, t)]\Delta q(\boldsymbol{r}, t)d\boldsymbol{r}\, dt \quad (4\text{-}3.7)$$

where the left side of equation follows from the definition in equation (4-3.2). This equation shows that the directional derivative of the $J(q)$ is a function of the directional derivative of the temperature $D_{\Delta q}T(\boldsymbol{d}_j, t;q)$. The directional derivative of temperature, i.e., the variation in temperature due to a variation in the heat flux, is typically referred to as the sensitivity function and defined as

$$\theta(\boldsymbol{r}, t;\Delta q) \equiv D_{\Delta q}T(\boldsymbol{r}, t;q) \quad (4\text{-}3.8)$$

The sensitivity function $\theta(\boldsymbol{r}, t;\Delta q)$ represents the variation in temperature $T(\boldsymbol{r}, t;q)$ due to the presence of an input heat flux function Δq.

4-4.0 Sensitivity Equations

The describing problem for the sensitivity function is derived from the definition of the directional derivative in equation (4-3.6). Evaluating the direct problem in equation (4-2.1 and 4-2.2) at $q + \mu\Delta q$ gives

$$\nabla \cdot (k(\boldsymbol{r})\nabla T(\boldsymbol{r}, t;q + \mu\Delta q))$$

$$= \rho C(\boldsymbol{r})\left[\frac{\partial}{\partial t}T(\boldsymbol{r}, t;q + \mu\Delta q) + \boldsymbol{v} \cdot \nabla T(\boldsymbol{r}, t;q + \mu\Delta q)\right], \quad \begin{matrix}(\boldsymbol{r}) \text{ in } \Omega \\ (t_0 < t \le t_f)\end{matrix} \quad (4\text{-}3.9)$$

$$-k_i \frac{\partial}{\partial \hat{\boldsymbol{n}}}T(\boldsymbol{r}, t;q + \mu\Delta q) + h_i\, T(\boldsymbol{r}, t;q + \mu\Delta q) = f_i(\boldsymbol{r}, t), \quad \begin{matrix}(\boldsymbol{r}) \text{ on } \Gamma_i, (i = 1, 2, 3) \\ (t_0 < t \le t_f)\end{matrix} \quad (4\text{-}3.10a)$$

$$-k(\boldsymbol{r})\frac{\partial}{\partial \hat{\boldsymbol{n}}}T(\boldsymbol{r}, t;q + \mu\Delta q) = q(\boldsymbol{r}, t) + \mu\Delta q(\boldsymbol{r}, t), \quad \begin{matrix}(\boldsymbol{r}) \text{ on } \Gamma_4 \\ (t_0 < t \le t_f)\end{matrix} \quad (4\text{-}3.10b)$$

$$T(\boldsymbol{r}, 0;q+\mu\Delta q) = T_o(\boldsymbol{r}),\ (\boldsymbol{r}) \text{ in } \Omega \tag{4-3.10c}$$

Defining $T_\mu = T(\boldsymbol{r}, t;q+\mu\Delta q)$ in equation (4-3.9) and (4-3.10), subtracting the direct problem in equation (4-2.1) and (4-2.2) with $T = T(\boldsymbol{r}, t;q)$, and dividing the result by μ gives

$$\nabla\cdot\left(k(\boldsymbol{r})\nabla\left(\frac{T_\mu - T}{\mu}\right)\right) = \rho C(\boldsymbol{r})\left[\frac{\partial}{\partial t}\left(\frac{T_\mu - T}{\mu}\right) + \underline{v}\cdot\nabla\left(\frac{T_\mu - T}{\mu}\right)\right] \quad , \quad \begin{matrix}(\boldsymbol{r}) \text{ in } \Omega \\ (t_0 < t \le t_f)\end{matrix} \tag{4-3.11}$$

$$-k_i\frac{\partial}{\partial\hat{\boldsymbol{n}}}\left(\frac{T_\mu - T}{\mu}\right) + h_i\left(\frac{T_\mu - T}{\mu}\right) = 0\,, \quad \begin{matrix}(\boldsymbol{r}) \text{ on } \Gamma_i,\ (i=1,\,2,\,3) \\ (t_0 < t \le t_f)\end{matrix} \tag{4-3.12a}$$

$$-k(\boldsymbol{r})\frac{\partial}{\partial\hat{\boldsymbol{n}}}\left(\frac{T_\mu - T}{\mu}\right) = \Delta q(\boldsymbol{r}, t)\,, \quad \begin{matrix}(\boldsymbol{r}) \text{ on } \Gamma_4 \\ (t_0 < t \le t_f)\end{matrix} \tag{4-3.12b}$$

$$\left(\frac{T_\mu - T}{\mu}\right)\Big|_{t=0} = 0\,,\ (\boldsymbol{r}) \text{ in } \Omega \tag{4-3.12c}$$

Taking the limit as $\mu \to 0$ of equation (4-3.11) and (4-3.12) while using the definition in equation (4-3.6) and the definition of the sensitivity function $\theta(\boldsymbol{r}, t;\Delta q) \equiv D_{\Delta q}T(\boldsymbol{r}, t;q)$, the describing problem for sensitivity function is

$$\nabla\cdot(k(\boldsymbol{r})\nabla\theta(\boldsymbol{r}, t)) = \rho C(\underline{r})\left[\frac{\partial}{\partial t}\theta(\boldsymbol{r}, t) + \boldsymbol{v}\cdot\nabla\theta(\boldsymbol{r}, t)\right], \quad \begin{matrix}(\boldsymbol{r}) \text{ in } \Omega \\ (t_0 < t \le t_f)\end{matrix} \tag{4-3.13}$$

$$-k_i\frac{\partial\theta(\boldsymbol{r}, t)}{\partial\hat{\boldsymbol{n}}} + h_i\,\theta(\boldsymbol{r}, t) = 0\,, \quad \begin{matrix}(\boldsymbol{r}) \text{ on } \Gamma_i,\ (i=1,\,2,\,3) \\ (t_0 < t \le t_f)\end{matrix} \tag{4-3.14a}$$

$$-k(\boldsymbol{r})\frac{\partial}{\partial\hat{\boldsymbol{n}}}\theta(\boldsymbol{r}, t) = \Delta q(\boldsymbol{r}, t)\,, \quad \begin{matrix}(\boldsymbol{r}) \text{ on } \Gamma_4 \\ (t_0 < t \le t_f)\end{matrix} \tag{4-3.14b}$$

$$\theta(\boldsymbol{r}, 0) = 0\,,\ (\boldsymbol{r}) \text{ in } \Omega \tag{4-3.14c}$$

The describing equations for the sensitivity function have a similar form to the equations derived for direct problem. The differential equation and boundary conditions have the identical form. Differences between the direct and sensitivity problems are that the sensitivity problem has homogeneous known boundary conditions, equation (4-3.14a), it has a zero initial condition equation (4-3.14c), and its driving term is the variation in the heat flux $\Delta q(\boldsymbol{r}, t)$ on surface Γ_4, equation (4-3.14b). Similarities in the form of the two problems (direct and sensitivity) allow for savings in the calculations required for the numerical solution of these two problems. It is shown in the subsequent section that the describing equations for the adjoint function have a similar form.

4-5.0 Adjoint Equations

To obtain the derivative, $\nabla J(q)$, an adjoint problem is derived which will allow the directional derivative to be written as the scalar product

$$D_{\Delta q} J(q) = \langle \nabla J, \Delta q \rangle_E \tag{4-4.1}$$

The current expression for $D_{\Delta q} J(q)$ in equation (4-3.7) is not separable into a scalar product that contains Δq, i.e., $\langle \text{function}, \Delta q \rangle_E$ where terms that comprise "function" would then be the gradient. Hence by developing an adjoint problem the directional derivative is written as a scalar product and the gradient is identified.

To derive such an adjoint problem the method of Lagrange multipliers is used. As posed, the problem is to determine a solution $q^*(\boldsymbol{r}, t)$ that minimize $J(q)$, subject to $q^*(\boldsymbol{r}, t)$ satisfying the direct problem, equation (4-2.1) and (4-2.2). Equations (4-2.1) and (4-2.2) are rewritten such that $A[T(\boldsymbol{r}, t;q)] = 0$, where A is an appropriate operator. A

necessary condition for $q^*(\boldsymbol{r}, t)$ to satisfy these conditions is that there exist Lagrange multipliers, $\lambda(\boldsymbol{r}, t)$, such that the Lagrangian function

$$\Lambda(\lambda, T, q) = J(T, q) + \int_t \int_{\Omega} \lambda(\boldsymbol{r}, t) A[T(\boldsymbol{r}, t; q)] d\boldsymbol{r}\, dt \tag{4-4.2}$$

is stationary at the solution, $q^*(\boldsymbol{r}, t)$. This implies that the directional derivative of $\Lambda(\lambda, T, q)$ is zero at $q^*(\boldsymbol{r}, t)$. (In equation (4-4.2), the integrations must be interpreted in the correct sense for the boundary conditions associated with operator A.)

Using Lagrange multipliers permits the temperature $T(\boldsymbol{r}, t; q)$ to be considered independent of the heat flux, $q(\boldsymbol{r}, t)$. This is possible because the interaction between the temperature and heat flux is forced in the constraint, eliminating the need to consider the temperature as a function of q.

Define a Lagrangian function which includes the criterion $J(q)$ and Lagrange multipliers $(\psi, \eta_i, \lambda_o)$ associated with the imposed constraints that the heat flux must satisfy the direct problem gives

$$\begin{aligned}\Lambda(\psi, \eta_i, \lambda_o, T, q) = J(T, q) &+ \int_{t_0}^{t_f} \int_{\Omega} \psi(\boldsymbol{r}, t) \left\{ \nabla \cdot (k(\boldsymbol{r}) \nabla T) - \rho C(\boldsymbol{r}) \left[\frac{\partial T}{\partial t} + \boldsymbol{v} \cdot \nabla T \right] \right\} d\boldsymbol{r}\, dt \\ &+ \sum_{i=1}^{3} \int_{t_0}^{t_f} \int_{\Gamma_i} \eta_i(\boldsymbol{r}, t) \left(k_i \frac{\partial T}{\partial \hat{\boldsymbol{n}}} - h_i T + f_i(\boldsymbol{r}, t) \right) d\boldsymbol{r}\, dt \\ &+ \int_{t_0}^{t_f} \int_{\Gamma_4} \eta_4(\boldsymbol{r}, t) \left(k(\boldsymbol{r}) \frac{\partial T}{\partial \hat{\boldsymbol{n}}} + q(\boldsymbol{r}, t) \right) d\boldsymbol{r}\, dt + \int_{\Omega} \lambda_o(\boldsymbol{r}) [T(\boldsymbol{r}, 0) - T_o(\boldsymbol{r})]\, d\boldsymbol{r}\end{aligned} \tag{4-4.3}$$

Applying Green's theorem and integrating by parts on time, the first integral in equation (4-4.3) can be rewritten as

$$\int_{t_0}^{t_f}\int_{\Omega}\psi(\boldsymbol{r},t)\left\{\nabla\cdot(k(\boldsymbol{r})\nabla T)-\rho C(\boldsymbol{r})\left[\frac{\partial T}{\partial t}+\boldsymbol{v}\cdot\nabla T\right]\right\}d\boldsymbol{r}\,dt =$$

$$\int_{t_0}^{t_f}\int_{\Omega}\left\{\nabla\cdot(k(\boldsymbol{r})\nabla\psi)+\left[\rho C(\boldsymbol{r})\frac{\partial\psi}{\partial t}+\boldsymbol{v}\cdot\nabla[\rho C(\boldsymbol{r})\psi]\right]\right\}T\,d\boldsymbol{r}\,dt$$

$$+\int_{t_0}^{t_f}\int_{\Gamma}\left[\psi k(\boldsymbol{r})\frac{\partial T}{\partial\hat{\boldsymbol{n}}}-k(\boldsymbol{r})T\frac{\partial\psi}{\partial\hat{\boldsymbol{n}}}\right]d\boldsymbol{r}\,dt-\int_{t_0}^{t_f}\int_{\Gamma}\rho C(\boldsymbol{r})\psi T[\boldsymbol{v}\cdot\hat{\boldsymbol{n}}]d\boldsymbol{r}\,dt$$

$$-\int_{\Omega}\rho C(\psi T)\Big|_{t=t_0}^{t_f}d\boldsymbol{r} \quad (4\text{-}4.4)$$

where $\Gamma = \Gamma_1 \cup \Gamma_2 \cup \Gamma_3 \cup \Gamma_4$. Substituting this integral into the Lagrangian in equation (4-4.3) gives

$$\Lambda(\psi,\eta_i,\lambda_o,T,q) = J(T,q)+\int_{t_0}^{t_f}\int_{\Omega}\left\{\nabla\cdot(k(\boldsymbol{r})\nabla\psi)+\rho C(\boldsymbol{r})\frac{\partial\psi}{\partial t}+\boldsymbol{v}\cdot\nabla[\rho C(\boldsymbol{r})\psi]\right\}T\,d\boldsymbol{r}\,dt$$

$$+\int_{t_0}^{t_f}\int_{\Gamma}\left[\psi k(\boldsymbol{r})\frac{\partial T}{\partial\hat{\boldsymbol{n}}}-k(\boldsymbol{r})T\frac{\partial\psi}{\partial\hat{\boldsymbol{n}}}\right]d\boldsymbol{r}\,dt-\int_{t_0}^{t_f}\int_{\Gamma}\rho C(\boldsymbol{r})\psi T(\boldsymbol{v}\cdot\hat{\boldsymbol{n}})d\boldsymbol{r}\,dt-\int_{\Omega}\rho C(\psi T)\Big|_{t=t_0}^{t_f}d\boldsymbol{r}$$

$$+\sum_{i=1}^{3}\int_{t_0}^{t_f}\int_{\Gamma_i}\eta_i(\boldsymbol{r},t)\left[k_i\frac{\partial T}{\partial\hat{\boldsymbol{n}}}-h_i\,T+f_i(\boldsymbol{r},t)\right]d\boldsymbol{r}\,dt+\int_{t_0}^{t_f}\int_{\Gamma_4}\eta_4(\boldsymbol{r},t)\left[k(\boldsymbol{r})\frac{\partial T}{\partial\hat{\boldsymbol{n}}}+q(\boldsymbol{r},t)\right]d\boldsymbol{r}\,dt$$

$$+\int_{\Omega}\lambda_o(\boldsymbol{r})[T(\boldsymbol{r},0)-T_o(\boldsymbol{r})]\,d\boldsymbol{r} \quad (4\text{-}4.5)$$

The Lagrangian has now been rewritten such that the differential operators in the first integral apply to the Lagrange multiplier ψ, instead of temperature T. The directional derivative of the Lagrangian function Λ, for fixed multipliers, is

$$\delta\Lambda(\psi,\eta_i,\lambda_o,T,q) = D_{\Delta T}\Lambda(\psi,\eta_i,\lambda_o,T,q)+D_{\Delta q}\Lambda(\psi,\eta_i,\lambda_o,T,q) \quad (4\text{-}4.6)$$

where $D_{\Delta T}\Lambda(\psi,\eta_i,\lambda_o,T,q)$ is the directional derivative at T in the direction ΔT evaluated at $(\psi,\eta_i,\lambda_o,q)$ and $D_{\Delta q}\Lambda(\psi,\eta_i,\lambda_o,T,q)$ is the directional derivative at q in the direction Δq evaluated at $(\psi,\eta_i,\lambda_o,T)$. An analogous expression, similar to equation (4-4.6), can be written for the directional derivative of $J(T,q)$. These directional

derivatives can be obtained by using a similar methodology to that given in equation (4-3.2).

The directional derivative of the Lagrangian criterion for fixed multipliers is

$$\delta\Lambda(\psi, \eta_i, \lambda_o, T, q) = \delta J(T, q) + \int_{t_0}^{t_f}\int_{\Omega}\left\{\nabla\cdot(k(\boldsymbol{r})\nabla\psi) + \rho C(\boldsymbol{r})\frac{\partial\psi}{\partial t} + \boldsymbol{v}\cdot\nabla[\rho C(\boldsymbol{r})\psi]\right\}\Delta T\, d\boldsymbol{r}\, dt$$

$$+\int_{t_0}^{t_f}\int_{\Gamma}\left[\psi k(\boldsymbol{r})\frac{\partial}{\partial\hat{\boldsymbol{n}}}\Delta T - k(\boldsymbol{r})\Delta T\frac{\partial\psi}{\partial\hat{\boldsymbol{n}}}\right]d\boldsymbol{r}\, dt - \int_{t_0}^{t_f}\int_{\Gamma}\rho C(\boldsymbol{r})\psi\Delta T(\boldsymbol{v}\cdot\hat{\boldsymbol{n}})d\boldsymbol{r}\, dt - \int_{\Omega}\rho C(\psi\Delta T)\Big|_{t=t_0}^{t_f} d\boldsymbol{r}$$

$$+\sum_{i=1}^{3}\int_{t_0}^{t_f}\int_{\Gamma_i}\eta_i(\boldsymbol{r}, t)\left[k_i\frac{\partial}{\partial\hat{\boldsymbol{n}}}\Delta T + -h_i\Delta T_i\right]d\boldsymbol{r}\, dt + \int_{t_0}^{t_f}\int_{\Gamma_4}\eta_4(\boldsymbol{r}, t)\left[k(\boldsymbol{r})\frac{\partial}{\partial\hat{\boldsymbol{n}}}\Delta T + \Delta q(\boldsymbol{r}, t)\right]d\boldsymbol{r}\, dt$$

$$+\int_{\Omega}\lambda_o(\boldsymbol{r})[\Delta T(\boldsymbol{r}, 0)]\, d\boldsymbol{r} \quad (4\text{-}4.7)$$

The solution of interest is for the case that the temperature satisfies the direct problem, i.e., $T = T(q)$. Hence, for this case $\Delta T \equiv \theta$ in equation (4-4.7), therefore the boundary conditions on sensitivity problem, equation (4-3.11) and (4-3.12), can be used to simplify this equation. Introducing the boundary and initial conditions from the sensitivity problem, the Lagrangian criterion in equation (4-4.7) simplifies to

$$\delta\Lambda(\psi, T(q), q) = \delta J(T(q), q) + \int_{t_0}^{t_f}\int_{\Omega}\left\{\nabla\cdot(k(\boldsymbol{r})\nabla\psi) + \rho C(\boldsymbol{r})\frac{\partial\psi}{\partial t} + \boldsymbol{v}\cdot\nabla[\rho C(\boldsymbol{r})\psi]\right\}\theta\, d\boldsymbol{r}\, dt$$

$$\sum_{i=1}^{3} I_{BC_i} - \int_{t_0}^{t_f}\int_{\Gamma_4}\left\{\psi\Delta q(\boldsymbol{r}, t) + \left[k(\underline{s})\frac{\partial\psi}{\partial\hat{\boldsymbol{n}}} + \rho C(\boldsymbol{r})(\boldsymbol{v}\cdot\hat{\boldsymbol{n}})\psi\right]\theta\right\} d\boldsymbol{r}\, dt$$

$$-\int_{\Omega}\rho C(\boldsymbol{r})(\psi\theta)\Big|_{t=t_f} d\boldsymbol{r} \quad (4\text{-}4.8)$$

where,

$$(i = 1)\quad I_{BC_1} = \int_{t_0}^{t_f}\int_{\Gamma_1}\left[k(\boldsymbol{r})\frac{\partial\theta}{\partial\hat{\boldsymbol{n}}} - \rho C(\boldsymbol{r})(\boldsymbol{v}\cdot\hat{\boldsymbol{n}})\theta\right]\psi d\boldsymbol{r}\, dt \quad (4\text{-}4.9)$$

$$(i \neq 1) \quad I_{BC_i} = \int_{t_0}^{t_f} \int_{\Gamma_i} \left[-k(\boldsymbol{r}) \frac{\partial \psi}{\partial \hat{\boldsymbol{n}}} + [h_i - \rho C(\boldsymbol{r})(\boldsymbol{v} \cdot \hat{\boldsymbol{n}})] \psi \right] \theta \, d\boldsymbol{r} \, dt \tag{4-4.10}$$

Notice that the criterion is no longer a function of the multipliers η_i and λ_o since the terms for these multipliers are zero from the boundary conditions on the sensitivity problem. It can be shown that

$$\delta J(T(q), q) = D_{\Delta q} J(q) \tag{4-4.11}$$

Defining the residual for the difference between the measured and calculated temperatures ($e_j(t) = Y_j(t) - T(\boldsymbol{d}_j, t, q)$) in the directional derivative $D_{\Delta q} J(q)$, equation (4-3.7), the directional derivative of the Lagrangian is

$$\begin{aligned}
&\delta \Lambda(\psi, T(q), q) = \\
&- \sum_{j=1}^{J} \int_{t_0}^{t_f} \int_{\Omega} [e_j(t) \delta(\boldsymbol{r} - \boldsymbol{d}_j)] \theta \, dV \, dt + \alpha_T \int_{t_0}^{t_f} \int_{\Gamma_4} [q(\boldsymbol{r}, t) - q_{pri}(\boldsymbol{r}, t)] \Delta q(\boldsymbol{r}, t) \, d\boldsymbol{r} \, dt \\
&\qquad + \int_{t_0}^{t_f} \int_{\Omega} \left\{ \nabla \cdot (k(\boldsymbol{r}) \nabla \psi) + \rho C(\boldsymbol{r}) \frac{\partial \psi}{\partial t} + \boldsymbol{v} \cdot \nabla [\rho C(\boldsymbol{r}) \psi] \right\} \theta \, d\boldsymbol{r} \, dt \\
&\qquad + \sum_{i=1}^{3} I_{BC_i} - \int_{t_0}^{t_f} \int_{\Gamma_4} \left\{ \psi \Delta q(\boldsymbol{r}, t) + \left[k(\boldsymbol{r}) \frac{\partial \psi}{\partial \hat{\boldsymbol{n}}} + \rho C(\boldsymbol{r})(\boldsymbol{v} \cdot \hat{\boldsymbol{n}}) \psi \right] \theta \right\} d\boldsymbol{r} \, dt \\
&\qquad\qquad - \int_{\Omega} \rho C(\boldsymbol{r})(\psi \theta) \big|_{t = t_f} \, d\boldsymbol{r}
\end{aligned} \tag{4-4.12}$$

Rearranging the terms in equation (4-4.12) to group similar integrals gives

$$\begin{aligned}
&\delta \Lambda(\psi, T(q), q) = \\
&\int_{t_0}^{t_f} \int_{\Omega} \left\{ \nabla \cdot (k(\boldsymbol{r}) \nabla \psi) + \rho C(\boldsymbol{r}) \frac{\partial \psi}{\partial t} + \boldsymbol{v} \cdot \nabla [\rho C(\boldsymbol{r}) \psi] - \sum_{j=1}^{J} e_j(t) \delta(\boldsymbol{r} - \boldsymbol{d}_j) \right\} \theta \, d\boldsymbol{r} \, dt \\
&\qquad + \alpha_T \int_{t_0}^{t_f} \int_{\Gamma_4} [q(\boldsymbol{r}, t) - q_{pri}(\boldsymbol{r}, t)] \Delta q(\boldsymbol{r}, t) \, d\boldsymbol{r} \, dt \\
&\qquad + \sum_{i=1}^{3} I_{BC_i} - \int_{t_0}^{t_f} \int_{\Gamma_4} \left\{ \psi \Delta q(\boldsymbol{r}, t) + \left[k(\boldsymbol{r}) \frac{\partial \psi}{\partial \hat{\boldsymbol{n}}} + \rho C(\boldsymbol{r})(\boldsymbol{v} \cdot \hat{\boldsymbol{n}}) \psi \right] \theta \right\} d\boldsymbol{r} \, dt \\
&\qquad\qquad + \int_{\Omega} \rho C(\boldsymbol{r})(\psi \theta) \big|_{t = t_f} \, d\boldsymbol{r}
\end{aligned} \tag{4-4.13}$$

Fix the Lagrange multiplier, $\psi(\boldsymbol{r}, t)$, as follows:

$$\nabla \cdot [k(\boldsymbol{r})\nabla\psi] + \rho C(\boldsymbol{r})\frac{\partial\psi}{\partial t} + \boldsymbol{v} \cdot \nabla[\rho C(\boldsymbol{r})\psi] - \sum_{j=1}^{J} e_j(t)\delta(\boldsymbol{r} - \boldsymbol{d}_j) = 0, \quad \begin{matrix}(\boldsymbol{r}) \text{ in } \Omega \\ (t_0 < t \le t_f)\end{matrix} \tag{4-4.14}$$

$$-k_i \frac{\partial}{\partial \hat{\boldsymbol{n}}}\psi(\boldsymbol{r}, t) + [h_i - \rho C(\boldsymbol{r})(\boldsymbol{v} \cdot \hat{\boldsymbol{n}})]\ \psi(\boldsymbol{r}, t) = 0, \quad \begin{matrix}(\boldsymbol{r}) \text{ on } \Gamma_i, (i = 1, 2, 3) \\ (t_0 < t \le t_f)\end{matrix} \tag{4-4.15a}$$

$$k(\boldsymbol{r})\frac{\partial}{\partial \hat{\boldsymbol{n}}}\psi(\boldsymbol{r}, t) + \rho C(\boldsymbol{r})(\boldsymbol{v} \cdot \hat{\boldsymbol{n}})\ \psi(\boldsymbol{r}, t) = 0, \quad \begin{matrix}(\boldsymbol{r}) \text{ on } \Gamma_4 \\ (t_0 < t \le t_f)\end{matrix} \tag{4-4.15b}$$

$$\psi(\boldsymbol{r}, t)\big|_{t = t_f} = 0, (\boldsymbol{r}) \text{ in } \Omega \tag{4-4.15c}$$

By defining the Lagrange multiplier as done in equation (4-4.14) and (4-4.15), the Lagrangian function in equation (4-4.13) reduces to

$$\delta\Lambda(\psi, T(q), q) = -\int_{t_0}^{t_f}\int_{\Gamma_4} \psi \Delta q(\boldsymbol{r}, t)\ d\boldsymbol{r}\ dt + \alpha_T \int_{t_0}^{t_f}\int_{\Gamma_4} [q(\boldsymbol{r}, t) - q_{pri}(\boldsymbol{r}, t)]\Delta q(\boldsymbol{r}, t) d\boldsymbol{r}\ dt \tag{4-4.16}$$

Instead of fixing the Lagrange multiplier as prescribed in equation (4-4.14) and (4-4.15), the negative of the Lagrange multiplier is calculated. Since the Lagrange multiplier is homogeneous except for the residual term, changing the sign of the residual term only changes the sign of the multiplier. Define the adjoint function as this Lagrange multiplier, with describing equations

$$\nabla \cdot [k(\boldsymbol{r})\nabla\psi] + \rho C(\boldsymbol{r})\frac{\partial\psi}{\partial t} + \boldsymbol{v} \cdot \nabla[\rho C(\boldsymbol{r})\psi] + \sum_{j=1}^{J} e_j(t)\delta(\boldsymbol{r} - \boldsymbol{d}_j) = 0, \quad \begin{matrix}(\boldsymbol{r}) \text{ in } \Omega \\ (t_0 < t \le t_f)\end{matrix} \tag{4-4.17}$$

$$-k_i \frac{\partial}{\partial \hat{n}} \psi(\boldsymbol{r}, t) + [h_i - \rho C(\boldsymbol{r})(\boldsymbol{v} \cdot \hat{\boldsymbol{n}})]\, \psi(\boldsymbol{r}, t) = 0, \quad \begin{matrix} (\boldsymbol{r}) \text{ on } \Gamma_i, (i = 1, 2, 3) \\ (t_0 < t \le t_f) \end{matrix} \tag{4-4.18a}$$

$$k(\boldsymbol{r}) \frac{\partial}{\partial \hat{n}} \psi(\boldsymbol{r}, t) + \rho C(\boldsymbol{r})(\boldsymbol{v} \cdot \hat{\boldsymbol{n}})\, \psi(\boldsymbol{r}, t) = 0, \quad \begin{matrix} (\boldsymbol{r}) \text{ on } \Gamma_4 \\ (t_0 < t \le t_f) \end{matrix} \tag{4-4.18b}$$

$$\psi(\boldsymbol{r}, t)\big|_{t = t_f} = 0, (\boldsymbol{r}) \text{ in } \Omega \tag{4-4.18c}$$

By defining the Lagrange multiplier in this manner, the directional derivative of the Lagrangian reduces to

$$\delta\Lambda(\psi, T(q), q) = \int_{t_0}^{t_f} \int_{\Gamma_4} \psi \Delta q(\boldsymbol{r}, t)\, d\boldsymbol{r}\, dt + \alpha_T \int_{t_0}^{t_f} \int_{\Gamma_4} [q(\boldsymbol{r}, t) - q_{pri}(\boldsymbol{r}, t)] \Delta q(\boldsymbol{r}, t) d\boldsymbol{r}\, dt \tag{4-4.19}$$

To determine the relationship between the directional derivative of the Lagrangian and the function J, consider that temperature T satisfies the equations given in equation (4-2.1) and (4-2.2), denoted $T(q)$, and the Lagrangian criterion simplifies to

$$\Lambda(\psi, T(q), q) = J(T(q), q) \tag{4-4.20}$$

This relationship is seen from equation (4-4.5) where all integral terms are zero for $T = T(q)$. Assuming fixed multipliers, the directional derivative of equation (4-4.20) is

$$\delta\Lambda(\psi, T(q), q) = \delta J(T(q), q) = D_{\Delta q} J(q) \tag{4-4.21}$$

Since equation (4-4.19) is also satisfied for $T(q)$, it can be rewritten using the result of equation (4-4.21) as

$$D_{\Delta q} J(q) = \int_{t_0}^{t_f} \int_{\Gamma_4} \psi(\boldsymbol{r}, t) \Delta q(\boldsymbol{r}, t) d\boldsymbol{r}\, dt + \alpha_T \int_{t_0}^{t_f} \int_{\Gamma_4} [q(\boldsymbol{r}, t) - q_{pri}(\boldsymbol{r}, t)] \Delta q(\boldsymbol{r}, t) d\boldsymbol{r}\, dt$$
$$= \langle \psi + \alpha_T (q - q_{pri}), \Delta q \rangle_E = \langle \nabla J, \Delta q \rangle_E \tag{4-4.22}$$

Finally, the equation is in the desired from to identify the gradient of J, which is obtained from equation (4-4.1)

$$\nabla J(\boldsymbol{r}, t, q) = \psi(\boldsymbol{r}, t) + \alpha_T[q(\boldsymbol{r}, t) - q_{pri}(\boldsymbol{r}, t)], (\boldsymbol{r}) \text{ on } \Gamma_4 \quad (4\text{-}4.23)$$

With the derivation of the gradient ∇J complete, the gradient search methods are discussed.

4-6.0 Optimization Method

The previous equations have presented the derivation for computing the gradient of function $J(q)$, which is minimized to determine the heat flux. Gradient search methods are applied to compute the unknown heat flux.

Methods of steepest descent and conjugate gradient are common approaches to compute the search direction. Steepest descent is quite inefficient and not recommended, but is simple and illustrative. Gradient search methods use iterative techniques to search for the minimum of an objective function. Beginning with an initial guess q^0 for the heat flux, at subsequent iterations the heat flux is

$$q^{n+1}(\boldsymbol{r}, t) = q^n(\boldsymbol{r}, t) + \Delta q(\boldsymbol{r}, t), (\boldsymbol{r}) \text{ on } \Gamma_4 \quad (4\text{-}5.1)$$

The correction to the heat flux is

$$\Delta q(\boldsymbol{r}, t) = -\rho^n p^n(\boldsymbol{r}, t), (\boldsymbol{r}) \text{ on } \Gamma_4 \quad (4\text{-}5.2)$$

where p^n is the search direction and ρ^n is a scalar step size. For the steepest descent method the search direction is

$$p^n(\boldsymbol{r}, t) = \nabla J(\boldsymbol{r}, t, q^n) \quad (4\text{-}5.3)$$

(It is actually the negative of the gradient, but the negative sign is incorporated in equation (4-5.2).) The conjugate gradient method, which typically converges more quickly, computes the search direction as follows (Arora, 1989)

$$p^n = \nabla J(\boldsymbol{r}, t, q^n) + \beta^n p^{n-1}(\boldsymbol{r}, t), \ (n \neq 0) \quad (4\text{-}5.3a)$$

$$p^0 = \nabla J(\boldsymbol{r}, t, q^0), n = 0 \tag{4-5.4b}$$

where,

$$\beta^n = \frac{\int_{t_0}^{t_f}\int_{\Gamma_4}\{\nabla J(\boldsymbol{r}, t, q^n)[\nabla J(\boldsymbol{r}, t, q^{n-1}) - \nabla J(\boldsymbol{r}, t, q^n)]\}d\boldsymbol{r}\, dt}{\int_{t_0}^{t_f}\int_{\Gamma_4}[\nabla J(\boldsymbol{r}, t, q^{n-1})]^2 d\boldsymbol{r}\, dt}$$

$$= \frac{\langle \nabla J(q^n), \nabla J(q^{n-1}) - \nabla J(q^n)\rangle_E}{\|\nabla J(q^{n-1})\|_E^2} \tag{4-5.5}$$

Procedures to calculated the gradient $\nabla J(\boldsymbol{r}, t, q^n)$ have been outlined previously. Computation of the step size ρ^n (a positive scalar) remains. The optimum step size is selected based on reducing $J(q)$ the greatest amount in the current search direction. Equivalently, the following function is minimized

$$\phi(\rho) = J(q^n - \rho^n p^n) \tag{4-5.6}$$

for $(\rho^n \geq 0)$. The optimal step size, denoted $\hat{\rho}^n$, satisfies

$$\left.\frac{d\phi}{d\rho^n}\right|_{\rho^n = \hat{\rho}^n} = \left.\frac{d}{d\rho^n}J(q^n - \rho^n p^n)\right|_{\rho^n = \hat{\rho}^n} = 0 \tag{4-5.7}$$

The sensitivity problem, which calculates the changes in temperature due to a variation of magnitude Δq in the heat flux, can be adapted to calculate the change in temperature due to a variation in heat flux of magnitude p^n. Then the calculated temperature, which is linear with respect to q^n, can be written as

$$T(\boldsymbol{r}, t, q^n - \rho^n p^n) = T(\boldsymbol{r}, t, q^n) - \rho^n \bar{\theta}(\boldsymbol{r}, t) \tag{4-5.8}$$

where $\bar{\theta}$ is the adapted sensitivity function computed from the problem

$$\nabla \cdot (k(\boldsymbol{r})\nabla\bar{\theta}(\boldsymbol{r}, t)) = \rho C(\boldsymbol{r})\left[\frac{\partial}{\partial t}\bar{\theta}(\boldsymbol{r}, t) + \boldsymbol{v} \cdot \nabla\bar{\theta}(\boldsymbol{r}, t)\right], \quad \begin{matrix}(\boldsymbol{r}) \text{ in } \Omega \\ (t_0 < t \leq t_f)\end{matrix} \tag{4-5.9}$$

$$-k_i \frac{\partial}{\partial \hat{n}} \bar{\theta}(\boldsymbol{r}, t) + h_i \, \bar{\theta}(\boldsymbol{r}, t) = 0 \quad , \quad \begin{matrix} (\boldsymbol{r}) \text{ on } \Gamma_i, (i = 1, 2, 3) \\ (t_0 < t \le t_f) \end{matrix} \tag{4-5.10a}$$

$$-k(\boldsymbol{r}) \frac{\partial}{\partial \hat{n}} \bar{\theta}(\boldsymbol{r}, t) = p^n(\boldsymbol{r}, t) \, , \quad \begin{matrix} (\boldsymbol{r}) \text{ on } \Gamma_4 \\ (t_0 < t \le t_f) \end{matrix} \tag{4-5.10b}$$

$$\bar{\theta}(\boldsymbol{r}, 0) = 0, (\boldsymbol{r}) \text{ in } \Omega \tag{4-5.10c}$$

The adapted sensitivity problem differs from the original sensitivity problem in equation (4-3.13) and (4-3.14), only by the right hand side of equation (4-5.10b). In the original sensitivity problem this is the function Δq. Using equation (4-2.4), the function $\phi(\rho^n)$ in equation (4-5.6) becomes

$$\phi(\rho^n) = J(q^n - \rho^n p^n) = \frac{1}{2} \sum_{j=1}^{J} \int_{t_0}^{t_f} [T(\boldsymbol{d}_j, t; (q^n - \rho^n p^n)) - Y_j(t)]^2 dt$$

$$+ \frac{1}{2} \alpha_T \int_{t_0}^{t_f} \int_{\Gamma_4} [q^n(\boldsymbol{r}, t) - q_{pri}(\boldsymbol{r}, t) - \rho^n p^n(\boldsymbol{r}, t)]^2 \, d\boldsymbol{r} \, dt \tag{4-5.11}$$

Substituting the variation in the calculated temperature from equation (4-5.8) gives

$$\phi(\rho^n) = \frac{1}{2} \sum_{j=1}^{J} \int_{t_0}^{t_f} [T(\boldsymbol{d}_j, t; q^n) - \rho^n \bar{\theta}(\boldsymbol{d}_j, t) - Y_j(t)]^2 dt$$

$$+ \frac{1}{2} \alpha_T \int_{t_0}^{t_f} \int_{\Gamma_4} [q^n(\boldsymbol{r}, t) - q_{pri}(\boldsymbol{r}, t) - \rho^n p^n(\boldsymbol{r}, t)]^2 d\boldsymbol{r} \, dt \tag{4-5.12}$$

After expanding the terms, equation (4-5.12) is rewritten as

$$\phi(\rho^n) = \frac{1}{2} \rho^{n^2} \sum_{j=1}^{J} \int_{t_0}^{t_f} [\bar{\theta}(\boldsymbol{d}_j, t)]^2 dt - \rho^n \sum_{j=1}^{J} \int_{t_0}^{t_f} [T(\boldsymbol{d}_j, t; q^n) - Y_j(t)] \bar{\theta}(\boldsymbol{d}_j, t) dt$$

$$+ \frac{1}{2} \sum_{j=1}^{J} \int_{t_0}^{t_f} [T(\boldsymbol{d}_j, t; q^n) - Y_j(t)]^2 dt +$$

$$\frac{1}{2} \alpha_T \int_{t_0}^{t_f} \int_{\Gamma_4} \{ [q^n(\boldsymbol{r}, t) - q_{pri}(\boldsymbol{r}, t)]^2 - 2\rho^n p^n(\boldsymbol{r}, t) [q^n(\boldsymbol{r}, t) - q_{pri}(\boldsymbol{r}, t)] + [\rho^n p^n(\boldsymbol{r}, t)]^2 \} d\boldsymbol{r} \, dt \tag{4-5.13}$$

Taking the derivative with respect to the step size and solving for the optimal step size $\hat{\rho}^n$, as shown in equation (4-5.7), gives

$$\hat{\rho}^n = \frac{\sum_{j=1}^{J} \int_{t_0}^{t_f} [T(\boldsymbol{d}_j, t; q^n) - Y_j(t)] \bar{\theta}(\boldsymbol{d}_j, t) dt + \alpha_T \int_{t_0}^{t_f} \int_{\Gamma_4} p^n(\boldsymbol{r}, t)[q^n(\underline{s}, t) - q_{pri}(\boldsymbol{r}, t)] d\boldsymbol{r}\, dt}{\sum_{j=1}^{J} \int_{t_0}^{t_f} [\bar{\theta}(\boldsymbol{d}_j, t)]^2 dt + \alpha_T \int_{t_0}^{t_f} \int_{\Gamma_4} [p^n(\boldsymbol{r}, t)]^2 d\boldsymbol{r}\, dt} \tag{4-5.14}$$

Utilizing the relationship between the directional derivative and gradient in equation (4-3.3) and the directional derivative in equation (4-3.7), the numerator of this function is

$$\sum_{j=1}^{J} \int_{t_0}^{t_f} [T(\boldsymbol{d}_j, t; q^n) - Y_j(t)] \bar{\theta}(\boldsymbol{d}_j, t) dt + \alpha_T \int_{t_0}^{t_f} \int_{\Gamma_4} p^n(\boldsymbol{r}, t)[q^n(\underline{s}, t) - q_{pri}(\boldsymbol{r}, t)] d\boldsymbol{r}\, dt = \langle \nabla J(q^n), p^n \rangle_E \tag{4-5.15}$$

The step size in equation (4-5.14) is rewritten as

$$\hat{\rho}^n = \frac{\int_{t_0}^{t_f} \int_{\Gamma_4} \nabla J(\boldsymbol{r}, t, q^n) p^n(\boldsymbol{r}, t) d\boldsymbol{r}\, dt}{\sum_{j=1}^{J} \int_{t_0}^{t_f} [\bar{\theta}(\boldsymbol{d}_j, t)]^2 dt + \alpha_T \int_{t_0}^{t_f} \int_{\Gamma_4} [p^n(\boldsymbol{r}, t)]^2 d\boldsymbol{r}\, dt} = \frac{\langle \nabla J(q^n), p^n \rangle_E}{\sum_{j=1}^{J} \left\| \bar{\theta}(\boldsymbol{d}_j, t) \right\|_E^2 + \alpha_T \left\| p^n \right\|_E^2} \tag{4-5.16}$$

4-7.0 Implementation of the Gradient Method

4-7.1 Whole Domain

The derivation to solve the IHCP using a gradient search method and adjoint equation approach have been presented. A summary of the solution with these methods, in the form of an algorithm for a whole domain implementation are given next. Equations presented in this section are identical to those derived earlier and are summarized here for clarity.

1) Select initial values for the function $q^0(\boldsymbol{r}, t)$ $(n = 0)$. A common choice is $q^0(\boldsymbol{r}, t) = 0$. If prior information is available set $q_{pri}(\boldsymbol{r}, t)$.

2 i) Solve the direct problem for the temperature $T(\boldsymbol{r}, t; q_n)$

$$\nabla \cdot (k(\boldsymbol{r})\nabla T(\boldsymbol{r}, t)) = \rho C(\boldsymbol{r})\left[\frac{\partial}{\partial t}T(\boldsymbol{r}, t) + \boldsymbol{v} \cdot \nabla T(\boldsymbol{r}, t)\right], \quad \begin{matrix}(\boldsymbol{r}) \text{ in } \Omega \\ (t_0 < t \le t_f)\end{matrix} \tag{4-6.1}$$

$$-k_i \frac{\partial}{\partial \hat{\boldsymbol{n}}}T(\boldsymbol{r}, t) + h_i\, T(\boldsymbol{r}, t) = f_i(\boldsymbol{r}, t), \quad \begin{matrix}(\boldsymbol{r}) \text{ on } \Gamma_i, (i = 1, 2, 3) \\ (t_0 < t \le t_f)\end{matrix} \tag{4-6.2a}$$

$$-k(\boldsymbol{r})\frac{\partial}{\partial \hat{\boldsymbol{n}}}T(\boldsymbol{r}, t) = q^n(\boldsymbol{r}, t) \quad , \quad \begin{matrix}(\boldsymbol{r}) \text{ on } \Gamma_4 \\ (t_0 < t \le t_f)\end{matrix} \tag{4-6.2b}$$

$$T(\boldsymbol{r}, 0) = T_o(\boldsymbol{r}) \ , (\boldsymbol{r}) \text{ in } \Omega \tag{4-6.2c}$$

2 ii) Evaluate the residuals

$$e_j(t_i) = Y_j(t_i) - T(\boldsymbol{d}_j, t_i; q^n) \tag{4-6.3}$$

3 i) Solve the adjoint problem to determine $\psi(\boldsymbol{r}, t)$

$$\nabla \cdot (k(\boldsymbol{r})\nabla \psi(\boldsymbol{r}, t)) + \left[\rho C(\boldsymbol{r})\frac{\partial}{\partial t}\psi(\boldsymbol{r}, t) + \boldsymbol{v} \cdot \nabla[\rho C(\boldsymbol{r})\psi(\boldsymbol{r}, t)]\right] + \sum_{j=1}^{J} e_j(t)\delta(\boldsymbol{r} - \boldsymbol{d}_j) = 0$$

$$\begin{matrix}(\boldsymbol{r}) \text{ in } \Omega \\ (t_0 < t \le t_f)\end{matrix} \tag{4-6.4}$$

$$-k_i \frac{\partial}{\partial \hat{\boldsymbol{n}}}\psi(\boldsymbol{r}, t) + [h_i - \rho C(\boldsymbol{r})(\boldsymbol{v} \cdot \hat{\boldsymbol{n}})]\ \psi(\boldsymbol{r}, t) = 0, \quad \begin{matrix}(\boldsymbol{r}) \text{ on } \Gamma_i, (i = 1, 2, 3) \\ (t_0 < t \le t_f)\end{matrix} \tag{4-6.5a}$$

$$k(\boldsymbol{r})\frac{\partial}{\partial \hat{\boldsymbol{n}}}\psi(\boldsymbol{r}, t) + \rho C(\boldsymbol{r})(\boldsymbol{v} \cdot \hat{\boldsymbol{n}})\ \psi(\boldsymbol{r}, t) = 0, \quad \begin{matrix}(\boldsymbol{r}) \text{ on } \Gamma_4 \\ (t_0 < t \le t_f)\end{matrix} \tag{4-6.5b}$$

$$\psi(\boldsymbol{r}, t)\big|_{t = t_f} = 0, (\boldsymbol{r}) \text{ in } \Omega \tag{4-6.5c}$$

3 ii) Evaluate the gradient $\nabla J(q^n)$

$$\nabla J(\boldsymbol{r}, t, q^n) = \psi(\boldsymbol{r}, t) + \alpha_T[q^n(\boldsymbol{r}, t) - q_{pri}(\boldsymbol{r}, t)], (\boldsymbol{r}) \text{ on } \Gamma_4 \text{ and } (t_0 < t \le t_f) \quad (4\text{-}6.6)$$

3 iii) Compute search direction p^n

$$p^n(\boldsymbol{r}, t) = \nabla J(\boldsymbol{r}, t, q^n) \text{ - Steepest Descent Method} \quad (4\text{-}6.7)$$

$$p^n(\boldsymbol{r}, t) = \nabla J(\boldsymbol{r}, t, q^n) + \beta^n p^{n-1}(\boldsymbol{r}, t), (n \neq 0) \text{ Conjugate Gradients} \quad (4\text{-}6.8)$$

$$p^0 = \nabla J(q^0), n = 0 \text{ Conjugate Gradients} \quad (4\text{-}6.9)$$

where,

$$\beta^n = \frac{\int_{t_0}^{t_f}\int_{\Gamma_4}\{\nabla J(\boldsymbol{r}, t, q^n)[\nabla J(\boldsymbol{r}, t, q^n) - \nabla J(\boldsymbol{r}, t, q^{n-1})]\}d\boldsymbol{r}\, dt}{\int_{t_0}^{t_f}\int_{\Gamma_4}[\nabla J(\boldsymbol{r}, t, q^{n-1})]^2 d\boldsymbol{r}\, dt}$$

$$= \frac{\langle \nabla J(q^n), \nabla J(q^{n-1}) - \nabla J(q^n)\rangle_E}{\|\nabla J(q^{n-1})\|_E^2} \quad (4\text{-}6.10)$$

4 i) Solve the (adapted) sensitivity problem for $\bar{\theta}(\underset{\sim}{r}, t)$

$$\nabla \cdot (k(\boldsymbol{r})\nabla\bar{\theta}(\boldsymbol{r}, t)) = \rho C(\underset{\sim}{r})\left[\frac{\partial}{\partial t}\bar{\theta}(\boldsymbol{r}, t) + \boldsymbol{v} \cdot \nabla\bar{\theta}(\boldsymbol{r}, t)\right], \quad \begin{matrix}(\boldsymbol{r}) \text{ in } \Omega \\ (t_0 < t \le t_f)\end{matrix} \quad (4\text{-}6.11)$$

$$-k_i \frac{\partial}{\partial \hat{\boldsymbol{n}}}\bar{\theta}(\boldsymbol{r}, t) + h_i\, \bar{\theta}(\boldsymbol{r}, t) = 0, \quad \begin{matrix}(i = 1, 2, 3) \\ (\boldsymbol{r}) \text{ on } \Gamma_i \\ (t_0 < t \le t_f)\end{matrix} \quad (4\text{-}6.12a)$$

$$-k(\boldsymbol{r})\frac{\partial}{\partial \hat{\boldsymbol{n}}}\bar{\theta}(\boldsymbol{r}, t) = p^n(\boldsymbol{r}, t), \quad \begin{matrix}(\boldsymbol{r}) \text{ on } \Gamma_4 \\ (t_0 < t \le t_f)\end{matrix} \quad (4\text{-}6.12b)$$

$$\bar{\theta}(\boldsymbol{r}, 0) = 0, (\boldsymbol{r}) \text{ in } \Omega \quad (4\text{-}6.12c)$$

4 ii) Compute the optimal step size $\hat{\rho}$

$$\hat{\rho}^n = \frac{\int_{t_0}^{t_f}\int_{\Gamma_4}\nabla J(\boldsymbol{r}, t, q^n)p^n(\boldsymbol{r}, t)d\boldsymbol{r}\, dt}{\sum_{j=1}^{J}\int_{t_0}^{t_f}[\bar{\theta}(\boldsymbol{d}_j, t)]^2 dt + \alpha_T\int_{t_0}^{t_f}\int_{\Gamma_4}[p^n(\boldsymbol{r}, t)]^2 d\boldsymbol{r}\, dt} = \frac{\langle \nabla J(q^n), p^n\rangle_E}{\sum_{j=1}^{J}\|\bar{\theta}(\boldsymbol{d}_j, t)\|_E^2 + \alpha_T\|p^n\|_E^2} \quad (4\text{-}6.13)$$

5) Compute the improved value for the heat flux

$$q^{n+1}(\boldsymbol{r}, t) = q^n(\boldsymbol{r}, t) - \hat{\rho}^n p^n(\boldsymbol{r}, t), (\boldsymbol{r}) \text{ on } \Gamma_4 \tag{4-6.14}$$

6) Check for convergence of the estimated heat flux

$$\int_{t_0}^{t_f}\int_{\Gamma_4} [q^{n+1}(\boldsymbol{r}, t) - q^n(\boldsymbol{r}, t)]^2 d\boldsymbol{r}\, dt = \|q^{n+1} - q^n\|_E^2 < \varepsilon \tag{4-6.15}$$

If convergence has not been obtained let $n = n + 1$ and return to step 2 with the updated heat flux. If convergence has been met, use the residual principle to verify that the correct magnitude of α_T was used. The residual principle is

$$J_S(q^n) = \sum_{j=1}^{J} \int_{t_0}^{t_f} [T(\boldsymbol{d}_j, q^n) - Y_j(t)]^2 dt \approx \tau\delta^2 \tag{4-6.16}$$

where δ^2 is the expected noise or error in the measurements and $\tau \geq 1$ is a relaxation parameter.

An iterative regularization method can be obtained in the above algorithm by allowing the regularization parameter α_T to go zero. However, convergence is not evaluated by checking that by changes in the heat flux are small as in equation (4-6.15). Instead, in iterative regularization, the residual principal is used to select the number of iterations such that equation (4-6.16) is satisfied and the sum-of-squares function is reduced to its expected value; once this is achieved the iteration process is stopped.

Sequentially implementing this method is discussed next. Insight to the solution procedures using the gradient method with adjoint equation approach is given in Section (4-8.0) at the end of this chapter.

4-7.2 Sequential Implementation

The usual application of a gradient method with adjoint equation approach would solve the three problems over the whole time domain ($t_0 < t \leq t_f$), obtaining the estimated function $q(\boldsymbol{r}, t)$ for all time. Consequently, any inaccuracies in the estimated function at later times might influences the estimated function at early times. This dependence results from simultaneously estimating the function for all time.

An alternative approach uses the sequential idea applied in function specification method. A sequential approach is quite effective for estimating the heat flux. In addition, it possesses other positive attributes. The components that are estimated at later times are not influenced by the early estimates, less computer storage (and possibly time) is required, and it is possible to linearize over the future interval and more efficiently solve non-linear problems. Benefits of a sequential method are discussed in more detail in Section 5-2.0.

The sequential procedure can also be implemented for a gradient method using an adjoint equation approach. This procedure applies the method over smaller time intervals. Assuming that the function $q(\boldsymbol{r}, t)$ is known for times $t \leq t_{m-1}$, the unknown heat flux over r-future time steps, $t_{m-1} < t \leq t_{m+r-1}$ is estimated. Equations for the whole domain implementation are identical to those for the sequential implementation; however, they are solved over the time interval $t_{m-1} < t \leq t_{m+r-1}$. After obtaining a solution, the time interval is shifted by one (or possibly more) time step(s) and the procedure is repeated until the whole time domain is covered. In contrast to function specification it is not required to assume a functional form for the heat flux, but such a procedure may be beneficial. With this sequential approach, many shorter duration problems are solved, compared to the whole domain approach that solves one large time duration problem. Operationally, it is

straight forward to use gradient search methods in a sequential manner. Implementing such a method, and the associated practical issues, are not as straight forward. Chapters 5 and 6 study and provide insight to this implementation.

It is anticipated that this sequential approach will result in great reductions in the use of computer memory and have the potential to substantially reduce computational time. More savings are expected as the number of measurements become very large. These potential benefits are to be explored and are important parts of the proposed research. A more in-depth discussion of the benefits associated with the sequential approach is given in the subsequent chapters (Section 5-2.0).

The formulation of the problem and the describing equations are nearly identical for a sequential implementation. However, the sequential implementation solves a series of smaller problems over the time domain. The time domain $(t_0 < t \leq t_f)$ is broken into a series of sequential intervals each of length $(t_{m-1} < t \leq t_{m+r-1})$ and solved for $m = 1, 2, \ldots . M$, where $M = (t_f - t_0)/\Delta t - r$, Δt is the time step, and r is the number of future time steps. Assume that the heat flux for the sequential intervals up to and including time t_{m-1} is known. It is desired to compute the heat flux for subsequent times. Similar to the whole domain implementation, the solution is presented in the form of an algorithm.

1 For the first sequential interval $(m = 1)$ and iteration $(n = 0)$ select the initial values for the function q^0. Future sequential intervals $(m > 1)$ use the estimates at the previous sequential interval to specify the initial value. A common choice is $q^0(\boldsymbol{r}, t) = 0$. If prior information is available set $q_{pri}(\boldsymbol{r}, t)$.

2 i) Solve the direct problem for $T(\boldsymbol{r}, t;q^n)$

$$\nabla \cdot (k(\boldsymbol{r})\nabla T(\boldsymbol{r}, t)) = \rho C(\boldsymbol{r})\left[\frac{\partial}{\partial t}T(\boldsymbol{r}, t) + \boldsymbol{v} \cdot \nabla T(\boldsymbol{r}, t)\right], \quad \begin{matrix}(\boldsymbol{r}) \text{ in } \Omega \\ (t_{m-1} < t \le t_{m+r-1})\end{matrix} \tag{4-6.17}$$

$$-k_i \frac{\partial}{\partial \hat{\boldsymbol{n}}}T(\boldsymbol{r}, t) + h_i\, T(\boldsymbol{r}, t) = f_i(\boldsymbol{r}, t) \quad , \quad \begin{matrix}(\boldsymbol{r}) \text{ on } \Gamma_i, (i = 1, 2, 3) \\ (t_{m-1} < t \le t_{m+r-1})\end{matrix} \tag{4-6.18a}$$

$$-k(\boldsymbol{r})\frac{\partial}{\partial \hat{\boldsymbol{n}}}T(\boldsymbol{r}, t) = q^n(\boldsymbol{r}, t) \quad , \quad \begin{matrix}(\boldsymbol{r}) \text{ on } \Gamma_4 \\ (t_{m-1} < t \le t_{m+r-1})\end{matrix} \tag{4-6.18b}$$

$$T(\boldsymbol{r}, t_{m-1}) = \hat{T}(\boldsymbol{r}, t_{m-1}), (\boldsymbol{r}) \text{ in } \Omega \tag{4-6.18c}$$

2 ii) Evaluate the residuals

$$e_j(t) = Y_j(t) - T(\boldsymbol{d}_j, t;q^n) \ , (t_{m-1} < t \le t_{m+r-1}) \tag{4-6.19}$$

3 i) Solve the adjoint problem to determine $\psi(\boldsymbol{r}, t)$

$$\nabla \cdot (k(\boldsymbol{r})\nabla \psi(\boldsymbol{r}, t)) + \left[\rho C(\boldsymbol{r})\frac{\partial}{\partial t}\psi(\boldsymbol{r}, t) + \boldsymbol{v} \cdot \nabla[\rho C(\boldsymbol{r})\psi(\boldsymbol{r}, t)]\right] + \sum_{j=1}^{J} e_j(t)\delta(\boldsymbol{r} - \boldsymbol{d}_j) = 0$$

$$\begin{matrix}(\boldsymbol{r}) \text{ in } \Omega \\ (t_{m-1} < t \le t_{m+r-1})\end{matrix} \tag{4-6.20}$$

$$-k_i \frac{\partial}{\partial \hat{\boldsymbol{n}}}\psi(\boldsymbol{r}, t) + [h_i - \rho C(\boldsymbol{r})(\boldsymbol{v} \cdot \hat{\boldsymbol{n}})]\ \psi(\boldsymbol{r}, t) = 0, \quad \begin{matrix}(\boldsymbol{r}) \text{ on } \Gamma_i, (i = 1, 2, 3) \\ (t_{m-1} < t \le t_{m+r-1})\end{matrix} \tag{4-6.21a}$$

$$k(\boldsymbol{r})\frac{\partial}{\partial \hat{\boldsymbol{n}}}\psi(\boldsymbol{r}, t) + \rho C(\boldsymbol{r})(\boldsymbol{v} \cdot \hat{\boldsymbol{n}})\ \psi(\boldsymbol{r}, t) = 0, \quad \begin{matrix}(\boldsymbol{r}) \text{ on } \Gamma_4 \\ (t_{m-1} < t \le t_{m+r-1})\end{matrix} \tag{4-6.21b}$$

$$\psi(\boldsymbol{r}, t)\big|_{t = t_{m+r-1}} = 0, (\boldsymbol{r}) \text{ in } \Omega \tag{4-6.21c}$$

3 ii) Evaluate the gradient $\nabla J(q^n)$

$$\nabla J(\boldsymbol{r}, t, q^n) = \psi(\boldsymbol{r}, t) + \alpha_T[q^n(\boldsymbol{r}, t) - q_{pri}(\boldsymbol{r}, t)], \quad \begin{matrix}(\boldsymbol{r}) \text{ on } \Gamma_4 \\ (t_{m-1} < t \le t_{m+r-1})\end{matrix} \tag{4-6.22}$$

3 iii) Compute search direction p^n

$$p^n(\boldsymbol{r}, t) = \nabla J(\boldsymbol{r}, t, q^n) \text{ - Steepest Descent Method} \tag{4-6.23}$$

$$p^n(\boldsymbol{r}, t) = \nabla J(\boldsymbol{r}, t, q^n) + \beta^n p^{n-1}(\boldsymbol{r}, t), \ (n \neq 0) \text{ Conjugate Gradients} \tag{4-6.24}$$

$$p^0 = \nabla J(q^0), \ n = 0 \text{ Conjugate Gradients} \tag{4-6.25}$$

where,

$$\beta^n = \frac{\int_{t_{m-1}}^{t_{m+r-1}} \int_{\Gamma_4} \{\nabla J(\boldsymbol{r}, t, q^n)[\nabla J(\boldsymbol{r}, t, q^n) - \nabla J(\boldsymbol{r}, t, q^{n-1})]\} d\boldsymbol{r}\, dt}{\int_{t_{m-1}}^{t_{m+r-1}} \int_{\Gamma_4} [\nabla J(\boldsymbol{r}, t, q^{n-1})]^2 d\boldsymbol{r}\, dt}$$

$$= \frac{\langle \nabla J(q^n), \nabla J(q^{n-1}) - \nabla J(q^n) \rangle_E}{\|\nabla J(q^{n-1})\|_E^2} \tag{4-6.26}$$

4 i) Solve the adapted sensitivity problem for $\bar{\theta}(\boldsymbol{r}, t)$

$$\nabla \cdot (k(\boldsymbol{r}) \nabla \bar{\theta}(\boldsymbol{r}, t)) = \rho C(\boldsymbol{r}) \left[\frac{\partial}{\partial t} \bar{\bar{\theta}}(\boldsymbol{r}, t) + \boldsymbol{v} \cdot \nabla \bar{\theta}(\boldsymbol{r}, t) \right], \quad \begin{matrix} (\boldsymbol{r}) \text{ in } \Omega \\ (t_{m-1} < t \leq t_{m+r-1}) \end{matrix} \tag{4-6.27}$$

$$-k_i \frac{\partial}{\partial \hat{\boldsymbol{n}}} \bar{\theta}(\boldsymbol{r}, t) + h_i \, \bar{\theta}(\boldsymbol{r}, t) = 0, \quad \begin{matrix} (\boldsymbol{r}) \text{ on } \Gamma_i, (i = 1, 2, 3) \\ (t_{m-1} < t \leq t_{m+r-1}) \end{matrix} \tag{4-6.28a}$$

$$-k(\boldsymbol{r}) \frac{\partial}{\partial \hat{\boldsymbol{n}}} \bar{\theta}(\boldsymbol{r}, t) = p^n(\boldsymbol{r}, t), \quad \begin{matrix} (\boldsymbol{r}) \text{ on } \Gamma_4 \\ (t_{m-1} < t \leq t_{m+r-1}) \end{matrix} \tag{4-6.28b}$$

$$\bar{\theta}(\boldsymbol{r}, 0) = 0, (\boldsymbol{r}) \text{ in } \Omega \tag{4-6.28c}$$

4 ii) Evaluate the optimal step size $\hat{\rho}$

$$\hat{\rho}_n = \frac{\int_{t_{m-1}}^{t_{m+r-1}} \int_{\Gamma_4} \nabla J(\boldsymbol{r}, t) p^n(\boldsymbol{r}, t) d\boldsymbol{r}\, dt}{\sum_{j=1}^{J} \int_{t_{m-1}}^{t_{m+r-1}} [\bar{\theta}(\boldsymbol{d}_j, t)]^2 dt + \alpha_T \int_{t_{m-1}}^{t_{m+r-1}} \int_{\Gamma_4} [p^n(\boldsymbol{r}, t)]^2 d\boldsymbol{r}\, dt}$$

$$= \frac{\langle \nabla J(q^n), p^n \rangle_E}{\sum_{j=1}^{J} \|\bar{\theta}(\underline{d}_j, t)\|_E^2 + \alpha_T \|p^n\|_E^2} \tag{4-6.29}$$

5 Compute the improved value for q

$$q^{n+1}(\boldsymbol{r}, t) = q^n(\boldsymbol{r}, t) - \hat{\rho}^n p^n(\boldsymbol{r}, t), \quad \begin{matrix}(\boldsymbol{r}) \text{ on } \Gamma_4 \\ (t_{m-1} < t \le t_{m+r-1})\end{matrix} \tag{4-6.30}$$

6 Check for convergence of the estimated heat flux

$$\int_{\Gamma_4}\int_{t_{m-1}}^{t_{m+I-1}} [(q^{n+1}(\boldsymbol{r}, t) - q^n(\boldsymbol{r}, t))]^2 dt\, d\boldsymbol{r} = \|q^{n+1} - q^n\|_E^2 < \varepsilon \tag{4-6.31}$$

If convergence has not been obtained let $n = n + 1$ and return to step 2 with updated heat flux. If convergence has been met, store the heat flux for sequential analysis interval (store I-components)

$$q_{est}(\boldsymbol{r}, t) = q^{n+1}(\boldsymbol{r}, t), \; (t_{m-1} < t \le t_{m+I-1}) \tag{4-6.32}$$

Then index sequential interval $m = m + I$ and reset iteration to $n = 0$. Use estimated heat flux from the current sequential interval to partially set initial guess for next sequential interval (an additional I-components must be specified to complete the initial guess). Return to solution of direct problem (step 2.)

7 After final sequential interval check that proper magnitude of α_T was used with the residual principle

$$J(q^n) = \sum_{j=1}^{J} \int_{t_0}^{t_f} [T(\boldsymbol{d}_j, q^n) - Y_j(t)]^2 dt \approx \tau\delta^2 \tag{4-6.33}$$

where δ^2 is the expected noise or error in the problem and $\tau \ge 1$ is a relaxation parameter.

The selection of the Tikhonov parameter for this case does not take advantage of the sequential implementation to improve the selection of the parameter during a solution. Selecting the parameter after completing the solution for the whole time domain was chosen to allow a direct comparison between a sequential and whole domain solution. It is

possible to sequentially select the magnitude of the Tikhonov parameter at each sequential interval. In a sequential selection of the parameter, equation (4-6.33) is evaluated at each sequential interval and criteria are specified to vary the magnitude of the Tikhonov parameter. In a sequential application of equation (4-6.33) the results would likely be more sensitivity to local errors, and some constraints based on previous values of the Tikhonov may be need to prevent large fluctuation in the parameter from one sequential interval to the next.

4-8.0 Parameterizing the Solution (Finite-Dimensional Problem)

The derivation up to this point does not assume information concerning the functional form of the unknown heat flux. The problem, in general, has been considered infinite dimensional. This approach permits estimating a functional representation of the heat flux without having to specify information concerning the unknown function. Of course for realistic problems, obtaining a solution requires a numerical procedure. Any numerical procedure chosen will require discretizing, both on space and time, and consequently making assumptions about the form of unknown function. These assumptions are not too restrictive for most cases and the function can be estimated at the discrete grid points. If however, information is available, or assumed, concerning the heat flux, the solution can be constructed as a special case of the generalized solution methodology presented for the infinite dimensional problem.

Consider the case that information about the form of the heat flux is known. A general form for the known information can be represented as

$$q(\boldsymbol{r}, t) = \sum_{k=1}^{P} \sum_{i=1}^{M} q_{i,k} \phi_i(t) \varphi_k(\boldsymbol{r}) \tag{4-7.1}$$

where $\phi_i(t)$ and $\varphi_k(\boldsymbol{r})$ are basis functions on time and space and $q_{i,k}$ is the parameterized heat flux. When the heat flux is represented in the form of equation (4-7.1), solving for an adjoint function is not required to compute the gradient ∇J. Standard differential calculus can be used to compute the partial derivative with respect to each component of heat flux $\partial J/\partial q_{i,k}$. When there are a relatively small number of components this approach is suggested. However, for the multi-dimensional problem a large number of components are required to represent the spatial, time varying heat flux. Hence, the solution for the finite dimensional representation of the heat flux is presented as a special case of the infinite dimensional problem.

As stated previously, solving realistic problems requires using a numerical procedure. Regardless of the numerical method selected (finite element, finite difference, boundary element, or finite control volume) the spatial and temporal domains required discretizing. Consequently, even the infinite dimensional problem requires the heat flux to be represented in a finite dimensional form, as shown in equation (4-7.1), when solving with a numerical procedure. For the finite control volume numerical method, assuming that the quantities are constant over the control volume, P is the number of control volumes on surface Γ_4 and M is the number of time steps. It is well understood that improved numerical accuracy is obtained by decreasing the size of the control volumes and time step when solving the direct problem. Although this improves the numerical accuracy of the direct solution, it also increases the number of spatial heat flux components and decreases the magnitude of the time step. Estimating a larger number of spatial components or at smaller time increments makes the inverse problem more ill-conditioned. Hence, refining

the spatial and temporal grid size for a numerical method will not necessarily improve the accuracy of the inverse problem, in fact it will likely produce a larger variability in the estimated function. If however, some smoothing or prior information is used, as in equation (4-7.1), accuracy will not be significantly affected.

Modifications of the solution for a heat flux represented as in equation (4-7.1) are mainly in the computation of the gradient. Implementing the finite dimensional case using an adjoint equation approach is given in Jarny et al. (1991) and Alifanov (1994). Assuming the update to the heat flux, $\Delta q(\boldsymbol{r}, t)$ has the same form as the heat flux, and substituting these approximations into the directional derivative in equation (4-4.22) gives

$$D_{\Delta q}J(q) = \sum_{k=1}^{P}\sum_{i=1}^{M}\int_{t_0}^{t_f}\int_{\Gamma_4}\psi(\boldsymbol{r}, t)\phi_i(t)\varphi_k(\boldsymbol{r})\Delta q(\boldsymbol{r}, t)d\boldsymbol{r}\,dt$$
$$+\alpha_T\sum_{l=1}^{P}\sum_{j=1}^{M}\sum_{k=1}^{P}\sum_{i=1}^{M}\int_{t_0}^{t_f}\int_{\Gamma_4}[\phi_i(t)\varphi_k(\boldsymbol{r})q(\boldsymbol{r}, t) - q_{pri}(\boldsymbol{r}, t)]\phi_j(t)\varphi_l(\boldsymbol{r})\Delta q(\boldsymbol{r}, t)d\boldsymbol{r}\,dt \tag{4-7.2}$$

Equation (4-7.2) can be arranged to determine the gradient

$$D_{\Delta q}J(q) = \sum_{k=1}^{P}\sum_{i=1}^{M}\nabla J_{i,k}\Delta q_{i,k} \tag{4-7.3}$$

where

$$\nabla J_{i,k} = \gamma_{i,k} + \alpha_T\sum_{l=1}^{P}\sum_{j=1}^{M}S_{i,k,j,l}[q(\boldsymbol{r}, t) - q_{pri}(\boldsymbol{r}, t)], \quad \begin{matrix}(i = 1, 2, \ldots, M)\\(k = 1, 2, \ldots, P)\end{matrix} \tag{4-7.4}$$

$$\gamma_{i,k} = \sum_{k=1}^{P}\sum_{i=1}^{M}\int_{t_0}^{t_f}\int_{\Gamma_4}\psi(\boldsymbol{r}, t)\phi_i(t)\varphi_k(\boldsymbol{r})d\boldsymbol{r}\,dt \tag{4-7.5}$$

$$S_{i,k,j,l} = \int_{t_0}^{t_f}\int_{\Gamma_4}\phi_i(t)\varphi_k(\boldsymbol{r})\phi_j(t)\varphi_l(\boldsymbol{r})d\boldsymbol{r}\,dt \tag{4-7.6}$$

Thus, once the adjoint function $\psi(\boldsymbol{r}, t)$ is available, $\gamma_{i,k}$ is computed by integrating with the known basis functions. Similarly the weighting for the regularization $S_{i,k,j,l}$ is computed by integrating.

Restricting the more general infinite dimensional problem to a finite dimensional domain is straight forward. After solving for the adjoint function, the gradient for the finite dimensional representation of the heat flux is an integration of the adjoint function with the associated basis function. Other quantities computed in the solution, such as parameters for the search direction and step size, are performed in the finite dimensional space, i.e., $\langle\ ,\ \rangle_{R^n}$ and $\|\ \|_{R^n}$.

4-9.0 Summary

A formulation to solve the multi-dimensional IHCP using a conjugate gradient search method with an adjoint equation approach was derived in Section 4-1.0 to 4-6.0. The describing differential equations for solving in a whole domain implementation, herein referred to as the whole domain gradient method (GM), were presented in algorithm format in Section 4-7.1. The formulation for a method that solves the IHCP sequentially in time was also given in an algorithm format in Section 4-7.2. Studying this sequential implementation, herein called the sequential gradient method (SGM), is a major objective of this dissertation. The algorithms, for both GM and SGM, were formulated for the most general case, allowing the estimated heat flux to be described as a function (infinite dimensional). As a special case, restricting the estimated heat flux to a finite dimensional space was discussed in Section 4-8.0.

Solving the IHCP with a gradient method requires solving three problems, which are denoted the direct, adjoint, and sensitivity problems. Results from the solution of each problem provides an input for the subsequent problem. Residuals computed from the solution of the direct problem, equations (4-6.17) and (4-6.18) are the driving term in the adjoint problem in equation (4-6.20) and (4-6.21). The search direction computed with information from the adjoint function is the driving term in the sensitivity problem in equation (4-6.27) and (4-6.28). If the measured temperatures are known "exactly" i.e., residuals are zero, all three problems have a homogeneous solution. For inexact data, as iterations progress the solution of the three problems should converge towards a homogeneous solution.

The remaining chapters study the solution of the IHCP using the GM and SGM. In Chapter 5 a detailed discussion of the benefits of a sequential implementation are addressed. Because many of these benefits are related to the numerical solution, a discussion of the numerical aspects are given first. In the remainder of Chapter 5 the methods are applied to the one-dimensional IHCP. Although a two-dimensional formulation is given, a one-dimensional solution is obtained as a special case of the two-dimensional formulation. In general, it is not recommended that this solution technique be applied to a one-dimensional problem. However, to gain insight to the SGM and understand it better, a one-dimensional solution is an appropriate beginning to the investigation. After investigating the one-dimensional problem, Chapter 6 progresses to study the two-dimensional problem.

Chapter 5

APPLICATION OF THE SEQUENTIAL GRADIENT METHOD: ONE-DIMENSIONAL IHCP

5-1.0 Introduction

Cases are presented in this chapter to study the sequential gradient method. The accuracy of the sequential implementation, as compared to the whole domain, is also quantified. Addressing issues of accuracy for inverse methods is an important topic. Though there are many methods for solving the IHCP, few methods have had detailed studies conducted on their accuracy. Investigations of the accuracy of inverse methods are presented by Beck and Murio (1986), Raynaud and Beck (1988), and Scott and Beck (1989). Beck and Murio (1986) compared a whole domain solution with a sequential implementation combining function specification and Tikhonov regularization. The work by Scott and Beck focussed on the sequential regularization method while Raynaud and Beck compared four methods for solving the IHCP. In these papers, however, simulated cases, with known heat flux, are analyzed to quantify the accuracy of the inverse methods. These ideas are also applied in this investigation. In particular, standard test cases for which the heat flux is known are analyzed and the accuracy is quantified for the sequential implementation as well as the whole domain approach, which is the usual application of this method. Hence in addition to studying the sequential method, this dissertation provides insight to the whole domain solution.

An important issue in an inverse analysis is the effect of measurement errors on the solution. Many researchers study this effect modeling the errors with standard statistical assumptions, which is beneficial and also pursued in this investigation. Additional insight is gained from an analysis with actual experimental measurements. Hence, in addition to the studies with simulated errors, an experimental case is presented. The case has the unique benefit, in that transient temperature and heat flux histories are both measured. Since the heat flux is measured, the "true" heat flux, within some experimental uncertainty, is known. This experiment permits comparison between the estimated and measured flux.

A new competitive sequential method is presented in this chapter. In addition to studying the sequential gradient method a modification of the sequential implementation is suggested that improves the computational requirements of the sequential method. The new method combines function specification with the sequential gradient method. Implementing a gradient solution, but assuming the heat flux is a prescribed function over the sequential interval is studied. Prescribing a functional form for the heat flux over the sequential interval is shown to reduce the computational requirements compared to a standard sequential implementation.

Associated benefits of a sequential implementation of gradient methods and the numerical procedures to obtain a solution are discussed in next section. Several test cases to simulate experimental data are given in Section 5-3.0. Results of the one-dimensional analyses with simulated exact data, data corrupted with measurement errors, and experimental data are presented in Section 5-4.0.

5-2.0 Advantages of a Sequential Method and Numerical Solution of the IHCP

This section discusses the benefits and advantages of a sequential implementation for solving the IHCP. Because these advantages are closely related to the numerical solution, the numerical method to solve the IHCP is discussed first.

5-2.1 Numerical Solution

A numerical solution for the two-dimensional IHCP is developed using a finite control volume (FCV) method. Numerically solving the IHCP using a gradient method and adjoint equation approach requires the solution of three partial differential equations representing the direct, adjoint, and sensitivity problems. Describing equations formulated for the three problems are given in equation (4-6.17) and (4-6.18), equation (4-6.20) and (4-6.21), and equation (4-6.27) and (4-6.28), respectively. Fortunately, the differential equations are similar and numerical computations required for one problem apply for the other problems. A detailed derivation of the FCV equations are given in Appendix A.

The numerical solution was developed for the two-dimensional problem using an alternating direction implicit (ADI) scheme. A one-dimensional solution is obtained as a special case. The FCV equations for the direct problem are represented as a two step solution

$$[K_1]\{T^{n+1/2}\} = \{D^n\} \tag{5-2.1}$$

$$[K_2]\{T^{n+1}\} = \{E^{n+1/2}\} \tag{5-2.2}$$

where $[K_1]$ and $[K_2]$ are the standard FCV tri-diagonal matrices, $\{T^n\}$ is a vector of unknown temperatures for time n, and $\{D^n\}$ and $\{E^{n+1/2}\}$ are vectors of known

information for the respective time steps. The two sets of equations represent the two steps of an ADI scheme.

All three problems, direct, adjoint, and sensitivity, require solving a set of equations similar to those shown in equation (5-2.1) and (5-2.2). Since the problems are similar, the tri-diagonal matrices ($[K_1]$ and $[K_2]$) are identical for the three problems and require computation only one time for constant thermal properties, i.e., a linear problem. Furthermore, when solving the tri-diagonal set of equations, computational savings are possible for the linear problem. This is true for a whole domain as well as sequential solution. However, for non-linear problems with a sequential solution it is possible to temporarily linearize and benefit from the computational savings associated with linear problems. Aspects of this procedure are discussed below.

5-2.2 Sequential Solution of IHCP

Benefits of applying a sequential solution for the IHCP are addressed. Several supporting reasons for a sequential solution are discussed. Although not all reasons are investigated in this dissertation, nor verified, it suggests the possibility of growth for the sequential gradient method.

1. A sequential method can be implemented in an on-line or "real" time mode. For example, in the monitoring of surface heating during the flight of a space vehicle, data can be collected for a short period then the surface heat flux can be computed in "real" time.
2. Estimated values much later in time do not affect the estimates at early times when solving sequentially. When solving in a whole domain approach, all temporal components are simultaneously estimated. Consequently, errors in estimated components will pervade all estimates. It is physically unreasonable that this occurs because of the parabolic nature of the describing equations. Furthermore, values near the final time, which

are known to be difficult to estimated, must be estimated and the errors in these components may impact the others. Since a sequential approach solves on a subset of the whole time region, or sequential region, estimates at later times do not impact early estimates, which is physically reasonable.

3. For nonlinear problems, due to temperature dependent thermal properties or other temperature dependent coefficients in the differential equation, the sequential method permits the problem to be temporarily linearized. This is an important point, because it is not possible when solving on the whole time domain. Since the problem is solved on the shorter sequential interval, it is valid to assume that the temperature dependent quantity is constant during the sequential interval (r-future time steps). The validity of this assumption depends on the degree of non-linearity in the problem. In most applications the non-linear term is not known with sufficient accuracy to justify accounting for the non-linearity during the temperature change seen in a sequential interval. To linearize, thermal properties and temperature dependent variables are evaluated at the initial temperature distribution of the sequential interval. Consequently, computing matrices $[K_1]$ and $[K_2]$ is required only at the beginning of each sequential interval. The matrices apply for all three problems and it is not required to recompute the matrices during the iteration procedure. Conversely, the whole domain approach requires re-computing the matrices at each time step as the temperature varies over the time domain. Matrices must be recomputed at every iteration.

4. Related to point 3., is the computational savings that can be realized in the solution of the tri-diagonal system of equations. Since the problem is linear (temporarily) for a sequential approach, the intermediate coefficients required to solve the tri-diagonal system can be saved after solving the direct problem and need not be computed until the next sequential interval, when the initial temperature, and coefficients, change. Examining the algorithm illustrates the point. Assuming the tri-diagonal matrix $[K_1]$ has main diagonal $C_{1,i}$ sub-diagonal $A_{1,i}$ and sup-diagonal $B_{1,i}$, the system is solving by the Thomas algorithm using the recursive relations (Anderson et al., 1984)

$$\beta_0 = C_{1,0} \tag{5-2.3a}$$

$$\beta_i = C_{1,i} - \frac{A_{1,i}B_{1,i-1}}{\beta_{i-1}}, \; i = 1, 2, \ldots N \tag{5-2.3b}$$

$$\gamma_0 = \frac{D_0^n}{\beta_0} \tag{5-2.3c}$$

$$\gamma_i = \frac{D_i^n - A_{1,i}\gamma_{i-1}}{\beta_i}, \; i = 1, 2, \ldots N \tag{5-2.3d}$$

The solution of the temperature is

$$T_N^{n+1/2} = \gamma_N \tag{5-2.4a}$$

$$T_i^{n+1/2} = \gamma_i - \frac{B_{1,i}T_{i+1}^{n+1/2}}{\beta_i}, \; i = N-1, N-2, \ldots 1, 0 \tag{5-2.4b}$$

Since the problem is linear (temporarily), the coefficients $A_{1,i}$, $C_{1,i}$, and, $B_{1,i}$ are the same for the direct, adjoint, and sensitivity problems. Consequently, after computing and storing β_i in equation (5-2.3b), this step is by-passed in subsequent solutions. A similar procedure is used to store the coefficients from the second step in the ADI scheme. Computations in the following steps, equation (5-2.3c) and (5-2.4a) and (5-2.4b), are required for every solution. For a linear problem, both the sequential and whole domain methods can benefit from this computational saving.

5. Solution of the adjoint and sensitivity problems can use the zero initial condition and fact that driving terms in the equations tend to have oscillating signs to reduce computations by marching on space and/or time. The possibly oscillating signed driving terms, residuals $e_j(t)$ in the adjoint problem and search direction $p^n(\boldsymbol{r}, t)$ in the sensitivity problem, will localize the effects. It may be possible to consider the solution on a subset of the time domain or physical domain because the effects are localized. A whole domain approach might benefit from such an approach, but because the sequential implementation focuses on a restricted time region it is more likely to benefit.

6. The magnitude of the Tikhonov regularization parameter can be adjusted in a sequential implementation. Again, this is not restricted to the sequential implementation, but is more practical to implement in a sequential method because current information is available to select the magnitude of the Tikhonov parameter. This permits more accurately estimating rapidly changing functions with less bias.
7. Additional heat flux components can be retained in a sequential implementation. This is an advantage compared to a standard function specification solution, because additional bias is not introduced with the function specification approximation. More components from the solution over a sequential interval therefore may be retained.

5-3.0 Simulated Test Cases

Several standard one-dimensional cases are examined. Test cases include heat flux functions that vary in a triangular, step, and sinusoidal manner with time. The one-dimensional geometry is a slab of thickness L with an unknown heat flux at $x = 0$, insulated on the surface at $x = L$, uniform initial temperature, and constant thermal properties. Since the IHCP is very sensitive to measurement errors, to reduce the possibility of numerical errors, analytical solutions (when possible) are employed to generate simulated data. Mathematically the problem is represented as

$$\frac{\partial^2 T_i^+}{\partial x^{+2}} = \frac{\partial T_i^+}{\partial t^+} \tag{5-3.1}$$

$$-\left.\frac{\partial T_i^+}{\partial x^+}\right|_{x^+ = 0} = q_i^+(t^+) = ? \tag{5-3.2a}$$

$$\left.\frac{\partial T_i^+}{\partial x^+}\right|_{x^+ = 1} = 0 \tag{5-3.2b}$$

$$T_i^+(x^+, 0) = 0 \tag{5-3.2c}$$

where $i = 1, 2, 3$ for the three prescribed heat fluxes studied. To remove the dimensional dependence and facilitate the investigation, dimensionless variables were introduced in equation (5-3.1) and (5-3.2). The dimensionless variables are

$$q_i^+ = \frac{q}{q_N} \tag{5-3.3}$$

$$T_i^+ = \frac{T_i - T_o}{(q_N L/k)} \tag{5-3.4}$$

$$t^+ = \frac{(k/\rho C)t}{L^2} \tag{5-3.5}$$

$$x^+ = \frac{x}{L} \tag{5-3.6}$$

Symbol q_N is a nominal value of the heat flux, k and ρC are the thermal properties, T_0 is the uniform initial temperature, and L is the plate thickness in equation (5-3.3) through (5-3.6).

Three forms of the prescribed (assumed unknown) heat flux (q_i^+) are examined. A triangular heat flux

$$q_1^+(t^+) = \begin{cases} 0 & (t^+ < 0) \\ t^+ & (0 \le t^+ \le t_h^+/2) \\ t^+ - 2(t^+ - t_h^+/2) & (t_h^+/2 < t^+ \le t_h^+) \\ 0 & (t^+ > t_h^+) \end{cases} \tag{5-3.7}$$

which increases linearly to a magnitude of $t_f^+/2$ then decreases linearly until reaching zero, and is zero elsewhere. The second variation is a step change in the heat flux

$$q_2^+(t^+) = \begin{cases} 0 & (t^+ < 0) \\ 1 & (0 \le t^+ \le t_h^+) \\ 0 & (t^+ > t_h^+) \end{cases} \tag{5-3.8}$$

which increases to a magnitude of one at $t^+ = 0$, remains constant until $t^+ = t_h^+$ and then returns to zero. The final heat flux is a sinusoidal heat flux. It represents one-half the period $\left(-\frac{\pi}{2}, \frac{3\pi}{2}\right)$ of a sine wave between zero and $t^+ = t_f^+$, and is zero elsewhere

$$q_3^+(t^+) = \begin{cases} 0 & (t^+ < 0) \\ \frac{1}{2}\left\{\sin\left[-\pi\left(2\frac{t^+}{t_h^+} + \frac{1}{2}\right)\right] + 1\right\} & 0 \le t^+ \le t_h^+ \\ 0 & (t^+ > t_h^+) \end{cases} \tag{5-3.9}$$

A constant is added to the sinusoidal heat flux to maintain a nonzero flux.

Analytical solutions are readily generated for these three cases. Solutions can be obtained using Greens functions (Beck et al., 1992). Although the test cases mentioned are standard cases and it is not difficult to solve for the temperature, closed form expressions are not typically given in the literature. Beck et al. (1985) give the closed form solution for a linear heat flux at the boundaries ($x = 0, L$). For completeness, the closed-form expressions for the temperature solutions with the three specified heat flux functions are provided.

For the triangular heat flux the solution is built using superposition of a heat flux which increases linearly with time ($q^+ = t^+$). The temperature due to the linearly varying heat flux is

$$\phi_1^+(x^+,t^+) = \frac{t^{+2}}{2} + \left[\frac{1}{2}x^{+2} - x^+ + \frac{1}{3}\right]t^+ + \left[\frac{1}{24}x^{+4} - \frac{1}{6}x^{+3} + \frac{1}{6}x^{+2} - \frac{1}{45}\right]$$
$$+ \frac{2}{\pi^4}\sum_{n=1}^{\infty}\frac{1}{m^4}\cos(m\pi x^+)[\exp(-m^2\pi^2 t^+)] \quad (5\text{-}3.10)$$

The temperature solution for the triangular heat flux in equation (5-1.7) follows as

$$T_1^+(x^+,t^+) = \begin{cases} 0 & (t^+ < 0) \\ \phi_1^+(x^+,t^+) & (0 \le t^+ \le t_h^+/2) \\ \phi_1^+(x^+,t^+) - 2\phi_1^+(x^+,t^+ - t_h^+/2) & (t_h^+/2 < t^+ \le t_h^+) \\ \phi_1^+(x^+,t^+) - 2\phi_1^+(x^+,t^+ - t_h^+/2) + \phi_1^+(x^+,t^+ - t_h^+) & (t^+ > t_h^+) \end{cases} \quad (5\text{-}3.11)$$

Similarly, the temperature solution for the step help flux is built using superposition of a constant heat flux.The temperature solution for a constant heat flux ($q^+ = 1$) is

$$\phi_2^+(x^+,t^+) = t^+ + \left[\frac{1}{2}x^{+2} - x^+ + \frac{1}{3}\right] - \frac{2}{\pi^2}\sum_{n=1}^{\infty}\frac{1}{m^2}\cos(m\pi x^+)\exp(-m^2\pi^2 t^+) \quad (5\text{-}3.12)$$

For the step change in the heat flux, equation (5-3.8), the temperature solution is

$$T_2^+(x^+,t^+) = \begin{cases} 0 & (t^+ < 0) \\ \phi_2^+(x^+,t^+) & (0 \le t^+ \le t_h^+) \\ \phi_2^+(x^+,t^+) - \phi_2^+(x^+,t^+ - t_h^+) & (t^+ > t_h^+) \end{cases} \quad (5\text{-}3.13)$$

The sinusoidal heat flux in equation (5-3.9) is the sum of a sine function and a constant, hence, superposition of these solutions is used. The sinusoidal part of the heat flux, $q^+ = \sin[-\pi(2t^+/t_h^+ + 1/2)]$, has a temperature solution

$$\phi_3^+(x^+,t^+) = \frac{t_h^+}{\pi}\cos\left[-\pi\left(2\frac{t^+}{t_h^+}+\frac{1}{2}\right)\right] + 4t_h^+\sum_{m=1}^{\infty}\left[\frac{1}{m^4\pi^4 t_h^{+2}+4\pi^2}\right]\cos(m\pi x^+)$$

$$\left\{2\pi\cos\left[-\pi\left(2\frac{t^+}{t_h^+}+\frac{1}{2}\right)\right] + m^2\pi^2 t_f^+\sin\left[-\pi\left(2\frac{t^+}{t_h^+}+\frac{1}{2}\right)\right] + m^2\pi^2 t_h^+\exp(-m^2\pi^2 t^+)\right\} \quad (5\text{-}3.14)$$

The temperature solution for the sinusoidal heat flux in equation (5-3.9) is

$$T_3^+(x^+,t^+) = \frac{1}{2}\begin{cases} 0 & (t^+<0) \\ \phi_3^+(x^+,t^+)+\phi_2^+(x^+,t^+) & (0\le t^+\le t_h^+) \\ \phi_3^+(x^+,t^+)-\phi_3^+(x^+,t^+-t_h^+)+\phi_2^+(x^+,t^+)-\phi_2^+(x^+,t^+-t_h^+) & (t^+>t_h^+) \end{cases} \quad (5\text{-}3.15)$$

Data for the simulated temperature and heat flux are shown in Figure 5-1, 5-2, and 5-3 for the triangular, step, and sinusoidal heat flux. All three cases demonstrate the effect that makes the IHCP difficult, mainly the lagged or delayed response in the temperature at the back surface due to the heat flux on the opposite surface. The temperature response is delayed relative to the application of the surface heat flux. The more gradual the variation in the surface heat flux is, the greater this delay becomes, as seen by comparing Figure (5-2) and (5-3). The temperature response at the sensor location is damped also. That is, the magnitude of the temperature response at the sensor location is smaller that the response at the surface where the heat flux is estimated. These temperature data are used to estimate the surface heat flux.

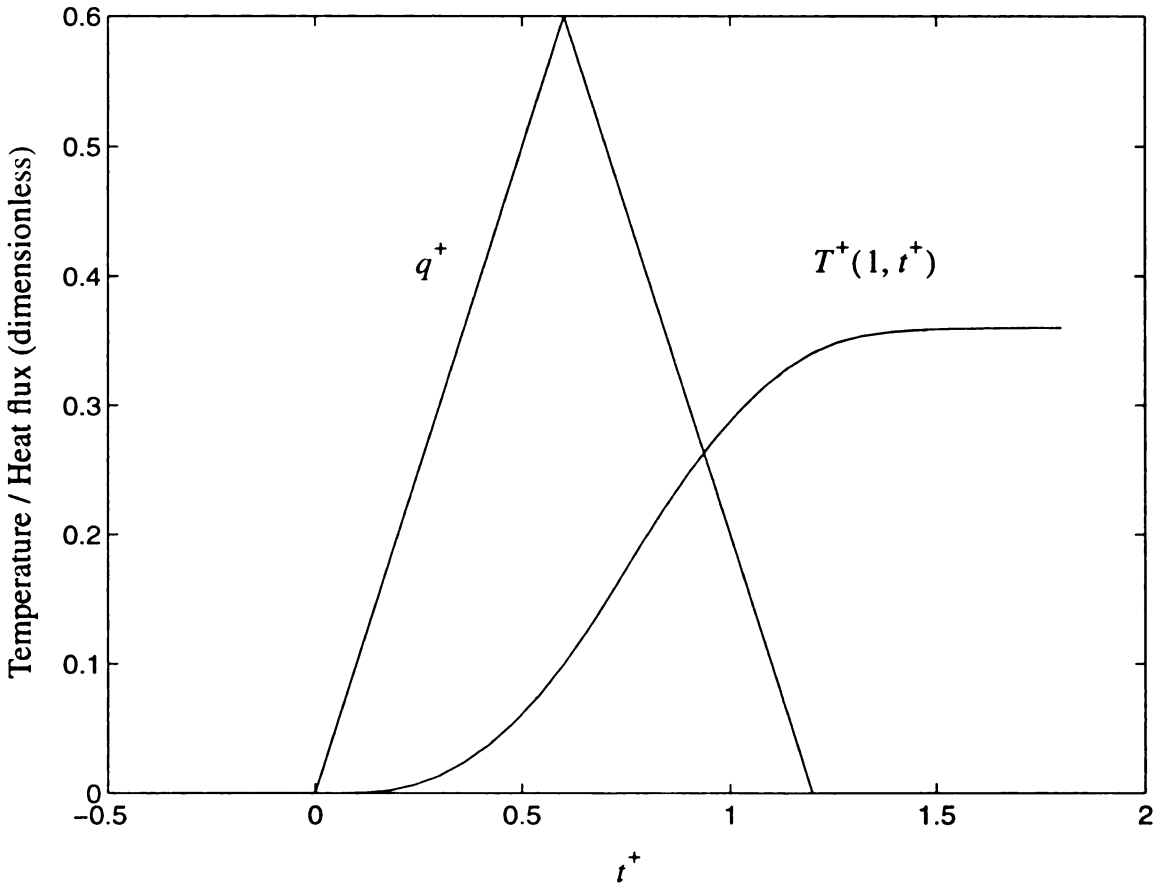

Figure 5-1 Simulated temperature and heat flux data for the one-dimensional triangular heat flux

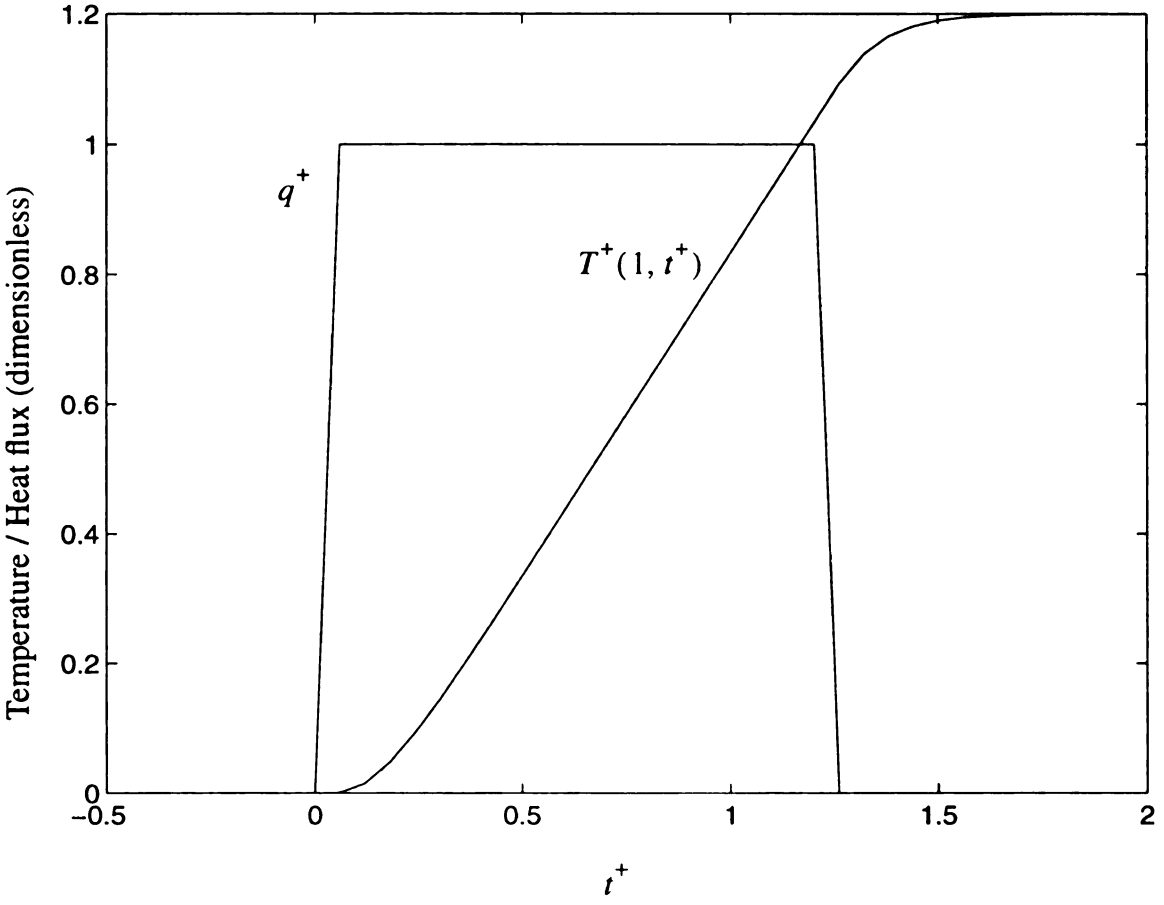

Figure 5-2 Simulated temperature and heat flux data for the one-dimensional step heat flux test case

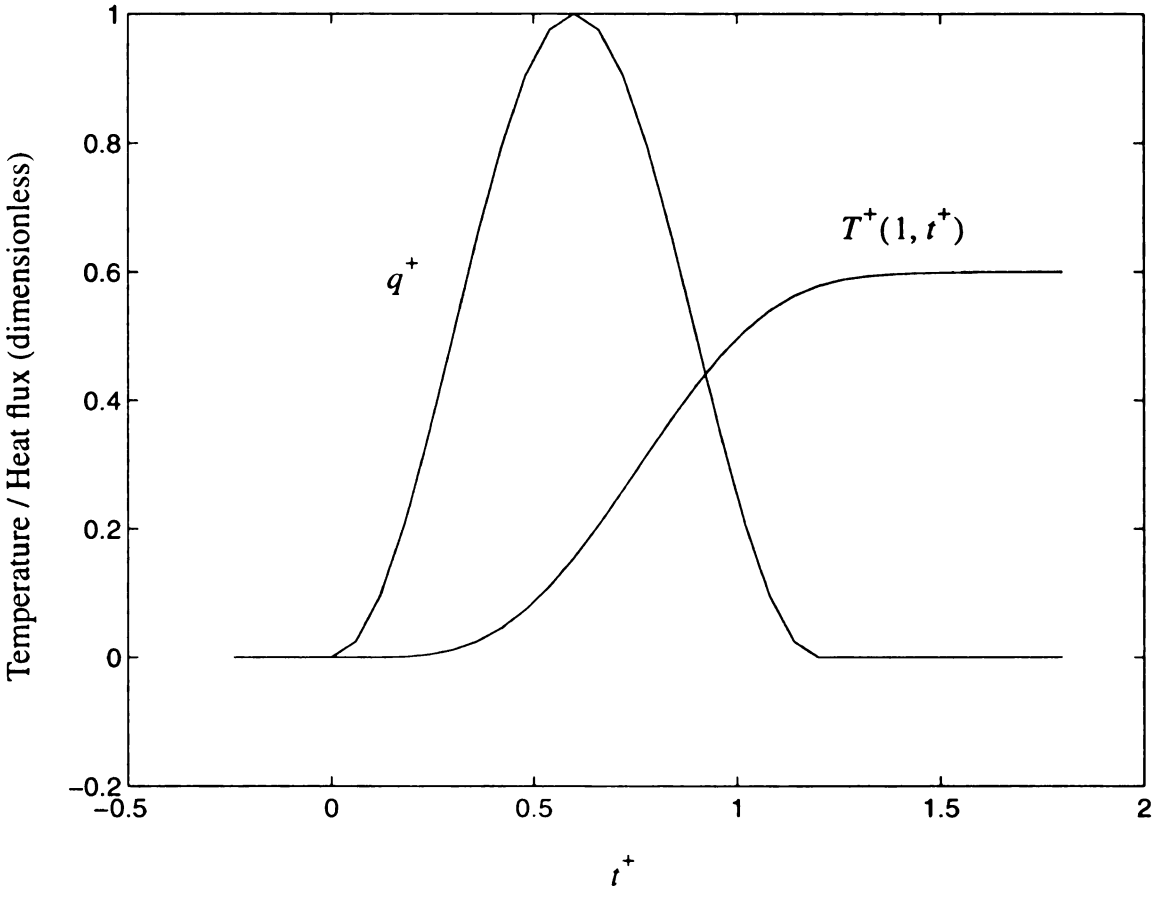

Figure 5-3 Simulated temperature and heat flux data for the one-dimensional sinusoidal heat flux test case

5-4.0 1D Results - Simulated Measurements

One-dimensional test cases are presented to study the sequential implementation. Implementing such a method is not recommended for the usual one-dimensional problems; it is applied in this case to develop an understanding of this new method. (Nonlinear problems may be an exception for using the sequential method for one-dimensional problems.) Three functional forms of the heat flux, triangular, step, and sinusoidal, serve as test cases. Investigations with exact data and data corrupted with errors are conducted. Errors, denoted $\varepsilon_n(\boldsymbol{d}_j, t)$, are assumed additive

$$Y(\boldsymbol{d}_j, t) = T(\boldsymbol{d}_j, t) + \varepsilon_n(\boldsymbol{d}_j, t) \tag{5-4.1}$$

with a normal distribution, zero mean, constant variance, and uncorrelated. The true temperature $T(\boldsymbol{d}_j, t)$ is computed from the analytical solutions, see Section 5-3.0. Random errors are generated with routines in MATLAB.

5-4.1 Exact Data (no Measurement Errors)

The three test cases are analyzed with exact data ($\varepsilon_n = 0$) for a dimensionless time step of 0.06 and a total of thirty time steps. Values selected for r are five, eight, and ten. Results are shown for the triangular heat flux in Figure 5-4. Graphic results are not shown for the step and sinusoidal test cases using exact data, but the analyses are discussed. Estimates for the final sequential interval ($t_f - r\Delta t < t < t_f$) at the end of the time region are not considered reliable and not reported. The results of the estimations are similar with less than a five-percent difference in the whole domain and sequential implementation; errors are largest near areas of sudden change in the surface heat flux.

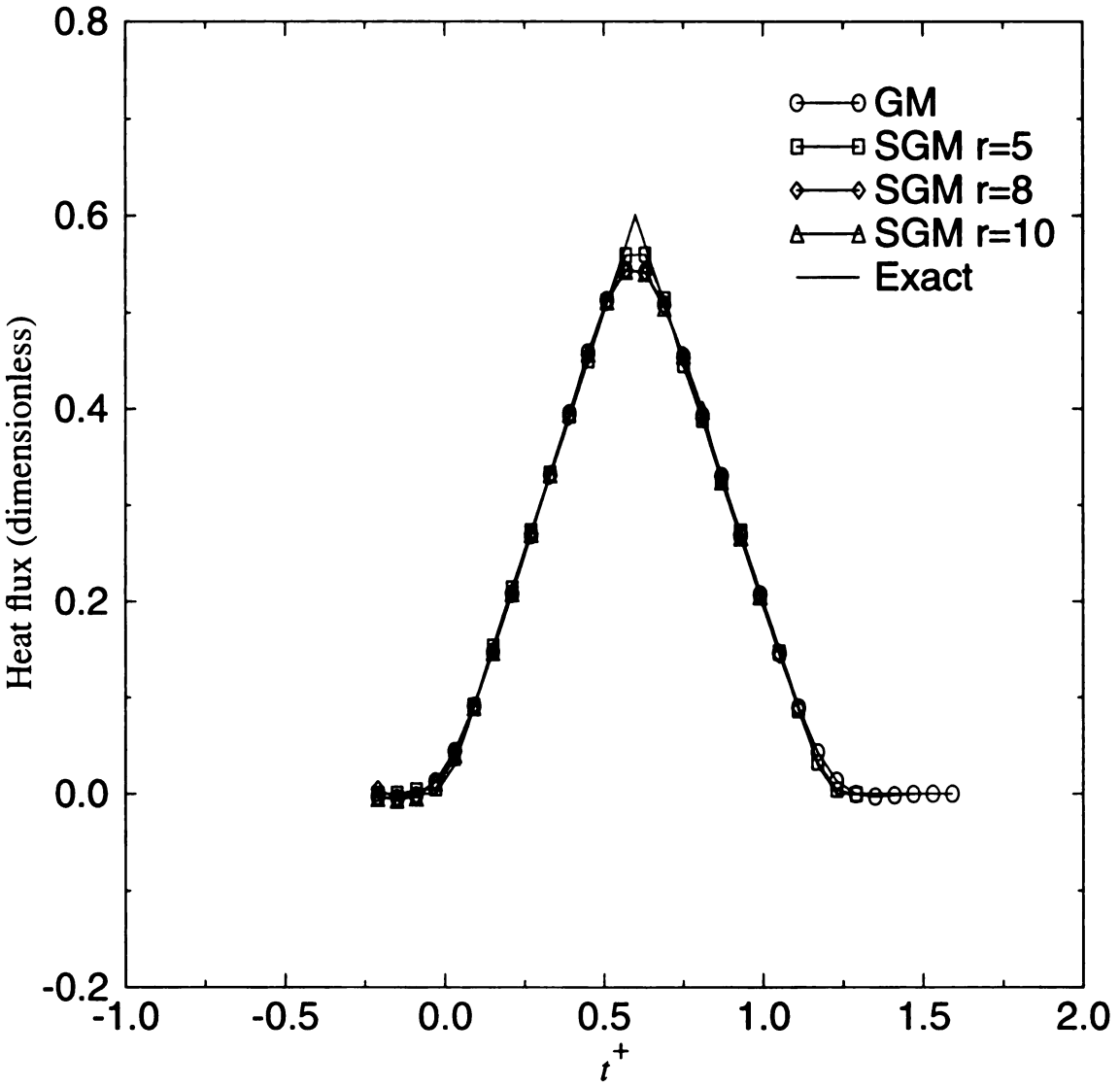

Figure 5-4 Estimated heat flux for one-dimensional triangular test case with exact data

Table 5-1 Estimation results for exact simulated data

Method	Analysis domain	Tikhonov α_T	Iterations		Comp time (sec)	S_Y $(°C)$	$\hat{\sigma}_D$ W/m^2
			total	per seq int			
Triangular Flux (σ = 0.0°C)							
GM	whole	0.001	7	-	2.14	8.59 E-04	0.0094
SGM	r = 5	0.00011	78	3.0	3.64	8.64 E-04	0.0046
SGM	r = 8	0.00087	87	3.8	6.86	8.72 E-04	0.0094
SGM	r = 10	0.00107	87	4.1	8.64	8.72 E-04	0.011
Step Flux (σ = 0.0°C)							
GM	whole	0.001	8	-	2.38	3.12 E-03	0.116
SGM	r = 5	0.00014	79	3.0	3.56	3.17 E-03	0.109
SGM	r = 8	0.0009	96	4.2	7.29	3.12 E-03	0.097
SGM	r = 10	0.001	102	4.9	9.85	3.08 E-03	0.101
Sinusoidal Flux (σ = 0.0°C)							
GM	whole	0.001	6	-	1.85	1.71 E-03	0.043
SGM	r = 5	0.00012	80	3.1	3.48	1.70 E-03	0.044
SGM	r = 8	0.0009	84	3.7	6.38	1.71 E-03	0.051
SGM	r = 10	0.001	86	4.1	8.34	1.71 E-03	0.050

Results from the analysis with exact data are given in Table 5-1 for estimating the three heat flux functions. The first column identifies the method, whole domain gradient method (GM) or a sequential gradient method (SGM). The second column lists the analysis domain investigated, either whole domain or sequential with the value of *r* specified. The Tikhonov regularization parameter is given in column three. Since exact data are used, the regularization parameter is specified as 0.001 for the whole domain analysis and

varied to produce the same sum-of-squares error (column seven) for the sequential analysis. The number of iterations, both total and average number per sequential interval, are given in columns four and five. Computational time is listed in column six. Measures of the error in temperature and heat flux are given in columns seven and eight, respectively. The error in the temperature is computed as

$$S_Y = \left\{ \frac{1}{J(N-1)} \sum_{j=1}^{J} \sum_{i=1}^{N} [T(\boldsymbol{d}_j, t_i) - Y_j(t_i)]^2 \right\}^{\frac{1}{2}} \tag{5-4.2}$$

Equation (5-4.2) represents a measure of the error in the sum-of-squares function J_S in equation (4-2.4). The residual (discrepancy) principle states that the error, S_Y in equation (5-4.2), should be reduced to its expected value, Alifanov (1994). Error in the estimated heat flux is

$$\hat{\sigma}_D = \left\{ \frac{1}{p(N-1)} \sum_{k=1}^{P} \sum_{i=1}^{N} [q(\boldsymbol{r}_k, t_i) - \hat{q}(\boldsymbol{r}_k, t_i)]^2 \right\}^{\frac{1}{2}} \tag{5-4.3}$$

where $q(\boldsymbol{r}_k, t_i)$ is the true heat flux at location $\boldsymbol{r}_k$ on Γ_4 and time t_i and $\hat{q}$ is the estimated value with no measurement errors. Equation (5-4.3) is referred to as the deterministic bias, or just bias, (Beck et al., 1985), since the estimated heat flux is computed without measurement errors. The deterministic bias represents the bias that is introduced by the inverse method itself; some bias is required to stabilize the ill-posed problem.

The estimated heat flux can more closely approximate the triangular shape for small r-values using the SGM, particularly near the peak, see Figure 5-4. A smaller Tikhonov parameter permits the SGM to more accurately reproduce the peak, with less bias or smoothing of the estimated heat flux. It is interesting that the Tikhonov parameter is

reduced for the SGM at small values of r. The problem is more ill-posed for the SGM compared to GM. Hence, it was anticipated that the Tikhonov parameter would increase, but it decreases instead. The decrease in the Tikhonov parameter is required, even though the problem is more ill-posed, to permit the solution the "flexibility" to reduce the sum-of-squares to the magnitude specified by the residual principle. Regularization, tends to "stiffen" the inverse problem. When solved in a sequential manner, estimates near the end of the sequential interval are biased low (discussed below). To compensate for the biased estimates near the end of the interval the Tikhonov parameter must be reduced to permit "flexibility" in the first components and obtain the correct magnitude for the sum-of-squares. Note that as r is increased, the Tikhonov parameter also increases towards the magnitude specified for the whole domain solution.

Several observations are drawn from the analysis with exact data. The computational time required for the sequential implementation was significantly more (by a factor or 2 or greater) than the whole domain solution. Larger magnitudes of r required additional computational time. Five was the minimum number of future times that could be used, which represents a dimensionless time based on the sensor depth of $t_e^+ = 0.3$. Fewer than five future steps, or more importantly a dimensionless time of 0.3, results in the estimated heat flux being biased low. The additional computational time required and minimum number of future time steps for the sequential implementation are explained by examining the characteristics of the gradient method near the end of the time interval.

For illustrative purposes, consider that the steepest descent method is the iterative search method used. In this case the search direction is (the negative of) the gradient, which is related to the adjoint function. The heat flux at iteration $n + 1$ is

$$q^{n+1}(\boldsymbol{r}, t) = q^{n}(\boldsymbol{r}, t) - \hat{\rho}^{n} p^{n}(\underline{r}, t), \boldsymbol{r} \ni \Gamma_4 \tag{5-4.4}$$

For the steepest descent method this becomes

$$q^{n+1}(\boldsymbol{r}, t) = q^{n}(\boldsymbol{r}, t) - \hat{\rho}^{n} \nabla J(\boldsymbol{r}, t), \boldsymbol{r} \ni \Gamma_4 \tag{5-4.5}$$

Substituting for the gradient from the relationship developed for the adjoint function, gives

$$q^{n+1}(\boldsymbol{r}, t) = q^{n}(\boldsymbol{r}, t) - \hat{\rho}^{n} \{ \psi(\boldsymbol{r}, t) + \alpha_T [q^{n}(\boldsymbol{r}, t) - q_{pri}(\boldsymbol{r}, t)] \}, \boldsymbol{r} \ni \Gamma_4 \tag{5-4.6}$$

Recalling that the adjoint function is prescribed to be zero at the final time, equation (4-6.21d), equation (5-4.6) shows that updates to the heat flux approach zero at the final time. Consequently, the estimated heat flux near the final time is biased. If no prior information is used, $q_{pri}(\boldsymbol{r}, t) = 0$, the estimated heat flux at the final time is approximately (the difference is the Tikhonov regularization term) the same as the initial guess $(n = 0)$, $q^{n+1}(\boldsymbol{r}, t_{m+r-1}) \approx q^{0}(\boldsymbol{r}, t_{m+r-1})$. For a zero initial guess the estimated value at the final time is identically zero, $q^{n+1}(\boldsymbol{r}, t_{m+r-1}) = 0$.

It is not unreasonable to specify that the flux components near the final time approach zero. Nor is it unreasonable to specify that the adjoint function be zero at the final time. Very little information is available concerning the flux components near the final times. Due to the lagging effect of the temperature response at the senor location to variations in the surface heat flux, there is not time enough for information about the components near the final times to reach the sensor. The magnitude of the lagging effect depends on the dimensionless time (based on the sensor depth). For the same reason, the adjoint function, which is shown to be closely related to the gradient, is insensitive to the components near the end of the time interval. Appropriately, it is specified as zero there to simplify its computation.

The inherent difficulty of estimating the heat flux near the end of the time domain is more influential for the sequential implementation because a smaller number of time steps are considered. As stated previously, for sequential intervals shorter than a dimensionless time of 0.3 (five steps for these cases) results in biasing of the estimated heat flux. At the threshold of 0.3, the response at the sensor and sensitivity is large enough such that the estimated heat flux is not biased at the first time step of the sequential interval (the one retained for a sequential interval). Components beyond the first time step are biased due to the insensitivity of the temperature to these components.

An anticipated benefit of a sequential implementation is an improvement in the computational efficiency. The expected improvement is based on the premise that after the first sequential interval ($t_0 < t < t_0 + r\Delta t$) an accurate initial guess for the estimated heat flux is available from the previous sequential interval. With an accurate initial guess it was expected that few iterations, possibly one, would be required to converge after the first sequential interval. Computational savings may not be realized for the one-dimensional problem because the conjugate gradient method is quite efficient. Results indicate that approximately the same number of iterations are required for all sequential intervals. A result that indicates the conjugate gradient search method is insensitive to the initial estimate. With a seemingly accurate initial estimate, convergence is expected within a couple of iterations, especially for the one-dimensional problem and should improve after the first sequential interval. This was not realized, the reason is discussed next.

The computational time required for the whole domain approach was 50-90% less than the time required for a sequential implementation for r=5, see Table 5-1. As more future time steps were considered, the computational time increases significantly, nearly

doubling for an increase from $r=5$ to $r=8$. Additional iterations, which in turn increases the computational time, are required for the sequential implementation because of the biasing in the estimated heat flux near the end of the sequential time interval. The biasing of the estimates to zero (or a prescribed constant) results from the definition of the adjoint function, which is prescribed to be zero at the final time. The sequential implementation accentuates this effect, which was not expected to have such a significant effect. This was not expected to be significant because only data at the first time step is checked for the convergence. What was not realized was that in a sequential interval, the estimates at the end of the time interval influence the estimates at the beginning of the time interval. Furthermore, predicting the effect of the biasing is a difficult proposition. Its influence depends on the variation of the (unknown) heat flux. Such an effect is difficult to predict or anticipate.

Examining the estimates at each iteration for a sequential interval gives insight to this effect. Estimated values for the triangular heat flux at each iteration for the sequential interval beginning at $t_e^+ = 0.12$ are shown in Figure 5-5a, b, and c, for r-values of 5, 8 and 10, respectively. For $r=5$ in Figure 5-5a the initial estimate ($n = 0$), set from values at the previous sequential interval, is inaccurate. Biasing of the estimated heat flux resulted in a 40% error in this component during the previous sequential interval. At larger magnitudes of r in Figure 5-5b and c, the effect at the beginning of the sequential interval is less pronounced. However, the estimate at the first time step, which is the component retained for a sequential interval, varies with iteration. For $r=10$ the converged estimate (at n=4) for the first component varies only 2-3% compared to the initial estimate (n=0). The first component varies 10-30% while iterating (n=1 and 2). Variations in the estimates are caused

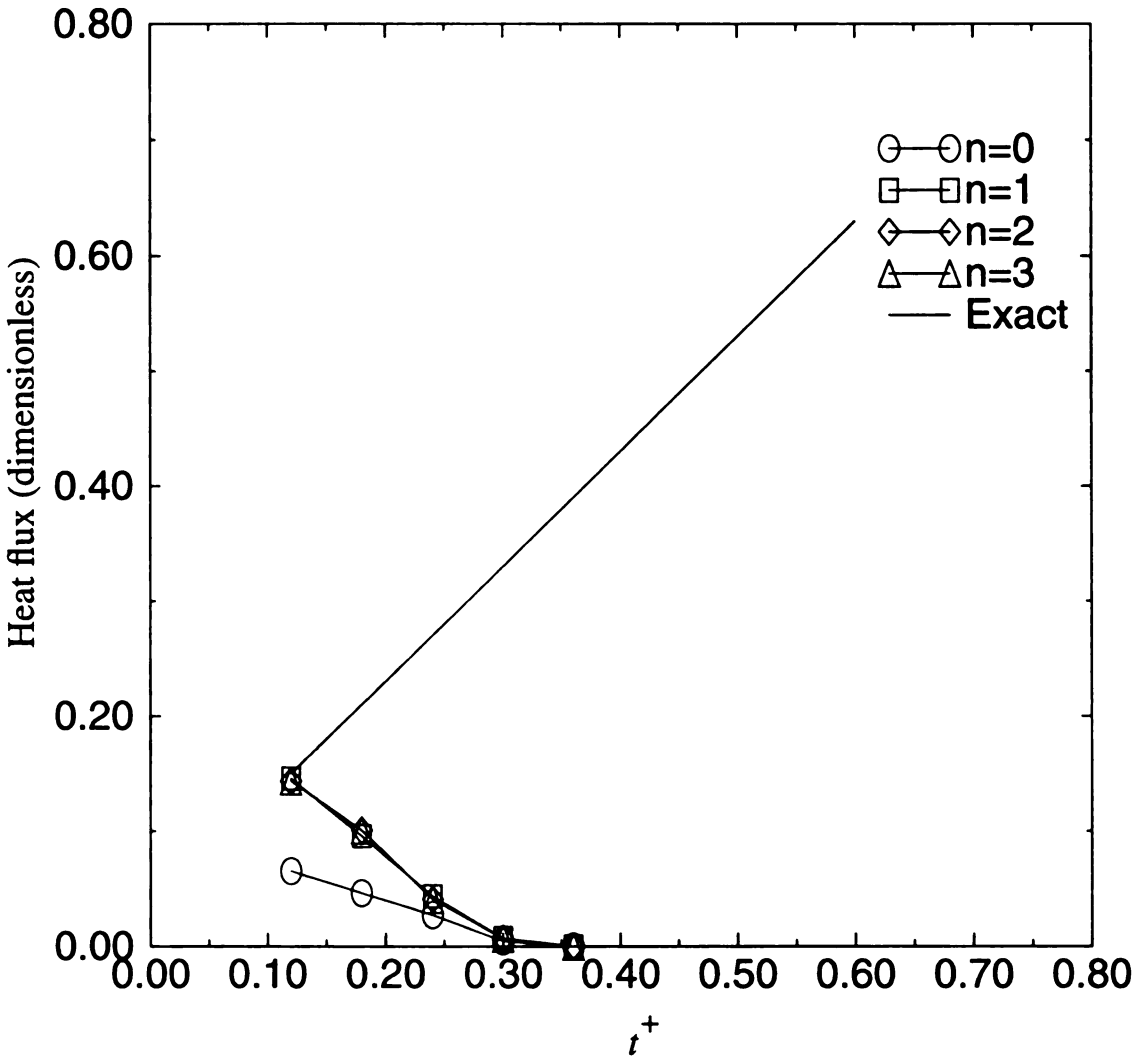

Figure 5-5a Estimated one-dimensional triangular heat flux with no measurement errors for sequential interval beginning at time 0.12 for $r = 5$

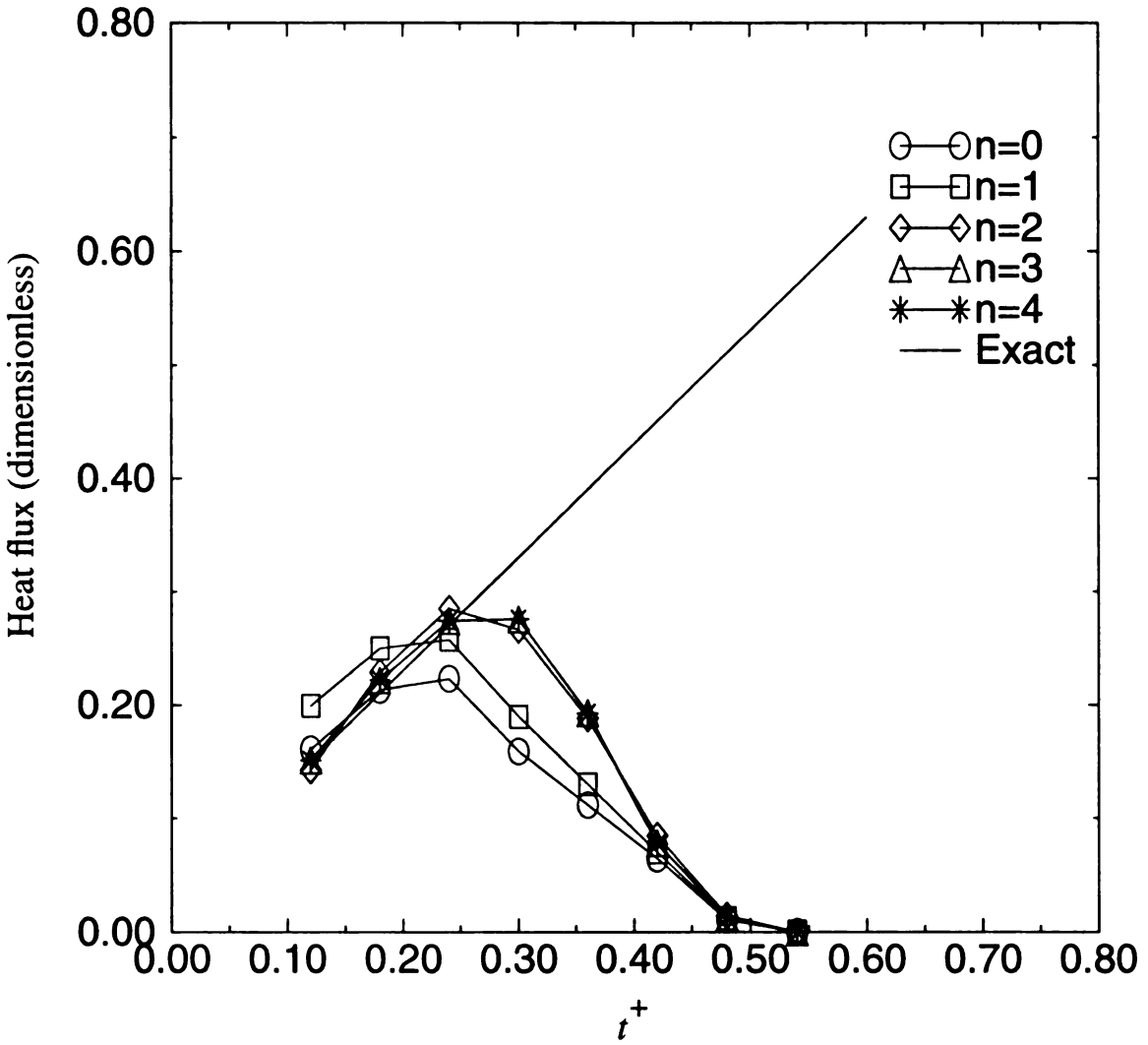

Figure 5-5b Estimated one-dimensional triangular heat flux with no measurement errors for sequential interval beginning at time 0.12 for $r = 8$

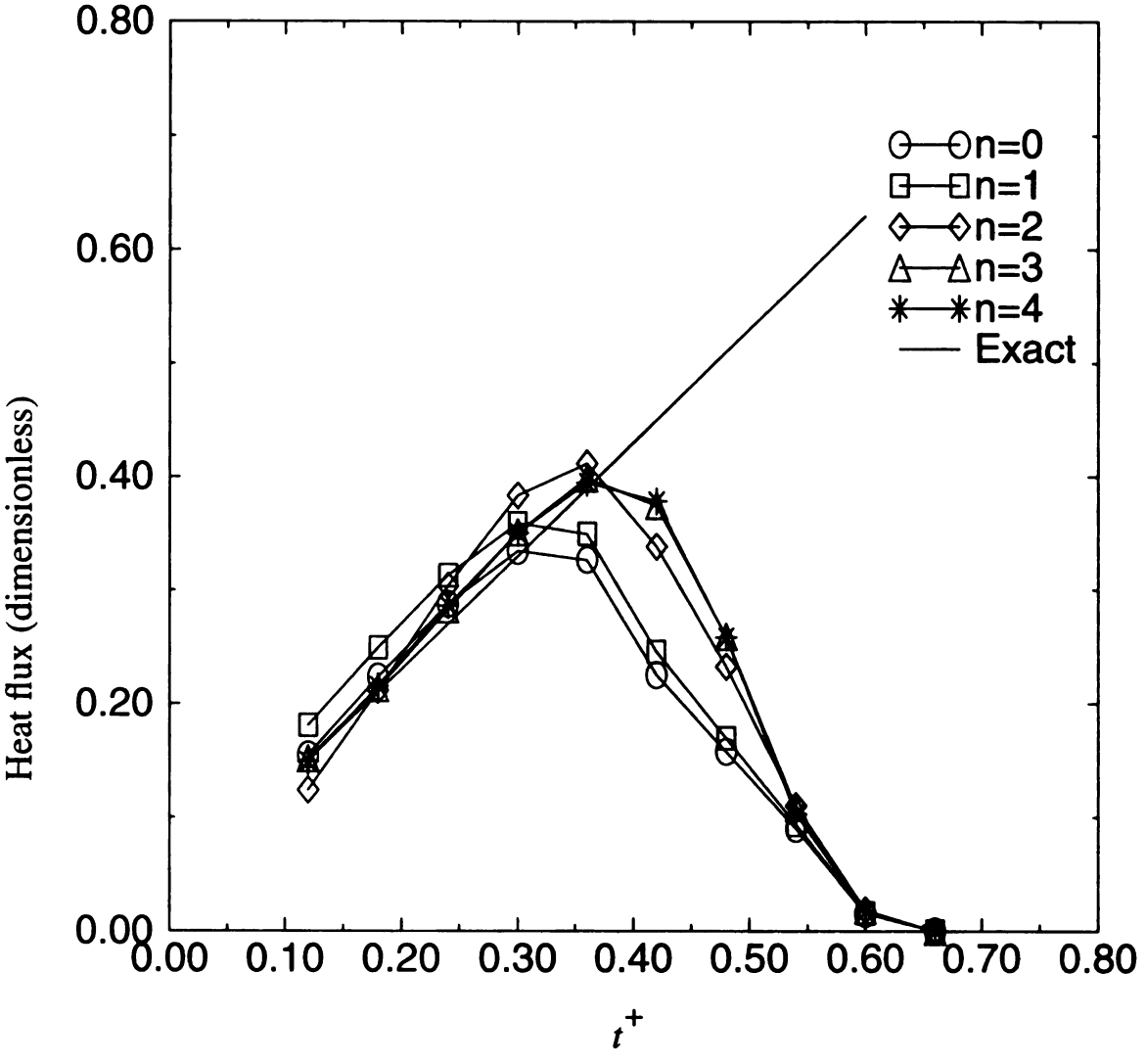

Figure 5-5c Estimated one-dimensional triangular heat flux with no measurement errors for sequential interval beginning at time 0.12 for $r = 10$

by the biasing at the end of the time region influencing estimates throughout the entire time region. In particular, estimates four to five time steps from the end (within a dimensionless time of 0.3) have the largest change, and hence the most influence on the required number of iterations. These components, not the one at the end of the interval, are the difficult ones. There is not enough sensitivity to estimate these component accurately, but there is enough to cause them to vary. Similar results were seen when estimating a constant heat flux.

Estimating the heat flux with exact data has indicated that a sequential implementation gives estimates within 5% (relative to maximum flux) of the whole domain method. Computational time required for the sequential solution was significantly greater. Computational time is 50-90% greater than the whole domain, and increases depending on the magnitude of r. Additional computational time is required because the sequential implementation is plagued by the inherent biasing of the components near the end of the time interval. This issue is addressed later by introducing some functional forms (function specification) over the sequential interval to control this effect.

5-4.2 Corrupted Data (Measurement Errors)

An important issue when investigating methods for solving the IHCP is the effect of measurement errors on the solution. Methods that are typically insensitive to measurement errors do so at the cost of introducing bias in the estimates. Conversely, methods that are unbiased or have a small bias, are typically sensitive to measurement errors. These conflicting objectives, minimal bias and sensitivity to measurement errors, are further discussed later. The one-dimensional simulated test cases were evaluated again after adding

random measurement errors to the experimental data. Only errors in the measured temperature are investigated. Errors have standard statistical assumptions and are described in equation (5-4.1).

Estimation of the triangular, step, and sinusoidal heat flux with measurement errors added to the data are shown in Figure 5-6, 5-7, and 5-8, respectively. Results from the

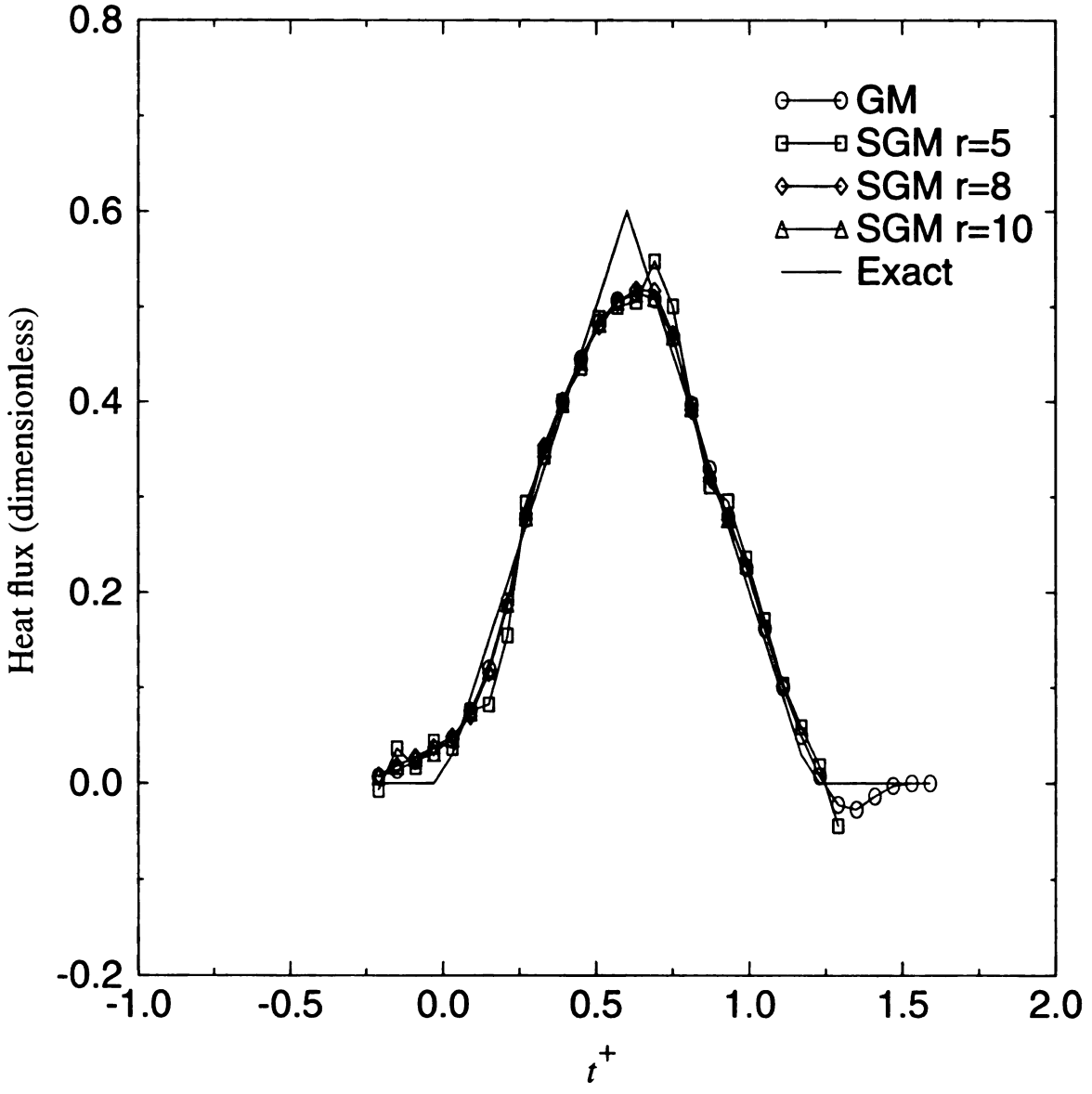

Figure 5-6 Estimated heat flux for one-dimensional triangular test case with measurement errors

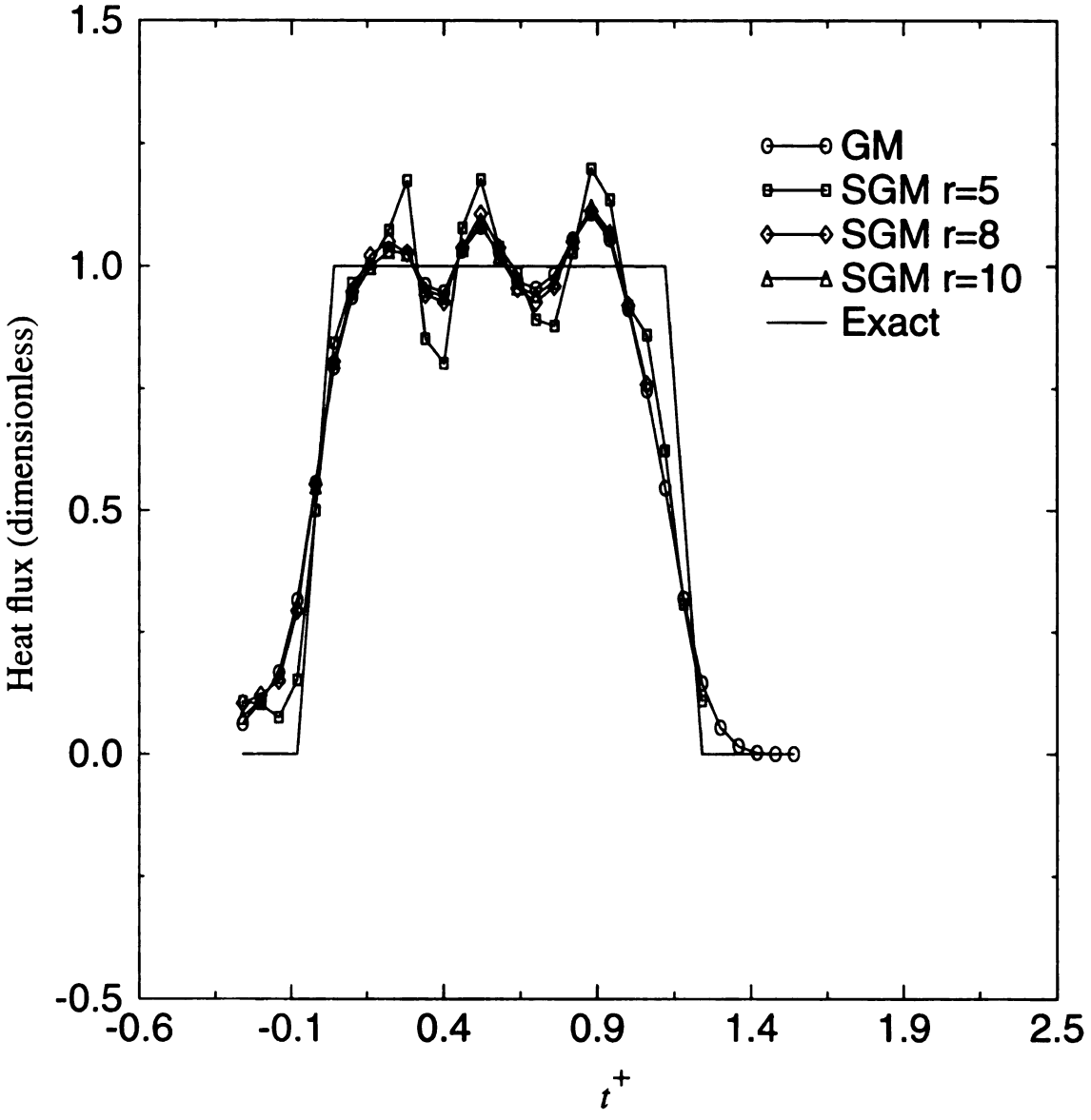

Figure 5-7 Estimated heat flux for one-dimensional step test case with measurement errors

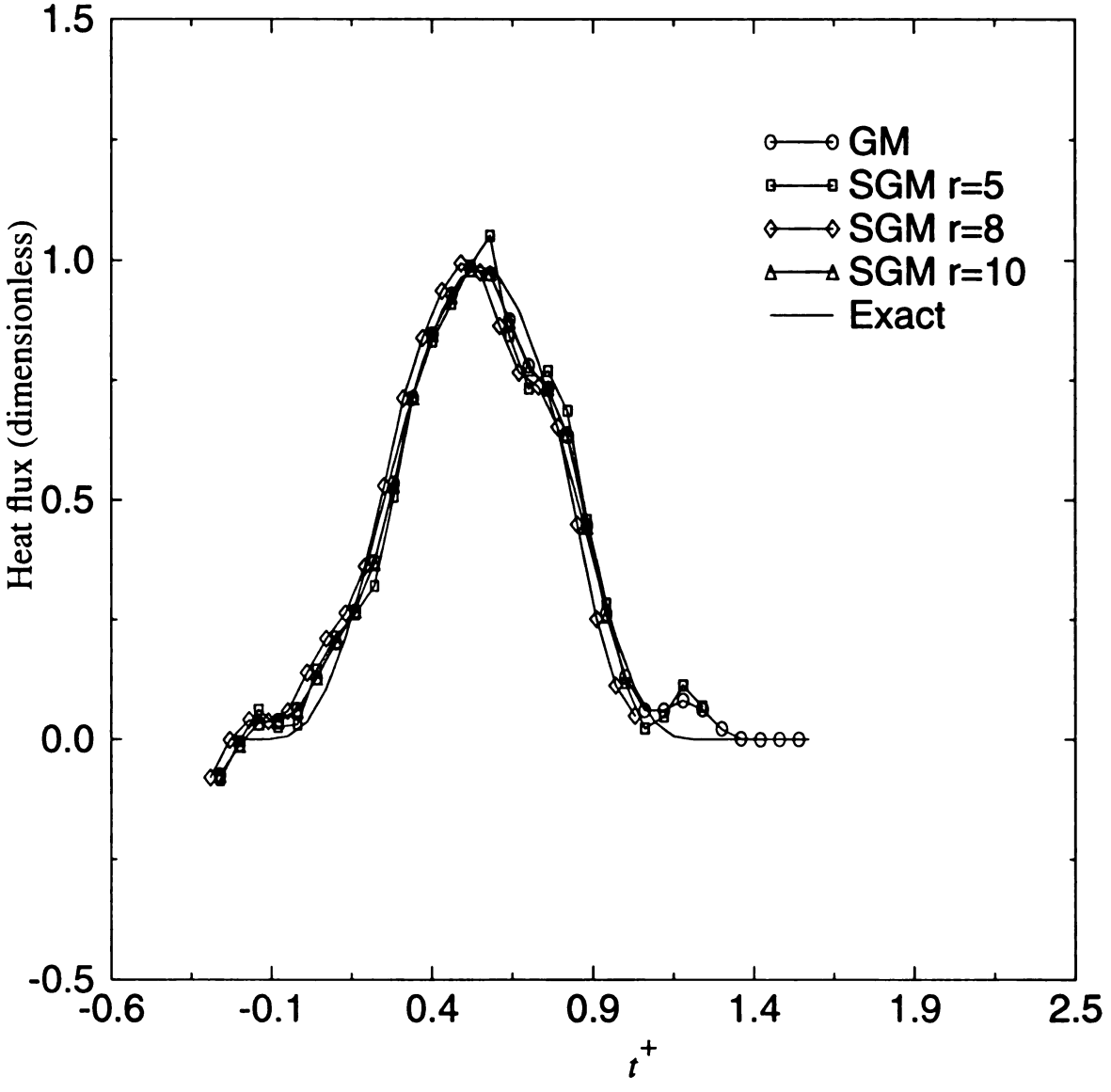

Figure 5-8 Estimated heat flux for one-dimensional sinusoidal test case with measurement errors

Table 5-2 Estimation results for simulated data corrupted with errors

Method	Analysis domain	Tikhonov α_T	Iterations		Comp time (sec)	S_Y $(°C)$	$\hat{\sigma}_{S_e}$ W/m^2
			total	per seq int			
Triangular Flux ($\sigma = 0.0036°C$)							
GM	whole	0.0028	6	-	1.84	3.63 E-03	0.034
SGM	r = 5	0.0021	77	2.9	3.48	3.65 E-03	0.050
SGM	r = 8	0.0019	91	4.0	6.95	3.64 E-03	0.040
SGM	r = 10	0.0026	88	4.2	8.50	3.62 E-03	0.039
Step Flux ($\sigma = 0.012°C$)							
GM	whole	0.0033	7	-	2.06	1.23 E-02	0.139
SGM	r = 5	0.0021	76	2.9	3.43	1.25 E-02	0.147
SGM	r = 8	0.0026	87	3.8	6.66	1.24 E-02	0.119
SGM	r = 10	0.0030	82	3.9	7.74	1.23 E-02	0.101
Sinusoidal Flux ($\sigma = 0.006°C$)							
GM	whole	0.0019	7	-	2.15	6.19 E-03	0.061
SGM	r = 5	0.0016	76	2.9	3.42	6.19 E-03	0.088
SGM	r = 8	0.0015	91	4.0	6.91	6.19 E-03	0.071
SGM	r = 10	0.0019	92	4.4	8.88	6.19 E-03	0.070

analysis are given in Table 5-2. The tabulated results are similar to that presented for the analysis with exact data. The type of analysis, whole domain (GM) or sequential (SGM), Tikhonov parameter, number of iterations, computational time, and temperature and heat flux errors are given in the table. In this case, which has measurement errors, the error in the estimated heat flux represents an error due to bias in the algorithm and the influence of measurement errors. This error is defined as the mean-squared error. The computation of

this error is identical to computation of the previous error in heat flux; however, the heat flux is estimated with random errors present in the measurements

$$\hat{\sigma}_{S_e} = \left\{ \frac{1}{P(N-1)} \sum_{k=1}^{P} \sum_{i=1}^{N} [q(r_k, t_i) - \hat{q}_e(r_k, t_i)]^2 \right\}^{\frac{1}{2}} \tag{5-4.7}$$

where $\hat{q}_e$ is the estimated heat flux with measurement errors in the temperature.

The residual principle was used to select the magnitude of the Tikhonov regularization parameter. As stated in the principle, the sum-of-squares function should be reduced to the expected level. Since random errors are used, this is specified as the standard deviation of the measurement errors.

The analysis with measurement errors, as expected, demonstrates similar computational aspects as the analysis without measurement errors, requiring significantly more time for the sequential method. It also showed that the whole domain method was superior to the sequential implementation in the accuracy of the estimated heat flux. Errors in the estimated flux were up to 50% less, depending on the magnitude of r, and were largest for smaller magnitudes of r. (Error in the estimated step heat flux was less for r-values of eight and ten; however, this did not include the step down in the heat flux because this region was within r steps of the final time.) These results show that, similar to the function specification method, the sequential gradient method requires a proper selection of r. However, it further shows that selecting a magnitude of r and the Tikhonov parameter (r, α_T), such that the residual principle is met, does not insure optimum results. Improved results may be obtained with another set of parameters. For smaller magnitudes of r the sequential method is more sensitive to measurement errors, but the method reduces α_T to meet the

residual principle. Although the whole domain method provides a more accurate estimate, the sequential method is competitive for a proper selection of *r*. If *r* is made large enough, the estimates are independent of *r* and are the same for both the sequential and whole domain solutions.

Quantifying the results of an estimation are discussed in Beck et al., (1985) and Scott and Beck (1989). The errors suggested for quantifying the results of an estimation are the deterministic error D and the mean-squared error S_e. These errors provide insight into the characteristics of an estimation algorithm. The errors are computed in equation (5-4.3) and (5-4.7) and are tabulated in Tables 5-1 and 5-2. For the deterministic error the heat flux is estimated with no measurement errors, while for the mean-squared error the heat flux is estimated with random errors in the measurements.

The deterministic errors, which show the bias of an algorithm, are smaller for the sequential approach for the *r=5*. The deterministic bias, in the final column of Table 5-1, is smaller because α_T is smaller for all three cases for *r=5*. Since there is less regularization the solution can more quickly respond to changes in the heat flux. However, as *r* increases (and α_T increases) the deterministic bias for the SGM becomes larger, and equals or exceeds the whole domain value. The mean-squared error, which can be compared to the deterministic error to determine the sensitivity to measurement errors, is exclusively better for a whole domain solution. The mean-squared error is shown in the final column of Table 5-2. A sequential method permits the Tikhonov parameter to be smaller at low *r*-values, however, this is at the cost of an increased sensitivity to measurement errors, as shown by a larger mean-squared error at these *r*-values. As *r* increases the SGM becomes less sensitive to measurement errors, of course in the limit the SGM and GM are the same.

Although the SGM provides comparable results to the GM, the computational requirements are significantly greater. A 100% (or more) increase in the computational time is typical for a sequential implementation compared to a whole domain solution. The increase in computational time is a direct consequence of the sequential implementation (of length r-steps) requiring approximately half as many iterations for each sequential interval as the whole domain requires for a complete solution. Since these results are for the one-dimensional problem, when the methods are extended to two-dimensions the requirements for the sequential implementation might be greater in comparison to the whole domain approach. As demonstrated previously, the additional computational requirements are caused by the inability to estimate components near the end of the sequential interval.

Several approach were investigated to improve the computational requirements of the sequential implementation. It was clear from observing the results during a sequential interval (see Figure 5-5) that the variation in components near the end of the interval result in an increased number of iterations. If these components over the end of the sequential interval could be controlled, or anticipated in their response, improvement in computational requirements is possible. Note that the components in the range 4-5 steps from the end of the interval (a dimensionless time of 0.25 to 0.3) are troublesome. On either side of these components the response of the heat flux is understood.

Approaches to improve the computational efficiency of the sequential method looked at three aspects of the sequential implementation. First is the setting of the initial condition for a sequential interval. Next, was using regularization to control the variation of certain components in a sequential interval. Lastly, was the use of prescribed functions over the

sequential interval, similar to the function specification method. As it turned out, only the final approach, using function specification over the sequential interval significantly improved the computational efficiency. Much was learned concerning the method, however, and is described below.

Setting the initial condition for the subsequent sequential interval, from the previous interval, has all the required information except for I-components, where I is the number of components retained on time for a sequential interval. Initially, all values from the past interval were carried to the next interval then the final I-values were specified to be zero. But it was noticed that the values near the end of the interval did not change with sequential interval. Another procedure was used. Estimates from the previous interval were used from the beginning and end of the sequential interval. The procedure is shown graphically in Figure 5-9. For a specified number of time steps, m_{end} (typically $m_{end} = 4$) from the end of the interval, the initial values were set from the previous interval

$$q^0(\boldsymbol{r}, t) = q^{Nconv}(\boldsymbol{r}, t - I\Delta t) \quad , t_{m+r-1-m_{end}+I} \le t \le t_{m+r-1} \tag{5-4.8}$$

where q^{Nconv} is the heat flux estimated at the previous sequential interval and q^0 is the initial estimate for the next interval. Equation (5-4.8) specifies that the initial values at the end of the sequential interval should be the same as they were at the end of the previous sequential interval. The components are shifted I-values in time because the time interval advances I-values for the next sequential interval. Initial values at the beginning of the time interval are specified directly from the previous interval

$$q^0(\boldsymbol{r}, t) = q^{Nconv}(\boldsymbol{r}, t) \quad , t_{m-1+I} \le t \le t_{m+r-1-m_{end}} \tag{5-4.9}$$

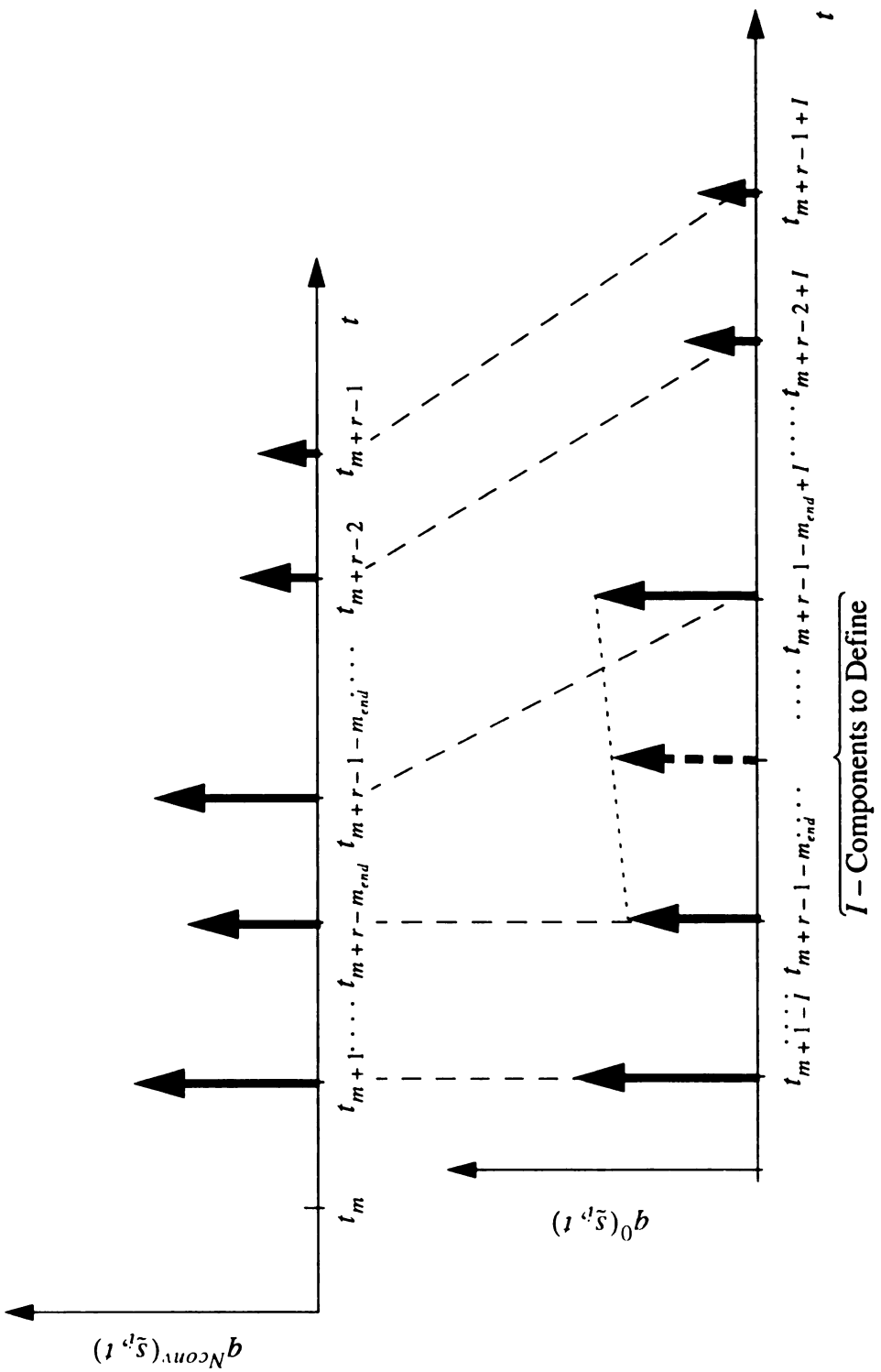

Figure 5-9 Procedure for specifying the initial condition using converged estimates from the previous sequential interval

This leaves I-values (where I is the number of retained components on time) to be specified, which are computed using linear interpolation to join the two previously defined regions.

Unfortunately, accurately specifying the initial condition from the previous interval was not causing the increased computations. Computational requirements were unchanged using the procedure outlined for setting the initial estimated. Rather, it was understanding that the estimated heat flux in the previous sequential interval was not as accurate as anticipated, particularly components about 4-5 steps (or $t_e^+ = 0.3$) from the end of a sequential interval. These components vary significantly from one sequential interval to the next, which influences other components in the interval.

The results in Figure 5-5a, b, and c show that the initial condition was not as accurate as believed. Furthermore, the components that cause the most difficulty in the sequential estimation are the last 4-5 components (covering the final 0.3 in dimensionless time of the interval). Consequently, regularization was used to attempt to control the change in these components. The Tikhonov regularization parameter was specified to be a function of time, with magnitudes larger near the end of the sequential interval. The larger regularization parameter drives the estimated heat flux to zero. This approach did eliminate changes in the component near the end of the sequential. But, the changes that would have occurred in these component migrated to other components. In retrospect this should have been anticipated, since the solution for the heat flux should conserve the total energy (for a specified r-value), by forcing some components to be zero (or a constant), other components will accommodate to conserve the total energy. Computational aspects were not improved.

A positive aspect of the gradient methods is their function estimation basis. The difficulties encountered in the sequential implementation, however, are due to the attempt to estimate a function over the sequential interval, even though, only one component of the function is typically retained. A final approach to reduce the computational requirements is to constrain the heat flux over the sequential interval so that not as much computational effort is needed to estimated all components on a sequential interval. Fewer parameters are estimated instead of a function. Specifying several functional forms over the sequential interval were tried: cubic, parabolic, linear, and constant. Additional constraints were imposed for the higher order functions, such as zero slope or zero second derivative at the end of the sequential interval, as required. Prescribing a single function over the sequential interval did not improve the computational aspects when higher order functions were used. However, specifying the heat flux be constant over the sequential interval did improve computational efficiency significantly.

The triangular heat flux case was re-evaluated using function specification over the sequential interval. Herein, this method is referred to as the sequential function specification gradient method (SFSGM). Maintaining the heat flux constant over the sequential interval stabilizes the problem and the Tikhonov regularization parameter is set to zero.

The results for the exact data are shown in Table 5-3 for the triangular heat flux using the function specification assumption; graphical results are not shown. The accuracy of the estimated heat flux is comparable to the whole domain. A direct comparison is not made because the Residual principle is not met by all r-values. The magnitude of the sum-of-squares error suggest an r between 4 and 5. In this range the error in the estimated heat flux is comparable, and more importantly computational requirements are reduced. For

Table 5-3 Estimation results for prescribing a constant heat flux over the sequential interval

Method	Analysis domain	Tikhonov α_T	Iterations		Comp time (sec)	S_Y $(°C)$	$\hat{\sigma}_D$ or $\hat{\sigma}_{S_t}$ W/m^2
			total	per seq int			
Triangular Flux ($\sigma = 0.0°C$)							
GM	whole	0.001	7	-	2.14	8.59 E-04	0.0094
SFSGM	r = 3	0.0	51	1.8	1.08	9.65 E-05	0.0054
SFSGM	r = 4	0.0	49	1.8	1.47	6.07 E-04	0.0052
SFSGM	r = 5	0.0	48	1.9	1.90	1.89 E-03	0.014
SFSGM	r = 6	0.0	48	1.9	2.24	9.13 E-04	0.025
Triangular Flux ($\sigma = 0.0036°C$)							
GM	whole	0.0028	6	-	1.84	3.63 E-03	0.034
SFSGM	r = 4	0.0	54	2.0	1.62	2.52 E-03	0.096
SFSGM	r = 5	0.0	50	1.9	1.98	3.27 E-03	0.039
SFSGM	r = 6	0.0	50	2.0	2.38	4.99 E-03	0.040
SFSGM	r = 8	0.0	46	2.0	2.93	1.07 E-02	0.048

r=5, using the function specification requirement (SFSGM) the computational time is reduced by nearly 50% compared to the standard SGM; computational time is 10% less than a whole domain solution.

The heat flux estimated with measurement errors added to the data is shown in Figure 5-10 when assuming the heat flux is constant over the sequential interval. Estimation results are also given in Table 5-3. With the heat flux held constant over the sequential interval the sequential implementation improves significantly in computational efficiency. Since only one components is estimated at each sequential interval, convergence is

obtained with few iterations. When the heat flux is held constant over the sequential interval, denoted SFSGM, a sequential solution is competitive with the whole domain solution.

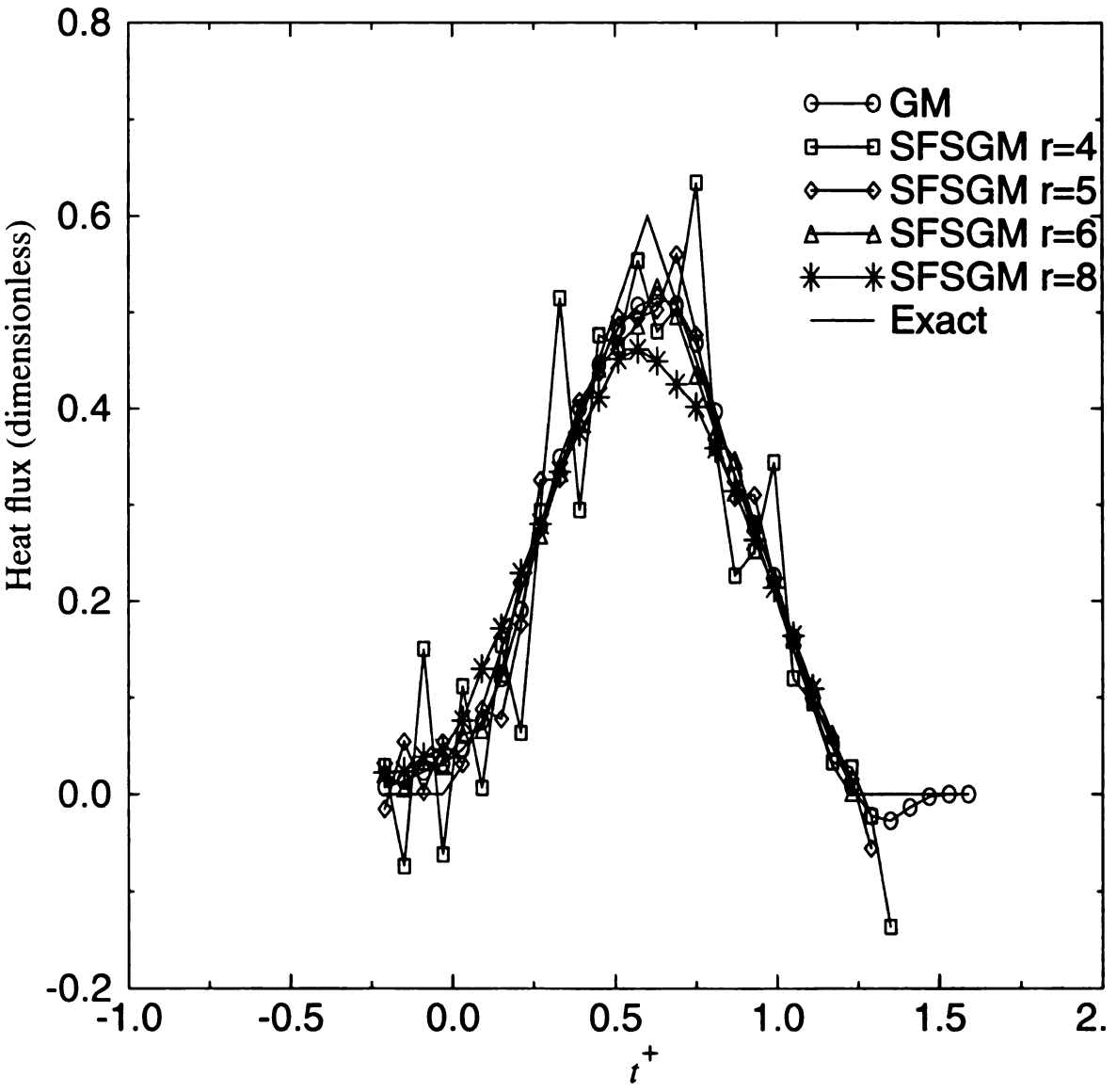

Figure 5-10 Estimated heat flux for one-dimensional triangular case with the heat flux held constant over future sequential interval

The computational time is further reduced for a sequential solution by using prior information. The prior information enters the solution in the Tikhonov regularization term of equation (4-2.4). Specifying the prior information as the initial estimate, which is set from values at the previous sequential interval, is shown to significantly improve the accuracy of the estimated heat flux as well as reduce the computational time required for a sequential solution. The use of the prior information is discussed in the next chapter. Results using prior information are not shown for the one-dimensional case.

5-4.3 Results - Experimental Measurements

Although simulated measurements provide insight to the behavior of the method, the true test is with experimental data. Gradient and iterative regularization methods are applied extensively in the literature to solve the IHCP. However, few of these investigations have applied the method to experimental data. Measured temperature and heat flux histories from the experiment to estimate the thermal conductivity are used. For this purpose, the problem is reversed and the estimated thermal properties and measured temperatures are used to recover the transient surface heat flux. Since electric heaters were used to generate the heating, the heat flux is also quantified. Consequently, a comparison between measured and estimated heat flux can be made.

The experimental apparatus is shown in Figure 2-1 and discussed in section 2-2.0. Electric heaters symmetrically heat the composite material while thermocouples measure the transient temperature. Since the experiment is symmetric, the measured power to the heaters quantifies the energy and heat flux to the specimens. In the thermal model of the experiment, shown in Figure 2-2, the thermal effects of the mica heater, and more

importantly the contact resistance, are included. An effective thermal conductivity, which represents the heater, contact resistance, and the cement used to install the thermocouples, is used to group these effects. Heat losses to the insulation are also included. Temperature measurements are made very close to the surface where the heat flux is estimated (a depth of 0.44 mm). However, the relatively low effective thermal conductivity of the mica heater/contact resistance results in the problem being more difficult than it appears. The Fourier number based on the depth of the closest sensor and thermal properties of the mica heater/contact resistance is approximately 0.06. The relative high thermal conductivity of the carbon-carbon specimen increases the difficulty of estimating the surface heat flux also. This is demonstrated by the limiting case, if the conductivity of the specimen were infinite, the sensitivity to the surface heat flux is zero and it is impossible to estimate it.

This case was also investigated by Beck et al. (1996), which among other things investigated the use of the residual principle for selecting the number of future time steps for the function specification method. Since seven reliable thermocouples were used to measure the temperature at nominally the same location, the error in the measurements could be quantified. Beck et al. suggested using the estimated standard deviation of seven measurements from the average temperature at each time. The standard deviation was approximately $0.04°C$ at the beginning and end of the experiment when the heater was not active and $0.12°C$ when the heat flux was active. A time average of this standard deviation was 0.083 C. This value was used as the level of noise for selecting the regularization parameters with the residual principle.

Beck et al. (1996) also compare several inverse methods. Function specification, Tikhonov regularization, iterative regularization, and specified functions over large time

regions using Green's functions were compared. Results indicate that estimates from the various methods are quite comparable. Although computational requirements were not the focus of the study in Beck et al. (1996), it was noted that certain methods require considerably more computational time.

Estimations of the surface heat flux are shown in Figure 5-11 for the experimental case. Several variations of the gradient method are compared to estimate the surface heat flux. Whole domain gradient method and sequential gradient method including specifying a constant flux over sequential internal are shown. A remarkable outcome of the different techniques is that about the same results is obtained. Results of the analysis are also listed in Table 5-4. Only for $r=4$ is there a significant difference between the whole domain and sequential solutions. Otherwise, the sequential solutions are as good as, or better than, a whole domain solution. The sequential solutions, denoted SGM in column one of Table 5-4 require about three iterations per sequential interval. Holding the heat flux constant over the sequential interval, denoted SFSGM in column one, requires about two iterations per sequential interval. This represents a reduction of approximately 30% in computations with SFSGM. A larger decrease in the computational time is achieved because the number of iterations required for SFSGM is actually less. Although the second iteration is started, frequently the gradient computed during the second iteration is very small (less than 1E-15) and based on the magnitude of the gradient iteration is stopped. So a full iteration is not completed (the sensitivity problem is not solved) and greater savings are realized. These additional savings increase with r.

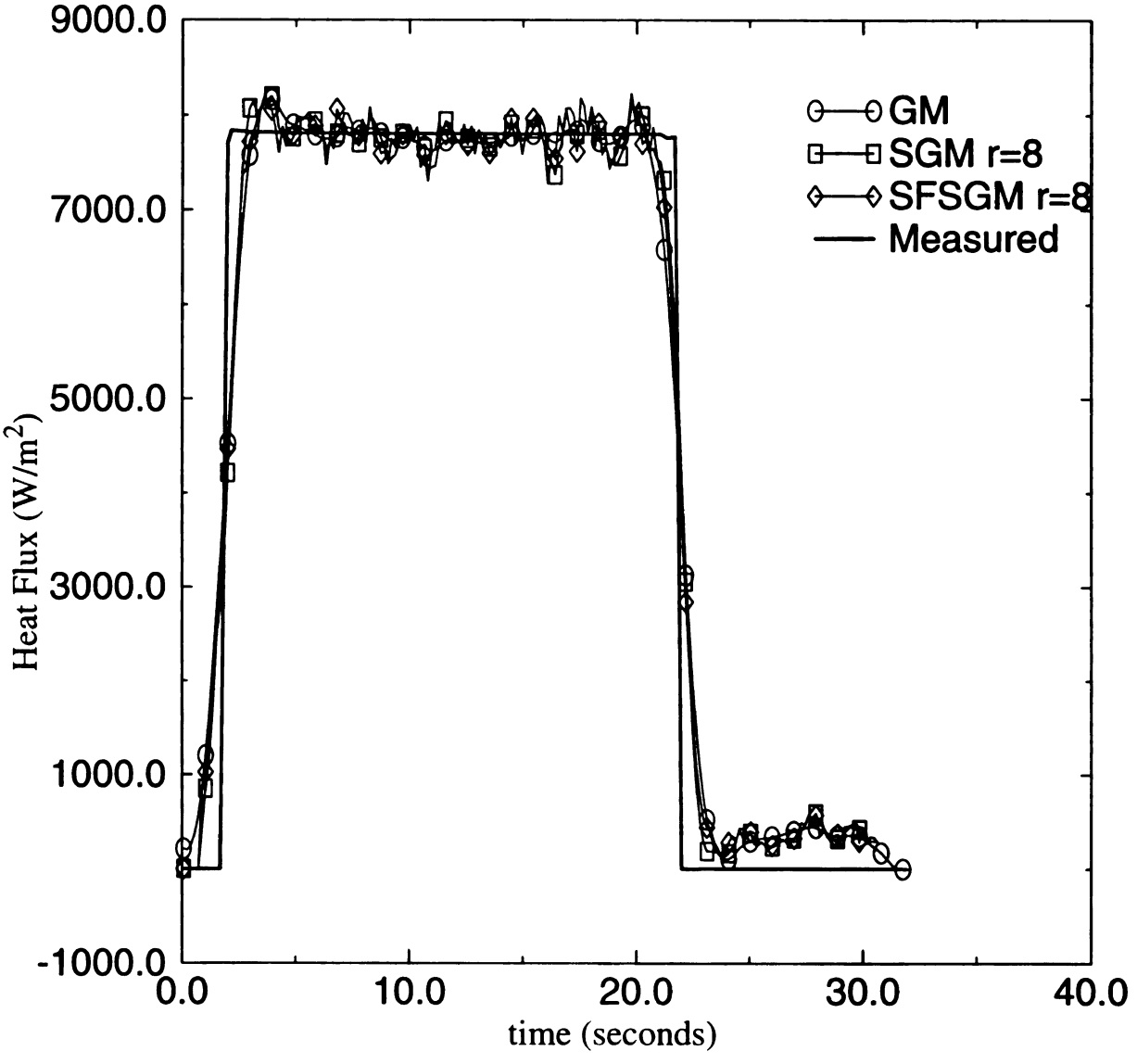

Figure 5-11 Estimate heat flux for one-dimensional experimental case 1010#30.1

Table 5-4 Estimation results for analysis of experimental case

Method	Analysis domain	Tikhonov α_T	Iterations		Comp time (sec)	S_Y (°C)	$\hat{\sigma}_q$ W/m^2
			total	per seq int			
Experiment Case 1010#30.1							
GM	whole	1.0 E-08	8	-	24.1	0.080	766
SGM	r=4	4.0 E-10	603	3.1	30.0	0.079	1400
SGM	r=6	2.0 E-09	564	2.9	47.4	0.077	754
SGM	r=8	4.5 E-09	560	2.9	64.7	0.079	716
SGM	r=10	7.0 E-09	565	2.9	80.2	0.078	726
SFSGM	r=4	0.0	382	1.9	16.5	0.039	2250
SFSGM	r=6	0.0	373	1.9	26.4	0.044	762
SFSGM	r=8	0.0	347	1.8	33.1	0.057	699
SFSGM	r=10	0.0	320	1.7	39.4	0.083	751
SFSGM	r=6	3.5 E-10	370	1.9	25.4	0.086	764
SFSGM	r=8	4.5 E-10	342	1.8	32.7	0.077	714
Experimental Case 1023 #403.1							
GM	whole	4.0 E-09	8	-	25.3	0.080	1230
SGM	r=6	9.0 E-10	578	3.0	47.0	0.084	1182
SGM	r=8	2.0 E-09	578	3.0	82.1	0.084	1141
SGM	r=10	3.0 E-09	576	3.0	82.5	0.079	1167
SFSGM	r=6	0.0	359	1.9	26.0	0.036	1234
SFSGM	r=8	0.0	342	1.8	34.2	0.052	1162
SFSGM	r=10	0.0	306	1.8	39.8	0.081	1261
SFSGM	r=6	1.5 E-10	359	1.9	26.0	0.080	1215
SFSGM	r=8	2.0 E-10	336	1.8	32.6	0.077	1180
SFSGM	r=10	1.2 E-10	307	1.6	39.9	0.084	1267

Chapter 6

APPLICATION OF THE SEQUENTIAL GRADIENT METHOD: TWO-DIMENSIONAL IHCP

6-1.0 Introduction

The solution of the two-dimensional IHCP is investigated in this chapter. Use of the sequential gradient method (SGM), possibly coupled with prescribing a functional form over the sequential interval (SFSGM) are studied. A comparison of sequential gradient methods with the standard whole domain gradient method (GM) is made. Some comparison with the standard function specification method, which does not use a gradient search method nor an adjoint equation approach, is presented. The two (or three) dimensional problem is the intended use of the proposed sequential methods. As demonstrated with the one-dimensional cases, assuming the heat flux is constant over the sequential interval improves the computational time of the sequential implementation, and makes it competitive with the whole domain approach. Additional steps may be required to improve the computational aspects for the two-dimensional problem also.

An approach similar to the one-dimensional analysis is pursued for the two-dimensional case. Several test cases for which the surface heat flux is known are studied to quantify the accuracy of the method for a two-dimensional analysis. The two-dimensional cases will demonstrate the ability to estimate spatially dependent fluxes. In addition to

simulated cases, an experimental case with a measured surface heat flux, which is two-dimensional and transient, is analyzed.

Several variations of the sequential gradient method are suggested in this chapter. Three methods are investigated. The standard whole domain gradient method (GM) solves for the heat flux with data from all measurement times. The sequential gradient method (SGM) solves for the heat flux using data from a sequential interval. The sequential function specification gradient method (SFSGM) solves for the heat flux over a sequential interval while prescribing a functional form for the heat flux on time, but allows for spatial variation. In addition, the use of prior information is suggested during the sequential solution to improve the sequential method. This is the first known application of prior information to improve a sequential solution.

The remainder of this chapter is summarized. The calculation of the simulated temperature data is discussed in the next section. Section 6-3.1 presents results for the simulated test cases with exact data. Test cases with measurement errors added to the simulated data are discussed in Section 6-3.2. An experimental case, with a measured surface heat flux is analyzed in Section 6-4.0.

6-2.0 Simulated Temperature Data

A rectangular domain of dimensions $[0, a]$ x $[0, b]$ is studied for the two-dimensional simulated cases. A schematic of the geometry is shown in Figure 6-1. One bounding surface of the two-dimensional body is assumed to have an unknown heat flux while all other surfaces are insulated. Furthermore, constant anisotropic thermal properties and a uniform initial temperature are assumed.

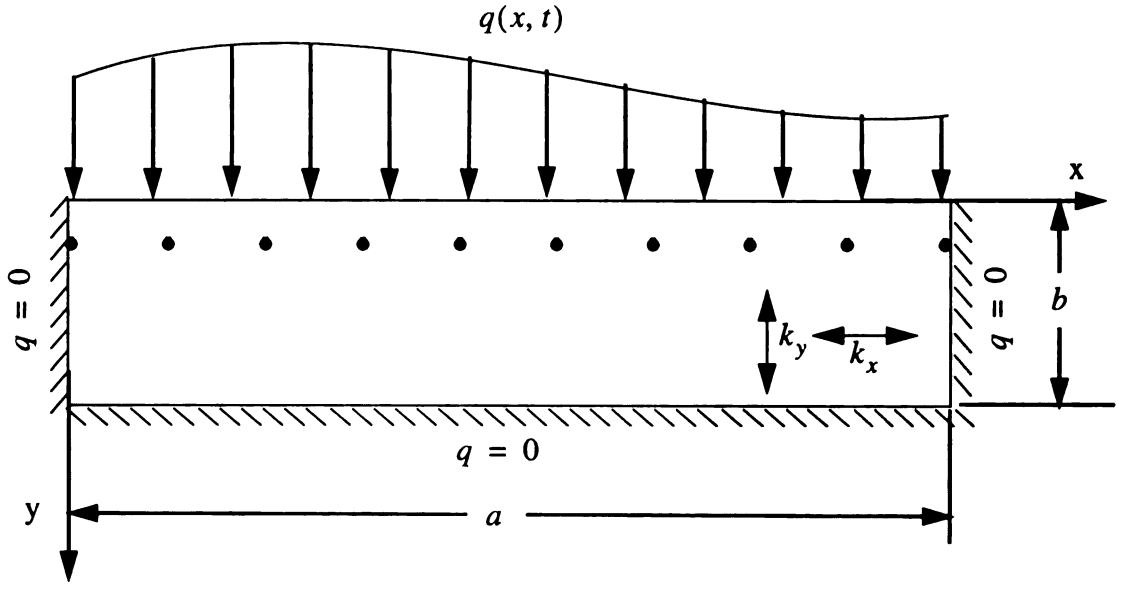

Figure 6-1 Two-dimensional geometry for simulated test cases

The problem can be mathematically written as

$$\left(\frac{b^2 k_x}{a^2 k_y}\right)\frac{\partial^2 T_i^+}{\partial x^{+2}} + \frac{\partial^2 T_i^+}{\partial y^{+2}} = \frac{\partial T_i^+}{\partial t^+} \tag{6-2.10}$$

$$-\left.\frac{\partial T_i^+}{\partial y^+}\right|_{y^+ = 0} = q_i^+(x^+, t^+) = ? \tag{6-2.11a}$$

$$\left.\frac{\partial T_i^+}{\partial y^+}\right|_{y^+ = 1} = 0 \tag{6-2.11b}$$

$$\left.\frac{\partial T_i^+}{\partial x^+}\right|_{x^+=0} = 0 \tag{6-2.11c}$$

$$\left.\frac{\partial T_i^+}{\partial x^+}\right|_{x^+=1} = 0 \tag{6-2.11d}$$

$$T_i^+(x^+, y^+, 0) = 0 \tag{6-2.11e}$$

where the following dimensionless variables were introduced

$$q_i^+ = \frac{q}{q_N} \tag{6-2.12}$$

$$T_i^+ = \frac{T_i - T_o}{(q_N b/k_y)} \tag{6-2.13}$$

$$t^+ = \frac{(k_y/\rho c)t}{b^2} \tag{6-2.14}$$

$$x^+ = \frac{x}{a} \tag{6-2.15}$$

$$y^+ = \frac{y}{b} \tag{6-2.16}$$

The subscript i indicates the prescribed heat flux. The estimation of two different prescribed heat fluxes is investigated for the two-dimensional case. A step change in heat flux on time (starting at $t^+ = 0$ and ending $t^+ = t_h^+$) and position (from $x^+ = 0$ to $x^+ = a_1$) is the first flux ($i = 1$) examined

$$q_1^+(x^+, t^+) = \begin{cases} 1 & (0 < t^+ < t_h^+), (0 \le x^+ \le a_1) \\ 0 & otherwise \end{cases} \tag{6-2.17}$$

The second flux (($i = 2$) examined also has a step change in time, but the spatial profile is triangular over the entire surface at ($y = 0$)

$$q_2^+(x^+,t^+) = \begin{cases} 2x^+ & (0<t^+<t_h^+),\left(0\le x^+\le \frac{1}{2}\right) \\ 2-2x^+ & (0<t^+<t_h^+),\left(\frac{1}{2}<x^+\le 1\right) \\ 0 & otherwise \end{cases} \tag{6-2.18}$$

Due to the complexity of obtaining analytical solutions for the two-dimensional problems, an accurate finite element code (TOPAZ2D) is used to solve for the two-dimensional temperatures. Data for the simulated cases are shown in Figure 6-2 and 6-3 for the step heat flux and triangular heat flux, respectively. Temperature data at the sensor locations and the heat flux at the surface are shown for the two cases. Both surface flux histories begin at time 0 and end at time t_h^+, which is prior to the end of the time domain, t_f^+. The temperature data are generated for eleven simulated sensor locations that are equally spaced along the x-plane at a depth of $y^+ = 0.1$. Lagging effects are similar to the one-dimensional problem. Notice that the spatial temperature profile is smoothed compared to the profile of the surface heat flux. The diffusive nature of the problem at the sensor depth makes it difficult to recover sharp spatial features.

6-3.0 2D Results - Simulated Measurements

6-3.1 Exact Data (No Measurement Errors)

A case with "exact" data is analyzed first. The dimensionless groups of interest for this geometry are $a/b = 2$ and $k_x/k_y = 1$. Measurements are available at eleven equally spaced locations ($x^+ = 0.0, 0.1. . . .,1.0$) beneath the surface of unknown heat flux at a depth of $y^+ = 0.1$. The dimensionless time step (Fourier number) based on the sensor

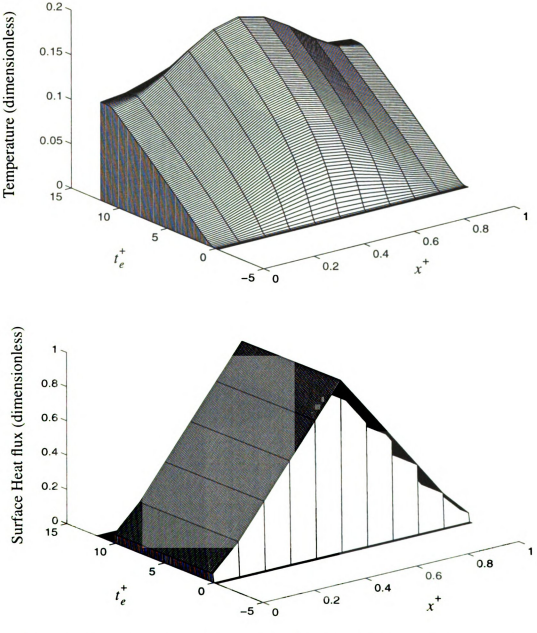

Figure 6-2 Simulated temperature and surface heat flux for a two-dimensional triangular heat flux

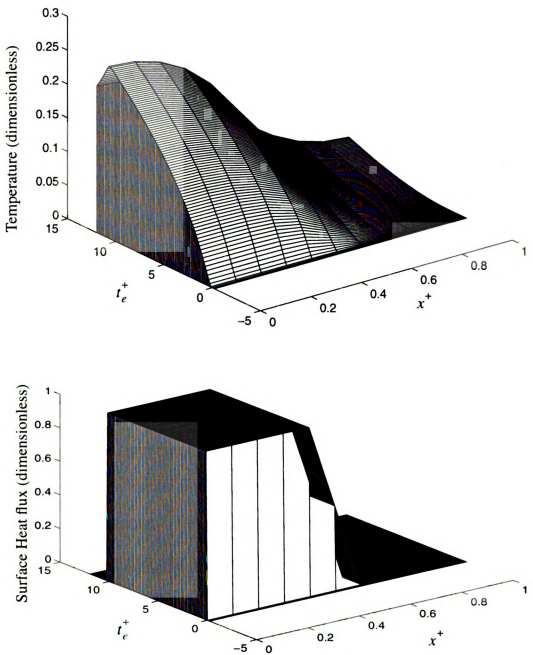

Figure 6-3 Simulated temperature and surface heat flux for a two-dimensional step heat flux

depth is $\Delta t_e^+ = 0.06$, which represents a difficult case; two-hundred time steps are considered in the analysis. "Exact" simulated temperature data are generated from the finite element solution using TOPAZ2D (Shapiro, 1986)

The geometry shown in Figure 6-1 is discretized for the numerical solution. A finite control volume mesh with eleven nodes in the x-direction and twenty-one nodes in the y-direction is used. A more coarse node spacing is specified for the x-direction. Because eleven sensors are located along this surface, eleven components of heat flux are to be estimated. It is possible to define more nodes along this surface and estimate a greater number of spatial components (discussed later). Alternately, more nodes can be defined along the surface and fewer spatial components, compared to the number of nodes, can be estimated by introducing some spatial smoothing using basis functions; see Section 4-8.0. In this study, it is not desired to impose spatial smoothing on the solution. Instead the number of nodes defined for the numerical solution are set based on the number of available sensors. Hence, eleven nodes are defined on the surface. The number of nodes is increased and more spatial components are estimated in a later analysis. Care is exercised to not have too few of nodes and incur numerical error from a coarse discretization.

The estimated surface heat flux for a whole domain solution (GM) and the sequential gradient method (SGM) with $r=6$ are shown in Figure 6-4a and b, respectively, for the triangular test case. The GM has the whole domain characteristic of over-shooting near regions where the heat flux has an abrupt change, at the beginning and ending times. The SGM reduces the effect of these characteristics. Both methods accurately estimate the surface heat flux.

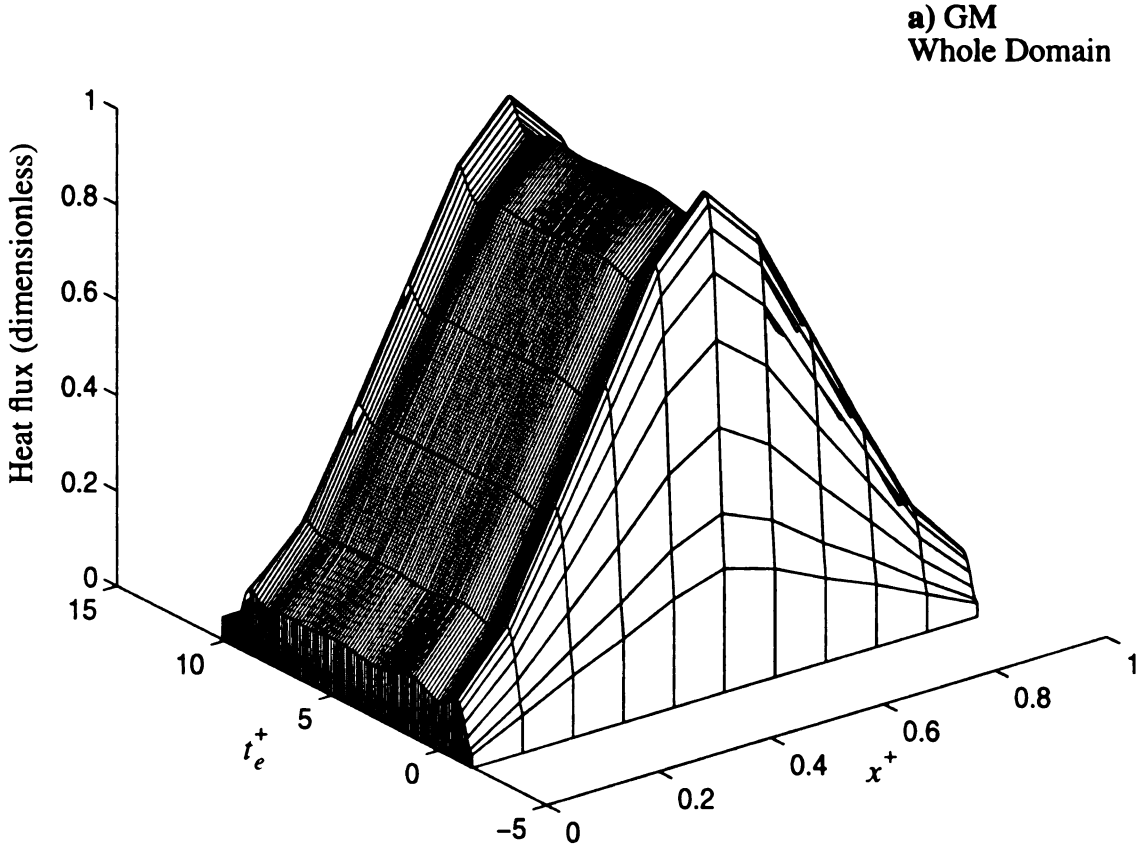

Figure 6-4a Estimated surface two-dimensional heat flux for triangular test case using data without measurement errors. Whole domain solution

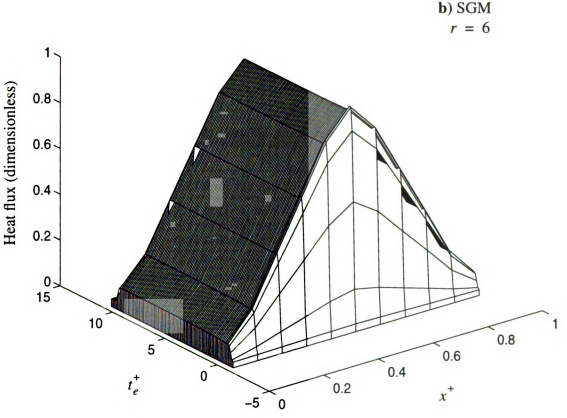

Figure 6-4b Estimated surface two-dimensional heat flux for triangular test case using data without measurement errors. Sequential solution with *r=6*

Table 6-1 Estimation results for the two-dimensional IHCP with exact simulated data

Method	Analysis domain r	Analysis domain I	Tikhonov α_T	Iterations total	Iterations per seq int	Comp time (sec)	S_Y $(°C)$	$\hat{\sigma}_D$ W/m^2
Triangular Flux (11 Components)								
GM	all	all	1.00 E-04	11	-	35.7	2.53 E-04	7.46 E-02
SGM	6	1	1.02 E-04	758	4.0	71.8	2.50 E-04	8.05 E-02
SGM	10	1	3.20 E-04	735	4.0	121.2	2.52 E-04	7.79 E-02
SFSGM	6	1	1.05 E-05	244	1.3	23.2	2.51 E-04	7.89 E-02
SFSGM	10	1	0.0	238	1.3	35.6	4.29 E-04	7.32 E-02
Step Flux (11 Components)								
GM	w	all	1.0 E-04	12	-	38.8	4.42 E-04	9.30 E-02
SGM	6	1	1.25 E-04	762	4.0	71.7	4.46 E-04	9.92 E-02
SGM	10	1	4.05 E-04	737	4.0	119.9	4.43 E-04	9.54 E-02
SFSGM	6	1	1.67 E-05	264	1.4	24.9	4.42 E-04	9.68 E-02
SFSGM	10	1	0.0	260	1.4	42.1	5.41 E-04	8.84 E-02
Triangular Flux (21 Components)								
GM	w	all	1.00 E-04	11	-	66.3	2.53 E-04	7.46 E-02
SGM	6	1	1.01 E-04	758	3.9	130.7	2.50 E-04	8.12 E-02
SGM	10	1	3.10 E-04	727	3.9	222.4	2.50 E-04	7.72 E-02
SFSGM	6	1	1.05 E-05	270	1.4	47.0	2.52 E-04	9.65 E-02
SFSGM	10	1	3.00 E-05	278	1.5	83.6	4.91 E-04	7.89 E-02

Pertinent information about the estimations with exact data are given in Table 6-1. The table lists the solution method and analysis domain, with the number of future time steps and number of components retained on time in the first three columns. Column four gives the magnitude of the Tikhonov parameter. The number of iterations, both total and

average per sequential interval are given in columns five and six. Computational time is listed in column seven. The errors in the sum-of-squares temperature and estimated heat flux (bias error) are shown in columns eight and nine. Values of $r = 6$ and $r = 10$ were studied for the number of future time steps. The Tikhonov regularization parameter was specified as 0.0001 for the whole domain solution (GM). Subsequent sequential solutions (SGM and SFSGM) varied the Tikhonov parameter to match the magnitude of the sum-of-squares, S_Y, to the level of the whole domain solution.

Estimation results with exact data for the triangular and step heat flux, given in Table 6-1, have trends similar to the one-dimensional case. A comparable heat flux to the whole domain (GM) solution is estimated with the sequential implementation (SGM), the bias error (last column of Table 6-1) is 6-8% larger for $r = 6$, but it requires approximately twice as much computational time. Increasing the r-value to ten reduces the bias error to a magnitude 2-4% larger than the GM, but requires a proportional increase in the computational time, i.e. computational time increases by $167\%(10/6)$, compared to the computational time for $r = 6$.

In the one-dimensional solution the computational aspects were improved by maintaining the heat flux constant (on time) over the future sequential interval, which is the standard function specification assumption. The same procedure was tried for the two-dimensional problem. Prescribing that the heat flux remain constant over the sequential interval (method SFSGM in Table 6-1), requires one-third the computational time of the SGM for $r = 6$, and has a bias error that is only 4-6% larger than the whole domain estimation. Improved accuracy was obtained when r was increased to ten, bias error was 2-5%

less than whole domain solution. Notice that the Tikhonov parameter was set to zero for the SFSGM with $r = 10$. Even with this parameter set to zero the sum-of-squares was not reduced to the required level. This is due to the effects of the Tikhonov parameter and the function specification approximation, which are discussed next. The SFSGM has superior computational aspects. It requires 35% less computational time than the GM for both the triangular and step test case for $r = 6$; computational requirements are comparable for $r = 10$.

One observes in Table 6-1 that the estimation with exact data requires a larger magnitude for the Tikhonov parameter when solving sequentially compared to whole domain. Since a larger magnitude of the Tikhonov parameter is used, the sequential solution is more biased than the whole domain solution, particularly near regions of variation in the heat flux. An increase in the Tikhonov parameter is expected because the shorter duration sequential problem is more ill-posed than the whole domain problem. For the one-dimensional solution, in general, a smaller Tikhonov parameter was required for the sequential solution compared to the whole domain solution, contrary to what was expected. It is believed that the one-dimensional problem required a smaller Tikhonov parameter to permit the solution algorithm the flexibility to reduce the sum-of-squares magnitude to the desired level. The reduction in the Tikhonov parameter is greater at small r-values. As r is increased the Tikhonov parameter for SGM approaches the magnitude of GM, in the one-dimensional case.

Applying the function specification approximation in the inverse solution provides significant regularization, which increases with r. As noted in Chapter 5, regularization imposes "stiffness" to the inverse solution. When maintaining the heat flux constant over

the sequential interval, considerable "stiffness" is imposed on the solution. Consequently, the Tikhonov parameter must be reduced in magnitude to permit obtaining the desired sum-of-squares magnitude, S_Y. At some level of r, the bias error becomes large enough such that even when the Tikhonov parameter is specified as zero, the sum-of-squares function can not be reduced any further. This is a result of the bias introduced when assuming the heat flux is constant over the sequential interval.

A noted benefit of the gradient method is that it is not required to specify the functional form of the unknown heat flux. Since a numerical solution is used, however, some approximation of the heat flux is required. The simplest numerical approximation of the heat flux is used, which assumes the heat flux is constant over a control surface surrounding the node. Consequently, the functional heat flux is numerically represented by P spatial components, where P is the number of nodes along the surface of the unknown heat flux. Specifying more nodes along this surface will improve the numerical accuracy of the direct problem, but requires estimating more spatial components, which may increase the difficulty of the inverse problem depending on sensor locations. A general rule is that the number of spatial components estimated should not exceed the number of sensors. Fewer spatial components of the heat flux, compared to the number nodes, can be estimated by prescribing a spatial functional form using basis functions, see Section 4-8.0. Prescribing a spatial functional form introduces regularization and helps stabilize the solution.

In the previous simulated cases, given in the first two blocks of Table 6-1, eleven nodes were defined along the x-direction and eleven spatial components were estimated. Now the triangular test case is analyzed with twenty-one nodes components on the surface and twenty-one spatial components are estimated, with eleven equally spaced sensors

along the surface. Results are given in the final block of Table 6-1. The estimated heat flux is nominally the same for the whole domain (GM); of course computational time is approximately doubled with twice as many nodes. The sequential method does not perform as well. Bias error is increased by 1% for the SGM, but increases 22% for the SFSGM with $r=6$. When estimating more spatial components than available sensors with a sequential method the spatial components between the sensor locations are biased low for $r=6$. This produces spatial oscillations in the estimated heat flux, a "zig-zag" pattern about the true flux value exists in the estimated heat flux. The oscillations are reduced by increasing the magnitude of r.

It appears that estimating more spatial components than available sensors is possible using the gradient method. At least for the case when sensors are evenly distributed along the surface it is possible. The method seems to have some spatial regularization inherent. Implementing a sequential solution degrades this characteristic for small values of r. These outcomes are influenced by the dimensionless time step based on the sensor depth, the spacing of the sensors along the surface relative to the sensor depth, and the amount of noise in the measurements, which was exact for this case.

6-3.2 Corrupted Data (Measurement Errors)

The two-dimensional test cases are analyzed with measurement errors added to the simulated temperatures. Standard statistical assumptions are used to describe the measurement errors. The errors are modeled as additive, with zero mean, constant variance, and a normal distribution. A magnitude of approximately 1% of the maximum temperature rise

was selected as the standard deviation of the measurement errors. This error corresponds to $0.0018°C$ and $0.0025°C$ for the triangular and step heat flux, respectively.

Estimation of the triangular heat flux with measurement errors is shown in Figure 6-5a for a whole domain solution and Figure 6-5b shows a sequential solution with *r=6*. The two solutions are quite different, whereas the whole domain solution is relatively smooth, the sequential solution has a significantly larger variability. It is not clear if the variability of the SGM estimated heat flux is larger on time or on space. The sequential results are certainly unacceptable in comparison to the whole domain solution for *r=6*.

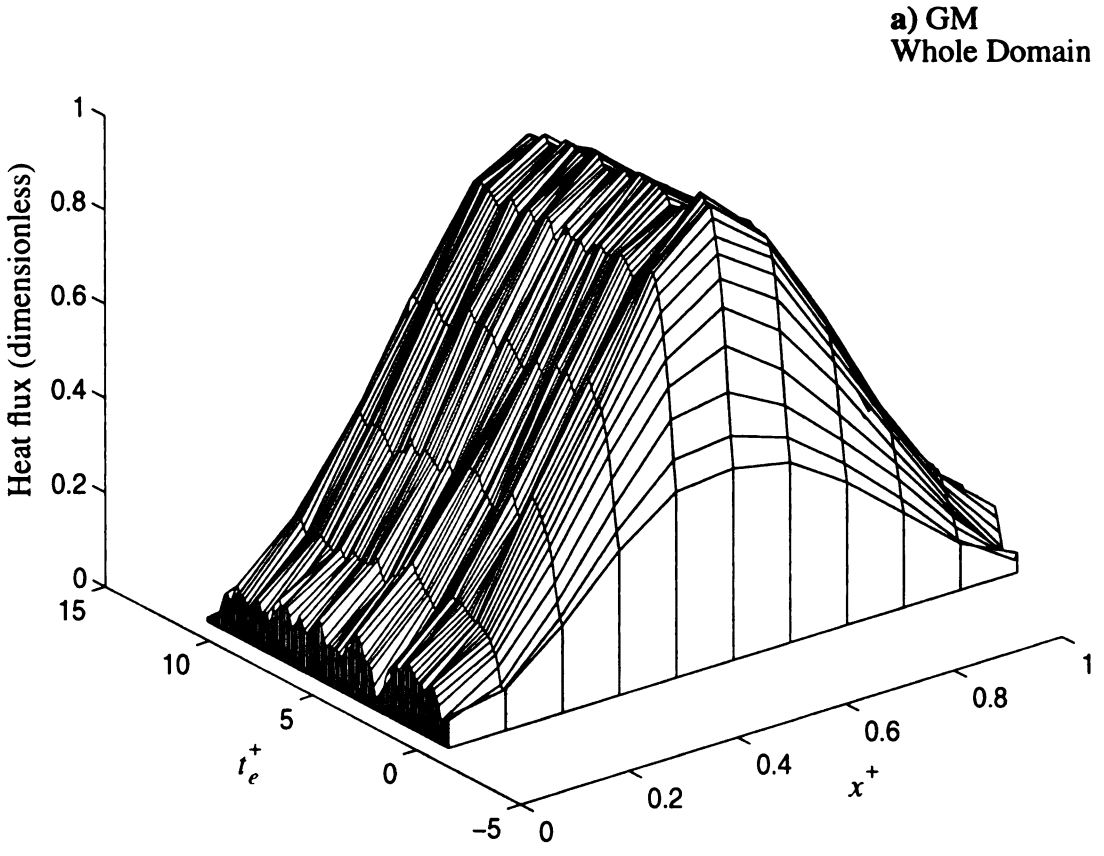

Figure 6-5a Estimated surface heat flux for triangular test case using data corrupted with measurement errors ($\sigma = 0.0018°C$). Whole domain solution.

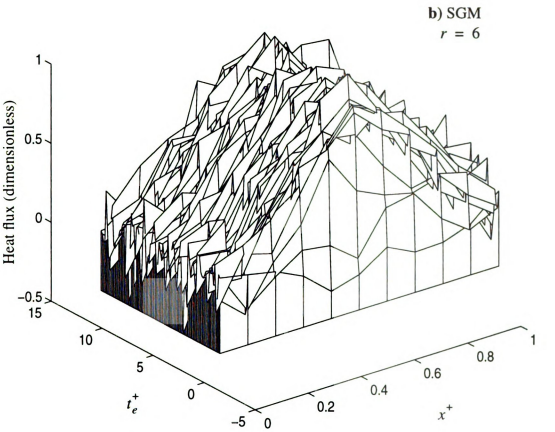

Figure 6-5b Estimated surface heat flux for triangular test case using data corrupted with measurement errors ($\sigma = 0.0018°C$). Sequential solution with *r=6*.

Table 6-2 Estimation results for two-dimensional IHCP with simulated data corrupted with random errors

Method	Analysis domain r	Analysis domain I	Tikhonov α_T	Iterations total	Iterations per seq int	Comp time (sec)	S_Y $(^\circ C)$	$\hat{\sigma}_{s_\epsilon}$ W/m^2
Triangular Flux ($\sigma = 0.0018^\circ C$) - 11 Spatial Components								
GM	all	all	1.70 E-03	9	-	31.8	1.82 E-03	8.57 E-02
SGM	6	1	2.20 E-04	764	4.0	77.8	1.81 E-03	1.36 E-01
SGM	8	1	4.50 E-04	758	4.0	96.0	1.80 E-03	1.02 E-01
SGM	10	1	7.00 E-04	746	4.0	119.0	1.80 E-03	9.19 E-02
SGM	15	1	1.25 E-03	718	4.0	173.7	1.80 E-03	8.65 E-02
SGM	20	1	1.50 E-03	759	4.3	246.9	1.80 E-03	7.53 E-02
SFSGM	6	1	5.00 E-05	767	4.0	77.1	1.81 E-03	1.57 E-01
SFSGM	8	1	8.30 E-05	769	4.1	96.3	1.80 E-03	1.12 E-01
SFSGM	10	1	1.1 E-04	761	4.1	120.2	1.80 E-03	9.71 E-02
SFSGM	15	1	9.50 E-05	693	3.8	167.2	1.87 E-03	8.97 E-02
Step Flux ($\sigma = 0.0025^\circ C$) - 11 Spatial Components								
GM	all	all	6.00 E-04	13	-	45.8	2.51 E-03	1.06 E-01
SGM	6	1	1.90 E-04	775	4.1	73.3	2.50 E-03	2.18 E-01
SGM	10	1	5.5 E-04	762	4.1	121.9	2.50 E-03	1.24 E-01
SGM	15	1	7.5 E-04	822	4.5	200.7	2.50 E-03	1.15 E-01
SGM	20	1	7.5 E-04	975	5.5	317.8	2.50 E-03	1.03 E-01
SFSGM	6	1	4.0 E-05	795	4.2	74.2	2.50 E-03	2.59 E-01
SFSGM	10	1	2.0 E-05	953	5.1	150.8	2.50 E-03	1.49 E-01
Triangular Flux ($\sigma = 0.0018^\circ C$) - 21 Spatial Components								
GM	all	all	1.70 E-03	9	-	54.7	1.84 E-03	8.50 E-02
SGM	6	1	2.20 E-03	760	4.0	137.9	1.82 E-03	1.33 E-01
SGM	15	1	1.25 E-03	718	4.0	328.2	1.82 E-03	8.44 E-02
SFSGM	6	1	5.50 E-05	786	4.1	141.6	1.82 E-03	1.65 E-01
SFSGM	15	1	9.50 E-05	693	3.8	314.4	1.88 E-03	9.29 E-02

Analysis of the triangular and step test cases with measurement errors are presented in Table 6-2. Numerical conditions similar to the exact cases were used, a dimensionless time step based on the sensor depth is $\Delta t_e^+ = 0.06$ with twenty-one nodes in the y-direction and eleven in the x-direction for the numerical solution. Data was assumed at two-hundred time steps and eleven components of the heat flux are estimated; twenty-two hundred heat flux components are estimated.

The step heat flux case was more difficult to estimate. Reproducing a step change spatially is considerably harder than the more gradual changing triangular case. Figures 6-6a and b show the whole domain and SGM for $r=15$ estimated heat flux for the step case. Estimates have more variability than the triangular test case. Tabulated results in the middle of Table 6-2 show that trends similar to the triangular case. The mean-squared error is as large as 25% of the maximum heat flux for small r-values. For the triangular case the mean-squared error did not exceed 16% of the maximum heat flux.

The whole domain (GM) approach was superior to the sequential approach (SGM and SFSGM) for both two-dimensional test cases for r less than 10. This superior performance is supported by the smaller mean-squared error, final column of Table 6-2, and the shorter computational time, column seven. The mean-squared error was 7 to 83% greater for sequential approach, compared to the whole domain approach for the triangular heat flux, depending on the choice of r. Results were worse for the step heat flux, which had a mean-squared error that was 17 to 144% (depending on r) greater for the sequential approach. Computational times were adversely affected by the sequential approach. The sequential

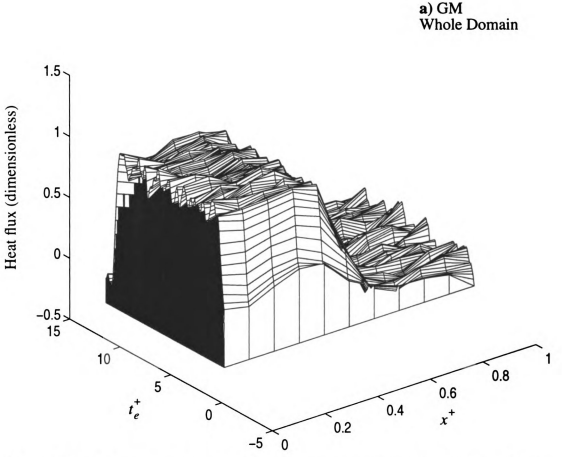

Figure 6-6a Estimated surface heat flux for step test case using data corrupted with measurement errors ($\sigma = 0.0025°C$). Whole domain solution

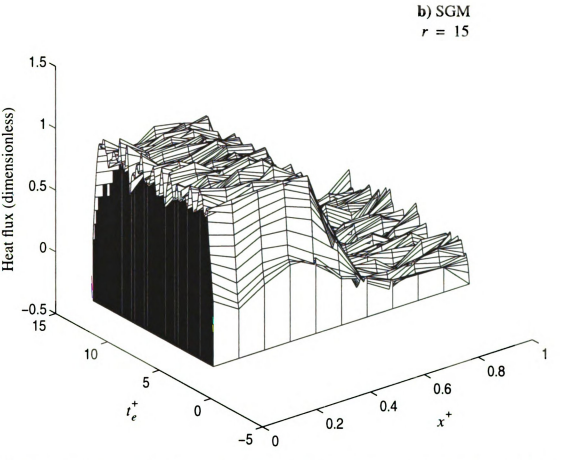

Figure 6-6b Estimated surface heat flux for step test case using data corrupted with measurement errors ($\sigma = 0.0025°C$). Sequential solution *r=15*

approach required 60 to 400% more computational time, compared to a whole domain solution. The computational time increases proportional to the increase in the number of future time steps, *r*.

The poor performance of the sequential approach for these cases can be attributed to two related factors. The first factor is that the sequential implementation is more ill-posed than the whole domain solution. Since the sequential solution solves over a shorter time domain, the effect of the measurement errors is more significant and results in a more ill-conditioned problem than the whole domain problem. Examining Table 6-2 shows that, even though the sequential problem is more ill-posed, the magnitude of the Tikhonov parameter in column four is decreased (except at large *r*-vales). Decreasing the Tikhonov parameter is contradictory to stabilize a more ill-conditioned problem. However to obtain the required magnitude in the sum-of-squares function, S_Y, the Tikhonov parameter must be decreased. The reason for this outcome (decreasing α_T for SGM) is the second factor in the poor performance of the sequential implementation. It is again the difficulty with the values near the end of the sequential interval influencing the early values. Much the same as was observed for the one-dimensional problem. Because the values near the end of the time region are biased, the regularization parameter must be decreased to provide the inverse solution "flexibility" to obtain the proper magnitude of the sum-of-squares function. Although decreasing the Tikhonov parameter reduces the temperature sum-of-squares, it results in an increase in the variability of the estimated heat flux.

In contrast to the one-dimensional solution, maintaining the heat flux constant over the sequential analysis interval does not improve the two-dimensional results. In the two-dimensional solution it does not work because the additional stability introduced by

maintaining the heat flux constant over the sequential interval requires a reduction in the Tikhonov parameter to obtain the desired sum-of-squares. The reduction in α_T in turn increases the variability in the estimated heat flux. If r is too large when using function specification, the sum-of-squares can not be reduced to the desired level, regardless of the Tikhonov parameter. The estimated results are actually worse when maintaining the heat flux constant (with time) over the sequential interval for the two-dimensional problem.

The sequential method performs poorly for small magnitudes of r, which are in the range that would typically be used for function specification. The estimated results for both test cases are improved as the number of future time steps is increased. Figure 6-7 demonstrates that the effects at the end of the interval are reduced by lengthening the sequential interval. At $r=15$ and 20 the mean-squared error in Table 6-2 is +1% and -12% of the mean-squared error of the whole domain estimation, respectively. The improved accuracy in the estimated heat flux using larger r-values is at the cost of a significantly increased computational requirement. Sequential solutions (SGM) for larger magnitudes of r require 500-800% (depending on r) more computational time than the whole domain solution. Computational time increases proportional to the increase in r. However, the potential benefits of an on-line (real time) method may outweigh the increased computational time.

For the one-dimensional problem, and the two-dimensional problem with exact data, an improvement in the computational speed, with a comparable accuracy in the estimated function, was obtained when the heat flux was maintained constant over the sequential interval, the method was denoted SFSGM. In the two-dimensional analysis with measurement errors the results are not improved when the heat flux is maintained constant over the

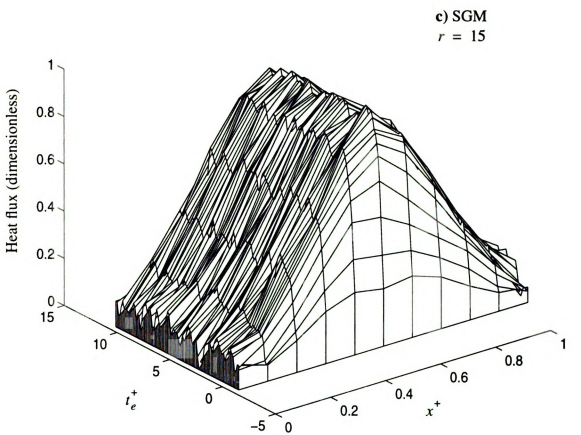

Figure 6-7 Estimated surface heat flux for triangular test case using data corrupted with measurement errors ($\sigma = 0.0018°C$). Sequential solution with *r=15*.

sequential interval. Although computational times are comparable (to the SGM) for a specified r-value, the error in the estimated heat flux actually increases, as seen in the final column of Table 6-2, when maintaining the heat flux constant over the sequential interval.

It was shown with exact data that a greater number of spatial components can be estimated than there are sensors available. The triangular case is reanalyzed for data with measurement errors and results are listed in the final block of Table 6-2. The outcome was similar to that seen in the analysis with exact data. A comparable heat flux, to that estimated with few spatial components, is obtained for a whole domain solution. Using the sequential method has a larger variability in the estimated heat flux for small r-values. The sequential method is improved by increasing r. Computational times are significantly greater using the sequential method.

Several approaches are possible to improve the sequential method. Before outlining these approaches, a summary explaining the effects that are resulting in the sequential method's poor performance is given. It is understood that the sequential method is more ill-posed. However, when solving with a sequential method the Tikhonov parameter is typically smaller than the whole domain solution; as r is increased the Tikhonov parameter increases for the sequential method. The reason that the Tikhonov parameter decreases (assuming that the residual principle is applicable), even though the sequential problem is more ill-posed, is due to the components near the end of the time interval. These components are difficult to estimate; when using a gradient method with the adjoint equation approach, these components are not estimated. Instead, the adjoint function, which is proportional to the computed update to the heat flux, is defined to be zero at the end of the time interval. Consequently, the heat flux estimated at the end of the time interval is "near"

the initial estimate specified for the heat flux. Its deviation from the initial estimate depends on the magnitude of the Tikhonov parameter.

As was demonstrated, lengthening the sequential interval improves the mean-squared error in the estimated heat flux; see Table 6-2 and Figures 6-7. Lengthening the sequential interval is also shown to increase the computational time in Table 6-2. An advantage of the SGM, compared to the SFSGM is that functional constraints are not imposed on the solution. Consequently more than one component may be retained for a sequential interval and the computational time can be reduced by having fewer sequential intervals. For example, when retaining 10 components for the triangular heat flux with $r=20$, the computational time is reduced to 30.8 seconds, which is about only 3% greater than the whole domain computational time. The mean-squared error for this case, shown in the final column of Table 6-3, is within 1% of the whole domain error; the mean-squared has increased 14% compared to retaining only one component for $r=20$. Although lengthening the sequential interval and retaining more components on time improves the computational aspects, the process may reduce the likelihood that non-linear problems can be linearized. Since larger sequential intervals are considered, it is less likely that the changes in thermal properties, due to the temperature variation during the sequential interval, are negligible. This is an important advantage of the sequential method. The validity of this assumption will depend on magnitude of non-linearity in the problem.

The one-dimensional problem was quite insensitive to the specified initial condition. Regardless of how the initial condition was specified, the solution required approximately the same number of iterations to converge. This same situation was found for the two-dimensional problem. Estimated heat flux and computational time were insensitive to the

procedure for setting of the initial condition for the two-dimensional problem. Whether the initial estimates for the next sequential interval were specified from the previous interval as outline in Section 5-4.2, or specified as zero, it did not significantly change the number of iterations.

A characteristic noticed for the one-dimensional problem, and two-dimensional test cases with measurement errors, was that the Tikhonov parameter decreases for the sequential problem, compared to its magnitude for the whole domain solution. The decrease in the Tikhonov parameter was more pronounced at smaller r-values and approached the magnitude of the whole domain solution as r was increased. A smaller Tikhonov parameter was not expected for the sequential solution because the problem is more ill-posed. It is the sequential implementation that forces the Tikhonov parameter to be reduced, at least for small r-values. Since the sequential solution is on the shorter time interval, the zeroth order Tikhonov regularization is more influential because the sensitivity (or in this case adjoint function) is not as large, particularly for r-values beyond four to five time steps from the end of the interval, which represents a dimensionless time of 0.3. The nature of zeroth order regularization is to bias or "drive" the estimates to zero, to reduce their variability. Consequently, to obtain the desired sum-of-squares, the Tikhonov parameter must be decreased so as not to "drive" the estimates towards zero. As r is increased to be farther away from this region the sensitivity (or adjoint function) is larger and the regularization has less affect on the solution.

When solving in a sequential manner, however, there is additional information available concerning the heat flux. The heat flux need not be "driven" to zero with the zeroth order regularization, instead it can be confined using the concept of prior information. The

prior information for the heat flux is specified from converged values at the previous sequential interval. The initial estimate for the sequential interval, which is specified from the converged estimates at the previous sequential interval, are set identically to be the prior information. The prior information is seen to enter the solution as $q_{pri}(r, t)$ in equation (4-2.4), which is the Tikhonov regularization term in the sum-of-squares function. Hence, instead of penalizing estimates that are different from zero, it penalizes estimates that are different from the previous estimates. For components that are far enough away from the end of the sequential interval the prior information has little influence. Near the end of the sequential interval, however, the prior information is more influential and helps control components in this region.

The results using prior information are given in Table 6-3. As shown in the table, by using the initial estimate as prior information, the sequential method is improved compared to no prior information. Figure 6-8 shows the estimated triangular heat flux for $r=6$. Compared to the estimated flux without prior information, see Figure 6-5b, results are significantly smoother. For $r=6$ the mean-square error is reduced by 15%, and the computational time is reduced in half with prior information. For larger magnitude of r the mean-squared error is comparable, while computational time is approximately one-half its former value without prior information. Similar trends are shown for the step heat flux case in Table 6-3. Notice that the magnitude of the Tikhonov parameter is greater when using prior information, but because it penalizes changes from the prior information (estimates at previous sequential interval) it does not bias the estimates as significantly. Prior information allows for smaller r-values to be considered and reduces computational time by requiring fewer iterations.

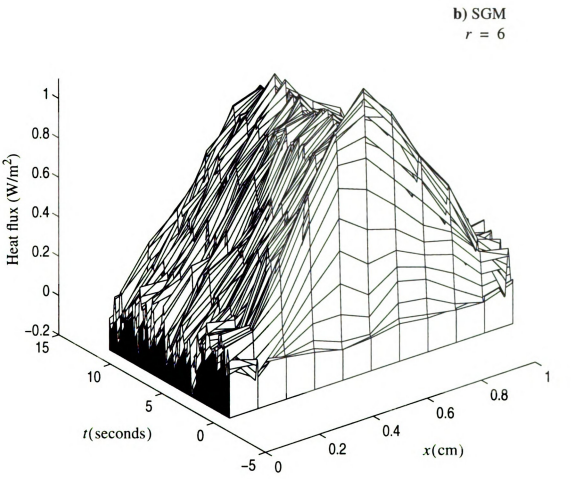

Figure 6-8 Estimated surface heat flux for triangular test case using data corrupted with measurement errors ($\sigma = 0.0018°C$). Sequential solution with r=6 using prior information.

Table 6-3 Estimation results for two-dimensional IHCP with simulated data corrupted with random errors using prior information

Method	Analysis domain		Tikhonov α_T	Iterations		Comp time (sec)	S_Y $(°C)$	$\hat{\sigma}_{s_t}$ W/m^2
	r	I		total	per seq int			
Triangular Flux ($\sigma = 0.0018°C$) - 11 Spatial Components								
GM	all	all	1.70 E-03	9	-	31.8	1.82 E-03	8.57 E-02
SGM[1]	6	1	1.40 E-03	396	2.1	37.6	1.80 E-03	1.16 E-01
SGM[1]	8	1	3.50 E-03	391	2.0	50.1	1.80 E-03	1.02 E-01
SGM[1]	20	10	3.00 E-03	59	3.2	19.4	1.82 E-03	8.21 E-02
SGM	20	10	1.20 E-03	90	5	30.8	1.80 E-03	8.51 E-02
SFSGM[1]	6	1	8.30 E-04	390	2.0	36.5	1.81 E-03	1.33 E-01
SFSGM[1]	8	1	2.50 E-03	384	2.0	48.9	1.82 E-03	1.11 E-01
Step Flux ($\sigma = 0.0025°C$) - 11 Spatial Components								
GM	all	all	6.00 E-04	13	-	45.8	2.51 E-03	1.06 E-01
SGM[1]	6	1	9.00 E-04	508	2.7	48.2	2.50 E-03	1.79 E-01
SGM[1]	10	1	3.50 E-03	423	2.3	67.8	2.51 E-03	1.30 E-01
SFSGM[1]	6	1	4.00 E-04	506	2.7	47.2	2.50 E-03	1.97 E-01
SFSGM[1]	10	1	3.00 E-03	388	2.1	61.8	2.52 E-03	1.19 E-01

[1] Prior information used for solution

A final procedure to improve the sequential method is discussed. Although the procedure is not numerically studied, it has promise for further improving the sequential method. For all results presented herein, the Tikhonov parameter was specified to be constant for the entire time region. Using the residual principle, the correct magnitude of the

Tikhonov parameter was identified. This procedure allowed for a direct comparison of computational time for the whole domain and sequential methods. An alternative method could vary the Tikhonov parameter during the sequential analysis. In regions that the heat flux is rapidly varying, the Tikhonov parameter could be reduced to minimize the effect of bias. Similarly, it could be increased in regions where the heat flux is relatively constant. In a sequential implementation information from previous sequential intervals is available to modify the magnitude of the Tikhonov parameter, as well as the magnitude of r. The whole domain solution does not have the necessary information to select these parameters.

6-4.0 Results - Experimental Measurements

The experimental configuration previously used to estimate the (orthotropic) thermal properties of the carbon-carbon composite is used to study the two-dimensional IHCP. Recall that transient temperatures and heat flux were measured to estimate the thermal properties in Chapter 3. Now the same transient temperature measurements, with the previously estimated thermal properties, are employed to estimate the two-dimensional transient surface heat flux. Surface heat flux is known for this experiment because the power to the heater is measured. Furthermore, the experiment is symmetrically designed and heat losses are negligible compared to the applied heat flux. Since the heater design has three independently controlled heaters, by activating only one of the three heaters a two-dimensional surface heat flux is experimentally prescribed. Additional details on the experimental configuration are discussed in Section 2-2.0 and 3-2.0.

An important issue in the study of the multi-dimensional IHCP is defining the spatial representation of the unknown heat flux. In the analysis of simulated data, it was shown that the gradient method could estimated more spatial components than the number of

sensors available. A rule used by the author is that the number of components estimated should not exceed the number of sensors. If more components than this are estimated, additional regularization is typically required to stabilize the solution. In the analysis of this experimental case, no assumptions on the spatial form of the heat flux are used. It is assumed that the heat flux is unknown only on the surface where the temperature sensors are located. All other boundary surfaces are insulated. See Figure 3-1. Hence, the heat flux that is estimated has a step change spatially and also a step change on time; a difficult case. The measured surface heat flux is shown if Figure 6-9a. Note that the surface with unknown heat flux, which is 7.62 cm long, has five sensors located above the heater at locations, x = 0.89, 1.91, 3.18, 4.45, and 6.73 cm.

The numerical solution for this problem uses twenty-one nodes along the x-direction for all materials. A schematic of the geometry is given in Figure 3-2. In the y-direction there are four nodes across the mica heater, eleven nodes across the carbon-carbon, and eleven nodes across the insulation. A numerical time step of 0.64 seconds, which is the same as the measurement time step, is used. Because effective properties have been estimated for the mica heater, the interface between the heater and specimen is modeled with perfect contact. Although the mica heater is quite thin (0.44 mm), because its properties include the contact resistance between the heater and the carbon-carbon, it is thermally significant. Based on the effective properties of the mica heater, the dimensionless time step (Fourier number) for the temperature sensors is 0.23. A dimensionless time step in this range does not represent a difficult one-dimensional case; however, in two-dimensions with a limited number of sensors, the problem is more difficult.

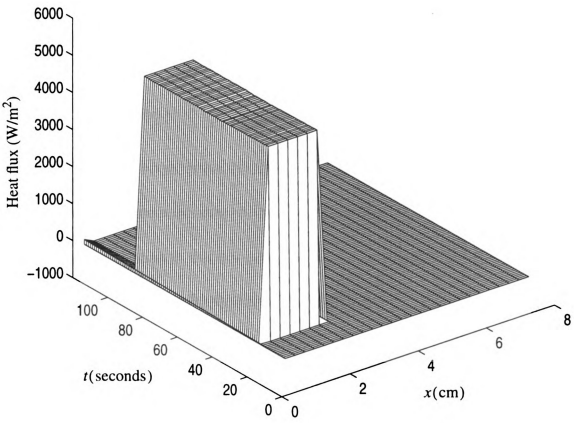

Figure 6-9a Measured surface heat for experimental case to estimate thermal properties of carbon-carbon

Selecting the appropriate Tikhonov parameter requires knowledge about the errors to apply the residual principle (Alifanov, 1994). For this two-dimensional experiment the temperature was measured at seven locations, but two measurements are available at all seven locations. The sensors located at the back surface of the carbon-carbon composite provide little information compared to the sensors near the surface. Therefore the five sensors located closest to the heater are used in the analysis. By comparing the two measured signals at each location an indication of the noise in the measurements is gained. The standard deviation of the redundant measurements, from the average, is computed as

$$\hat{\sigma}_{\overline{Y}_k}(t) = \left\{ \frac{1}{J_k - 1} \sum_{l=1}^{J_k} [\overline{Y}_k(t) - Y_{k,l}(t)]^2 \right\}^{\frac{1}{2}} \tag{6-4.1}$$

where $\overline{Y}_k(t)$ is the average temperature (for J_k sensors) for sensor location k, $Y_{k,l}(t)$ is the measured temperature for sensor location k and sensor number l, and J_k is the number of sensors at location k. For this experiment $J_k = 2$ for all k. Since so few sensors are available, by substituting for the average temperature

$$\overline{Y}_k(t) = \frac{Y_{k,1}(t) + Y_{k,2}(t)}{2} \tag{6-4.2}$$

equation (6-4.1) simplifies to

$$\hat{\sigma}_{\overline{Y}_k}(t) = \left\{ \frac{1}{2} [Y_{k,1}(t) - Y_{k,2}(t)]^2 \right\}^{\frac{1}{2}} \tag{6-4.3}$$

Notice that this error is a function of time and sensor location k. An approximation of the total error is obtained by averaging the error in equation (6-4.3) over time and sensor location. The average magnitude is $0.1°C$. This is about 20% larger than the measurement

error estimated for the one-dimensional experiment. The one-dimensional experiment had a larger sample set, $J_k = 7$.

The estimated heat flux is shown in Figure 6-9b and c for the whole domain and sequential method. The two methods are remarkable similar. Table 6-4 shows results from the analysis. The mean-squared errors are within 5% of the GM for all cases considered, except when prior information is used. For r=6, however, the computational time 77% greater for the SGM, which increases to 203% greater for $r=10$. The computational time is reduced to the level of whole domain solution by retaining more than one component. With $r=6$ and retaining two components, the computational time is cut in half and the mean-squared error is reduced by 3%, compared to the estimates while retaining only one component. Similar improvements are seen when retaining five components for $r=10$.

For a comparison, another program for estimating the surface heat flux is used to analyze the same data. The program QUENCH2D (Osman and Beck, 1989) computes surface heat flux from internal measurements using a combined function specification regularization method (CFSRM). In the CFSRM algorithm function specification on time and Tikhonov regularization on space is applied. The finite element direct solver TOPAZ2D is used in this program. Heat flux estimated with QUENCH2D is shown in Figure 6-9d for $r=6$. The Tikhonov parameter was specified to have the same magnitude as the whole domain solution. Similar numerical aspects as used in the gradient method's FCV solution were defined for the finite element solution. Approximately the same number of nodes and time step were specified for the numerical solution.

The estimated heat flux is again quite similar. For the CFSRM only seven spatial components are estimated because of program limitations. Because QUENCH2D required two

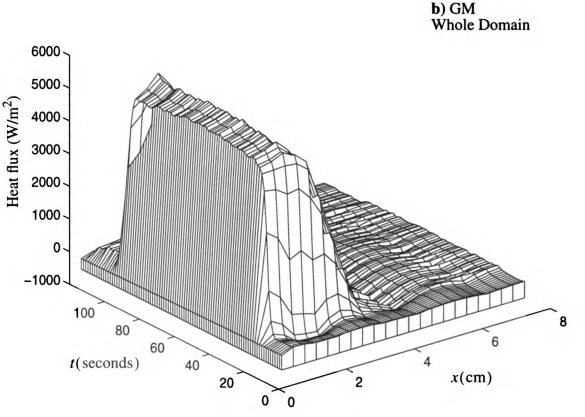

Figure 6-9b Estimated surface heat flux for experimental case. Whole domain solution.

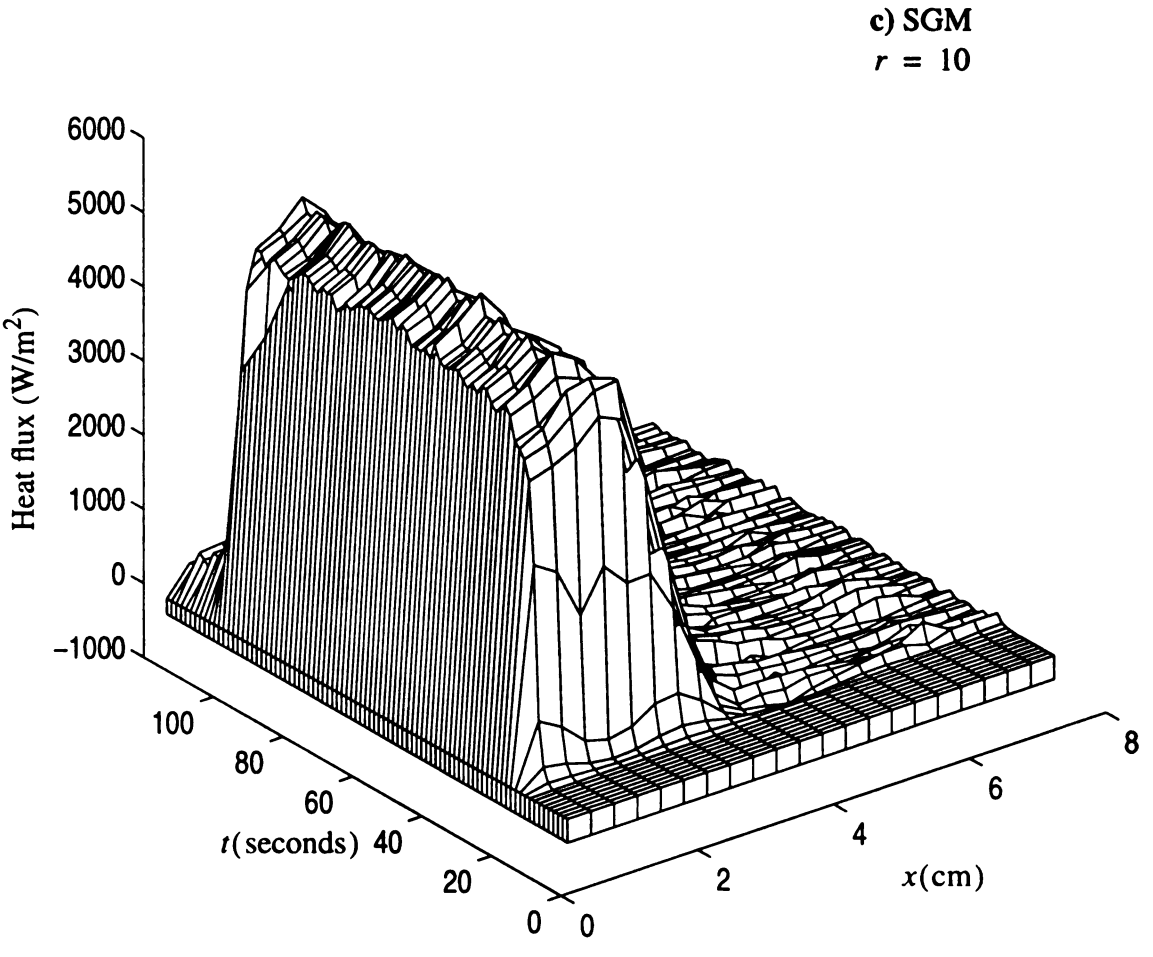

Figure 6-9c Estimated surface heat flux for experimental case. Sequential solution with *r=10.*

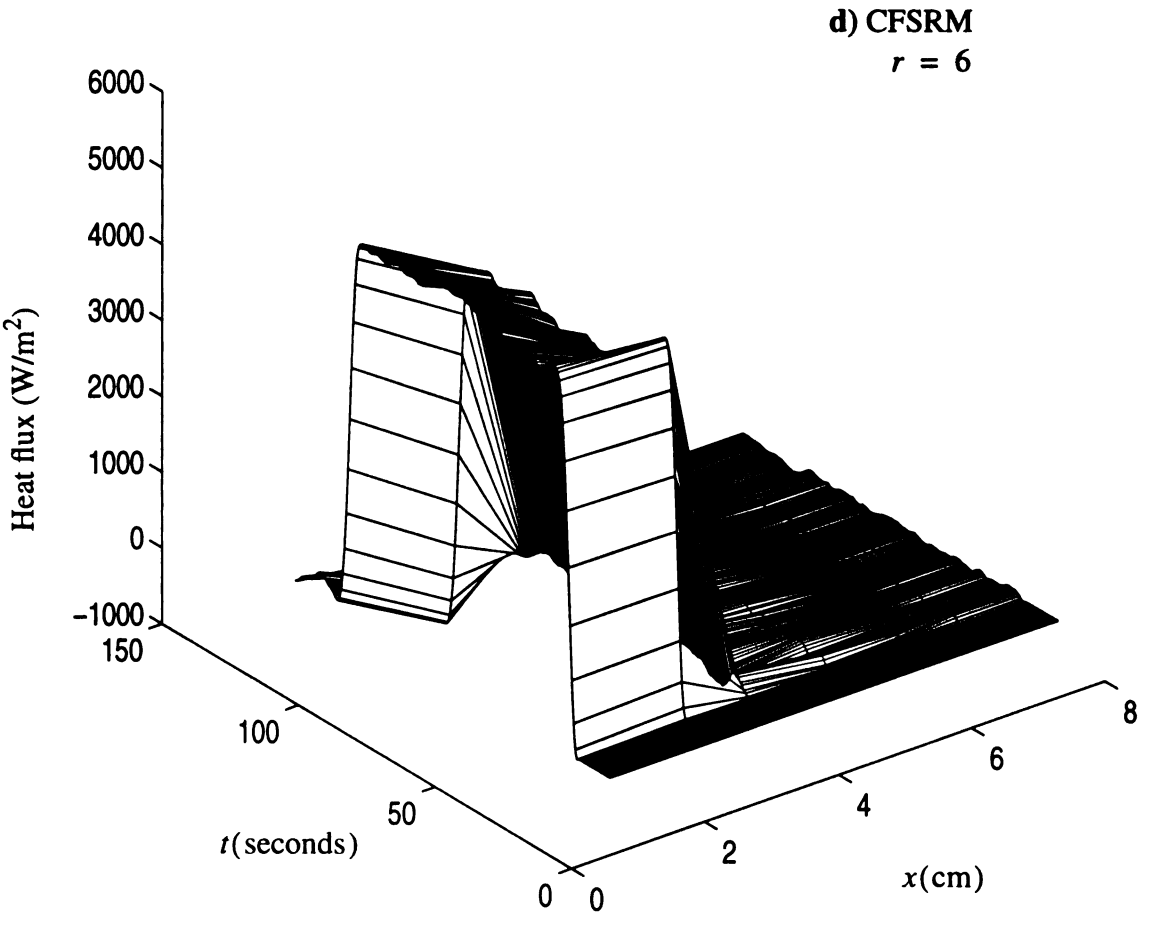

Figure 6-9d Estimated surface heat flux for experimental case. Combined function specification regularization method with *r=6*.

Table 6-4 Estimation results for two-dimensional IHCP with experimentally measured heat flux

Method	Analysis domain		Tikhonov α_T	Iterations		Comp time (sec)	S_Y $(°C)$	$\hat{\sigma}_q$ W/m^2
	r	I		total	per seq int			
Experimental Case 1020&65 - 21 Components								
GM	all	all	1.5 E-06	13	-	89.5	1.00 E-01	648
SGM	6	1	3.0 E-06	763	4.3	159	1.04 E-01	660
SGM	6	2	2.4 E-06	429	4.9	89.3	1.03 E-01	637
SGM[1]	6	1	1.3 E-05	486	2.8	101	1.01 E-01	878
SGM	10	1	3.6 E-06	825	4.8	298	1.01 E-01	679
SGM	10	5	2.9 E-06	215	6.3	78.3	1.07 E-01	635
Experimental Case 1020&65 - 7 Components								
SGM	6	1	2.6 E-08	504	3.3	104	1.04 E-01	500
SGM[1]	6	1	2.0 E-07	371	2.2	76.8	1.00 E-01	389
CFSRM	6	1	1.5 E-06	-	-	7200	7.88 E-02	399
CFSRM	10	1	1.5 E-06	-	-	7200	1.65 E-01	518

[1] Prior information used

hours to obtain a solution the appropriate α_T, based on the residual principle, was not identified. It appears the appropriate (r, α_T) for CFSRM is between the two cases listed in Table 6-4. The estimated heat flux is not sensitive to these parameters. The biggest distinction between the two programs is the computational time. The gradient method requires on the order of 100 seconds, while CFSRM requires on the order of 7000 seconds. These computational times can not be directly compared because different direct solvers are

used. The gradient methods employ a ADI method, which typically is much faster than the finite element method used in QUENCH2D. To understand the computational difference, the time required to obtain one direct solution with comparable numerical conditions was conducted. The ADI solution required 3.6 seconds while the FEM required 110 seconds; a factor of 30. Indicating that the gradient methods are more computational efficient because the inverse solution required a factor of 70 more computational time. Furthermore, the CFSRM only estimated seven components, compared to 21 for the GM. As more spatial components are estimated the CFSRM requires solving additional problems, some computational savings are carried from previous solutions, however. In contrast, the gradient methods do not require solving additional problems when more components are considered. A very good feature for the multi-dimensional problems. It appears that the gradient methods are more efficient for higher dimensional problems, but further cases, with similar direct solvers, or more detailed studies are need. Comparing the gradient methods with standard function specification was not a thrust of this dissertation. Early indications are that the gradient methods are very promising for multi-dimensional problems.

Chapter 7

SUMMARY AND CONCLUSIONS

A study of multi-dimensional inverse thermal problems was presented. Two main problems were studied. Parameter estimation techniques were applied to characterize thermal properties of a carbon-carbon composite material. The second problem developed the sequential implementation of a gradient method, utilizing an adjoint equation approach, for estimating the surface heat flux from internal temperature measurements. Both problems addressed multi-dimensional cases.

Thermal properties, represented by two components of thermal conductivity and the volumetric heat capacity, were estimated for the carbon-carbon composite. One- and two-dimensional transient experiments were analyzed to estimate the thermal properties up to $500°C$. Several conclusions are supported:

1. The thermal properties of the carbon-carbon are described by a parabolic temperature dependence, given in equation (3-40) and (3-41) for the $k^e_{y,\,cc}$ and $(\rho C)^e_{cc}$, and by a linear temperature function, given in equation (3-37) for $k^e_{x,\,cc}$.
2. Experimental uncertainty in the estimated thermal properties was a maximum of 5.8% in $(\rho C)^e_{cc}$ and 2.4% in $k^e_{y,\,cc}$ for one-dimensional experiments. Two-dimensional experimental uncertainty was a maximum of 6.0% in $(\rho C)^e_{cc}$ and $k^e_{y,\,cc}$ and 4.4% in $k^e_{x,\,cc}$.

3. One and two-dimensional results for $(\rho C)_{cc}^{e}$ and $k_{y,cc}^{e}$ correlate within the experimental uncertainty.
4. An orthotropic model adequately describes the carbon-carbon material studied.

A sequential gradient method was developed to solve the IHCP. Several one and two dimensional cases, using simulated and experimental measurements, were investigated to characterize the sequential method. A comparison between the sequential method and a whole domain solution was made. The following conclusions are drawn concerning the sequential gradient method, and variations of the method that were proposed:

1. A sequential gradient method has an accuracy comparable to the whole domain gradient method, but in certain cases requires significantly more computational time.
2. In one-dimensional cases the minimum length of the sequential interval was a dimensionless time of 0.3. The dimensionless time is based on the depth of the sensor nearest the location of the estimated surface heat flux.
3. Applying function specification on time, in conjunction with the sequential gradient method, reduced the computational requirements and allowed for sequential intervals to be shorter than 0.3 for the one-dimensional cases. Computational requirements were comparable for the sequential function specification gradient method and whole domain method.
4. The two-dimensional cases required the dimensionless time to be greater that 1.0 to obtain comparable accuracy between the sequential and whole domain solutions. The dimensionless time is based on the depth of the sensor nearest the location of the estimated surface heat flux.
5. Applying function specification on time, in conjunction with the sequential gradient method, did not improve the computational requirements when errors were present in the data for the two-dimensional case.
6. Retaining more than one component for a sequential interval improved computational requirements without affecting the accuracy of the sequential gradient method for the two-dimensional case.
7. Using prior information with the sequential gradient method for the two-dimensional case was shown to improve the accuracy, permitted smaller sequential intervals, and made the computational requirements competitive with the whole domain solution.

Chapter 8

RECOMMENDED FUTURE WORK

In the course of this dissertation several topics for future work were realized. The topics are separated according to the parameter estimation or inverse heat conduction problem.

Experiments conducted to estimate the thermal properties of the carbon-carbon composite material measured transient temperature and heat flux histories for discrete experiments spanning the desired temperature range. Experiments with one- and two-dimensional heat flow were analyzed independently, assuming the thermal properties were constant for the analysis of each experiment. In the end, the discrete experiments were combined to determine a temperature dependence for the thermal properties. One and two-dimensional results were also compared. Topics of future direction are noted:

1. Analysis of currently available data to directly estimate temperature-dependent thermal properties is of interest. A sequential analysis using prior information is used to accomplish this.
2. The optimal experiment for estimating two components of thermal conductivity and volumetric heat capacity is needed for the case of a relatively high thermal conductivity material (which this particular carbon-carbon has). The optimal conditions for the design of a *series* of experiments is an important concept that needs attention. The experimental *series* may included one- and two-dimensional experiments. As the complexity of the experiments increase, more frequently several experiments may be required to fully characterize complex materials or compound structures.
3. The model of the carbon-carbon composite can be extended to include the silicon-carbide layer. This case of a thin layer on a thick substrate represents an important problem. Work to estimate the thermal properties of the thin layer, in conjunction with the underlying material, is of interest.

4. Methods, both experimental and analytical, should be generalized to the three-dimensional case. Developing the analysis is straight forward. Experimental techniques, including the experimental design, are extremely important for higher dimensions and will require significant effort.

The sequential gradient method has several areas for potential growth of the method.

1. The procedure to linearized nonlinear problems in the sequential gradient solution suggests large savings in computational time without significantly affecting accuracy, the procedure needs investigating.
2. Implementing on-line logic for selecting the regularization parameter, number of future time steps, and/or the number of retained components would enhance the sequential method. Quite frequently, the selection of these parameters is not trivial and requires experience and an understanding of inverse problems. Since the accuracy of the solution may be sensitive to correctly selecting these parameters, the method would be enhanced to logically select the parameter.
3. In the sequential formulation presented, zeroth order Tikhonov regularization was used. Extending the method to include first order Tikhonov regularization is appropriate.
4. Prior information to spatially filter the heat flux could provide spatial regularization.
5. Implementing the methods for the three-dimensional case is of interest.

APPENDIX

APPENDIX A

FINITE CONTROL VOLUME METHOD

A-1.0 Introduction

Many methods exist for discretizing partial differential equations. Two popular methods are finite differences and finite element. An alternate approach applies conservation of energy directly to a control volume. That method is applied to discretize the heat conduction equation here.

The problem considered is the heat conduction equation with constant thermal properties, a spatially time dependent volume energy source

$$\frac{\partial}{\partial x}\left(k_x \frac{\partial T}{\partial x}\right)+\frac{\partial}{\partial y}\left(k_t \frac{\partial T}{\partial y}\right)+g(x, y, t) = \rho C\left[\frac{\partial T}{\partial t}+u_o \frac{\partial T}{\partial x}\right] \tag{A-1.1}$$

$$-k \left.\frac{\partial T}{\partial n_i}\right|_{\Gamma_i} = q_i(s_i, t) \quad (i=1, 2, 3, 4) \tag{A-1.2a}$$

$$\text{OR } T|_{\Gamma_i} = T_i(s_i, t) \quad (i=1, 2, 3, 4) \tag{A-1.2b}$$

$$T|_{t=0} = T_o(x, y) \tag{A-1.2c}$$

The thermal conductivity is assumed orthotropic. First or second kind boundary conditions are allowed on the four bounding surfaces (Γ_i). Conditions may have temporal and spatial variation. The outward normal of surface i is n_i. Since a regular geometry is used this is the unit normal in the x or y direction.

The FCV procedure uses energy conservation principles to derive a discretized set of equations to solve for the temperatures. In contrast, a finite difference scheme would discretize the problem presented in equation (A-1.1) and (A-1.2), i.e. use a finite difference approximation for the derivatives, to obtain a numerical solution. The FCV procedure is preferred over a finite difference approach because it is more general and applies energy conservation principles to derive the equations.

To implement the FCV procedure the spatial domain is discretized with uniform mesh points (nodes)

$$(x, y) = (i\Delta x, j\Delta y) \qquad i = (0, 1, 2.....,I),\ j = (0, 1, 2.....,J) \tag{A-1.3}$$

where the mesh lengths are

$$\left(\Delta x = \frac{L_x}{I}\right), \left(\Delta y = \frac{L_y}{J}\right) \tag{A-1.4}$$

Control volumes are the region ($\Delta x \Delta y$) surrounding the nodes with the node centrally located. The control surfaces are at the mid-plane between the nodes. Figure A-1 shows a schematic of the nodes, control volumes, and control surfaces.

The integral energy equation (Beck et al., 1992)

$$\int_{\text{c.s.}} (-\boldsymbol{q} \cdot \hat{\boldsymbol{n}}) dA + \int_{\text{c.v.}} g dv = \int_{\text{c.v.}} \rho C \frac{\partial T}{\partial t} dv + \int_{\text{c.s.}} \rho u (\underset{\sim}{v} \cdot \hat{\boldsymbol{n}}) dA \tag{A-1.5}$$

is applied to each control volume on the domain to obtain the FCV equations. The integral energy equation can be used to derive the describing differential equation in equation (A-1.1) as well. The energy balance for a typical node in the interior is shown in Figure A-2. Using the simplified approximation of equation (A-1.5), which assumes the quantities are

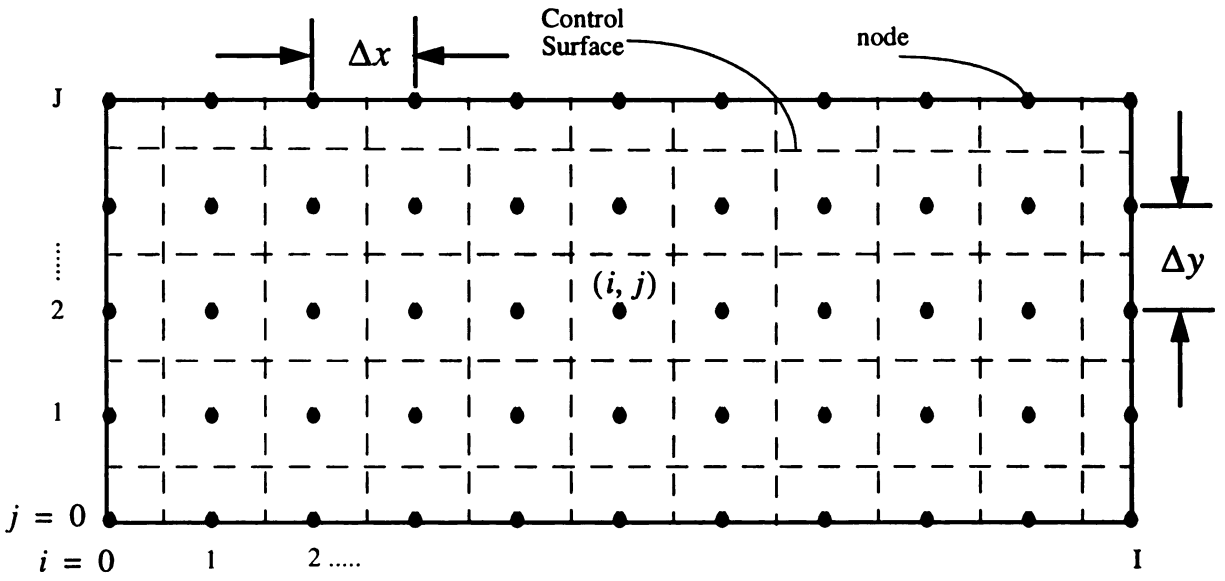

Figure A-1 Computational nodes and control surfaces

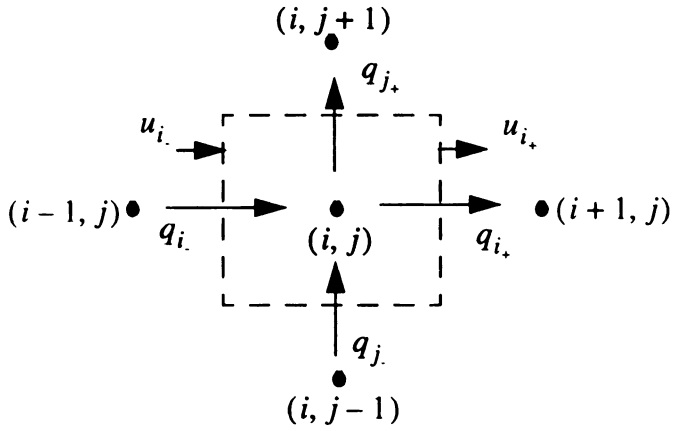

Figure A-2 Typical energy balance for an interior node

constant over the control volume and surface, gives

$$-(-q_{i_-}A_{i_-}+q_{i_+}A_{i_+}-q_{j_-}A_{j_-}+q_{j_+}A_{j_+})+gV=\rho C\frac{\partial T}{\partial t}V+\rho v_o u_{i_+}A_{i_+}-\rho v_o u_{i_-}A_{i_-} \quad \text{(A-1.6)}$$

The heat fluxes are taken as the mean values over the control surface and are approximated as

$$q_{i_-}=-k_x\frac{(T_{i,j}-T_{i-1,j})}{\Delta x} \quad \text{(A-1.7)}$$

$$q_{i_+}=-k_x\frac{(T_{i+1,j}-T_{i,j})}{\Delta x} \quad \text{(A-1.8)}$$

$$q_{j_+}=-k_y\frac{(T_{i,j+1}-T_{i,j})}{\Delta y} \quad \text{(A-1.9)}$$

$$q_{j_-}=-k_y\frac{(T_{i,j}-T_{i,j-1})}{\Delta y} \quad \text{(A-1.10)}$$

Assuming that the velocity is positive, the flow terms are evaluated at the upwind locations to avoid the known difficulties associated with central differences for this term (Anderson et al.,)

$$u_{i_+}=C_pT_{i,j} \quad \text{(A-1.11)}$$

$$u_{i_-}=C_pT_{i-1,j} \quad \text{(A-1.12)}$$

The areas are $(A_{i_-}=A_{i_+}=\Delta y)$ and $(A_{j_-}=A_{j_+}=\Delta x)$ and the volume is $(\Delta x\Delta y)$. Substituting equation (A-1.7) through (A-1.12) with areas and volume into the energy balance gives

$$-k_x\frac{(T_{i,j}-T_{i-1,j})}{\Delta x}\Delta y+k_x\frac{(T_{i+1,j}-T_{i,j})}{\Delta x}\Delta y-k_y\frac{(T_{i,j}-T_{i,j-1})}{\Delta y}\Delta x+k_y\frac{(T_{i,j+1}-T_{i,j})}{\Delta y}\Delta x$$

$$+g\Delta x\Delta y=\rho C\Delta x\Delta y\frac{\partial T_{i,j}}{\partial t}+\rho Cv_o\Delta y(T_{i,j}-T_{i-1,j}) \quad \text{(A-1.13)}$$

Defining the following constants

$$\lambda'_x = \frac{k_x}{\rho C(\Delta x)^2} \; ; \; \lambda'_y = \frac{k_y}{\rho C(\Delta y)^2} \tag{A-1.14}$$

and simplifying equation (A-1.13) results in an equation that represents an energy balance on a finite control volume

$$\left[\left(\lambda'_x + \frac{v_o}{\Delta x}\right)T_{i-1,j} - \left(2\lambda'_x + \frac{v_o}{\Delta x}\right)T_{i,j} + \lambda'_x T_{i+1,j}\right] + \left[-\lambda'_y T_{i,j-1} - 2\lambda'_y T_{i,j} + \lambda'_y T_{i,j+1}\right]$$

$$+ \frac{g_{i,j}}{\rho C} = \frac{\partial T_{i,j}}{\partial t} \tag{A-1.15}$$

For boundary conditions that are prescribed temperature only, after approximating the time derivative in equation (A-1.15) the equation can be written for each interior node and numerically solved for the all discrete temperatures. However, if flux boundary conditions are prescribed, a FCV procedure performs an energy balance on the boundaries and results in an equations to describe the energy balance there.

The FCV equations to represent the boundary conditions apply an energy balance at the boundary FCV. Two possible configurations on the boundary are shown in Figure A-3. The first is along a bounding surface but not on a corner and the second is at a corner.

The energy balance for the bounding surface node is

$$-(-q_{i_+}A_{i_+} - q_{j_-}A_{j_-} + q_{j_+}A_{j_+} + \hat{q}_{s_1,j}A_s) + gV = \rho C\frac{\partial T}{\partial t}V + \rho v_o u_0 A_i - \rho v_o u_1 A_{i_+} \tag{A-1.16}$$

The heat fluxes $(q_{i_+}, q_{j_-}, q_{j_+})$ and flow term (u_{i_+}) are the same as for an interior grid point and given in equation (A-1.8) through (A-1.10) and equation (A-1.11). The flow term at the boundary surface is evaluated using the average temperature, $u_i = C_p(T_{0,j} + T_{1,j})/2$. The areas are $A_{j_+} = A_{j_-} = \Delta x/2$, $A_{i_+} = A_s = \Delta y$ and the

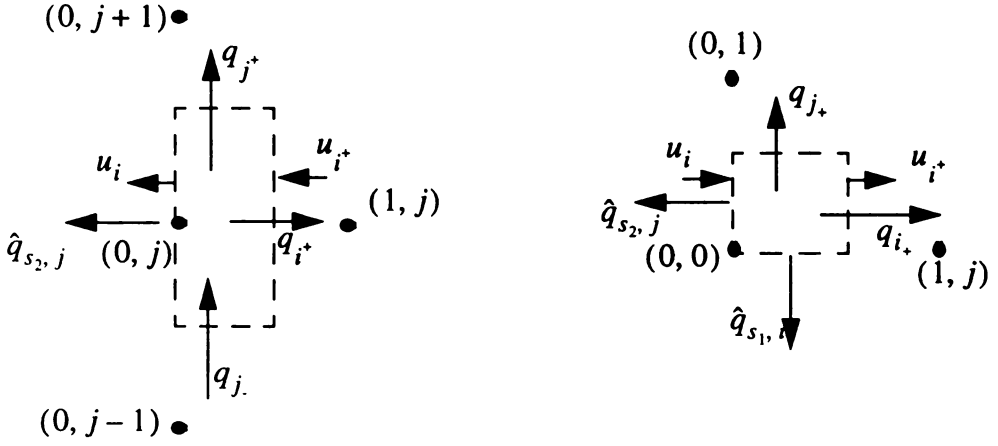

a) Bounding surface node
$x = 0$

b) Corner node
$(x = 0, y = 0)$

Figure A-3 Finite control volumes along the boundary of the domain

volume is $V = \Delta x \Delta y/2$. Substituting these relations into equation (A-1.16) and simplifying gives

$$\left[\left(-2\lambda'_x + \frac{v_o}{\Delta x}\right)T_{0,j} + \left(2\lambda'_x - \frac{v_o}{\Delta x}\right)T_{1,j}\right] + [\lambda'_y T_{0,j-1} - 2\lambda'_y T_{0,j} + \lambda'_y T_{0,j+1}]$$

$$- \frac{2\hat{q}_{s_2,j}}{\rho C \Delta x} + \frac{g_{0,j}}{\rho C} = \frac{\partial T_{0,j}}{\partial t} \quad \text{(A-1.17)}$$

where λ'_x and λ'_x are given in equation (A-12). The prescribed heat flux $\hat{q}_{s_2,j}$ is the heat flux on surface s_2 at node j.

Using the same procedure the following equation is derived to represent the energy balance at a corner node

$$\left[\left(-2\lambda'_x + \frac{v_o}{\Delta x}\right)T_{0,0} + \left(2\lambda'_x - \frac{v_o}{\Delta x}\right)T_{1,0}\right] + [-2\lambda'_y T_{0,0} + 2\lambda'_y T_{0,1}]$$

$$- \frac{2\hat{q}_{s_1,i}\Delta x + 2\hat{q}_{s_2,i}\Delta y}{\rho C(\Delta y \Delta x)} + \frac{g_{i,j}}{\rho C} = \frac{\partial T_{i,j}}{\partial t} \quad \text{(A-1.18)}$$

The equations derived for the boundary conditions, equation (A-17) and (A-18), apply along boundary $x = 0$ and at corner $(x = 0, y = 0)$. Similar expressions can be derived for the remaining boundary surfaces and corners.

A-2.0 Alternating Direction Implicit Method (ADI)

Discrete equations derived can be solved using an explicit or implicit method. The explicit is more easily implemented, however, may be unstable depending on thermal properties and the time and space discretization. In contrast, an implicit method is more complicated to implement, but unconditionally stable. A fully implicit method has five unknowns for each interior node (see Figure A-2 and equation (A-1.15)) and requires solving a penta-diagonal system for each time step. A more efficient method is the ADI (alternating direction implicit) scheme, which requires solving two tri-diagonal system of equations at each time step.

The time domain is uniformly discretized

$$t = n\Delta t \qquad n = (1, 2....., N) \quad \text{(A-2.1)}$$

In the ADI method, two solutions are obtained for each time step. For the first half time step the FCV equations are solved implicit in the x-direction and explicit in the y-direction. For the second half time step the difference equations are implicit in the y-direction and explicit in the x-direction. Hence, the ADI method is a two step solution. An

intermediate solution at time $(n + 1/2)\Delta t$ is obtained after the first step. The second results in the solution at the end of the time step.

A-2.1 ADI Equations (n+1/2)

The FCV equations using an ADI scheme proceed over the first half time step. These equations are implicit in the x-direction and explicit in the y-direction. For illustrative purposes consider the FCV equations in equation (A-1.13), (A-1.15), and (A-1.16). Introducing the forward difference for the time derivative and the implicit/explicit ADI scheme for the first half time step produces the following equations

Interior Node: $(0 < i < I)$, $(0 < j < J)$

$$\left[\left(\lambda_x + \frac{v_o \Delta t}{\Delta x}\right) T_{i-1,j}^{n+1/2} - \left(2\lambda_x + \frac{v_o \Delta t}{\Delta x}\right) T_{i,j}^{n+1/2} + \lambda_x T_{i+1,j}^{n+1/2}\right]$$

$$+ (\lambda_y T_{i,j-1}^{n} - 2\lambda_y T_{i,j}^{n} + \lambda_y T_{i,j+1}^{n}) + \frac{g_{i,j}^{n}}{\rho C} = \frac{(T_{i,j}^{n+1/2} - T_{i,j}^{n})}{\Delta t/2} \quad \text{(A-2.2)}$$

Flux B.C.$(i = 0)$ and$(0 < j < J)$

$$\left[\left(-2\lambda_x - \frac{v_o \Delta t}{\Delta x}\right) T_{0,j}^{n+1/2} + \left(2\lambda'_x - \frac{v_o \Delta t}{\Delta x}\right) T_{1,j}^{n+1/2}\right]$$

$$+ (\lambda_y T_{0,j-1}^{n} - 2\lambda_y T_{0,j}^{n} + \lambda_y T_{0,j+1}^{n}) - 2\frac{\hat{q}_{s_1,j}^{n}}{\rho C \Delta x} + \frac{g_{0,j}^{n}}{\rho C} = \frac{(T_{0,j}^{n+1/2} - T_{0,j}^{n})}{\Delta t/2} \quad \text{(A-2.3)}$$

Flux B.C. $(i = 0)$ and $(j = 0)$

$$\left[\left(-2\lambda_x - \frac{v_o \Delta t}{\Delta x}\right) T_{0,0}^{n+1/2} + \left(2\lambda'_x - \frac{v_o \Delta t}{\Delta x}\right) T_{1,j}^{n+1/2}\right]$$

$$+ (-2\lambda_y T_{0,0}^{n} + 2\lambda_y T_{0,1}^{n}) - 2\frac{\hat{q}_{s_1,0}^{n}\Delta x + \hat{q}_{s_2,0}^{n}\Delta y}{\rho C(\Delta y \Delta x)} + \frac{g_{0,0}^{n}}{\rho C} = \frac{(T_{0,0}^{n+1/2} - T_{i,j}^{n})}{\Delta t/2} \quad \text{(A-2.4)}$$

The first equation is for an interior node and the next two equations are for a surface and corner node for a prescribed flux boundary condition. For the case of temperature boundary conditions only, the first equation is sufficient for numerically solving the problem. Using a similar procedure, equations for the remaining surfaces and corner can be written. After deriving all the FCV equations, they can be rearranged to group known information on the left hand side of the equation and unknowns on the right. The equations represent a set of simultaneous equations, which can be written for each j, ($j = 0, 1 \ldots, J$), the jth set of equations are

$$\left(2(\lambda_x + 1) - \frac{v_o \Delta t}{\Delta x}\right) T_{0,j}^{n+1/2} + \left(-2\lambda'_x + \frac{v_o \Delta t}{\Delta x}\right) T_{1,j}^{n+1/2} = D_0^n \quad (i = 0) \tag{A-2.5a}$$

$$\left(-\lambda_x - \frac{v_o \Delta t}{\Delta x}\right) T_{i-1,j}^{n+1/2} + \left(2(\lambda_x + 1) + \frac{v_o \Delta t}{\Delta x}\right) T_{i,j}^{n+1/2} - \lambda_x T_{i+1,j}^{n+1/2} = D_i^n \quad (0 < i < I) \tag{A-2.5b}$$

$$\left(-2\lambda_x - \frac{v_o \Delta t}{\Delta x}\right) T_{I-1,j}^{n+1/2} + \left(2(\lambda_x + 1) + \frac{v_o \Delta t}{\Delta x}\right) T_{I,j}^{n+1/2} = D_I^n \quad (i = I) \tag{A-2.5c}$$

The right hand sides are also a function of j,

for $i = 0$

$$D_0^n = 2(1 - \lambda_y) T_{0,0}^n + \lambda_y T_{0,1}^n + g_{0,0}^n \frac{\Delta t}{\rho C} + \hat{q}_{s_1,0}^n \frac{2\Delta t}{\rho C \Delta y} + \hat{q}_{s_2,0}^n \frac{2\Delta t}{\rho C \Delta x} \quad (j = 0) \tag{A-2.6a}$$

$$D_0^n = \lambda_y T_{0,j-1}^n + 2(1 - \lambda_y) T_{0,j}^n + \lambda_y T_{0,j+1}^n + g_{i,j}^n \frac{\Delta t}{\rho C} + \hat{q}_{s_1,j}^n \frac{2\Delta t}{\rho C \Delta x} \quad 0 < j < J \tag{A-2.6b}$$

$$D_0^n = \lambda_y T_{0,J-1}^n + 2(1 - \lambda_y) T_{0,J}^n + g_{0,J}^n \frac{\Delta t}{\rho C} + \hat{q}_{s_2,J}^n \frac{2\Delta t}{\rho C \Delta x} + \hat{q}_{s_3,0}^n \frac{2\Delta t}{\rho C \Delta y} \quad (j = J) \tag{A-2.6c}$$

for $0 < i < I$

$$D_i^n = 2(1 - \lambda_y) T_{i,0}^n + \lambda_y T_{i,1}^n + g_{i,0}^n \frac{\Delta t}{\rho C} + \hat{q}_{s_1,i}^n \frac{2\Delta t}{\rho C \Delta y} \quad (j = 0) \tag{A-2.7a}$$

$$D_i^n = \lambda_y T_{i,j-1}^n + 2(1-\lambda_y)T_{i,j}^n + \lambda_y T_{i,j+1}^n + g_{i,j}^n \frac{\Delta t}{\rho C} \quad (0 < j < J) \tag{A-2.7b}$$

$$D_i^n = \lambda_y T_{i,J-1}^n + 2(1-\lambda_y)T_{i,J}^n + g_{i,J}^n \frac{\Delta t}{\rho C} + \hat{q}_{s_3,i}^n \frac{2\Delta t}{\rho C \Delta y} \quad (j = J) \tag{A-2.7c}$$

for $(i = I)$

$$D_I^n = 2(1-\lambda_y)T_{I,0}^n + \lambda_y T_{I,1}^n + g_{I,0}^n \frac{\Delta t}{\rho C} + \hat{q}_{s_1,0}^n \frac{2\Delta t}{\rho C \Delta y} + \hat{q}_{s_4,0}^n \frac{2\Delta t}{\rho C \Delta x} \quad (j = 0) \tag{A-2.8a}$$

$$D_I^n = \lambda_y T_{I,j-1}^n + 2(1-\lambda_y)T_{I,j}^n + \lambda_y T_{I,j+1}^n + g_{i,j}^n \frac{\Delta t}{\rho C} + \hat{q}_{s_4,j}^n \frac{2\Delta t}{\rho C \Delta x} \quad 0 < j < J \tag{A-2.8b}$$

$$D_I^n = \lambda_y T_{I,J-1}^n + 2(1-\lambda_y)T_{I,J}^n + g_{I,J}^n \frac{\Delta t}{\rho C} + \hat{q}_{s_3,I}^n \frac{2\Delta t}{\rho C \Delta y} + \hat{q}_{s_4,J}^n \frac{2\Delta t}{\rho C \Delta x} \quad (j = J) \tag{A-2.8c}$$

A-2.2 ADI Equations (n+1)

The FCV equations for the second-half time step for the ADI scheme proceed from the intermediate solution at n+1/2 to the n+1 time step. For this second half step the FCV equations are implicit in the y-direction and explicit in the x-direction (the opposite of the first-half time step). Using the same procedure as before, the forward difference approximation is used to represent the time derivative, a simultaneous set of equations are written for i, $(i = 1, 2 \ldots, I)$, the ith set of equations are

$$2(\lambda_y + 1)T_{i,0}^{n+1} - \lambda_y T_{i,1}^{n+1} = E_0^{n+1/2} \quad (j = 0) \tag{A-2.9a}$$

$$-\lambda_y T_{i,j-1}^{n+1} + 2(\lambda_y + 1)T_{i,j}^{n+1} - \lambda_y T_{i,j+1}^{n+1} = E_j^{n+1/2} \quad 0 < j < J \tag{A-2.9b}$$

$$-\lambda_y T_{i,J-1}^{n+1} + 2(\lambda_y + 1)T_{i,J}^{n+1} = E_J^{n+1/2} \quad (j = J) \tag{A-2.9c}$$

The right hand side constants are a function of i:

for $j = 0$

$$E_0^{n+1/2} = \left(2(1-\lambda_x) - \frac{v_o \Delta t}{\Delta x}\right)T_{0,0}^{n+1/2} + \left(2\lambda_x - \frac{v_o \Delta t}{\Delta x}\right)T_{1,0}^{n+1/2}$$

$$+ g^{n}_{0,0}\frac{\Delta t}{\rho C} + \hat{q}^{n}_{s_1,0}\frac{2\Delta t}{\rho C \Delta y} + \hat{q}^{n}_{s_2,0}\frac{2\Delta t}{\rho C \Delta x} \quad (i = 0) \text{ (A-2.10a)}$$

$$E^{n+1/2}_{0} = \left(\lambda_x + \frac{v_o \Delta t}{\Delta x}\right) T^{n+1/2}_{i-1,0} + \left(2(1-\lambda_x) - \frac{v_o \Delta t}{\Delta x}\right) T^{n+1/2}_{i,0} + \lambda_x T^{n+1/2}_{i+1,0}$$

$$+ g^{n}_{i,0}\frac{\Delta t}{\rho C} + \hat{q}^{n}_{s_1,i}\frac{2\Delta t}{\rho C \Delta y} \quad 0 < i < I \text{ (A-2.10b)}$$

$$E^{n+1/2}_{0} = \left(2\lambda_x + \frac{v_o \Delta t}{\Delta x}\right) T^{n+1/2}_{I-1,0} + \left(2(1-\lambda_x) - \frac{v_o \Delta t}{\Delta x}\right) T^{n+1/2}_{I,0}$$

$$+ g^{n}_{I,0}\frac{\Delta t}{\rho C} + \hat{q}^{n}_{s_1,I}\frac{2\Delta t}{\rho C \Delta y} + \hat{q}^{n}_{s_4,0}\frac{2\Delta t}{\rho C \Delta x} \quad (i = I) \text{ (A-2.10c)}$$

for $0 < j < J$

$$E^{n+1/2}_{j} = \left(2(1-\lambda_x) - \frac{v_o \Delta t}{\Delta x}\right) T^{n+1/2}_{0,j} + \left(2\lambda_x - \frac{v_o \Delta t}{\Delta x}\right) T^{n+1/2}_{1,j}$$

$$+ g^{n}_{0,j}\frac{\Delta t}{\rho C} + \hat{q}^{n}_{s_2,j}\frac{2\Delta t}{\rho C \Delta x} \quad (i = 0) \text{ (A-2.11a)}$$

$$E^{n+1/2}_{j} = \left(\lambda_x + \frac{v_o \Delta t}{\Delta x}\right) T^{n+1/2}_{i-1,j} + \left(2(1-\lambda_x) - \frac{v_o \Delta t}{\Delta x}\right) T^{n+1/2}_{i,j} + \lambda_x T^{n+1/2}_{i+1,j}$$

$$+ g^{n}_{i,j}\frac{\Delta t}{\rho C} \quad 0 < i < I \text{ (A-2.11b)}$$

$$E^{n+1/2}_{j} = \left(2\lambda_x + \frac{v_o \Delta t}{\Delta x}\right) T^{n+1/2}_{I-1,j} + \left(2(1-\lambda_x) - \frac{v_o \Delta t}{\Delta x}\right) T^{n+1/2}_{I,j}$$

$$+ g^{n}_{I,j}\frac{\Delta t}{\rho C} + \hat{q}^{n}_{s_4,j}\frac{2\Delta t}{\rho C \Delta x} \quad (i = I) \text{ (A-2.11c)}$$

for $j = J$

$$E^{n+1/2}_{J} = \left(2(1-\lambda_x) - \frac{v_o \Delta t}{\Delta x}\right) T^{n+1/2}_{0,J} + \left(2\lambda_x - \frac{v_o \Delta t}{\Delta x}\right) T^{n+1/2}_{1,J}$$

$$+ g^{n}_{0,J}\frac{\Delta t}{\rho C} + \hat{q}_{s_2,J}\frac{2\Delta t}{\rho C\Delta x} + \hat{q}_{s_3,0}\frac{2\Delta t}{\rho C\Delta y}\ (i = 0) \quad \text{(A-2.12a)}$$

$$E^{n+1/2}_{J} = \left(\lambda_x + \frac{v_o\Delta t}{\Delta x}\right)T^{n+1/2}_{i-1,J} + \left(2(1-\lambda_x) - \frac{v_o\Delta t}{\Delta x}\right)T^{n+1/2}_{i,J} + \lambda_x T^{n+1/2}_{i+1,J}$$

$$+ g^{n}_{i,J}\frac{\Delta t}{\rho C} + \hat{q}_{s_3,i}\frac{2\Delta t}{\rho C\Delta y}\ 0 < i < I \quad \text{(A-2.12b)}$$

$$E^{n+1/2}_{J} = \left(2\lambda_x + \frac{v_o\Delta t}{\Delta x}\right)T^{n+1/2}_{I-1,J} + \left(2(1-\lambda_x) - \frac{v_o\Delta t}{\Delta x}\right)T^{n+1/2}_{I,J}$$

$$+ \frac{g^{n}_{I,J}\Delta t}{\rho C} + \hat{q}_{s_3 I}\frac{2\Delta t}{\rho C\Delta y} + \hat{q}_{s_4,J}\frac{2\Delta t}{\rho C\Delta x}\ (i = I) \quad \text{(A-2.12c)}$$

A-2.3 Summary of ADI Equations

The ADI scheme results in two tri-diagonal sets of equations to solve for the temperature

$$\{A1\}_i T^{n+1/2}_{i-1,j} + \{C1\}_i T^{n+1/2}_{i,j} + \{B1\}_i T^{n+1/2}_{i+1,j} = D^{n}_{i} \quad \text{(A-2.13)}$$

$$\{A2\}_j T^{n+1}_{i,j-1} + \{C2\}_j T^{n+1}_{i,j} + \{B2\}_j T^{n+1}_{i,j+1} = E^{n+1/2}_{j} \quad \text{(A-2.14)}$$

where the coefficients, $\{A1\}_i$, $\{C1\}_i$, $\{B1\}_i$, are given in equation (A-2.5) and D^{n}_{i} is given in equation (A-2.6) through (A-2.8) and coefficients $\{A2\}_j$, $\{C2\}_j$, $\{B2\}_j$, are given in equation (A-2.9) and $E^{n+1/2}_{j}$ is given in equation (A-2.10) through (A-2.12).

LIST OF REFERENCES

LIST OF REFERENCES

Alifanov, O. M., Artyukhin, E. A., and Rumyantsev, S. V., 1996, *Extreme Methods for Solving III-Posed Problems with Applications to Inverse Heat Transfer Problems,* Begell House Inc., New York.

Alifanov, O.M., 1994, *Inverse Heat Transfer Problems*, Springer-Verlag, New York.

Alifanov, O. M. and Egorov, Y. V., 1985, "Algorithms and Results of Solving the Inverse Heat Conduction Problem in a Two-Dimensional Formulation," *Journal Engineering Physics*, Vol. 48, No. 4, 489-496.

Alifanov, O. M. and Kerov, N. V., 1981, "Determination of External Thermal Load Parameters by Solving the Two-Dimensional Inverse Heat-Conduction Problem," *Journal Engineering Physics*, Vol. 41, No. 4, 1049-1053.

Anderson, D. A., Tannehill, J. C., and Pletcher, R. H., *Computational Fluid Mechanics and Heat Transfer*, Hemisphere, New York, Chapter 4, pp. 128.

Arora, J. S., Introduction to Optimum Design, McGraw-Hill, New York.

Artyukhin, E. A., 1996, "Account for Smoothness when Estimating Temperature-Dependent Thermophysical Characteristics," Proceeding of the Second International Conference on Inverse Problems in Engineering: Theory and Practice, eds. D. Delaunay, K. Woodbury, and M. Raynaud, 9-14 June 1996, LeCroisic, France, ASME Engineering Foundation.

Artyukhin, E. A., and Gedzhadze, I. Yu., 1994, "Sequential Regularization Solution of a Boundary Inverse Heat Conduction Problem," 2nd Joint Russian-America Workshop on Inverse Problems in Engineering, August 1994, St. Petersberg, Russia.

Balageas, D.L. and Luc, A.M., 1986, "Transient Thermal Behavior of Directional Reinforced Composites: Applicability Limits of Homogeneous Property Model," *AIAA Journal*, Vol. 24, No. 1, p. 109-114.

Bass, B. R., 1980, "Application of the Finite Element Method to the Nonlinear Inverse Heat Conduction Problem using Beck's Second Method," *ASME Journal Heat Transfer*, Vol. 102, pp. 168-176.

Baumeister, J., 1987, *Stable Solution of Inverse Problems*, Friedr. Vieweg and Sohn, Braunschweig.

Beck, J. V., Blackwell, B., and Haji-Sheikh, A., 1996, "Comparison of some inverse heat conduction methods using experimental data," *International Journal of Heat and Mass Transfer*, Vol. 39, No. 17, pp. 3649-3657.

Beck, J. V., 1996, "Parameter Estimation Concepts and Modeling: Flash Diffusivity Application," Proceeding of the Second International Conference on Inverse Problems in Engineering: Theory and Practice, eds. D. Delaunay, K. Woodbury, and M. Raynaud, 9-14 June 1996, LeCroisic, France, ASME Engineering Foundation.

Beck, J. V., 1993, "Comparison of the Iterative Regularization and Function Specification Algorithms for the Inverse Heat Conduction Problem," *Inverse Problems in Engineering: Theory and Practice*, eds. N. Zabaras, K. Woodbury and M. Raynaud, ASME.Engineering Foundation.

Beck, J. V., Cole, K, Haji-Sheikh, A., and Litkouhi, B., 1992, *Heat Conduction using Green's Functions*, Hemisphere, New York.

Beck, J. V., Petrie, T. W., and Courville, G. E., 1991, "Using Parameter Estimation to Analyze Building Envelope Thermal Performance," In-Situ Heat Flux Measurements in Buildings - Applications and Interpretation of Results, Steven N. Flanders, Editor, US Army Cold Regions Research and Engineering Laboratories, Hanover, NH., Special Report 91-3, pp. 161-191.

Beck, J.V., and Osman, A.M., 1991, "Sequential Estimation of Temperature-Dependent Thermal Properties," *High Temperature-High Pressure*, Vol. 23, pp. 255-266.

Beck, J. V. and Murio, D. A., 1986, "Combined Function Specification-Regularization Procedure for Solution of Inverse Heat Conduction Problem," *AIAA*, Vol. 24, No. 1, pp. 180-185.

Beck, J.V., Blackwell, B.,and St. Clair, C.R., 1985, *Inverse Heat Conduction*, Wiley, New York.

Beck, J.V. and Arnold, K.,1977, *Parameter Estimation in Engineering and Science*, Wiley, New York.

Bines, E. B., 1993, "The Protection of Carbon-Carbon Against Oxidation at Elevated Temperature," *Essential of Carbon-Carbon Composites*, ed. C.R. Thomas, Royal Society of Chemistry, Cambridge, p. 228.

Busby, H.R. and Trujillo, D.M., 1985, "Numerical Solution to a Two-Dimensional Inverse Heat Conduction Problem," *International Journal for Numerical Methods in Engineering*, Vol. 21, pp. 349-359.

Chamis, C.C., 1973, "Computerized Multilevel Analysis for Multilayer Fibre Composites," *Computers and Structures*, Vol. 3, pp. 467-482.

Dowding, K., and Beck, J. V., 1994, "Measurements of Transient Temperatures and Heat Fluxes in a Composite Material for the Estimation of Thermal Properties - Part II: Property Determination and Heat Flux Estimation," Michigan State University, MSU-ENGR-004-94, East Lansing, MI.

Emery, A.F. and Fadale, T. D., 1996, "Design of Experiments Using Uncertainty Information," *ASME Journal of Heat Transfer*, Vol. 118, pp. 532-538.

Fadale, T. D., Nenarokomov, A. V., and Emery, A.F., 1995a, "Two Approaches to Optimal Sensor Locations," *ASME Journal of Heat Transfer*, Vol. 117, pp. 373-379.

Fadale, T. D., Nenarokomov, A. V., and Emery, A.F., 1995b, "Uncertainties in Parameter Estimation: the Inverse Problem," *International Journal of Heat Transfer and Mass Transfer*, Vol. 38, no. 3, pp. 511-518.

Garnier, B., Delaunay, D.and Beck, J.V., 1993, "Measurement of Surface Temperature of Composite Materials for the Optimal Estimation of Their Thermal Properties," Proceedings of the 13th European Conference on Thermophysical Properties, Lisbon, Portugal.

Garnier, B., Delaunay, D., and Beck, J.V., 1992, "Estimation of Thermal Properties Without Instrumentation Inside the Samples," *International Journal of Thermophysics*, Vol. 13, No. 6, pp. 1097-1111.

Guo, L. and Murio, D., 1991, "A Mollified Space-Marching Finite-Difference Algorithm for the Two-Dimensional Inverse Heat Conduction Problem with Slab Symmetry," *Inverse Problems*, Vol. 7, pp. 247-259.

Haji-Sheikh, A. and Buckingham, F.P., 1993, "Multidimensional Inverse Heat Conduction Using the Monte Carlo Method," *ASME Journal Heat Transfer*, Vol. 115, pp. 26-33.

Han, L.S. and Cosner, A.A., 1981, "Effective Thermal Conductivities of Fibrous Composites," *ASME Journal of Heat Transfer*, Vol. 103, pp. 387-392.

Harris, J.P., Yates, B., Batchelor, J., and Garrington, P.J., 1982, "The Thermal Conductivity of Kevlar Fibre-Reinforced Composites," *Journal of Materials Science*, 17, pp. 2925-2931.

Hensel, E., 1991, Inverse Theory and Applications for Engineers, Prentice-Hall, New Jersey.

Hensel, E. and Hills, R., 1989, "Steady-State Two-Dimensional Inverse Heat Conduction," *Numerical Heat Transfer, Part B*, Vol. 15, pp. 227-240.

Hsu, T., Sun, N. G., Chen, G. G., and Gong, Z., 1992, "Finite element formulation for two-dimensional inverse heat conduction analysis, *ASME Journal Heat Transfer*, Vol. 114, pp. 553-557.

Imber, M., 1975, "Two-Dimensional Inverse Conduction Problem - Further Observations," *AIAA Journal*, Vol. 13, No. 1, pp. 114-115.

Imber, M., 1974, "Temperature Extrapolation Mechanism for Two-Dimensional Heat Flow," *AIAA Journal*, Vol. 12, No. 8, pp. 1089-1093.

Incropera, F. P. and DeWitt, D. P., 1990, *Introduction to Heat Transfer*, Second Edition, Wiley, NY.

Ingham, D.B. and Yuan, Y., 1994, *The Boundary Element Method for Solving Improperly Posed Problems*, Computational Mechanics, Southampton, U.K.

Jarny, Y. C. and Beck, J. V., 1995, "Tutorial Solution of a Heat Conduction Parameter Estimation Problem Using the Adjoint Method," Proceeding of Seventh Inverse Problems in Engineering Seminar, Busby, H. R. and Guo, L. eds., Ohio State University, Columbus, OH.

Jarny, Y., Ozisik, N. M., and Bardon, J. P., 1991, "A General Optimization Method Using Adjoint Equation for Solving Mulitdimensional Inverse Heat Conduction," *International Journal Heat and Mass Transfer*, Vol. 34, No.11, pp. 2911-2919.

Kerov, N.V., 1983, "Solution of the Two-Dimensional Inverse Heat Conduction Problem in Cylindrical Coordinate System," *Journal of Engineering Physics*, Vol. 45, No. 5, pp. 1245-1249.

Kulkarni, M. R. and Brady, R. P., 1997, "A Model of Global Thermal Conductivity in Laminated Carbon/Carbon Composites," *Composites Science and Technology*, Vol. 57, No. 3, pp. 277-285.

Kurpisz, K. and Nowak, A.J., 1995, *Inverse Thermal Problems*, Computational Mechanics, Southampton, U.K.

Lamm, P. K., 1995, "Future-Sequential Regularization Methods for Ill-Posed Volterra Equations: Applications to the Inverse Heat Conduction Problem," *Journal Math. Analysis and Applications*, Vol. 195, pp. 469-494.

Lamm, P. K., 1993, "Inverse Problems and Ill-posedness," Proceeding of the First International Conference on Inverse Problems in Engineering: Theory and Practice, eds

N. Zabaras, K. Woodbury, and M. Raynaud, 13-18 June 1993, Palm Coast, FL, ASME Engineering Foundation, pp. 1-10.

Lamm, P. K., 1990, "Regularization and the Adjoint Method of Solving Inverse Problems," Lectures given at 3rd Annual Inverse Problems in Engineering Seminar, Michigan State University, East Lansing, MI, 25-26 June 1990.

Lawson, C.L., 1974, *Solving Least Squares Problems*, Prentice-Hall, Englewood Cliffs, New York.

Lee, H,J., and Taylor, R.E., 1975, "Thermophysical Properties of Carbon/Graphite Fibers and MOD-3 Fiber-Reinforced Graphite," *Carbon*, Vol. 13, pp. 521-527.

Loh, M. and Beck, J. V., 1991, "Simultaneous Estimation of Two Thermal Conductivity Components from Transient Two-Dimensional Experiments," paper 91-WA/HT-11 presented at ASME Winter annual meeting, Atlanta, GA.

Loulou, T., Artyukhin, E. A., and Bardon, J. P., 1996, "Estimation of the Time-Dependent Thermal Contact Resistance at the Mold-Casting Interface," Proceeding of the Second International Conference on Inverse Problems in Engineering: Theory and Practice, eds. D. Delaunay, K. Woodbury, and M. Raynaud, 9-14 June 1996, LeCroisic, France, ASME Engineering Foundation.

Luenberger, D. G., 1973, *Introduction to Linear and Nonlinear Programming*, Addison-Wesley, Massachusetts.

Minkowycz, W.J., Sparrow, E.M., Schneider, G.E., and Pletcher, R.H.(eds.), 1988, *Handbook of Numerical Heat Transfer*, Wiley Science, New York.

Murio, D.A., 1993a, *The Mollification Method and the Numerical Solution of Ill-Posed Problems*, Wiley, New York

Murio, D., 1993b, "On the Numerical Solution of the Two-Dimensional Inverse Heat Conduction Problem by Discrete Mollification," Proceeding of the First International Conference on Inverse Problems in Engineering: Theory and Practice, eds. N. Zabaras, K. Woodbury, and M. Raynaud, 13-18 June 1993, Palm Coast, FL, ASME Engineering Foundation, Florida, pp. 17-21. .

Osman, A. M., Dowding, K. J., and Beck, J. V., 1997, "Numerical Solution of the General Two-Dimensional Inverse Heat Conduction Problem (IHCP)," *ASME Journal of Heat Transfer*, Vol. 119, pp. 38-45.

Osman, A. M. and Beck, J. V., 1990, "Investigation of Transient Heat Transfer Coefficients in Quenching Experiments," *ASME Journal Heat Transfer*, Vol. 112, pp. 843-848.

Osman, A.M. and Beck, J.V., 1989, "Nonlinear Inverse Problem for the Estimation of Time-and-Space Dependent Heat Transfer Coefficients," *Journal of Thermophysics and Heat Transfer*, Vol. 3, No. 2, pp. 146-152.

Osman, A.M. and Beck, J.V., 1989, "QUENCH2D: A General Computer Program for Two-Dimensional Inverse Heat Transfer Problems," Heat Transfer Group, Department of Mechanical Engineering, Michigan state University, Report. MSU-ENGR-89-017, October 1, 1989.

Ozisik, N. M., 1993, *Heat Conduction*, 2nd edition, Wiley Science, New York.

Pasquetti, R., and Le Niliot, C., 1991, "Boundary Element Approach for Inverse Heat Conduction Problems: Application to a Bidimensional Transient Numerical Experiment," *Numerical Heat Transfer, Part B*, Vol. 20, pp. 169-189.

Raynaud, M. and Beck J. V., 1988, "Methodology for Comparison of Inverse Heat Conduction Methods," *ASME Journal of Heat Transfer*, Vol. 110, pp. 30-37

Reinhardt, H. J. and Hao, N. H., 1996a, "A Sequential Conjugate Gradient Method for the Stable Numerical Solution to Inverse Heat Conduction Problems," *Inverse Problems*, Vol. 2, pp. 263-272.

Reinhardt, H. J. and Hao, N. H., 1996b, "On the Numerical Solution of Inverse Heat Conduction Problems by Gradient Methods," Proceeding of the Second International Conference on Inverse Problems in Engineering: Theory and Practice, eds. D. Delaunay, K. Woodbury, and M. Raynaud, 9-14 June 1996, LeCroisic, France, ASME Engineering Foundation.

Savage, G., 1993, *Carbon-Carbon Composite*, Chapman and Hall, London.

Scott, E.P., and Beck, J. V., 1992a, "Estimation of Thermal Properties in Carbon/Epoxy Matrix Materials During Curing," *Journal of Composite Materials*, Vol. 26, No. 1, pp. 21-36.

Scott, E.P., and Beck, J. V., 1992b, "Estimation of Thermal Properties in Epoxy Matrix/ Carbon Fiber Composite Materials," *Journal of Composite Materials*, Vol. 26, No. 1, pp. 132-149.

Scott, E. P. and Beck, J.V., 1989, "Analysis of Order of the Sequential Regularization Solutions of Inverse Heat Conduction Problems," *ASME Journal of Heat Transfer*, Vol. 111, pp. 218-224.

Shapiro, A. B., 1986, "TOPAZ2D a Two-Dimensional Finite Element Code for Heat Transfer Analysis, Electrostatic, and Magnetostatic Problems," Lawrence Livermore National Laboratory, CA.

Taktak, R., Beck, J.V., and Scott, E., 1993, "Optimal Experimental Design for Estimating Thermal Properties of Composite Materials," *International Journal of Heat Mass Transfer*, Vol. 36, No. 12, pp. 2977.

Taktak, R., 1992, "Design and Validation of Optimal Experiments for Estimating Thermal Properties of Composite Materials," Ph.D thesis, Michigan State University, East Lansing, Michigan.

Taylor, R.E., Jortner, J., and Groot, H., 1985, "Thermal Diffusivity of Fiber-Reinforced Composites using the Laser Flash Technique," Carbon, Vol. 23, No. 2, pp. 215-222.

Tikhonov, A.N. and Arsenin, V.Y., 1977, *Solutions of Ill-Posed Problems*, Winston and Sons, Washington D.C.

Truffart, B., Jarny, Y., and Delaunay, D., 1993, "A General Optimization Algorithm to Solve 2-d Boundary Inverse Heat Conduction Problems Using Finite Elements," *Proceedings of Inverse Problems in Engineering: Theory and Practice*, ASME, Florida, pp. 53-60.

Tseng, A.A. and Zhao, F. Z., 1996, "Multidimensional Inverse Transient Heat Conduction Problems by Direct Sensitivity Coefficient Method using a Finite-Element Scheme," *Numerical Heat Transfer, Part B*, Vol. 29, pp. 365-380.

Tseng, A.A., Chen, T.C., and Zhao, F. Z., 1996, "Direct Sensitivity Coefficient Method for Solving Two-Dimensional Inverse Heat Conduction Problems by Finite-Element Scheme," *Numerical Heat Transfer, Part B*, Vol. 27, pp. 291-307.

Tuan, P.-C., Ji, C.-C., Fong, L.-W., and Huang, W.-T., 1996, "An Input Estimation Approach to On-Line Two-Dimensional Inverse Heat Conduction Problems," *Numerical Heat Transfer, Part B*, Vol. 29, pp. 345-363.

Ulbrich, A., Beck, J. V., and Dowding, K., 1993, "Measurements of Transient Temperatures and Heat Fluxes in a Composite Material for the Estimation of Thermal Properties - Part I: Experimental Aspects," Michigan State University, MSU-ENGR-009-93, East Lansing, MI.

Zabaras, N. and Yang, G., 1996, "Inverse Design and Control of Microstructural Development in Solidification Processes with Natural Convection," presented at the 31st National Heat Transfer Conference Houston, Texas, 3-6 August, 1996, edited by V. Prasad et al., ASME, New York.

Zabaras, N. and Liu, J., 1988, "An Analysis of Two-Dimensional Linear Inverse Heat Transfer Problems Using an Integral Method," *Numerical Heat Transfer*, Vol. 13, pp. 527-533.